Applied Materials Today 29 (2022) 101614

Contents lists available at ScienceDirect

Applied Materials Today

journal homepage: www.elsevier.com/locate/apmt

Flexible solar and thermal energy conversion devices: Organic photovoltaics (OPVs), organic thermoelectric generators (OTEGs) and hybrid PV-TEG systems

Anirudh Sharma [a,1], Saeed Masoumi [b,1], Desta Gedefaw [c], Seamus O'Shaughnessy [b], Derya Baran [a], Amir Pakdel [b,*]

[a] KAUST Solar Center (KSC), Physical Sciences and Engineering Division (PSE), King Abdullah University of Science and Technology (KAUST), Thuwal, 23955, Saudi Arabia
[b] Department of Mechanical, Manufacturing, and Biomedical Engineering, Trinity College Dublin, The University of Dublin, Dublin D02PN40, Ireland
[c] School of Agriculture, Geography, Environment, Ocean and Natural Sciences (SAGEONS), The University of South Pacific, Suva, Fiji

ARTICLE INFO

Keywords:
Organic semiconductors
Organic photovoltaics
Organic solar cells
Organic thermoelectrics
Hybrid PV-TEG
Wearable electronics

ABSTRACT

Solar and thermal energy conversion are two major renewable energy technologies highly sought after in the past two decades by academia, industry, and policymakers. Besides the traditionally large-size solar and thermal energy convertors, more recently, lightweight, flexible solar cells and thermoelectric generators (TEGs) based on organic semiconductor materials have attracted much attention due to the booming development of wearable electronics. In this article, we comprehensively review the scientific advances in the field of organic photovoltaics and organic thermoelectric materials and devices, focusing both on the fundamental processes as well as the development of flexible devices. This review brings together state-of-the-art technological advancements in the field of hybrid photovoltaic-thermoelectric energy harvesters, with overarching relevance and implications for the development of self-powered wearable electronics for internet-of-things (IoT) applications.

1. Introduction

1.1. Photovoltaic technology

The beginning of solar cell technology can be associated with the discovery of the photovoltaic effect by a young French scientist named Edmond Becquerel, who in 1839 [1], measured the impact of a photochemical reaction between two chemically dissimilar liquids. It was not until 40 years after the discovery of the photoelectric effect that the first working photoactive device based on selenium was reported by Charles Fritts in 1883 [2]. In 1953 at Bell Laboratories, Gerald Pearson and Calvin Fuller, in an accidental discovery, found that doped silicon responds to light. This discovery led to the first-ever silicon-based solar cell fabricated by Chaplin et al., which was reported in 1954 [3]. This was later followed by the fabrication of the first silicon solar cell module for outdoor purposes in 1955 [4]. For the next 20 years, spacecraft provided the primary application field for photovoltaics [4]. The potential of solar cells was further demonstrated when 'Vanguard, the first American satellite equipped with solar cells, was launched [5]. The mid 1970's witnessed a sudden growth of module technology due to oil embargoes and the application of photovoltaics in large telecommunication systems, resulting in the first modern module which was designed in 1976 [4]. Although in the last several decades, silicon-based solar cells dominated the photovoltaics markets, and have steadily matured to possess high efficiency, stability, and a reduced energy payback time [6], the downside is brittle nature, energy-intensive manufacturing, and considerable module weight.

In 1960, over a century after the discovery of the photovoltaic effect, anthracene was the first organic compound in which photoconductivity was observed [7]. In 1977, Heeger, MacDiarmid, and Shirakawa showed that polyacetylene, the most straightforward polyconjugated system, can be rendered electrically conductive by reaction with bromine or iodine vapors. The exposure of polyacetylene to halogen vapor resulted in the oxidation of the polymer chain, and an increase in conductivity from a semiconductor to 38 S cm^{-1} was observed [8]. This striking discovery inspired researchers to develop a variety of non-acetylenic

* Corresponding author.
E-mail address: pakdela@tcd.ie (A. Pakdel).
[1] These authors contributed equally to this work.

https://doi.org/10.1016/j.apmt.2022.101614
Received 22 April 2022; Received in revised form 15 July 2022; Accepted 3 August 2022

polymers in both neutral and oxidized states such as poly(p-phenylene)s, polypyrroles, poly(p-phenylenevinylene)s, polythiophenes and polyanilines (leucoemeraldine) [9–13]. In order to impart solubility and tune optoelectronic properties, side-chain(s) introduction was widely used which led to the synthesis of alkyl-substituted semiconductors [14]. Further efforts to produce materials with extended optical coverage, finely tuned molecular energy levels, desired solubility, and ideal intramolecular and intermolecular interactions at solid-state was the impetus to the development of many structures for applications in organic electronics [15–18]. As a result, the last two decades have seen an explosion of academic as well as industry interest in utilizing conjugated polymers, oligomers, and small molecular semiconductors [19] across a range of electronic devices [20]. Particularly after the discovery of electro-luminescence in conjugated polymers [21], this class of materials has been used extensively to design optoelectronic devices such as diodes, transistors [22], organic photovoltaic (OPV) devices [23], organic photodetectors [24], and thermoelectric devices [25]. The research progress in this field is well reflected in the application of organic semiconductors in modern-day smart electronics such as flexible solar cells and high-resolution curved displays, which are not science fiction anymore.

1.2. Thermoelectric technology

Thermoelectric (TE) technology is based on the direct conversion of thermal energy to electrical energy and vice versa through the thermoelectric effect [26]. The TE effect consists of the Seebeck, the Peltier, and the Thomson effects, dating back to early 19th century [27]. Particularly, the Seebeck effect is responsible for converting the temperature differences to electricity, and this principle is the basis for operation of all thermocouples [28]. A device that can produce electricity from a temperature gradient is called a TE generator (TEG). TEGs possess several interesting characteristics such as silent operation, simple design, and a wide range of operating temperatures. Generally, these devices are constructed from *n*- and *p*-type semiconducting materials as TE legs in order to produce electrical power from waste heat. Recently, thermal energy harvesting from complex surfaces which act as the heat sources has triggered significant research focus on flexible TEGs [29]. Based on the TE effect, by applying a temperature difference along a sample, the charge carriers of the hot side transport to the cold side, producing an electrical voltage. The TE efficiency of a material is evaluated by a dimensionless figure of merit, $ZT = \frac{S^2\sigma}{k}T$, where S, σ, k, and T are the Seebeck coefficient, the electrical conductivity, the thermal conductivity, and the absolute temperature, respectively [30]. Therefore, to have a good thermoelectric efficiency, a material should be electrically conductive but thermally insulating.

Several classes of TE material have been developed for use in a wide range of working temperatures, such as chalcogenides, skutterudites, oxides, half-Heuslers, Zintl phases, clathrates, SiGe alloys, organic semiconductors, and semiconducting composites [31–33]. For high-temperature applications, oxides, Zintl phases, SiGe alloys, and Half-Heuslers have been used as high ZT (in the range of 1-1.5) TE materials [34]. In the mid-temperature range, Skutterudites, Half-Heuslers, and Clathrates have been introduced as TE materials that possess ZT of 1.3–2.2 [35]. At low temperatures, Chalcogenide and organic materials with the ZT of 0.4–1.86 have been used [35]. It has been reported that nanostructured, low dimensional, and super lattice forms of these materials can significantly improve the ZT value due to quantum confinement and filtering of charge carriers at the interfaces [36]. The characteristics of inorganic TE materials such as high fabrication costs, rigidity, and toxicity, have hindered their applications in flexible TEGs [33]. Accordingly, organic TE materials have been introduced as a new class of TE materials which not only overcome the limiting factors of their inorganic counterparts but also illustrate promising compatibility with flexible TEGs [37]. For instance, organic TE materials are compatible with solution-based fabrication methods which can significantly reduce the costs associated with flexible TEGs [38].

1.3. Flexible TEG and PV devices for wearable applications

Recently, wearable electronics with multi-functional features that can fit the human body curvatures have attracted much attention due to the booming fields of Internet of Things (IoT) and sensor networking [39–41]. Wearable devices should be small, lightweight, flexible, and portable [42]. Although development of wearable technology has grown rapidly over the past decade, it is still in its infancy and is confronted by several obstacles towards widespread application. One of the main issues with wearable electronic devices is the lack of a sustainable power source in place of conventional batteries for powering the operating sensors and actuators [43]. Such power sources must overcome the problems associated with traditional batteries such as large size, rigidity, high weight, and limited lifetime [44]. This bottleneck has induced a new wave of interest in self-powered wearable devices that utilize energy harvesting technologies for providing power from surrounding energy sources [45]. In this regard, solar and thermal energy sources are easily available from the sunlight and the human body. Therefore, flexible PV and TEG systems are two types of energy conversion devices that can convert sunlight and human thermal energies to electricity, respectively, for supplying the required power for wearable devices [46]. Flexible, thin, and conformal TEGs and PVs should be made of light-weight materials that can be easily processed and allow for stretching and bending for integration into curved surfaces [47]. Recently, research about hybrid TEG/PV devices has gained much interest for synergetic energy harvesting that could be a large driving force for self-powered wearable electronics [48]. Consequently, appropriate organic materials for applications in flexible and wearable TEGs and PVs have become remarkable vectors of innovation [49,50].

2. Organic semiconductors

Materials that fall within this category of semiconductors are a large family of carbon-based compounds comprising alternating single and double bonds of carbon atoms, also known as a conjugated system [19]. Conjugated materials with high molecular weights are commonly classified as polymers, whereas materials with a lower molecular weight are classified as small molecules and oligomers. In such units, the electrons are delocalized because of the sp^2 hybridization of the carbon atoms, imparting semiconducting behavior to organic materials.

Unlike inorganic semiconductors, which consist of a 3D crystal lattice in which energy levels form conduction and valence bands throughout the material, in the case of organic solids, the molecules are bound with weak van der Waals forces. As a result, the occupied and unoccupied states are usually localized, and the electronic structure of a single molecule or a polymeric chain is preserved (Fig. 1) [51].

The validity of band theory in such systems is limited, and the charge transport proceeds with a hopping mechanism between the localized states, resulting in reduced charge carrier mobility in organic solids compared to crystalline inorganic semiconducting solids. Thus, the chemical design of materials which determines the energies and distribution of molecular frontal orbitals in π-conjugated materials [52] plays a vital role in determining their electronic and optical properties.

Most organic semiconductors intrinsically have relatively high absorption coefficients ($\sim \geq 10^5\ cm^{-1}$) [53]. Therefore, a 100 nm thin film is usually enough to get sufficient photogeneration in the photoactive organic film for optimum device performance [54]. Unlike inorganic semiconductors where free charge carriers are generated, primary photo excitations in organic semiconductors, due to their low dielectric constant, lead to electron-hole pairs. The photo-generated electron-hole pairs, also called excitons are bound with Coulomb forces and require strong electric fields to dissociate due to their high binding energy [55].

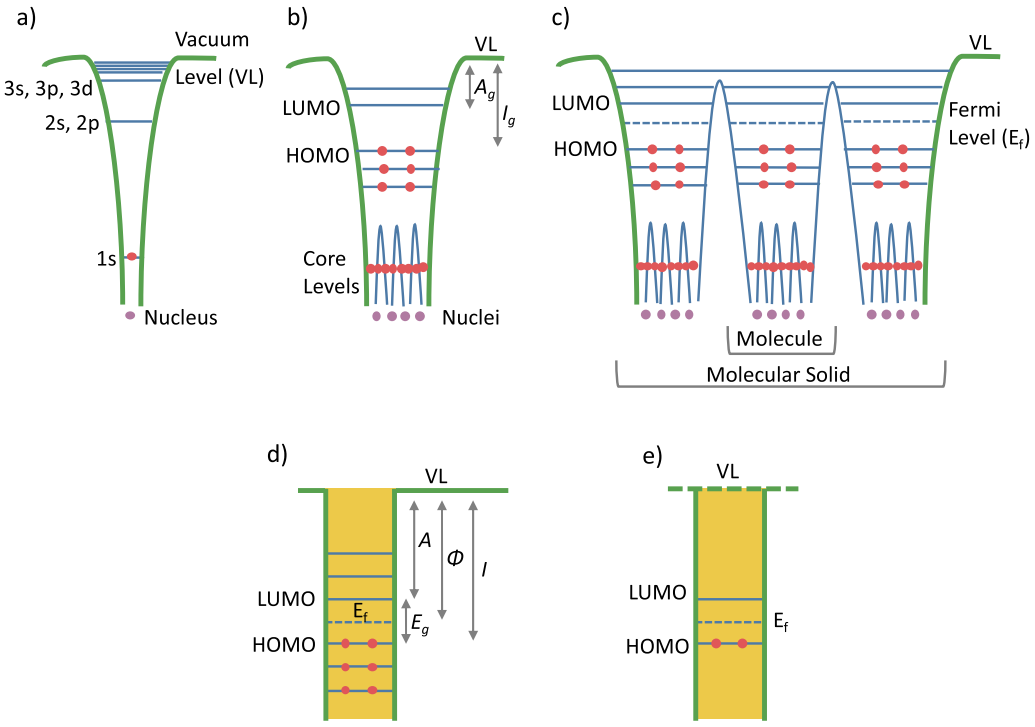

Fig. 1. Schematic depicting the electronic structure using potential well in the case of (a) hydrogen atom, (b) molecules with more than one atom, (c) solid organic, (d) and (e) simplified energy level diagram of a molecular solid shown in (c). I_g, A_g, and I and A are the gas phase and solid phase ionization energy and electron affinity, respectively. Φ denotes the work function, and E_g is the band-gap between the HOMO and LUMO. (Schematic adapted from Ref. [51]).

3. Organic solar cells

The interest in the research and development of organic solar cells (OSCs) has rapidly progressed in the last two decades [56] due to their ability to be lightweight, solution-processable, mechanically flexible, and the potential to tune the color, transparency, and other electrical properties. The first reported OSCs were fabricated by sandwiching a thin organic light-absorbing layer between two electrodes of different work function [57], where one of the electrodes is transparent (such as indium tin oxide) to allow for light to reach the organic layer.

When a photon incident on the device is absorbed by the photoactive layer, an electron in the highest occupied molecular orbital (HOMO) is excited and jumps to the lowest unoccupied molecular orbital (LUMO), forming a neutral excited state or exciton in the organic semiconductor [58] with a binding energy of 0.1 - 1 eV [59]. In order for the charges to be transported to the respective electrodes, the photo-generated exciton need to dissociate.

A significant breakthrough was achieved in the field of OPVs in 1986 when Tang introduced the concept of bilayer hetero-junction and reported an efficiency of ~ 1% from a device made by sandwiching two organic semiconducting materials (phthalocyanine and a derivative of perylenetetracarboxylic acid) [60]. The performance enhancement observed in bilayer devices was attributed to the improved dissociation of charges at the donor-acceptor interface. However, in the case of bilayer devices, the efficiency is often limited by the small diffusion length [61] of the photo-generated exciton. This problem was subsequently overcome through the concept of bulk hetero-junction (BHJ) first reported by two different research groups led by Heeger and Holmes in 1995, by creating polymer-fullerene and polymer-polymer mixtures [62,63]. The BHJ approach depends on creating a complex morphology of electron donor and acceptor materials such that the phases are separated by a distance less than the exciton diffusion length, where the charge dissociation happens at the donor-acceptor interface.

The significantly increased interfacial area between the donor and acceptor in BHJ devices as compared to the bilayer structures, dramatically enhances the charge dissociation [64]. Unlike bilayer devices where the donor and acceptor materials are selectively in contact with the anode and cathode, in the case of BHJ devices, a bi-continuous and interpenetrating network of the donor and acceptor materials is responsible for electron and hole transport to the respective electrodes. Therefore, the device performance of BHJ device is susceptible to the nanoscale morphology of the active layer as well as the charge transport/selective layers used between the active layer and the electrodes [65]. Simultaneous optimization of active and interlayer material properties and device design has thus led to the development of highly efficient OSCs with power conversion efficiencies (PCEs) now reaching 19% [66]. Meanwhile, to enhance the performance of OSCs by complementary and efficient photo-absorption, strategies such as tandem [67] and ternary [68] solar cells have also been studied and developed. More recently, this approach of a multi-component active layer in OSCs has been further extended to quaternary systems [69], even utilizing machine learning-enabled experimental setup for quick and automated optimization and characterization of such complex systems. In this section, we review the progress made in single-junction OSCs, with emphasis on the development of materials, interface engineering, morphology control, and processing of devices.

3.1. Organic solar cell materials

3.1.1. Donor materials

Attempts to improve charge transport and other optoelectronic properties of conjugated materials have led to the synthesis of a variety of simple to complex high molecular weight polymers, oligomers, and molecules. The conjugated polymers can be categorized into first, second, and third generation. Polyacetylene [19] represents the first generation which witnessed the initial efforts to fabricate OSCs. Some of the most studied second-generation semiconducting polymers are poly (paraphenylene) (PPP), poly(phenylene vinylene) (PPV) and polythiophenes (PTh) (Fig. 2) [70]. These materials were used in the fabrication of solar cells to yield reasonable PCE. Moreover, the development

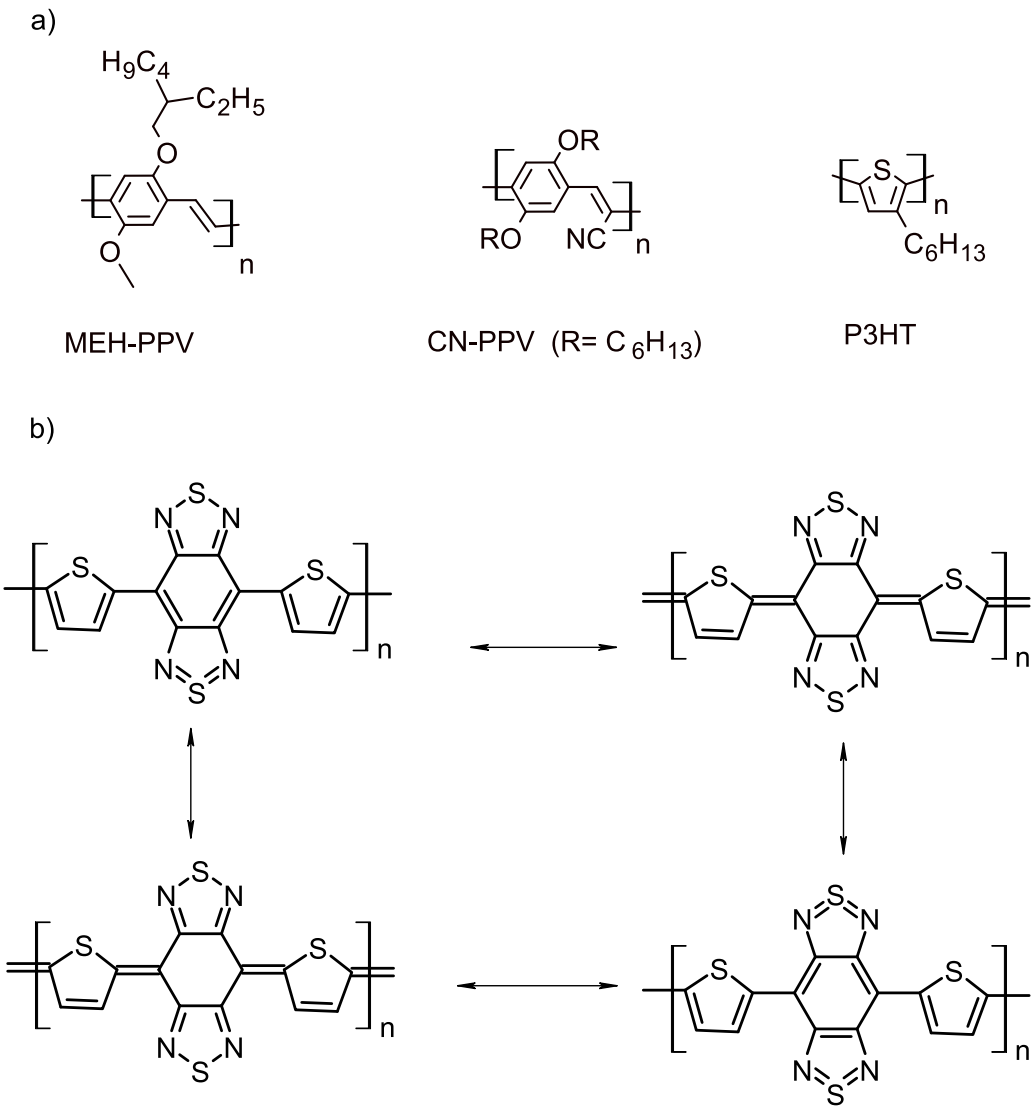

Fig. 2. (a) Examples of second-generation homopolymers. (b) Resonance contributors of thiophene-benzobisthiadiazole chain.

of these materials and their use in solar cells have served as a benchmark to enhance the understanding of film microstructures and device optimization techniques.

One of these is PPV based materials, which are among the first class of materials investigated in-depth due to their unique physical properties such as conductivity, electroluminescence, and solubility of their derivatives. For instance, MEH-PPV and CN-PPV are electron donor and electron-deficient conjugated polymers, respectively, used to study charge transfer in BHJ solar cells. Indeed, the study [63] revealed that the blend of the two materials provides an interpenetrating network in solid-state, and a relatively efficient charge generation was observed in solar cells. Moreover, the blend allowed pathways towards the opposite electrodes for charge collection in devices [63]. A further investigation of a blend of MEH-PPV and CN-PPV in solar cells yielded a PCE up to 1.7% under white light illumination [71]. Another class of homopolymers that have garnered the attention of researchers in the field of OPVs are polythiophenes. Even though the first report on the synthesis of polythiophenes dates back to 1884, the synthesis of polythiophenes with many repeating units was not achieved until the Yamamoto group developed the Grignard coupling reaction using 2,5-dibromothiophene as a monomer in 1980 [72]. The Grignard coupling reaction gave a relatively longer thiophene chain. However, the solubility in organic solvents of the material was minimal and hence difficult to process. The introduction of alkyl and aryl substituents to improve solubility and processability was a key development in polythiophenes that led to the synthesis of alkyl or aryl substituted thiophene based monomers and polymers. In 1986, soluble and processable oligothiophenes were prepared by introducing alkyl side chains on to the backbone of the thiophene-based polymer. The side chains played a role in reducing polymer chains organization, crystallization, and hence promoting solubility in organic solvents [73]. To improve the electrical property of the polyalkyl thiophenes, the synthesis of regioregular polyalkylthiophene by McCullough and coworkers reported in 1992 and 1993 was a decisive step [74,75]. In their work, Kumada cross-coupling reaction on 2-bromo-5-bromomagnesio-3-dodecylthiophene in the presence of Ni(dppp) Cl_2 as catalyst gave a polymer with high regioregularity (91% head-tail coupling) and high electrical conductivity (up to 1000 S cm^{-1}) for the I_2 doped polymer. Poly (3-hexyl thiophene) (P3HT) is undoubtedly one of the structures widely used in photovoltaic research due to its remarkable electrical and optical properties as well as its better balance between the solubility and electric properties [76,77]. PCE up to 7.4% using P3HT as a donor and indene C_{70} bisadduct as an acceptor with solvent additive have been reported [78]. Even though the PCE of P3HT based devices have shown improvement, the polymer still has an inherent drawback of mismatched absorption ranges, with an onset of absorption of 650 nm that can allow the harvesting of only up to 22.4% of the available

photons, giving a maximum theoretical current density of 14.3 mAcm^{-2}. Research has shown that extending the onset of absorption to 1000 nm will allow the harvesting of 53% of the available photons and could enable the generation of a maximum current density of 33.9 mAcm^{-2} [79]. Moreover, P3HT has a relatively higher-lying HOMO energy level (~-5.0 eV) that will result in lower open-circuit voltages (V_{OC}) in devices and eventually reduce the PCE of the final solar cell device [80]. Such drawbacks of polythiophenes and other homopolymers have served as an impetus for researchers to find alternative ways to extend the optical absorption coverage of the materials to a longer wavelength region and to produce materials with deeper HOMO energy levels to fulfill the requirements for successful solar cell materials. One of the key developments to circumnavigate these inherent problems in homopolymers is the emergence of the donor-acceptor (D-A) design motif, where the backbone of the polymer/oligomer/molecule is constructed from an electron-rich (D) and electron-deficient (A) aromatic segments linked together by a covalent bond using reactions such as metal-catalyzed cross-coupling reactions (e.g., Suzuki and Stille). The role of the D-A design motif to reduce band gap and to engineer the molecular energy levels of the polymers was first observed by Havinga et al. [81]. The intramolecular charge transfer interaction between the D and A units enhances the double bond character between the repeating units, stabilizes the quinoid form, reduces the bond length alternation and hence results in low bandgap materials [82,83]. For example, a D-A polymer

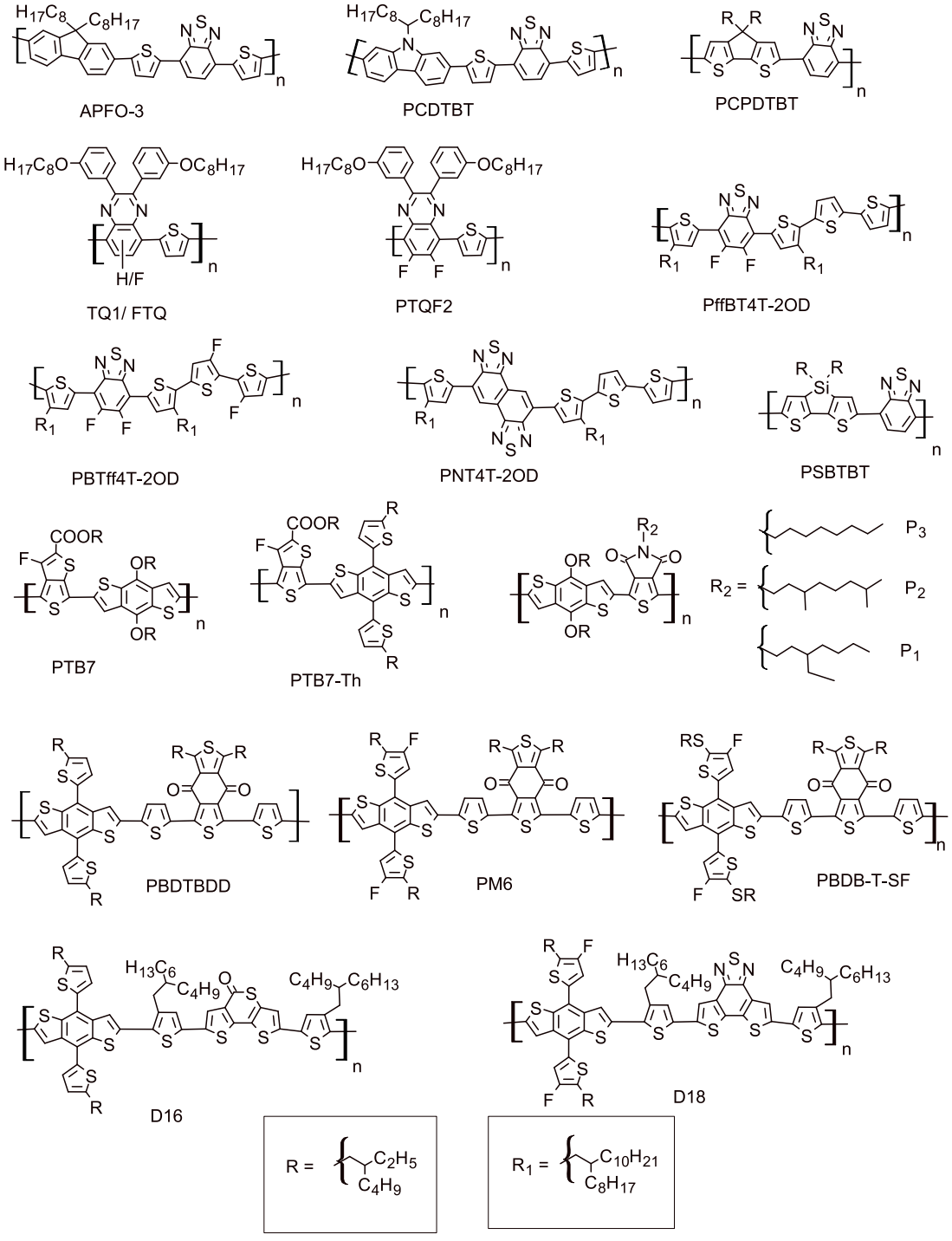

Fig. 3. Examples of D-A solar cell polymers.

containing thiophene (D) and benzobisthiadiazole (A) forms four resonance structures due to the intramolecular interaction between thiophene and bisthiadiazole (Fig. 2). The unhybridized donor (thiophene) has higher-lying HOMO and LUMO energy levels while the unhybridized benzobisthiadiazole acceptor has deeper-lying HOMO and LUMO energy levels. The covalent bonding of thiophene and benzobisthiadiazole will cause the mixing of the orbitals of the two units that bring the HOMO and LUMO energy levels of the coupled system closer, giving a narrower bandgap and optimized HOMO and LUMO energy levels (Fig. 2).

Subsequently, the synthesis of D-A polymers with various combinations of donors and acceptors became a common practice that led to the development of numerous structures, and their optical, electrical, and device properties were studied. The following section offers only a glimpse of the structures developed with the D-A strategy, focusing only on benchmark and historically significant materials. Among the first class of D-A polymers are polyfluorenes (Fig. 3). Polyfluorenes were studied for solar cell applications owing to the relative ease of synthesis, deep HOMO, and high stability. For example, Andersson's group developed poly(2,7-(9,9-dioctyl-fluorene)-*alt*-5,5-(4',7'-di-2-thienyl-2', 1', 3'-benzothiadiazole)) (APFO-3) which consist of a fluorene donor and benzothiadiazole acceptor with thiophene aromatic unit inserted as a π-spacer (Fig. 3). Devices fabricated from a blend of APFO-3 and $PC_{61}BM$ ([6,6]-phenyl C61-butyric acid methyl ester), have yielded up to 3.5% PCE, which was one of the highest achievements in the early days of OPVs [84]. Several other electron-deficient aromatic structures such as quinoxaline and pyrazinoquinoxaline were developed by the same group to prepare numerous APFO series D-A polymers. Structures with multiple chromophores in the backbone of the polymers (which are nowadays called terpolymers) were also among the structures developed with the intention of manipulating the optoelectronic properties [85–88].

The introduction of nitrogen at C-9 of the fluorene structure resulted in an analog donor molecule known as carbazole, where the first synthesis of D-A polymers based on 2,7-carbazole was reported in 2001 with an alkyl group attached to the nitrogen atom of the structure to promote the solubility and influence the inter-polymer chain interactions [89,90]. Poly[N-9'-heptadecanyl-2,7-carbazole-alt-5,5-(4', 7'-di-2-thienyl-2',1', 3'-benzothiadiazole)] (PCDTBT) (Fig. 3) is among the first carbazole based polymers, which consist of a benzothiadiazole acceptor and thiophene π-bridge. PCDTBT has an absorption onset of 660 nm and an estimated HOMO and LUMO of -5.5 and -3.6 eV. A 1:4 blend of PCDTBT and $PC_{61}BM$ in a BHJ device gave a PCE of 3.6% with short circuit current (J_{SC}) = 6.92 $mAcm^{-2}$, V_{OC} = 0.89 V, and FF = 63% [91]. Further optimization of the processing conditions and device parameters of PCDTBT based solar cells have resulted in a PCE over 7% [92].

The development of cyclopentadithiophene (CPDT) and silicon bridged CPDT is an essential step towards lowering the bandgap of polymers. Poly[2,6-(4,4-bis(2-ethylhexyl)-4H-cyclopenta[2,1-b; 3,4-b']dithiophene)-alt-4,7-(2,1,3-benzothiadiazole)] (PCPDTBT) and poly[(4,4'-bis(2-ethylhexyl)dithieno[3,2-b:2', 3'-d]silole)-2,6-diyl-alt-(2,1,3-benzothiadiazole)-4,7-diyl] (PSBTBT) (Fig. 3) are examples of CPDT- based polymers and were found to possess an excellent optical absorption that extends to the near IR region (up to 900 nm). PCPDTBT showed a PCE of 3.2% in combination with $PC_{71}BM$ in photovoltaic devices [19]. On the other hand, the silicon heteroatom-containing polymer (PSBTBT) revealed an improved PCE due to the higher crystallinity content and high hole mobility. Interestingly, PSBTBT showed three times higher hole mobility (3×10^{-3} $cm^2V^{-1}s^{-1}$) than PCPDTBT. A PCE as high as 5.1% was reported from a PSBTBT-based device [93, 94].

Thiophene is a commonly used electron-rich molecular unit used in numerous D-A polymers such as poly[2,3-bis-(3-octyloxyphenyl) quinoxaline-5,8-diyl-alt-thiophene-2,5-diyl] (TQ1), which is a copolymer of thiophene and quinoxaline monomers (Fig. 3). TQ1 is endowed with interesting properties such as easy synthesis, excellent solubility, ideal molecular energy levels (HOMO = -5.7 eV and LUMO = -3.3 eV), good film-forming, and other beneficial electrical properties. Andersson's group in 2010 reported a 6% PCE by blending TQ1 with $PC_{71}BM$ in a 1:3 ratio, processed with *o*-dichlorobenzene (ODCB). The solar cell device gave a corresponding J_{SC} = 10.5 $mAcm^{-2}$, V_{OC} = 0.89 V, and FF = 64% [95]. Further optimization of the nanomorphology of a blend of TQ1 and $PC_{71}BM$ with the use of solvent additives such as 1,8-octanedithiol (ODT), 1,8-diiodooctane (DIO), diphenylether (DPE), and 1-chloronaphthalene (CN)) to ODCB processing solvent, resulted in an improved PCE of over 7% [96]. Other modifications of TQ based polymers (poly(6-fluoro-2,3-bis-(3-octyloxyphenyl)quinoxaline-5,8-dyl-alt--thiophene-2,5-diyl), FTQ and poly[6,7-difluoro-2,3-bis(3-(octyloxy) phenyl)quinoxaline-alt-thiophene], PTQF2) with the use of a mono and difluorinated quinoxaline as acceptors were reported [97,98].

Oligothiophenes as donors were also used in various structures. For instance, a combination of oligothiophene with benzothiadiazole and bisbenzothiadiazole yielded D-A polymers referred to as poly [(5,6-difluoro-2,1,3-benzothiadiazol-4,7-diyl)-alt-(3,3‴-di(2-octyldodecyl)-2,2′;5′,2″;5″,2‴-quaterthiophen-5,5‴-diyl)] (PffBT4T-2OD), (poly[(2,1,3-benzothiadiazol-4,7-diyl)-alt-(4',3',-difluoro-3,3‴-di(2-octyldodecyl)-2,2';5',2'';5'',2'''-quaterthiophen-5,5'''-diyl)] (PBTff4T-2OD) and poly[(naphtho[1,2-c:5,6-c']bis[1,2,5]thiadiazol-5,10-diyl)-alt-(3,3'''-di(2-octyldodecyl)-2,2';5',2'';5'',2'''-quaterthiophen-5,5'''-diyl)] (PNT4T-2OD) (Fig. 3). These polymers were found to give an optimum morphology when combined with different fullerene-based acceptors. The photovoltaic device performances were insensitive to thickness of the films. The films possessed a high crystallinity and yet reasonably small domains that needed for efficient charge generation yielding a FF over 70% and PCE over 10.8% [99].

Benzodithiophene (BDT) is another popular electron-rich aromatic structure used in D-A polymers. The BDT molecular structure is known for its rigidity and planarity, allow the formation of an extended π-conjugation and favorable inter-chain π-π interaction in polymers. The synthesis of BDT based monomers is reasonably easy and scalable. Alkoxy, alkyl, and aryl containing substituents can be introduced as a side group to manipulate the optoelectronic properties [100–102]. An important class of materials is the PTB family where the BDT based donor and thieno[3,4-b]thiophene based acceptor monomers are linked covalently with or without the insertion of a π-linker. It is known that the thieno[3,4-b] thiophene molecular aromatic unit is known to enhance the quinoidal character and hence leads to the formation of narrower bandgap polymers. Among the PTB family, poly [[4,8-bis[(2-ethylhexyl)oxy]benzo[1,2-b:4,5-b']dithiophene-2,6-diyl][3-fluoro-2-[(2-ethylhexyl)carbonyl] thieno[3,4-b]thiophenediyl]] (PTB7) (Fig. 3) consists of a 2-ethylhexyloxy substituted BDT and a fluorinated and 2-ethylhexyloxy ester modified thieno[3,4-b]thiophene core structure. PTB7 was found to have good solubility in organic solvents and was prepared in high molecular weight. The hole mobility of the polymer was determined to be in the order of 10^{-4} cm^2/Vs. A blend of PTB7 and $PC_{71}BM$ gave a PCE of 7.4% when processed with a mixture of ODCB and 3% DIO solvent. An inverted structure using a water-soluble PFN polymer and MoO_3 as an electron and hole transporting layer, respectively, resulted in a PCE of over 9% [103]. To optimize the polymer structure, alkyl thiophene was introduced to the BDT core unit and used together with the thieno[3,4-b]thiophene acceptor to yield 2D π-extended system (poly[4,8-bis(5-(2-ethylhexyl) thiophen-2-yl)benzo[1,2-b;4,5-b']dithiophene-2,6-diyl-alt-(4-(2-ethylhexyl)-3-fluorothieno[3,4-b]thiophene-)-2-carboxylate-2-6-diyl)], PTB7-Th). PTB7-Th showed a relatively deeper HOMO (-5.22 eV) compared to PTB7, and hence PTB7-Th is expected to give a higher V_{OC} in solar cells. The use of PTB7-Th devices together with $PC_{71}BM$ processed from a DIO (1.5% V/V) and NMP (1.5% V/V) mixed solvent additive to ODCB as the primary solvent gave a high PCE of 10.8%, indicating the potential of the BDT- thieno[3,4-b]thiophene D-A system for high performing solar cells [104].

Another versatile electron-deficient unit widely known is the thieno [3,4-c]pyrrole-4,6(5H)-dione (TPD), which is known for its structural

flexibility for tuning the solubility and packing property in conjugated polymers. For instance, different alkyl groups were attached to the TPD unit to optimize the molecular structure and combined with a BDT donor unit to give three polymers (Fig. 3). The polymers were blended with $PC_{61}BM$ in solar cells which resulted in a PCE ranging between 4.0% and 6.8%, depending on the size and shape of the alkyl solubilizing groups [105].

Benzodithiophene-dione (BDD) is another successful acceptor that was combined with BDT to yield high performing solar cell materials (Fig. 3). The first solar cell polymer in the series is made from an alkoxy BDT donor and BDD acceptor units without the introduction of thiophene as a π-bridge. The material resulted in a low PCE of 0.73%, mainly due to the backbone twisting due to an unfavorable interaction and low charge carrier mobility of the device [106]. However, the use of a 2D-BDT as a donor (with an attachment of alkyl thiophene) and the insertion of a thiophene ring between the donor and acceptor yielded poly[(2,6-(4,8-bis(5-(2-ethylhexyl)thiophen-2-yl)-benzo[1,2-b:4,5-b']dithiophene))-alt-(5,5-(1',3'-di-2-thienyl-5',7'-bis(2-ethylhexyl)benzo[1',2'-c:4',5'-c']dithiophene-4,8-dione)] (PBDTBDD, *aka* PBDB-T) (Fig. 3). A mixture of this polymer with $PC_{61}BM/PC_{71}BM$ gave an improved PCE in the range of 6.67 to 7.45%. The polymer was blended with 3,9-bis(2-methylene-(3-(1,1-dicyanomethylene)-indanone))-5,5,11,11-tetrakis(4-hexylphenyl)-dithieno [2,3-d:2',3'-d']-s-indaceno[1,2-b:5,6-b']dithiophene (ITIC) (Fig. 5) (non-fullerene acceptor) to fabricate a solar cell (ITO)/ZnO/BHJ-layer/MoO_3/Al) that showed a J_{SC} =16.80 mAcm^{-2}, V_{OC} = 0.899 V, and FF = 74.2%, yielding a PCE of 11.21%. The improvement of the solar cell with the use of ITIC (compared to that of $PC_{61}BM/PC_{71}BM$) is attributed to the complementary optical absorption behavior of the materials and the improved and balanced electron and hole mobility of the blend (3.13×10^{-4} cm^{2}V^{-1}s^{-1} and 2.10×10^{-4} cm^{2}V^{-1}s^{-1}) [107,108]. The introduction of fluorine to the 2D-BDT unit employed in the synthesis of the PBDTBDD structure resulted in another polymer, represented as PM6 (Fig. 3), with a deeper HOMO of -5.45 eV (-5.25 eV for PBDTBDD), which is known to benefit the generation of high V_{OC} for the PM6 based solar cell devices. An inverted configuration solar cell with a device structure of ITO/PFN/PM6: $PC_{71}BM/MoO_3$/Au resulted in a high PCE of 9.2% with 75 nm thin film [109].

In another work, poly[(2,6-(4,8-bis(5-(2-ethylhexyl-3-fluoro)thiophen-2-yl)-benzo[1,2-b:4,5-b']dithiophene))-alt-(5,5-(1',3'-di-2-thienyl-5',7'-bis(2-ethylhexyl)benzo[1',2'-c:4',5'-c'] dithiophene-4,8-dione)] (PM6) was blended with a non-fullerene acceptor NFA (IDIC) (2,2'-((2Z, 2'Z)-((4,4,9,9-tetrahexyl-4,9-dihydro-s-indaceno[1,2-b:5,6-b']dithiophene-2,7-diyl) bis(methanylylidene)) bis(3-oxo-2,3-dihydro-1H-indene-2,1-diylidene)) dimalononitrile) with a complimentary optical absorption in the range of 300 to 800 nm, which facilitates obtaining high J_{SC} in PSCs. The structure of the NFA-PSCs used to probe the photovoltaic properties was ITO/PEDOT: PSS/PM6: IDIC/PFN-Br/Al, where the champion device gave a PCE of 11.9% [110]. A ladder-type multi-fused ring low bandgap acceptor (2,2'-((2Z, 2'Z)-((12,13-bis (2-ethylhexyl)-3,9-diundecyl-12,13- dihydro-[1,2,5] thiadiazolo[3,4-e] thieno[2,''3'':4',5'] thieno[2',3':4,5], Y6) (Fig. 5) with a benzothiadiazole core unit was reported by Yuan et al. [111], and used as an acceptor with PM6 donor material to fabricate a conventional device solar cell (ITO/PEDOT: PSS/PM6: Y6/PDINO/Al) to yield up to 15.7% PCE.

The BDT donor was modified with the attachment of a thioalkyl side chain and the introduction of fluorine, which was combined with the BDD-based acceptor to yield a polymer represented as poly[(2,6-(4,8-bis(5-(2-ethylhexylthio)-4-fluorothiophen-2-yl)-benzo [1,2-b:4,5-b']dithiophene))-alt-(5,5-(1',3'-di-2-thienyl-5',7'-bis(2-ethylhexyl) benzo[1',2'-c:4',5'-c']dithiophene-4,8-dione)] (PBDB-T-SF) (Fig. 3). The polymer showed a moderate optical band gap of 1.80 eV and enhanced absorption peak, showing strong π–π intermolecular interactions. The hole and electron mobility of PBDB-T-SF and IT-4F (9-bis(2-methylene-((3-(1,1-dicyanomethylene)-6,7-difluoro)-indanone))-5,5,11,11-tetrakis (4-hexylphenyl)-di) (non-fullerene acceptor) were found to be slightly improved compared to the parent structures (PBDB-T and ITIC). Photovoltaic properties of the polymer were investigated by blending the polymer with IT-4F (Fig. 5) (ITO/ZnO/active layer/MoO_3/Al) to yield a PCE of 13% [112].

Most recently, a 2D-BDT donor unit was combined with a three-membered thioolactone acceptor ring with alkyl thiophene inserted in between to give D16 (Fig. 3). D16 possesses an optical band gap of 1.95 eV estimated from the onset of the optical absorption of the polymer. The HOMO and LUMO energy levels of the polymer were determined to be -5.48 eV and -2.83 eV using cyclic voltammetry (CV). A conventional solar cell device with a configuration of ITO/PEDOT:PSS/active layer/PDIN/Ag was fabricated to evaluate the photovoltaic properties of the polymer. An NFA (in this case, Y6) was used as a counterpart that led to a PCE of 16.72% with corresponding V_{OC} = 0.85 V, J_{SC} = 26.61 mA cm^{-2}, and FF = 73.8%. The high performance of the polymer in solar cells was explained in terms of the balanced and relatively higher electron and hole mobility (in the order of 10^{-4} cm^2 V^{-1} s^{-1}). The blend also revealed a clear nanofiber morphology with a diameter around 16 nm which favors exciton dissociation and charge transport, thus leading to high J_{SC} and FF [113].

The use of a fused ring dithienobenzo[1,2-c][1,2,5]thiadiazole (DTBT) acceptor and a fluorinated 2D-BDT gave D18 (Fig. 3). The polymer showed an optical band gap of 1.98 eV, similar to D16. The HOMO and LUMO energy levels, as estimated from a CV measurement, are -5.51 eV and -2.77 eV, respectively. A solar cell device with a structure of ITO/PEDOT: PSS/D18: Y6/PDIN/Ag was made to evaluate the performance of D18. The D/A ratio, active layer thickness, additive content, and solvent vapor annealing (SVA) time were optimized to give a PCE of 18.22%. The high hole mobility (in the order of 10^{-3} cm^2 V^{-1} s^{-1}), favorable morphology and aggregation tendency were suggested as the reasons for the high performance of the devices [114].

3.1.2. Small donor molecules

Like conjugated polymers, the development and characterization of electron donor small molecules have gained the attention of the scientific community in the last few decades. It is known that small molecules can be synthesized in high purity, unlike conjugated polymers that suffer from batch-to-batch variations in terms of solubility, molecular weight, polydispersity, and purity, which leads to different processing properties and performances. There are many reported cases where different batches of polymers perform differently and provide completely different photovoltaic properties. The unique advantage of small molecular donors is that they are relatively immune from such differences [115,116].

Among the wide array of small molecules developed in the past, 5,5'-bis([4-(7-hexylthiophen-2-yl)thiophen-2-yl]-[1,2,5]thiadiazolo[3,4-c] pyridine)-3,3'-di-2-ethylhexylsilylene-2,2-bithiophene ($DTS(PTTh_2)_2$) (Fig. 4) developed by Sun et al. possesses an acceptor/donor/acceptor backbone composed of thiadiazolo[3,4-c]pyridine (acceptor) sandwiched between an electron-rich segment containing dithienosilol (DTS) and bithiophene electron-rich units. The molecule showed an ideal optical property with a solid-state absorption onset extending to 815 nm. The molecular energy levels (HOMO = -5.2 eV, LUMO = -3.6 eV) were estimated with CV. A solar cell device with a structure of ITO/MoOx/$DTS(PTTh_2)_2$:$PC_{71}BM$/Al was fabricated by blending $DTS(PTTh_2)_2$ with $PC_{71}BM$ and processing the film with chlorobenzene and DIO solvent additive. The best device gave a PCE of 6.70%, J_{SC} = 14.5 mAcm^{-2}, V_{OC} = 0.78 V and FF = 59.3%% when processed from chlorobenzene with 0.25% (V/V) DIO additive [116].

Another small donor molecule is benzodithiophene terthiophene rhodanine (BTR) (Fig. 4), which is composed of a core 2D-BDT unit sandwiched between two segments made up of terthiophene and rhodanine groups. BTR displayed absorption onset and absorption maximum (λ_{max}) of 681 nm and 523 nm, respectively. The HOMO and LUMO of BTR were estimated from a CV measurement to be -5.34 eV and -3.52 eV, respectively. The planar and extended conjugated system displayed hole mobilities up to 0.1 and 1.6×10^{-3} cm^2 V^{-1} s^{-1} recorded by an organic field-effect transistor (OFET) and space-charge-limited

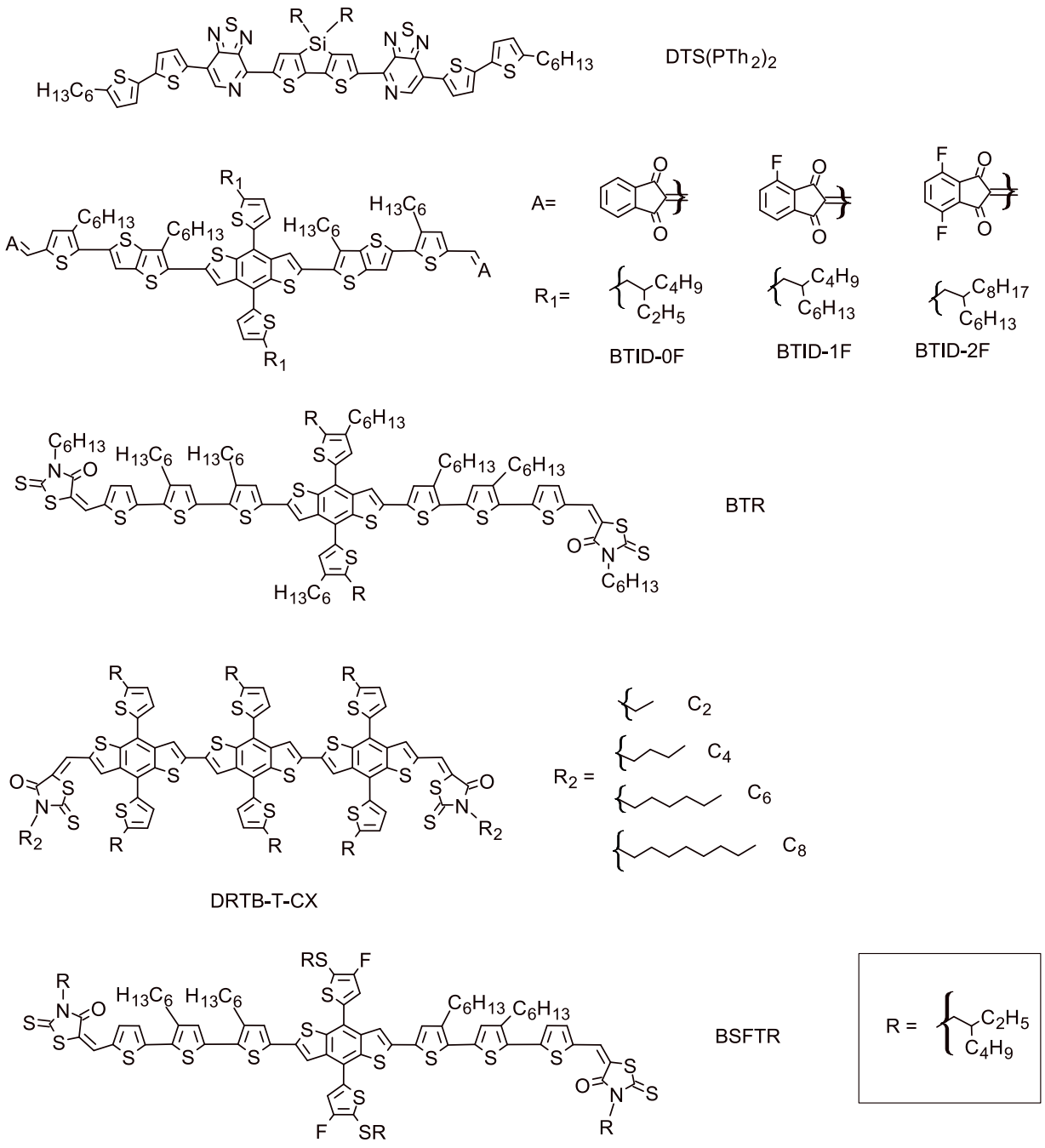

Fig. 4. Small molecular donor structures.

current (SCLC) methods, respectively. A blend of BTR: $PC_{71}BM$ sandwiched between PEDOT: PSS coated ITO and a Ca/Al back cathode resulted in a PCE of 9.3% with a J_{SC} of 13.90 mA cm^{-2}, V_{OC} of 0.90 V and a high FF of 74.0% [117]. A thickness-dependent solar cell performance of BTR was also carried out, and the performance varied from 6.8% (80 nm thick film) to 8.3% (250 nm thick film). The FF remained close to 70% even at a 400 nm thick film, which showed less sensitivity of the material to thickness.

Three medium bandgap molecules with an electron-rich segment made up of thiophene, thienothiophene, and BDT and end-capped with 0, 1 and 2 F atoms modified H-indene-1,3(2H)-dione were developed (Fig. 4) which showed excellent molecular properties, such as low HOMO levels (-4.91 to -5.05 eV), good crystallinity and high hole mobility. The materials were used in solar cells and yielded a 8.21%, 10.37% and 11.08% PCE when blended with $PC_{71}BM$ in an inverted device structure of ITO/ZnO/active layer/MoOx/Ag) [118].

A BDT triamer was end-capped with rhodanine, and different alkyl groups, namely, ethyl, *n*-butyl, *n*-hexyl, and *n*-octyl were attached to yield DRTB-TCX small molecules (Fig. 4). The molecular structure shifted from edge-on to face-on as the alkyl side chain length increased, affecting the photovoltaic properties. The four compounds show identical absorption spectra with an absorption maximum at 500–600 nm, and absorption onsets in the films were found in the range 620 nm–629 nm. A CV study revealed the HOMO levels to be in the range of ~-5.50 eV–5.52 eV. The photovoltaic properties were investigated by blending with IT-4F (Fig. 4) and using a device structure of ITO/ZnO/DRTB-TCX: IT-4F/MoO_3/Al, yielding a PCE of 9.52%, 11.24%, 10.52% and 9.4% for the devices prepared based on C2, C4, C6, and C8, respectively. The high PCE is closely related to the enhancement in charge mobility and the correlation length of π-π stacking [119].

A modification of BTR (discussed above), gave BSFTR. This was achieved with the introduction of a thioalkyl thiophene and fluorine atom on the 2D-BDT and a solubilizing group attached to the rhodanine end-capping electron-deficient unit. BSFTR was studied in depth using spectroscopic and electrochemical methods. It was also used as donor material to fabricate solar cells. Shown in Fig. 5, Y6, with complementary absorption that extends to longer wavelengths, was used as an acceptor counterpart for the fabrication of solar cells. BSFTR was found to have a HOMO and LUMO of -5.59 eV and -3.69 eV, respectively. The optical absorption range of the photovoltaic blend was 300 nm to 930 nm. The photovoltaic properties of a blend of BSFTR and Y6 were tested using a device structure of ITO/PEDOT: PSS/BSFTR: Y6/ZrAcac/Al, to give a PCE of 13.69%, with an active layer processed from chloroform solution and treatment of the film with solvent vapor and thermal annealing [120].

3.1.3. Acceptor materials

Fullerenes are a class of roughly spherical carbon-based molecules predominantly made up of sp2 bonds. These molecules, such as C_{60} and C_{70}, have a high EA and good electron conductance ($\sim 10^{-4}$ S cm^{-1}), resulting in them being one of the most used acceptors in heterojunction OSCs. Photoinduced electron transfer from a conjugated polymer to C_{60} was first reported by Sariciftci et al. [121]. Morita and colleagues [122] later observed that the conductivity in a C_{60} - conjugated polymer blend improved with C_{60}. Relatively more soluble derivatives of C_{60} were then used as acceptors in polymer-fullerene solar cells [123–125]. Subsequently, a range of fullerene derivatives were synthesized and studied as acceptor materials in OPV devices (Fig. 5) [126–129].

Despite the early success in the development of polymer-fullerene solar cells [130], organic solar cell performance and stability were limited mainly due to the weak absorption of PCBM in the visible and near infra-red (NIR) region [131], poor mechanical and morphological stability [132], as well as the inability to significantly alter their electron affinity (EA) and ionization energy (IE) using modifications to their chemical structure, which limits the generation of high V_{OC} in devices.

Recently, a range of NFA materials, both polymers as well as small molecules, have emerged as an efficient replacement of fullerene derivatives in OSCs [133]. The use of *n*-type polymeric acceptors together with *p*-type polymers has demonstrated long-term optical, thermal, environmental, mechanical, and morphological stabilities, which are

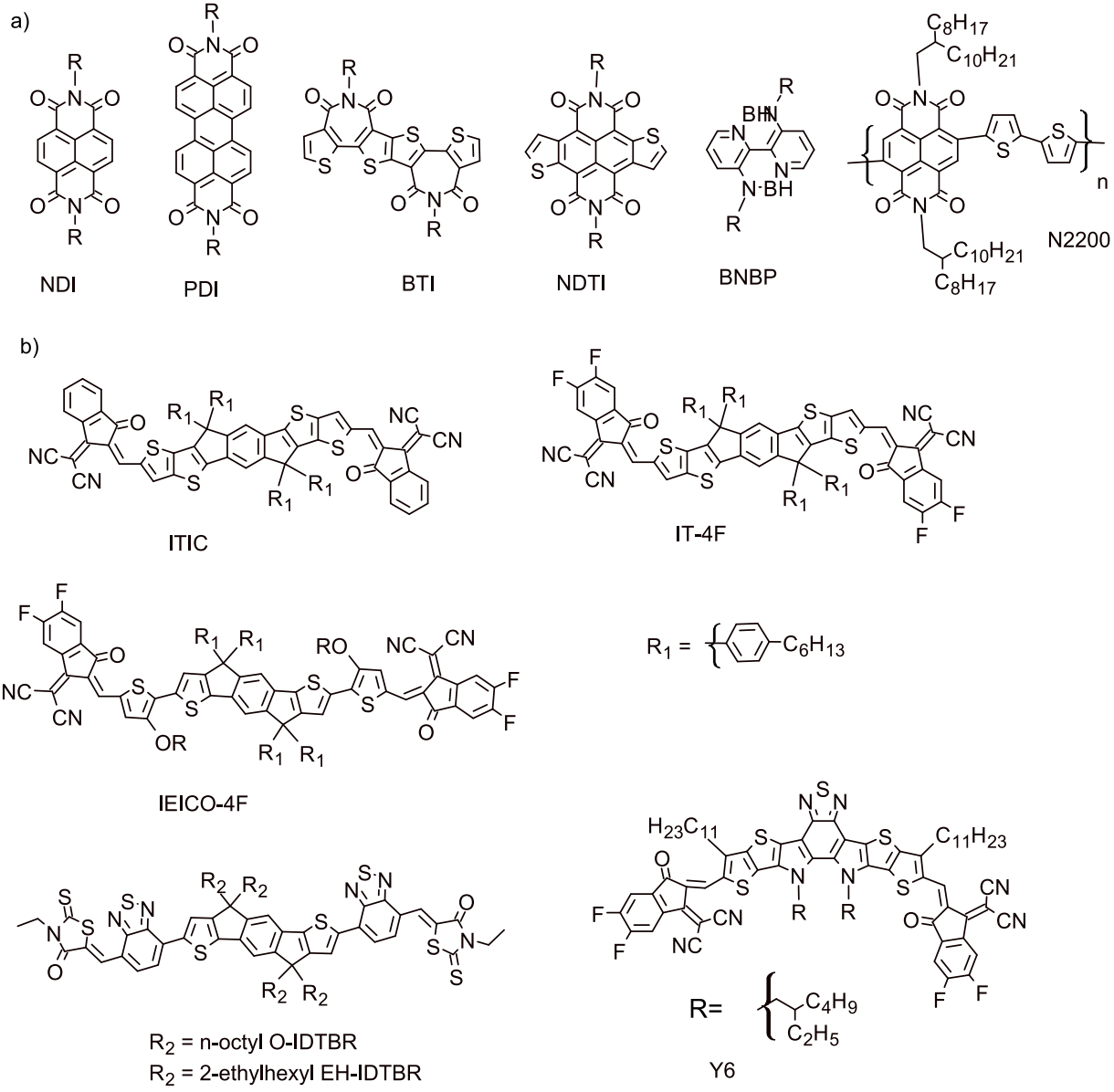

Fig. 5. (a) Electron deficient non-fullerene core units and *n*-type polymer. (b) non-fullerene *n*-type molecular acceptors.

properties required in large-area and flexible devices. The most widely known electron-deficient core units to synthesize *n*-type polymers include naphthalene diimide (NDI) [134], naphthodithiophene diimide (NDTI) [135], perylene diimide (PDI) [136], B'N bridged bipyridine (BNBP) [137] and bithiophene imide (BTI) [138] (Fig. 5).

For example, *n*-type polymers based on a naphthalene diimide (poly ([N,N'-bis(2-octyldodecyl)-naphthalene-1,4,5,8-bis(dicarboximide)-2,6-diyl]-alt-5,5'-(2,2'-bithiophene)), N2200) (Fig. 5) [139] or a perylene diimide [140] core have been demonstrated as efficient acceptor materials in OSCs. After the structure showed high performance in organic thin-film transistors [141], N2200 became popular as an NFA for OSCs. For instance, Mu et al. blended N2200 with a NT-based donor polymer to give a promising PCE of 5% due to the relatively favorable morphology of the NT: N2200 blends [139]. However, due to the rigid, planar, and strong π-π intermolecular interactions, N2200 can easily become overly crystalline, which can result in unsatisfactory morphology and give rise to poor PCE in solar cells. The use of random terpolymers is currently being investigated as a strategy to tune properties such as crystallinity, optical absorption, and molecular energy levels. For instance, thiophene, furan or selenophene have been added as a third component to a combination of NDI and bithiophene to yield three terpolymers: PNDI-Fu10, PNDI-Th10, and PNDI-Se10 [142], having a 10% of NDI-furan, 10% of NDI-thiophene and 10% of NDI-selenophene, respectively, in the backbone of the polymers.

The polymers were used as *n*-type acceptors together with FTQ (donor) (Fig. 3) in solar cells. Devices (ITO/PEDOT: PSS/ active layer/ PDINO/Al) based on PNDI-Fu10, PNDI-Th10, and PNDI-Se10 gave PCEs of 4.75%, 5.88% and 5.25%, respectively. For comparison, a device based on the reference alternating copolymer P(NDI2OD-T2) (N2200) yielded a PCE of 5.36%. All terpolymers based films give a smooth surface with root mean square (rms) roughness in the range of 0.81–0.92 nm (AFM). However, PNDI-Th10 based films revealed a preferential π-face-on crystal orientation with relatively large crystallites. Such orientation of PNDI-Th10 chains minimizes bimolecular/ geminate recombination in devices and hence yields higher J_{SC}, FF, and overall PCE.

A wide range of other *n*-type polymers based on moieties such as DPP, isoindigo, 2,1,3-benzothiadizole and [2,2′-bipyridine-3,3′-diaminato] tetrafluorodiboron adduct (BNBP) have also been developed [143].

Unlike PCBM, the ability to tune the optical and electronic properties of NFA materials has led to the emergence of a range of small molecule NFA materials with fused-ring acceptor-donor-acceptor type moiety such as ITIC, IDTBR, IEICO, Y6 (Fig. 5). These NFA acceptors have a strong visible-NIR light-harvesting capability and excellent electron mobility, significantly contributing towards improvement in OSC performance [144–148]. PCEs of upto19% have already been accomplished for single-junction OSC, [66,114] and are estimated to surpass 20% [149].

For instance, ITIC is a multicyclic system with a push-pull intramolecular interaction between electron-rich and electron-deficient units installed in the structure, developed by Lin et al. in 2015 (Fig. 5) [150]. ITIC revealed strong and broad optical absorption with an onset extending to 780 nm, low LUMO (-3.83 eV) and HOMO (-5.48 eV) energy levels, good electron transportability (3.0×10^{-4} $cm^2 V^{-1} s^{-1}$), and good miscibility with polymer donors materials; all important features needed for high performance in solar cells. ITIC was blended with PTB7-Th (Fig. 3) to yield a PCE of 6.8% compared to a 7.52% PCE when PC_{71} BM was used as an acceptor. This potential NFA was combined with various donor materials to yield promising PCE as high as 11.21% [108, 151]. The modification of ITIC by the introduction of fluorine atoms resulted in a molecular acceptor called IT-4F (Fig. 5), which was subsequently used in solar cells. The use of PBDTBDD and IT-4F as a photoactive material in a device structure of (ITO)/ZnO/active layer/MoO_3/Al resulted in a high efficiency of 13.1%, attributed to down-shifted molecular energy levels, broad optical absorption range, and enhanced absorption coefficient [112]. Another molecule is IEICO-4F (Fig. 5) [152], constructed based on indaceno [1,2-b:5,6-b'] dithiophene and 2-(3-oxo-2,3-dihydroinden-1-ylidene)malononitrile. The NFA showed a PCE of up to 10% when combined with PTB7-Th (Fig. 3).

IDTBR acceptors [153] (Fig. 5) were reported to have an indacenodithiophene (IDT) core sandwiched between benzothiadiazole rings and terminated with rhodanine rings. The structures were reported to be planar due to the increased quinoidal character of the phenyl-thienyl bond. A device structure of glass/ITO/ZnO/P3HT: IDTBR/MoO_3/Ag was used to evaluate the photovoltaic properties with P3HT used as a donor. The blend resulted in well-matched optoelectronic properties and gave an optimized morphology that enabled a PCE of up to 6.4%. Y6 (Fig. 5) was also combined with another D-A copolymer (D-18) (Fig. 3) to yield a PCE of 18% [114].

3.1.4. Transparent electrode materials

The electrodes are an essential component of a device as it acts as a medium between the semiconducting/photoactive layer and the external circuit. Ideally, they should be chemically stable and unreactive to the functional material layers, have very low resistance, and must possess high transmission to be used as a transparent electrode in OSC. The majority of OSC devices use a conducting metal electrode and a transparent conducting electrode, usually an oxide such as ITO or fluorine-doped tin oxide (FTO) due to their wide bandgap and transparency to wavelengths of over 400 nm. For better-performing devices, the low sheet resistance of the electrodes is desirable to minimize charge losses, as the direct correlation of device area and degradation in device performance is well known and has been attributed to the high sheet resistance of underlying electrodes.

With an increased focus on the development of flexible OSC and flexible electronics in general [154], research efforts have intensified on developing a low-cost and scalable replacement for the expensive and brittle ITO despite its high transparency, low sheet resistance, and high tolerance to bending. A range of organic and inorganic materials [155] have been explored as transparent electrode materials for OSC. In the last few years, alternative approaches have also emerged utilizing nano-composite materials consisting of carbon nanotubes, graphene, conducting polymers, and silver nano-wires [156,157]. Such materials show promise as transparent electrode materials with excellent electrical and optical properties and demonstrated compatibility with the roll-to-roll processing and printing [158,159]. Even though ITO is still the most widely used transparent electrode material in OSC due to relatively low sheet resistance and high transmittance, examples of ITO-free devices are available [160]. Recently, Han et al. have reported the use of a silver-copper grid as a transparent electrode in large area OSC, achieving a PCE of over 12% [161]. Another approach using bimodal silver nanowire (AgNW-BM) films composed of silver nanowires of two different aspect ratios has been utilized to achieve highly transparent electrodes with optical transmission of ~80% over the visible spectrum and sheet resistance of 10 Ω sq^{-1} when used in conjunction with a thin layer of PEDOT: PSS [162]. Semitransparent OSC based on PTB7-Th: IEICO4F and utilizing AgNW-BM electrodes resulted in a PCE of 7.49%, with an average visible transmittance of 33%. Although silver nanowire composites and silver grids have shown great promise for use as transparent electrodes, research efforts should focus on further reducing the sheet resistance of composite electrodes and increasing the tolerance of such electrodes to repeated bending and deformation, for applications in flexible devices.

3.2. Charge generation and energetics

The efficiency of OSC is often limited by the dissociation of the strongly bound Frenkel excitons into free charges [163,164]. As discussed in Section 3, in order to overcome the exciton binding energy and separate the coulombically bound excitons [59] generated upon

photoabsorption, a heterojunction between two semiconductors ("donor" – material with lowest IE and "acceptor" – material with highest EA) having different electrochemical potential (Fig. 6a, b) is used [60]. The photo-generated exciton can dissociate via two channels: (i) the photo-excited electron from the "donor" can be transferred to the high EA material, and (ii) when the acceptor is excited, a ground-state electron is transferred from the "donor" to the "acceptor" [165]. In BHJ OSC, these two channels of exciton dissociation are believed to be driven by the energetic offset between the EA and the IE of the "donor" and "acceptor" materials, respectively.

However, due to the low dielectric constant of the organic semiconductors, the electron-hole pair formed at the donor-acceptor interface due to the exchange of charge carriers experiences a coulombic attraction, and is commonly known as the charge transfer (CT) state (Fig. 6) [166]. The CT state can dissociate into separated charges by using excess energy from the singlet state or by thermal excitation from the relaxed CT state [167]. However, CT excitons can also recombine to the ground state either radiatively or non-radiatively. Thus, the CT states are believed to play a significant role in the charge generation of OSC, and the ultimate functionality of OSC depends on the dissociation of these excitons. The excitonic character of the CT state can be demonstrated by the sub-bandgap photo-absorption [168] and the corresponding photoluminescence of the CT state [169], as well as by applying an external bias to a solar cell injecting free charges which recombine from the lowest available energy state (CT state) resulting in electroluminescence radiation [170]. A complete understanding of the existence of CT state and the mechanism behind the charge separation into free charges and CT recombination, is a matter of continuing research [171] and has been reviewed comprehensively in the literature [167,172].

Kästner et al. has demonstrated a significant dependence of the CT states on the molecular order and local morphology at the donor-acceptor interface (Fig. 6), highlighting the importance of developing a clearer understanding on the correlation between the CT energy (E_{ct}) and the morphology-dependent material energetics, to give valuable insights for quantifying energy losses in OSC [170,173]. This is of high significance as the molecular frontal orbital energies, namely the IE and EA of organic semiconductors are also known to be dependent on the morphology [174]. The impact of material energetics on the resultant charge generation and device performance of OSCs has therefore attracted a lot of research interest [175].

In the case of fullerene-based OSC, fullerene molecules have been commonly used as the electron acceptor [176], and empirically a EA offset of ~ 0.3 eV has been estimated as a minimum driving force required for charge generation [177]. However, contrary to previous observations, Kawashima et al. in 2015 reported OSC based on a naphthobisoxadiazole-based polymer and PCBM, demonstrating a reduced energy loss of around 0.5 eV attributed to the small EA offset of ~ 0.12 eV [178]. To accomplish further improvements in OSC performance and to design high-performing materials, the field of OSC is in

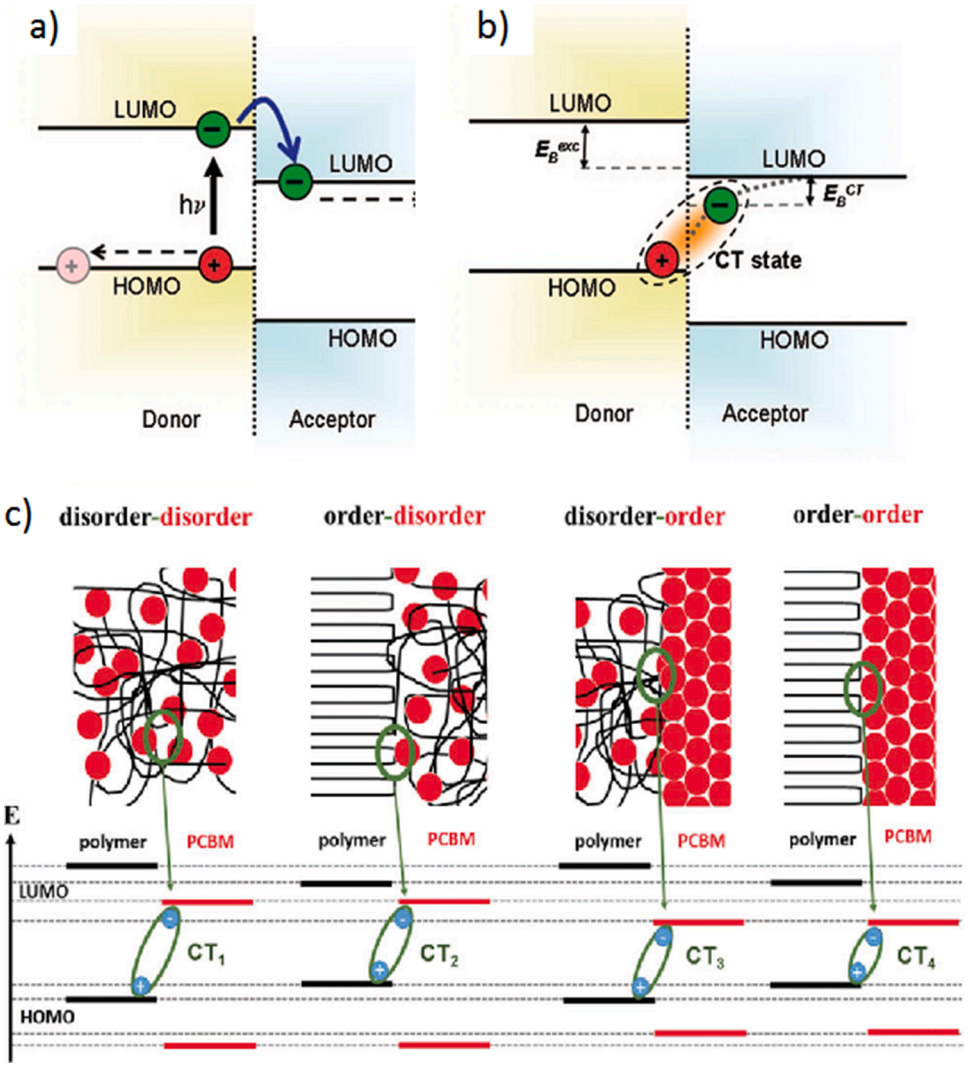

Fig. 6. (a) A schematic depicting the photoexcitation of an electron into the LUMO level of a donor, and subsequent transfer into the LUMO of the acceptor before the separated charges migrate away from the donor-acceptor interface. (b) The formation of a bound interfacial charge transfer (CT) state, where E_B^{exc} and E_b^{CT} are the excitons and CT state binding energies, respectively. (Reprint permission from Ref. [166]) (c) Schematic depiction of the correlation between different morphological phases at the polymer-PCBM interface to the intermolecular CT state transition energies. (Reprint permission from Ref. [170]).

need of a scientific consensus on the minimum driving force required for efficiently separating the charges [179–184]. The recent emergence of NFA molecules as efficient acceptor materials in OSC has further intensified research activities in this direction.

In 2016 Li et al. reported a indacenodithiopheno-indacenodiselenophene based novel fused ring NFA acceptor (IDTIDSe-IC), which in combination with a wide bandgap donor polymer (J51) and having a small IE offset of 0.1 eV, demonstrated efficient hole transfer [185]. Consistent with these findings, Chen et al. in 2017 reported a wide-bandgap donor polymer PvBDTTAZ, which along with an NFA O-IDTBR and having a small IE offset of ~0.4 eV, resulted in OSC with high PCE of over 11% and low energy losses [186]. These observations were later confirmed by Li et al., where they studied six different donor-acceptor systems with IE offset ranging from -0.05 eV to 0.21 eV [187]. The authors demonstrated that NFA OSC made of PTQ10-HC-PCIC as the donor-acceptor system with an IE offset of 0 eV resulted in PCEs of 10.42%, whereas for an active layer composed of PBDB-TF: HC-PCIC having an IE offset of 0.06 eV between the donor and acceptor, a PCE of 11.75% was achieved [187]. While the authors found a retarding effect of a negative IE offset on the hole transfer, the same study found an ultra-fast hole transfer ($\leq$ 4.6 ps), which was independent of an IE offset of more than 0 eV. Another donor-acceptor system composed of PBDBTF as a donor and a novel quinoxaline containing fused core NFA AQx-2 with a negligible driving force for charge separation was shown to have good hole transfer and suppressed charge recombination [188]. This resulted in OSC with PCEs of over 16% and FF of over 76%. Utilizing a polymer PTQ10 as an electron donor (IE = -5.6 eV) systematically with pristine as well as alloys of ZITI-S (-5.8 eV) and ZITI-N (-5.53 eV) as NFA acceptor materials, Zhang et al. has shown that only a low IE offset of ~ 40 meV is essential for efficient exciton dissociation [184]. Recently, Zhong et al. studied blends of m-ITIC NFA with a range of donor materials with varying IE, namely P3HT, PBTTT, J61, and PCDTBT and reported an intrinsically fast hole transfer on a sub-picosecond time scale even for an IE offset of close to 0 eV [189].

Similarly, reduced EA offset between the donor and NFA has also been shown to result in an efficient electron transfer [182,190]. Baran et al. reported efficient charge separation in OSC with an active layer composed of a PffBT4T-2DT: FBR blend, having a small EA offset of less than 0.1 eV [191], resulting in high V_{OC} of 1.12 V and a PCE of 7.8%. Chen et al. using PffBT2T-TT (EA = 3.55 eV, IE = 5.51 eV) as the donor and O-IDTBR (EA = 3.52 eV, IE = 5.42 eV) as the acceptor materials, further demonstrated that by minimizing both the EA and IE offset, efficient hole and electron transfer can still be achieved [192]. PffBT2T-TT and O-IDTBR-based OSC with negligible EA and IE offset resulted in a PCE of 10.4% and a small voltage loss of 0.55 eV.

Yang et al. investigated the influence of the energetic offset on the exciton dissociation efficiency and performance of OSC made of PBDB-TF as a donor and several variants of the NFA ITIC with different frontal orbital energies [179]. Contrary to the above findings, the authors found a direct correlation between the EA and /or IE offsets to the exciton dissociation, where IE offset > 0.2 eV was found to result in higher exciton dissociation efficiency compared to an IE offset of close to 0 eV. Such a dependence on the IE offset was also confirmed by Jin et al. for all polymer OSC based on PBDB-T (IE = 5.33 eV), PTQ1 (IE = 5.4 eV), PTP8 (IE = 5.56 eV) as donor polymers and N2200 as the acceptor polymer. The highest PCE of 6.35% was achieved for PBDB-T-N2200 devices as compared to 4.3% and 3.3% for PTQ1 and PTP8 devices. Importantly, the hole transfer rate from N2200 to PBDB-T was found to be the fastest (~ 5 ps), as compared to PTQ1 and PTP8 (~ 100 ps) devices, which was attributed to the relatively larger IE offset and better crystal orientation. Systematically using block copolymers consisting of a P3HT donor block linked to a push-pull polymer acceptor, Aplan et al. also demonstrated the importance of energetic offset for exciton dissociation [193]. More recently, Karuthedath et al. demonstrated that in the case of low-bandgap non-fullerene donor acceptor BHJ blends, to achieve high internal quantum efficiencies and efficient charge transfer, an IE offset of around 0.5 eV is essential [175].

The findings of the current literature are therefore not conclusive as to why some donor-acceptor combinations undergo efficient charge separation with negligible EA and/or IE offsets, while the others do not. Thus, in order to present a design rule for future NFA solar cells with an optimal current-voltage tradeoff, a more thorough understanding of the design of high performing donor and NFA molecules [194] is required. For example, the barrier-less charge generation has been reported in state-of-the-art low energetic offset PM6-Y6 donor- NFA systems [195,196], where the photocurrent has been found to be independent of the external bias. Efficient charge transfer in this system has been attributed to low energetic disorder and is believed to be primarily driven by entropy [197]. Thus the efficient dissociation of excitons in NFA solar cells having near-zero EA and IE offsets suggests the presence of a possible internal driving force intrinsic to the molecule, and perhaps the mechanism of charge generation in NFA solar cells may be different to that previously known [198].

In 2019, Yao et al. reported OSCs comprising a novel polymer donor PTO2 and IT-4F as the NFA, to have a high PCE of 14.7%, where efficient charge generation was attributed to the molecular electrostatic potential (ESP) and the intermolecular electric field [199]. As discussed in Section 3.1.3, since the NFA molecules are often designed with an electron-donating (D), and electron-withdrawing units (A), NFA molecules themselves may also be susceptible to an internal electric field or polarization, as a result of photoinduced intramolecular charge transfer [200], role of which should be further understood in future studies to unravel efficient charge generation in NFA OSC. Furthermore, charge-quadrupole moments of NFAs are also known to have an orientation-dependent impact on the IE and EA of molecular films [201], such that different molecular orientation could provide the required driving force for charge dissociation [202,203].

In 2020, Dong et al. has demonstrated that in the case of polycrystalline films of α-sexithiophene (α-6T), the boundaries between the crystalline domains of α-6T with different orientations can have electrostatically driven energetic offsets. When used as homo-junction solar cells, upon photo-excitation, such interfaces can efficiently dissociate charges by enabling the formation of hybridized singlet and charge transfer states [204]. Recently, Wu et al. have also reported single component OSCs based on a donor-acceptor block co-polymer PBDB-T-b-PYT [205]. These devices achieved a high PCE of over 11%, had better operational stability and reduced non-radiative voltage loss compared to binary devices. These early demonstrations of single component OSCs opens up exciting avenues for designing organic solar cell materials and devices, which will potentially simplify device fabrication, besides providing better control over structural stability and modulation of material energetics.

3.3. Interfacial engineering

3.3.1. Energy levels

In addition to discovering new and high-performing materials, the field of OSC has also witnessed an increased focus on developing a better understanding of interfacial processes at metal-organic and organic-organic interfaces [206–208]. For device interfaces, the energetics such as the work function [209], IE, and EA of materials govern the electronic transport through the device under operating conditions. In this regard, the frontier molecular orbital energies of organic materials have been extensively studied [210–212]. Though non-trivial, developing an understanding of how the energetics of organic semiconductors evolve when such semiconductors are molecularly mixed in BHJ blends could give further insights into the voltage-limiting and charge generation mechanisms at the donor-acceptor interface in binary and ternary device systems.

3.3.2. Metal-organic interfaces

In this section, we briefly introduce and discuss some basic concepts

of energy level alignment at interfaces in the context of understanding the role of *n*-type and *p*-type charge transport / work function modification layers used in OSC. We refer the readers to thorough reviews on the interfacial energetics, for more details [51,208]. When OSC are fabricated, organic materials are often sequentially deposited over an electrode surface, forming a metal-organic interface [51], which are often not atomically sharp. The underlying electrode surfaces can have native oxide and hydrocarbon contaminations due to ambient exposure, electronically and physically decoupling the continuum of states between the electrode and the organic thin film. When an organic semiconductor is deposited on a conducting electrode, it results in a shift of the vacuum level across the electrode-semiconductor interface and is explained by the integer charge transfer (ICT) model (Fig. 7) [208].

Since π-conjugated materials are electronically soft materials, the addition or removal of electronic charges can induce self-localized polaronic or bipolaronic states within the bandgap, due to lattice deformation. Therefore, the energy needed to remove one electron from the molecule / polymer resulting in a fully relaxed state is called the positive integer charge-transfer state (E_{ICT+}), whereas the energy gained by adding an electron to the molecule/polymer resulting in a fully relaxed state is called the negative integer charge-transfer state (E_{ICT-}).

As per the ICT model, in the case of weakly interacting electrode-organic semiconductor interfaces, the energy level alignment depends on the electrode work function (ϕ_{sub}) relative to the negative (E_{ICT-}) or positive (E_{ICT+}) integer charge transfer energy of the organic material. Three possible scenarios can occur, as shown in Fig. 7: (a) when the substrate work function is larger than the E_{ICT+} of the semiconductor, electrons will flow from the semiconductor to the electrode, and the Fermi level is pinned to the E_{ICT+} of the semiconductor, (b) no Fermi level pinning takes places when the Fermi level of the substrate is between E_{ICT-} and E_{ICT+}, and the resultant work function is substrate-dependent, and (c) when the substrate work function is smaller than the E_{ICT-} of the semiconductor, electrons will flow from the substrate to the semiconductor, and the Fermi level will be pinned to the E_{ICT-} of the semiconductor.

It must be noted that although the validity of the ICT models in limited to weakly interacting interfaces, it explains most of the metal-organic interface phenomenon observed experimentally. Given the importance of interfacial properties in tuning the charge injection barriers across the electrode-semiconducting interface, the ICT model has been widely accepted and used as a guide for the selection of interfacial materials at the interface.

3.3.3. *n-type and p-type interlayers*

In OSC, interlayers are often used between the electrode and the active layer to modify the electrode work function, such that it matches that of the charge carriers resulting in ohmic contact. In OSC, both inorganic and organic materials have been used as *n*-type (between the cathode and active layer) and *p*-type (between the anode and the active layer) interlayer in an energetically favorable manner, enabling unipolar extraction of photo-generated charges and an enhanced charge selectivity [214].

In conventional OSC, PEDOT: PSS is the most commonly used hole transport layer (HTL), which is known to increase the ITO work function as well as reduce the surface roughness. On the other hand, calcium (Ca) or lithium fluoride (LiF) was widely employed as an electron transport layer (ETL) in early days of OSC [215,216], where a thin layer of LiF between the active layer and the metal electrode has been shown to significantly reduce the electrode work function by inducing an energetically favorable dipole, resulting in enhanced electron transport and hence better performing devices. Over the years, various oxide materials have been effectively used as charge transport layers in OSC. For interested readers, the interfacial energetics of metal-organic, and organic-organic interfaces is reviewed in detail [51,206,208,217,218].

Though the interface materials are beneficial in enhancing the device performance, the degradation of devices due to interfacial instability has been an issue. For example, the acidic and hygroscopic nature of PEDOT: PSS is known to etch the ITO electrode, resulting in indium and tin migration in the PEDOT: PSS layer [219] which can be detrimental to the device performance [220]. Similarly, the oxygen-sensitive nature of the low work function materials used at the ETLs has also been shown to be a significant driver of device degradation [221].

Inverted device structures, in which the transparent electrode (ITO in most cases) acts as a cathode and the high work function metal electrode behaves like an anode have been shown to improve the stability of devices [222]. However, with an increased focus on scalable methods of fabricating flexible OSC such as printing, high-temperature processing of thin films of metal oxides [223–227] makes them incompatible with the plastic substrates such as polyethylenenaphthalate (PEN) and polyethyleneterephthalate (PET). This has led to much research activity on the development and use of organic interlayer materials in OSC.

Recently, modified fullerenes [228], polyelectrolytes [229], π-conjugated [230], amine and pyridine based materials [231–234] and small molecules [235] have emerged as work function reducing interlayers, which have been shown to improve the electrical properties and energetics of the active layer and the cathode interface. Zhou et al. demonstrated the use of a simple aliphatic amine-containing polymer ethoxylated poly-ethylenimine (PEIE), to significantly reduce the electrode work function [236]. PEIE has been further demonstrated to effectively modify the work function of PEDOT: PSS to be used as an ETL [160] and is capable of passivating oxide surfaces for enhanced device lifetimes [237]. Zheng et al. have reported a conjugated polymer poly(3, 3′-([(9′,9′-dioctyl-9H,9′H-[2,2′-bifluorene]-9,9-diyl)bis(4,1-phenylene)] bis(oxy))bis(N,N-dimethylpropan-1-amine)) (PFPA-1), which was demonstrated to reduce the surface work function and alter the surface energy of the underlying electrode [238]. Due to the incompatibility of large scale roll-to-roll fabrication technologies with toxic chlorinated solvents commonly used for processing semiconducting organic materials, there has been a prominent shift in focus towards green solvents [239], especially for *n-type* interlayers [240]. In recent years, a range of alcohol processable interlayer materials [241] such as poly [(9,9-bis (3′-(N, N - dimethylamino) propyl)-2,7-fluorene)- alt -2,7-(9, 9–dioctylfluorene) (PFN) [242], poly(4–vinylpyridine) [232], poly[N, N'-bis(3-dimethylaminopropyl)naphthalene-1,4,5,8-bis(dicarboximide)-2,6-diyl]-alt-2,5-thiophene) (PNDIT10N) [231], Phen-NaDPO [235], P2G [23], perylene diimide derivative PDIN and PDINO [243] has been reported.

Though amine-containing interlayers have been demonstrated to work remarkably well with the polymer-fullerene OSC [231], they have not been found to be universally compatible with NFA materials. Hu et al. reported an unfavorable interaction between ITIC and PEIE, where PEIE was found to act as a nucleophile with C=O moiety of ITIC, resulting in altered optical properties of ITIC due to severely impacted intramolecular charge transfer [244]. Xiong et al. has recently proposed the protonation of PEIE using water as a strategy to make it compatible with NFA materials and reported a PCE of 12.5% in PTB7-Th-IEICO-4F OSC using protonated PEIE as an *n-type* interlayer [245]. Recently, You et al. reported an amine-functionalized perylene-diimide (PDINN) interface material which has been demonstrated to be compatible with non-fullerene active layers, and resulted in a high PCE of 17.23% for OSC with PM6: Y6 as the photoactive materials [246].

In OSC, PEDOT: PSS has been one of the most used organic HTLs so far due to its suitable work function, transparency, and good electrical conductivity. PEDOT: PSS is hydrophilic in nature and has mostly been used in conventional device structures. It is not equally well suited to be coated over the hydrophobic active layer in inverted device structures due to poor wetting issues. To overcome this issue, various strategies such as the use of fluorosurfactant [247] and metal oxide-polymer composites [248] have been employed. Recently, Zheng et al. reported a tungsten oxide (WO_x) nanoparticles - PEDOT: PSS composite as a novel HTL in NFA solar cells, which resulted in enhanced PCE of over 14.5% and a remarkable fill factor of 80.79% [249]. However, the acidic nature

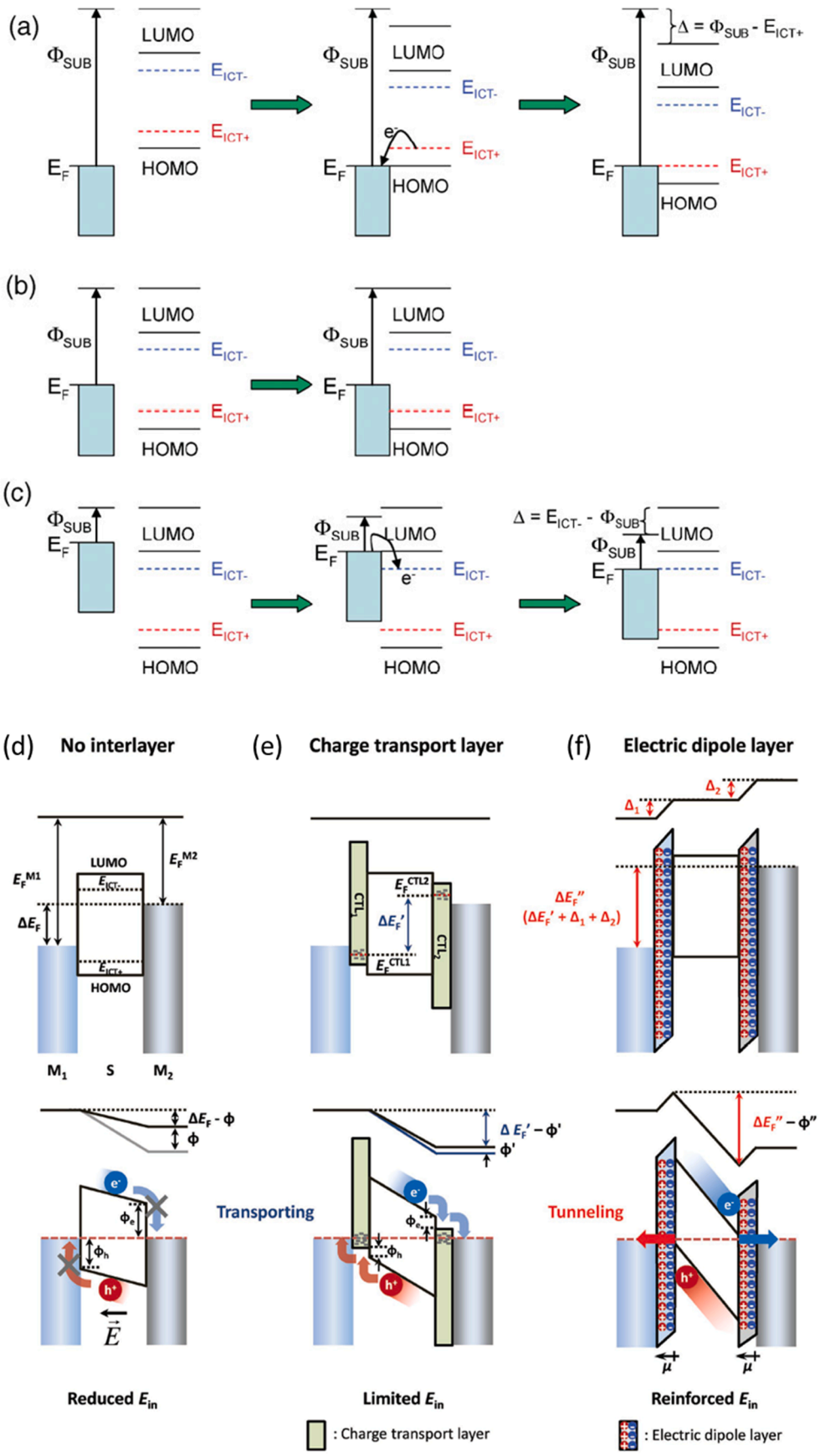

Fig. 7. Schematic representation of the energy-level alignment at the interface of a conducting electrode and a π-conjugated organic molecule or polymer when (a) $\phi_{sub} > E_{ICT+}$, (b) $E_{ICT-} < \phi_{sub} < E_{ICT+}$, and (c) $\phi_{sub} < E_{ICT-}$. (Reprint permission from Ref. [208]) Energy-level diagrams depicting the evolution of built-in internal fields (E_{in}) in metal-semiconductor-metal devices when in open circuit (top) and short-circuit (bottom) with (d) no interlayer, (e) paired CTLs, and (f) EDLs. Δ shows the change in vacuum energy level, Φ is the energetic barrier, and μ is the electric dipole moment. (Reprint permission from Ref. [213]).

of PEDOT: PSS remains an issue for its interactions with the active layer as well as long-term device stability. This has led to research on the development of PH-neutral HTL materials [250]. Cui et al. reported a novel *p*-type conjugated polymer PCP-Na, which was found to be self-doping in nature [251] and with tunable work function controlled by the size of the counter ion used [252]. Lee et al. found that when a pair of strong *p*-type and *n*-type EDLs (*p*-doped PFPs and PFN for example) are used in a device as compared to a pair of traditionally used charge transport layers (CTLs) (PEDOT:PSS and ZnO for instance), the difference in the effective work function of the electrodes is maximized, resulting in a relatively higher internal built-in field (Fig. 7d–f), hence better charge extraction [213].

With the emergence of 2D hybrid materials, transition metal disulfides has also been studied as CTLs in OSC [253]. Lin et al. have reported the use of WS_2 as an efficient HTL in OSC, achieving PCEs of 17% for a ternary BHJ solar cell [254]. The use of self-assembled monolayers (SAM) is another well-established example in the literature which has been used to improve charge injection in organic electronic devices via work function modification of electrodes [255]. Recently, the use of a carbazole-based SAM with phosphonic acid linkers has been demonstrated as an efficient hole selective material in OSC, resulting in 18% PCE [256]. Overall, compared to the emergence of new ETL materials, progress in the development of HTL materials for OSC has been limited and should be the focus of future work, in particular of the *p*-type polyelectrolyte and polymer interlayer materials.

3.4. Morphology and thermal stability

Operational lifetime and thermal stability of OSC are still significant challenges that need to be addressed. In particular, the thermal stability of organic semiconductors and their blends are an essential prerequisite, as OSC are often exposed to increased temperatures [132] during fabrication and operation. Thus, in order to be certified as thermally stable as per the International standard ASTM E 1171 requirements [257], OSC must be stable under repeated thermal treatments to at least 85 °C.

The BHJ active layers of OSC comprise of at least partially immiscible blend of conjugated electronic materials such as polymer-polymer or polymer-small molecules, where the optimal device performance significantly depends on the nanostructure morphology of the active layer. For efficient devices, an intermediate degree of phase separation between the donor and acceptor materials is desirable, which results in a high interfacial area between donor and acceptor domains, enabling efficient charge separation. At the same time, it is also essential to have percolating domains of pure donor and acceptor phases to minimize charge recombination during transport to the electrode [258]. The as-deposited semiconducting material is 'frozen in morphology' and is often not in thermodynamic equilibrium. The morphology of polymeric materials and blends can continue to evolve until the polymer chains relax to their lowest energy conformation, altering the optoelectronic properties.

Over the years, several strategies such as the use of different solvents and additives [259], self-organization of polymer blends [260], modified fullerene derivatives [261], molecular engineering [262], processing treatments [263], and aggregation of polymers [99], have been employed to tune the active layer morphology of both fullerene and non-fullerene solar cells.

However, the exposure of active layers composed of donor-acceptor blends to elevated temperatures higher than the glass transition temperature (T_g) of the BHJ blend components can change the blend morphology and microstructure [264], impacting the device performance. For BHJ blends composed of semi-crystalline donor polymers such as P3HT and $PC_{61}BM$, thermal treatment at temperatures higher than the T_g can improve [265] the device performance, and the crystallization of P3HT has been shown to result in blends with higher thermal stability [266]. However, annealing of BHJ blend films composed of an amorphous donor polymer poly[2, 3-bis-(3-octyloxyphenyl)quinoxaline-5,8-diyl- alt -thiophene-2,5-diyl] (TQ1) and PCBM [95], at temperatures higher than the T_g results in crystallization of PCBM and is detrimental for device performance [267]. For such donor-acceptor systems, the use of a ternary OSC approach incorporating acceptor alloys [268] has been used to prevent large scale crystallization of PCBM. A combination of $PC_{61}BM$ and $PC_{71}BM$ acceptors was shown to hinder large scale crystallization for PCBM due to vetrification [264], whereas pure fullerenes were used as nucleation sites to arrest large scale crystallization in TQ1:PCBM blends when added as a third component (Fig. 8a) [257].

In the case of non-fullerene acceptors such as the widely studied small molecule ITIC, the mechanism of crystallization has been found to be fundamentally different from that in fullerenes. ITIC molecules were found to be fully localized and 'frozen' at temperatures below 0.8 x T_g. However, ITIC has been shown to undergo a glass-crystal transition of low-temperature polymorphs (polymorph I) (Fig. 8b) [269], resulting in the formation of nanoscale crystallites which can arrest further crystal growth up to the high T_g temperature of 180°C, making such materials thermally very stable. Further annealing above T_g but below the melting temperature (T_m) resulted in long-range mass transport leading to the formation of larger polymorph II crystals.

It is clear from these studies that the intrinsic thermal properties, in particular, the T_g of organic semiconductors and their blends, determines the thermal stability of BHJ morphology. To establish design rules for thermally stable OSC, it is therefore imperative to measure the T_g of organic semiconductors precisely [270], and understand the correlation between molecular structures, thermal transition, and stability [271]. An improved understanding of thermomechanical properties of semiconducting polymers and small molecules is becoming urgent with the rapid evolution of printable and wearable electronic devices, which involve a higher degree of mechanical strain and physical deformation [272].

Differential scanning calorimetry (DSC) is one of the most widely applied techniques for determining the T_g of polymers [273]. For organic semiconductors, which are believed to possess a large fraction of the amorphous phase, measuring T_g using DSC is non-trivial. On the other hand, a new class of high performing polymer materials comprising more complex moiety such as naphthalene diimide (NDI), diketopyrrolopyrroles (DPP), isoindigo copolymers and indacenodithiophene-based polymers are known to have disordered aggregate morphology with no long-range order and little or no amorphous phase [274,275] (Fig. 8c–e). Since only the amorphous fraction of the polymer exhibits a glass-transition, measuring a traceable signal in such materials using DSC is often difficult.

This led to the use and development of alternative methods to measure the T_g of conjugated polymers. Variable temperature ellipsometry [277], combinations of UV-vis [278] with optical microscopy [264], plasmonic nano spectroscopy [279], oscillatory shear rheometry [280], and fast scanning calorimetry [281] have been explored. Hopkinson et al. used dynamic mechanical thermal analysis (DMTA) in cantilever bending mode to perform direct measurement of the T_g of P3HT and P3HT:PCBM blends. However, the results had a significant signal-to-noise issues [282]. Schroeder et al. used a polyimide template for measuring thermo-mechanical properties of conjugated polymers using DMTA [283]. Recently, Sharma et al. reported a glass fiber-based DMTA method with high sensitivity to measure not only the T_g of organic semiconductors but also the *sub*-T_g and melt transitions of pure materials [284]. This technique was further applied to a range of polymers, polymer-polymer blends, and polymer-small molecule blends, with high precision [24,269,275,285–289]. Sharma et al. demonstrated that polymers with flexible backbones and large alkyl side chains have two thermal transitions originating from the side chain as well as from the backbone, more resembling classical polymers that have both crystalline and amorphous phases in varying amounts. On the other hand, in the case of polymers with rigid backbone and long branched side chain,

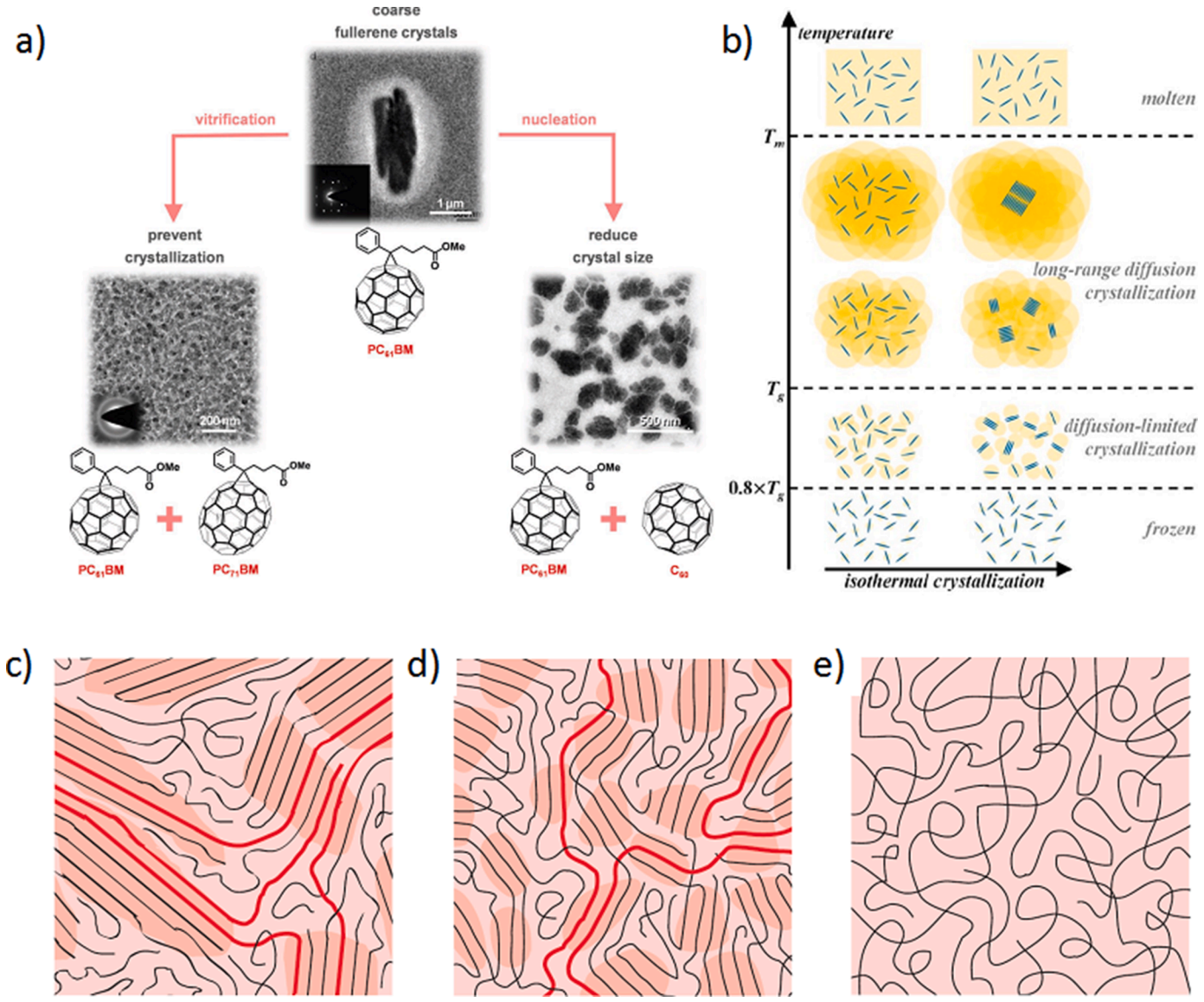

Fig. 8. (a) Vitrification using $PC_{71}BM$ and nucleation using C_{60} are presented as two different methods to avoid the formation of large fullerene crystals otherwise found in TQ1: PC61BM binary blends when exposed to elevated temperatures (Reprint permission from Refs. [257,264,268,276]) (b) depiction of isothermal crystallization of ITIC molecules at different temperatures. ITIC molecules are depicted in blue, whereas concentric yellow circles show the accessible volume. (Reprint permission from Ref. [269]) Schematic depiction of the semiconducting polymer thin film with different microstructures: (c) semicrystalline polymer film with ordered domains (darker shadowed areas) interconnected by long polymer chains (red lines), (d) polymer films with short-range/disordered aggregate along with some amorphous phase, represented by spaghetti-like structures, and (e) a fully amorphous polymer film. (Reprint permission from Ref. [274]) (For interpretation of the references to color in this figure legend, the reader is referred to the web version of this article.).

the thermal transitions from the side chain can be the most dominant and the relaxation of the backbone is seldom detected, implying almost no amorphous phase in such materials [275].

3.5. Towards flexible OPVs: processing and scalability

3.5.1. Reel-to-reel compatible fabrication

With PCE of single-junction OSC now approaching 20% and the cost of industrially produced modules estimated to be under €10 m^{-2} [290], OSC technology seems commercially more relevant than ever before. However, the upscaling of OSC technology currently faces several challenges. Success in transitioning this technology from the lab-scale to an industrial scale (Fig. 9) would largely depend on the ability to produce cost-effective and stable devices using industrially scalable methods [291] and compatible materials [292]. Research has intensified on the development of industrially relevant fabrication methods for OSC [293] to realize the low-cost potential and high power-to-weight ratio that this technology promises. This has resulted in various attempts to apply existing reel-to-reel compatible fabrication and coating technologies such as slot-die coating [294] screen printing [295], knife-over-edge coating [296], aerosol jet printing [297], brush painting [298], thin-film transfer printing [299], inkjet printing [159], electrospraying [300], blade coating [301], and lamination [302] to fabricate OSC. Such reel-to-reel compatible fabrication methods for manufacturing OSC [296] has the potential to enable cost-effective large-area production of OSC [303]. However, continuing research efforts are needed to reduce the scaling problem between the lab-scale device efficiencies and those achieved using scalable methods [304] since the choice of coating method can have a significant impact on the resultant morphology and device behavior [305].

Fabrication methods such as lamination [302], which involves sandwiching various material layers by lamination rather than

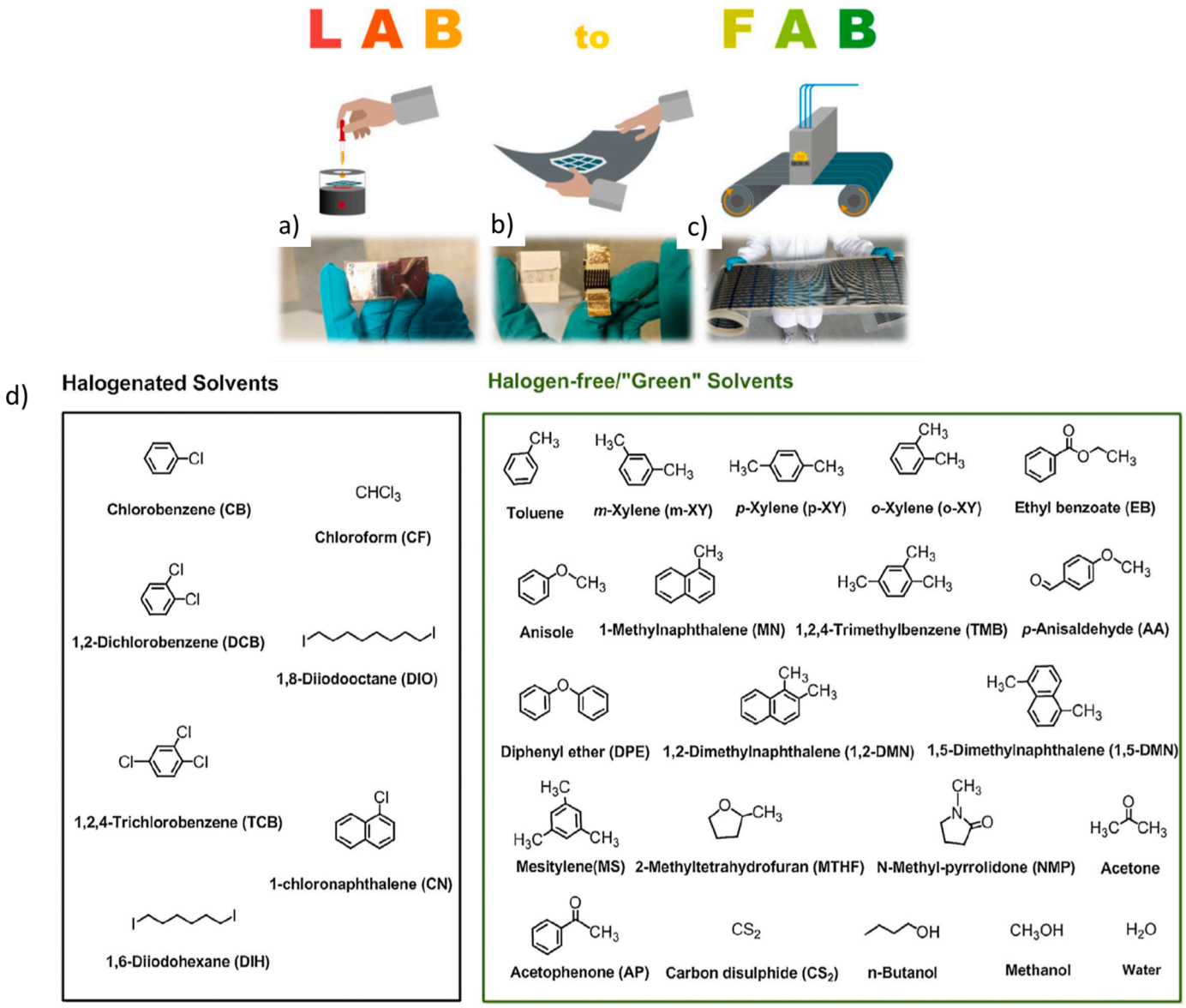

Fig. 9. Schematic showing the transitioning of the OSC fabrication from (a) lab-scale using non-scalable methods, to (b) flexible devices fabricated in the lab, and (c) scalable manufacturing of flexible OSC using reel-to-reel methods. (Reprint permission from Ref. [325]) (d) Chemical structures of halogenated (left) and non-halogen-free (right) solvents utilized for the processing of OSC. (Reprint permission from Ref. [326]).

sequential deposition, have received renewed research attention in the past few years. Lamination is a promising technique as it is not only compatible with reel-to-reel processing, but it also offers greater control over the optimization of each material layer. Laminated devices are self-encapsulated, and thus by a selection of an appropriate barrier substrate, an additional encapsulation step [306] could potentially be avoided, making the entire fabrication process a relatively less sophisticated and cost-effective method. A laminated OSC with a polymer-polymer bi-layer structure was reported by Granstrom et al. in 1998 [307]. Since then, not much research was conducted in this field until 2008 when Yang's group published an organic heterojunction solar cell fabricated by lamination [308]. As the device performance of OSC is improving rapidly, research groups around the world have recently focused on various lamination methods to fabricate OSC. Bergqvist et al. in 2018 reported flexible semitransparent ITO free polymer-PCBM solar cells utilizing slot-die coated PEDOT: PSS electrodes, and achieved a maximum PCE of over 4% [160].

3.5.2. *Industrially relevant non-halogenated solvents*

Though the field of OSC has witnessed tremendous progress in the development of solution-processed scalable methods of fabricating flexible devices [309], the commonly used halogenated solvents are toxic and incompatible with scalable industrial fabrication, and counter to the environmentally friendly nature of OSC technology [310,311]. This has led to a push towards green solvent (Fig. 9d) processing of OSC [312].

Research efforts have been multidimensional to process existing active layer materials via non-halogenated solvents [313], design and development of donor [15], acceptor and interlayer materials that can be processed using environmentally benign solvents [230,234, 314–317], and the use of water or alcohol-based organic nanoparticle suspensions as active layer inks in OSC. Recently, several non-halogenated solvents [318] including anisole [319], 2-methyl-tetrahydrofuran (MeTHF) [320], o-xylene [321], o-methylanisole [322], 1,2, 4-trimethylbenzene (TMB) [323], and mesitylene [324], have been successfully used to fabricate fullerene and non-fullerene OSC. The use of non-halogenated solvents for depositing the active layer has, in

several cases, been shown to enable devices with better PCE and stability than their counterparts processed using chlorinated solvents [325]. However, the use of non-halogenated organic solvents is cost-ineffective due to their high cost and the required solvent recovery system, and their large-scale use can still be a risk to the ecosystem. More work needs to be done towards the use of sustainable and economically viable and industrially relevant green solvents, which has the potential to truly revolutionize the scalability of OSCs.

3.5.3. Solar paints

High performing OSC fabricated using water or alcohol-based solar inks have the potential to be one of the ideal ways to achieve cost-efficient, scalable and eco-friendly processing of OSC. Emerging solar paint or colloidal nanoparticle ink technology is a promising method to realize such devices [327], circumventing the complexities of designing water or alcohol processable materials. For OSC applications, the semiconducting nanoparticles can either be produced using a mini-emulsion method [328] or a precipitation method [327]. While the mini-emulsion method results in a more stable particle suspension with the help of surfactants [329], this method is known to occur in nanoparticles with a core-shell structure [330], in contrast to the thoroughly blended nanoparticle morphology formed using the precipitation method [331]. Xie et al. demonstrated a robot-based optimization procedure of P3HT:ICBA nanoparticles prepared using the precipitation method, and the resulting OSC exhibited an impressive PCE of 4.5% for an alcohol-based suspension [332]. For PBDTTPD:$PC_{71}BM$ system, D'Olieslaeger et al. used the mini-emulsion method and reported a PCE of 3.8% [333].

Due to the reproducibility of the mini-emulsion method in achieving stable nanoparticle suspensions, this method has been applied to a range of polymer-fullerene and polymer-NFA systems including TQ1:$PC_{71}BM$ [334], PTNT:$PC_{71}BM$ [286], P3HT:$IC_{61}BA$ [335], P3HT: $PC_{71}BM$ [336], PBDTTPD:$PC_{71}BM$ [333], PCDTBT:$PC_{71}BM$ [337], PDPP5T:PCBM [330], PTB7-T H:EH-IDTBR [338]. However, the PCEs of most of these systems still fall short compared to their optimized BHJ counterparts, with non-ideal nanoparticle morphology and the use of insulating surfactant being the two primary performance limiting factors. While an excess of surfactant has been demonstrated to be detrimental for devices [330], Xie et al. have reported the use of poloxamer as a temperature modulated stabilizer and reported a PCE of 5.3% and 7.5% for P3HT: o-IDTBR and PBQ-QF: ITIC nanoparticle solar cells, respectively [339]. On the other hand, the core-shell structure of nanoparticles results in weak exciton dissociation and enhanced bimolecular charge recombination, resulting in lower photo-generated currents, smaller fill factors and thus low PCEs [330].

In recent years a range of strategies [340] such as the use of polymers with different molecular weight [341], vacuum-assisted mini-emulsion methods [335], the use of high boiling point solvent for particle synthesis [337], and thermal annealing of nanoparticles close to the glass transition temperature of the polymer [334], has been applied to tune the donor-acceptor morphology within the nanoparticles. Holmes et al. used thermal annealing to engineer an intermixed three-phase microstructure (Fig. 10) from pristine P3HT and PCBM nanoparticles, which resulted in a significant improvement in the exciton dissociation efficiency [285], highlighting the importance of the interconnecting pathways between the donor and acceptor phases. Future work on nanoparticle solar cells should thus be focused on synthesizing smaller nanoparticles with a narrow size distribution, as well as on developing alternative methods of stabilizing nanoparticle suspensions.

3.5.4. Flexible/ultra-thin OSCs for wearable electronics

As we embark upon the era of IoT, flexible and lightweight OSC offer a promising platform that could be used as a portable power source for rapidly growing flexible and wearable electronic devices [342], including biomedical and sensing applications [343]. Key aspects to this are the use of (a) flexible bottom and top electrodes with high bending durability, and (b) thin and mechanically flexible substrates. ITO is one of the most commonly used and commercially available transparent electrodes, even though its brittle nature and high-temperature processing make it not so compatible with plastic substrates. This has led to the development of a range of flexible transparent electrodes based on conducting polymers, silver nanowires, nanocomposites, ultra-thin metal films and carbon-based materials such as graphene and carbon nanotubes, as also discussed in Section 3.1.4 [344]. Here we discuss selected recent examples of the development of flexible (> 10 μm) and

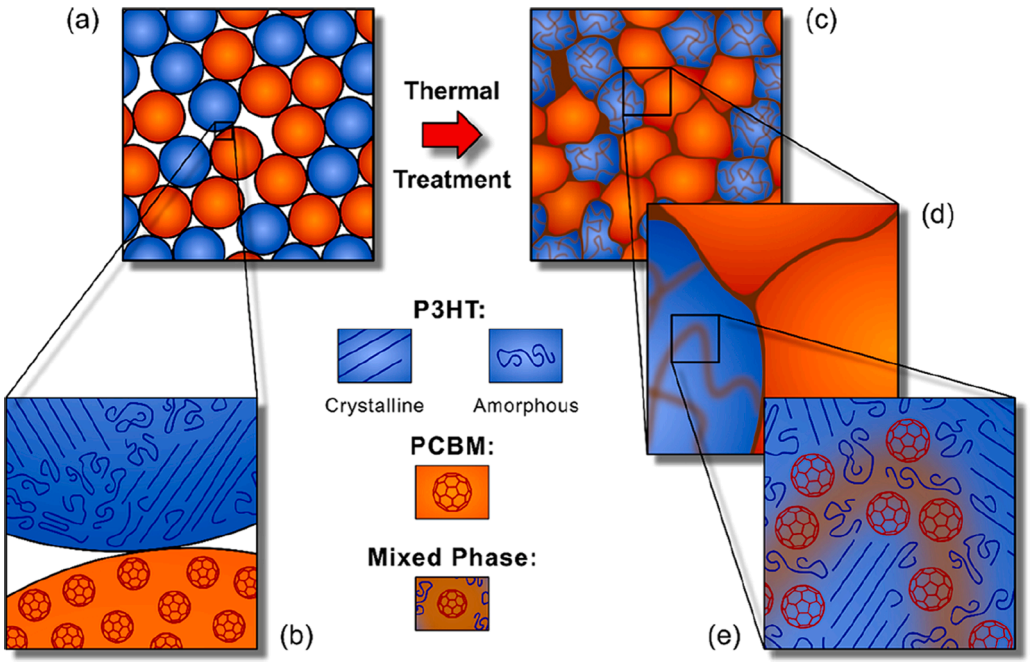

Fig. 10. Morphology evolution of thin films composed of P3HT and PCBM nanoparticles as a result of thermal treatment: (a) film with two-phase microstructure, (b) composition of two different phases, highlighting the presence of crystalline as well as amorphous P3HT subdomains in the P3HT phase, (c) formation of a continuous film when nanoparticles are sintered, (d, e) an intermixed phase is formed. (Reprint permission from Ref. [285]).

ultra-thin (1–10 μm) OSC, and their demonstrated applications.

A large part of the research on flexible OSC has employed substrates (~ 100–300 μm) based on plastic materials such as PET and PEN, which enabled scalable manufacturing of flexible OSC [345,346]. However, due to the relatively low T_g of PET and PEN as compared to glass substrates, these devices are prone to low thermal stability, in addition to being sensitive towards mechanical deformation [347]. In the last few years, paper [348], silk fibroin [349], and fabric [350] have also been demonstrated as non-plastic alternative substrates for flexible OSC. Recently, Wang et al. used flexible glass substrates (100 μm thick) to fabricate ITO-free OSC based on a BQR: $PC_{71}BM$ donor-acceptor system and achieved a PCE of 8% [351]. Nevertheless, Xiong et al. has reported flexible OSC fabricated on an ITO coated PET substrate, using water processable PEIE as an ETL and PTB7-Th: IEICO-4F as the donor-acceptor system, demonstrating a high PCE of 12.5%. The cell was found to be reasonably stable to mechanical bending and retained 90% of its initial PCE after 2000 cycles of bending with a radius of 5 mm [245]. Yan et al. used a ternary approach to fabricate flexible OSC on a PET substrate using PEDOT: PSS as the transparent electrode and PM6: Y6: $PC_{71}BM$ as the BHJ active layer. The flexible ternary device achieved a PCE of over 14%, an impressive FF of > 72%, and retained over 90% PCE after 500 cycles of bending with a small diameter of 2 mm [352].

Low-weight and conformability is the key to realize the full potential of OSC, for example in providing self-powering functionality to skin-interfaced health monitoring devices. For these devices to adhere conformably to skin or textiles [353], an ultra-thin flexible substrate, with a thickness of ~ < 10 μm is preferred. PET [354], and various biocompatible materials including cellulose [355], PDMS, ecoflex, solaris, silbione and parylene have been used as flexible substrates for organic electronic devices [343].

Kaltenbrunner et al. in 2012 reported a flexible and low-weight OSC on an ultra-thin PET foil substrate with a thickness of ~ 1.4 μm (Fig. 11a), where high conductivity PEDOT: PSS was used as transparent electrode and P3HT:PCBM as the BHJ blend. These devices resulted in a PCE of 4%, and the device was found to be mechanically resilient to up to 70% compression and 50% stretching, with minimal loss in the performance [356].

Jean et al. used a vapor-deposited ultra-thin parylene substrate coated with indium zinc oxide films as the transparent electrode, to fabricate flexible and ultra-light (3.6 g m^{-2}) bilayer OSC [359]. The photoactive layer in these devices was deposited by evaporating DBP and C_{60} as the donor-acceptor system, resulting in a PCE of 2.2%. Though modest, this PCE corresponds to a weight specific power of more than 6 W g^{-1}, demonstrating the potential of this technology as a

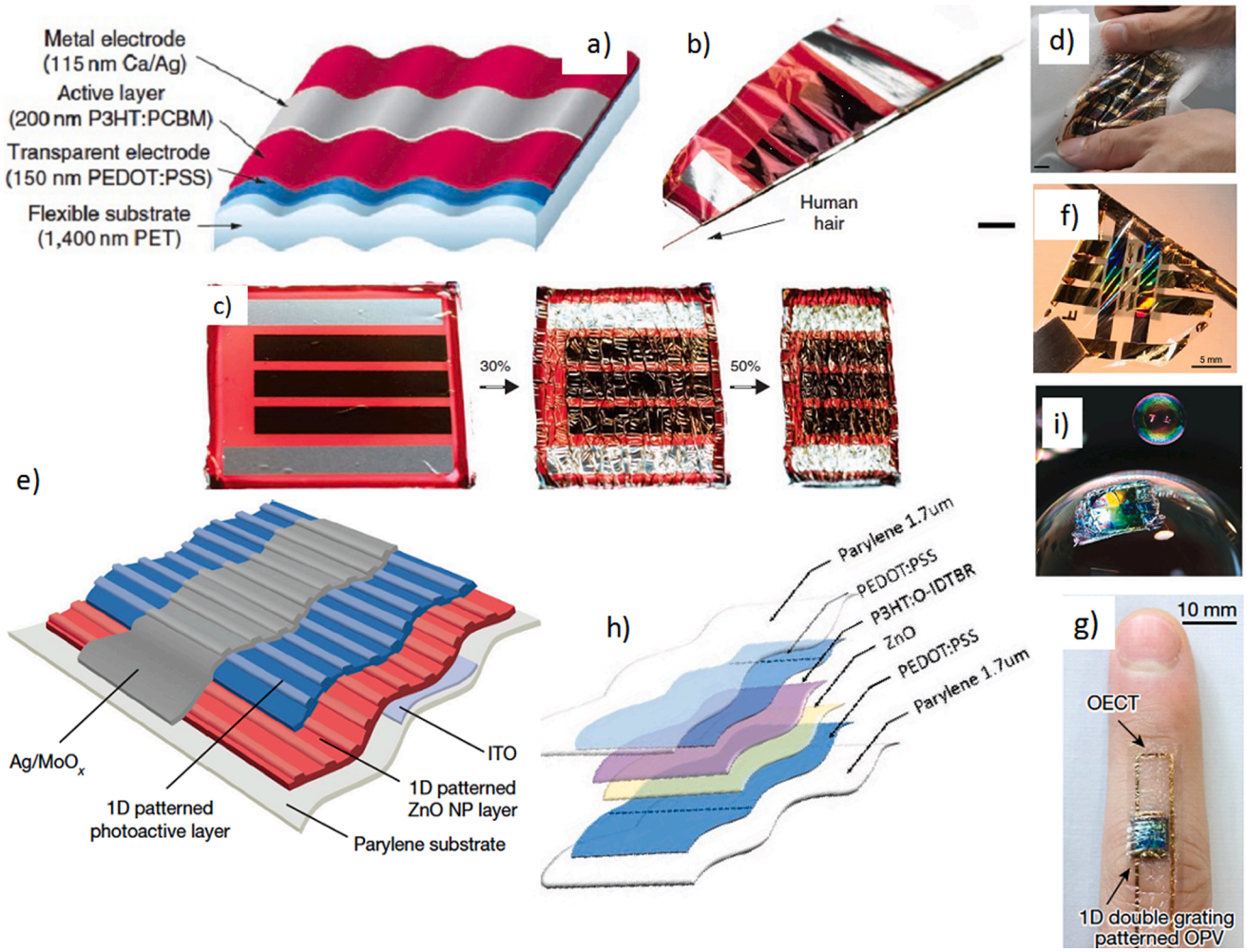

Fig. 11. (a) Schematic of an OSC fabricated on an ultra-thin PET substrate. (b) Demonstration of the ability to bend flexible OSC around a human hair. (c) Demonstrated stretchability of OSC when attached to an elastomer under the varying amount of compression. (Reprint permission from Ref. [356]) (d) Image depicting an ultra-flexible and washable OSC. (Reprint permission from Ref. [357]) (e) Schematic representation of a flexible OSC structure with 1D gratings. (f) Image of an ultra-thin OSC wrapped around a rod. (g) Image showing a flexible OSC integrated with OECT in a wearable sensor. (Reprint permission from Ref. [358]) (h) Schematic of an ink-jet printed flexible and ultra-light OSC device structure. (i) Image of the ultra-light OSC inside a soap bubble. (Reprint permission from Ref. [159]).

portable power-source for wearable electronics. Subsequent progress was made in the development of ultra-thin OSC, when Jinno et al. reported a highly flexible and stretchable OSC fabricated on a 1 μm thin parylene substrate, incorporating an air-stable PNTz4T: $PC_{71}BM$ active layer resulting in a PCE of 7.9% and a high FF of over 70% (Fig. 11d) [357]. Besides being conformal to human skin and textile, the encapsulation of devices with an acrylic elastomer (3M VHB Y-4905) provided mechanical stretchability while simultaneously making them water stable. OSC encapsulated by the elastomer on both sides retained 80% of their PCE after 100 min of water exposure, and 20 cycles of being mechanically compressed by 52%. In another work, Park et al. have designed an ultra-thin OSC (3μm with encapsulation) on an ITO coated parylene substrate and used this as a power source for organic electrochemical transistors (OECT) as a sensor for detecting cardiac signals (Fig. 11e–g) [358]. In this study, ZnO, and PBDTTT-OFT:$PC_{71}BM$ comprised the ETL and BHJ active layer respectively, and a 1D grating pattern was formed on both these layers using sequential molding with a PDMS mold to maximize optical gains. This resulted in devices with PCE of 10.49%, corresponding to a weight-specific power of 11.46 W g^{-1}. Jakešová et al. later utilized parylene based ultra-thin H_2P_c and PTCDI bilayer OSC, which gave voltages of 2.5–4.5 V when connected in series or in tandem, to power the high resistance electrophoretic ion pumps [360].

Xu et al. reported the use of a transparent polyamide as the ultra-thin polymer substrate for flexible OSC. Besides high transparency, the use of polyamide is of particular interest due to its high T_g of 265°C, which makes it compatible with high-temperature fabrication processes. OSC comprising a BHJ layer of PBDTTT: $PC_{71}BM$ and fabricated on a 1.3 μm polyamide substrate were highly flexible with a bending radius of 10 μm and resulted in high PCE of 10% [361]. High thermal stability of the active layer, as well as that of the polyamide substrate, enabled the integration of the ultra-flexible OSC to textile using a hot-melt process at 120°C, with no significant deterioration observed in the device performance. Koo et al. has further utilized thin films of polyimide as a transfer carrier and substrate for graphene electrodes, achieving high transmittance of over 92% [347]. Flexible polyimide-based graphene, when used as a transparent electrode in OSC based on PM6: Y6 photoactive layer, resulted in a high PCE of 15.2% and exceptional mechanical stability retaining over 90% of PCE after 1000 bending cycles at a bending radius of 2 mm. In another work, a transparent and conformal electrode stack based on PPZA (polyimide, silver nanowires, ZnO, and polystyrene spheres) was used to fabricate flexible ternary OSC consisting of PM6: N3:$PC_{71}BM$ as the photoactive layer [362]. These devices resulted in a high PCE of 16.1% and retained over 85% of the performance when repeatedly bent with a small radius of 1 mm, over 5000 cycles. Recently, Bihar et al. designed an inkjet-printed, low-weight, and conformal OSC on ultra-thin (1.7 μm) parylene substrate (Fig. 11i) [159]. In this study, the authors utilized GOPS as a cross-linking agent for PEDOT: PSS, which was used as the transparent electrode. The photo-active layer composed of P3HT: O-IDTBR and fully inkjet-printed ultra-thin OSC resulted in a PCE of 3.6%, and importantly encapsulated devices were found to be stable in aqueous environments, which is imperative for biological and skin-interfaced applications.

The above discussed works successfully demonstrate the feasibility of producing ultra-thin and lightweight OSC with efficiencies comparable to their ITO/glass counterparts. The compatibility of scalable methods such as ink-jet printing for manufacturing ultra-thin OSC devices further makes it industrially relevant, and such flexible and light weight OSC have immense potential for applications in wearable electronics.

4. Organic thermoelectric (OTE) materials & generators (OTEGs)

Organic materials provide a fertile platform for next generation flexible TEGs due to several notable characteristics, particularly their intrinsic low thermal conductivity [33]. Different types of organic TE materials such as coordination polymers, conducting polymers, small molecules, single molecules, carbon-based materials, and their composites, have been developed to obtain high performance flexible and wearable TEGs. The recent progress of ZT at 300K for *p*-and *n*-type OTE materials is shown in Fig. 12a, b. Furthermore, a development timeline for OTEGs and their applications is illustrated in Fig. 12c. In the following sections these organic TE materials are classified and analyzed.

4.1. p-Type organic TE materials

4.1.1. Conducting polymers

Conducting polymers are a major class of organic TE materials. They have many advantages such as high solubility in various solvents, tunability of electrical and thermal properties via molecular doping, and a variety of molecules that can be used for their doping. The presence of both amorphous and crystalline phases in the structure of a typical conducting polymer makes it difficult to precisely control its structural properties [384]. The π-conjugated units in the backbone of these polymers determine their electronic properties and the miscibility of dopants with the polymers [385]. Oxidation and reduction of conjugated polymers result in *p*-type and *n*-type doping through the removal and addition of π-orbital electrons, respectively. During oxidation, an electron is removed from the backbone of a polymer and a polaron is created (a quasiparticle with a positive charge). Subsequent oxidation (further doping) by removing another electron results in a bipolaron with a double positive charge (Fig. 13). Increasing the doping level in a conjugated polymer can transform bipolaron levels to a bipolaron band and reduce the electronic band gap [386].

Polyvinylidene fluoride (PVDF), polyacetylene, polypyrrole, poly (3,4-ethylenedioxythiophene), polythiophene, poly(2,7-carbazolylene vinylene), poly(3-octylthiophene), poly(3-hexylthiophene), poly(aniline), and poly(3-methylthiophene) are some of the well-established conducting polymers as TE materials. Their chemical structures are shown in Fig. 14.

A derivative of polythiophene, known as poly(3,4-ethylenedi oxythiophene) or PEDOT, possesses good chemical and physical stability, biocompatibility, transparency, and adjustable electrical properties. The solubility of PEDOT in water is very low, but compounding PEDOT and polystyrenesulphonic (PSS) makes it dispersible in water [388]. PEDOT:PSS is a well-known *p*-type conducting polymer whose charge carrier concentration can be controlled by various doping processes [389]. For instance, treatment of PEDOT:PSS with H_2SO_4 resulted in a high electrical conductivity of 4380 S cm^{-1} due to the creation of a structure with highly ordered chains [390]. Also, a comparison of PEDOT doping with ClO_4^-, PF_6^- and bis (trifuoromethylsulfonyl)imide (BTFMSI) has revealed BTFMSI to be the most efficient for improving the TE properties, resulting in a power factor (PF) of 147 μW $m^{-1}K^{-2}$, corresponding to a three-fold increase of electrical conductivity while keeping the Seebeck coefficient in the same order of magnitude [391]. Improvement was also reported in the case of PEDOT:PSS treated with a dielectric solvent, dimethyl sulfoxide (DMSO). For example, Scholdt et.al. [392] reported that the treatment of PEDOT:PSS (both PH750 and PH500 types) with 5 vol% DMSO resulted in a ZT of 9.2×10^{-3} at 300 K. In another report, Chu et al. [393] used formic acid, methanol, polyethylene glycol, and ethylene glycol (EG) as secondary dopants to PEDOT:PSS which resulted in electrical conductivities of 1900, 1300, 800, 640 S cm^{-1}, respectively, whereas the Seebeck coefficient decreased to ~20 μV K^{-1}. A ZT of 0.32 was achieved for the PEDOT:PSS treated with formic acid. These enhancements were attributed to the improvement of the electrical conductivity by increasing the charge carrier mobility, more ordered PEDOT: PSS chains, and keeping the oxidation level of PEDOT constant [393].

Bubnova et al. [364] reported that the TE properties of PEDOT-Tos can be regulated by the alteration of the oxidation level through exposure to tetrakis(dimethylamino)ethylene (TDAE). In this case, a PF of 324 μW $m^{-1}K^{-2}$ and a ZT of 0.25 were achieved at room temperature (RT) at an oxidation level of 22%. Following these results, as a proof of

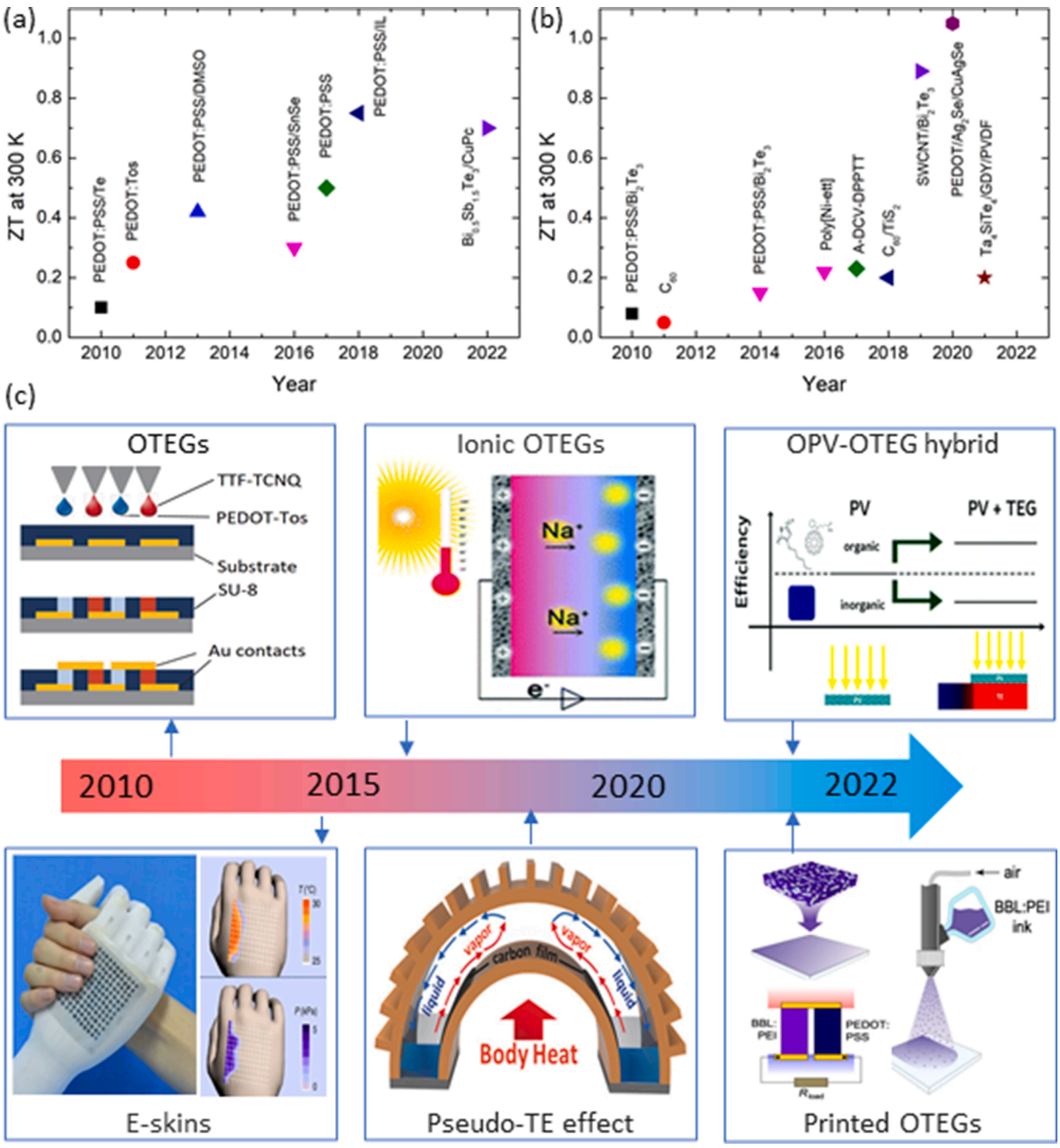

Fig. 12. Progress of ZT at 300 K over time for OTE materials, (a) *p*-type (PEDOT:PSS/Te (Reprint permission from Ref. [363]), PEDOT:Tos (Reprint permission from Ref. [364]), PEDOT:PSS/DMSO (Reprint permission from Ref. [365]), PEDOT:PSS/SnSe (Reprint permission from Ref. [366]), PEDOT:PSS (Reprint permission from Ref. [367]), PEDOT:PSS/IL (Reprint permission from Ref. [368]), $Bi_{0.5}Sb_{1.5}Te_3$/CuPc (Reprint permission from Ref. [369])). (b) *n*-type (PEDOT:PSS/Bi_2Te_3 (Reprint permission from Ref. [370]), C_{60} (Reprint permission from Ref. [371]), PEDOT:PSS/Bi_2Te_3 (Reprint permission from Ref. [372]), poly(Ni-ett) (Reprint permission from Ref. [373]), A-DCV-DPPTT (Reprint permission from Ref. [374]), C_{60}/TiS_2 (Reprint permission from Ref. [375]), SWCNT/Bi_2Te_3 (Reprint permission from Ref. [376]), PEDOT/Ag_2Se/CuAgSe (Reprint permission from Ref. [377]), Ta_4SiTe_4/GDY/PVDF (Reprint permission from Ref. [378])). (c) Development roadmap for OTEGs and their applications over time (OTEG (Reprint permission from Ref. [364]), E-skins (Reprint permission from Ref. [379]), ionic OTEGs (Reprint permission from Ref. [380]), Pseudo-TE technology (Reprint permission from Ref. [381]), OPV-OTEG hybrid (Reprint permission from Ref. [382]), Printed OTEGs (Reprint permission from Ref. [383])).

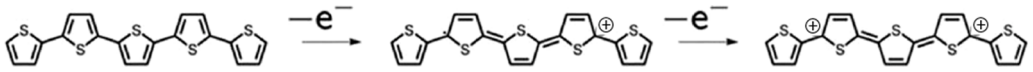

Fig. 13. The oxidation process of an oligothiophene (left structure): the creation of a polaron (middle structure), and a bipolaron (right structure). (Reprint permission from Ref. [386]).

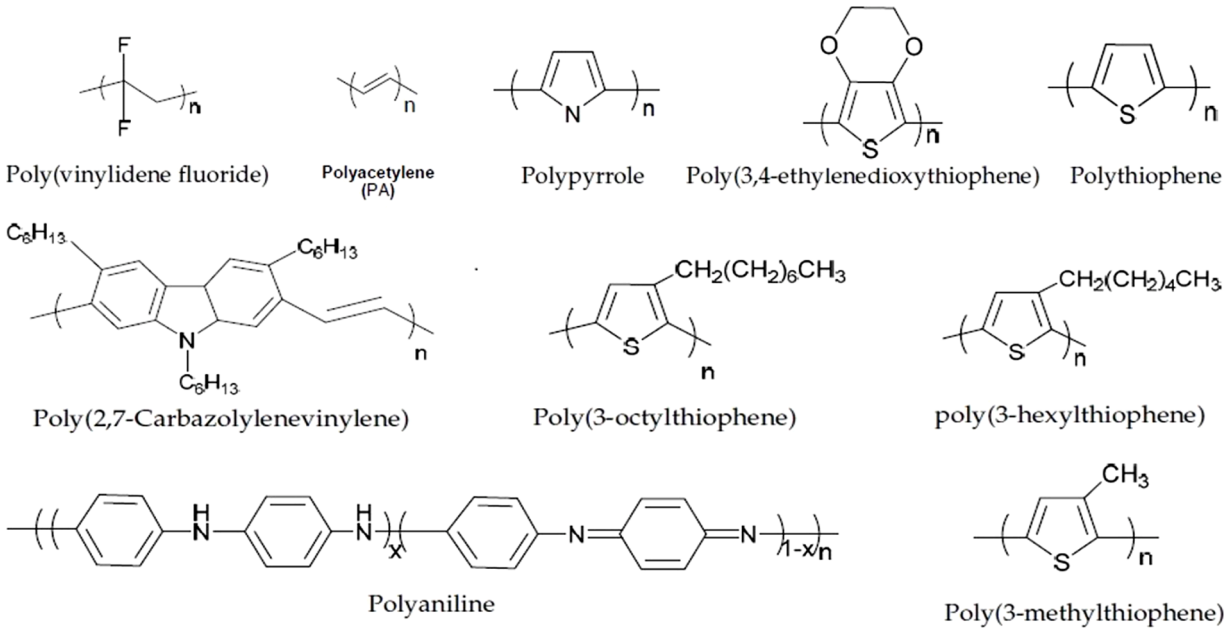

Fig. 14. Chemical structures of the state-of-the-art conducting polymers as organic TE materials. (Reprint permission from Ref. [387]).

concept, a TE unicouple made of PEDOT-Tos (*p*-type leg), carbon black (*n*-type leg), and gold (electrode) was fabricated by ink-jet printing. The fabricated TE unicouple, when connected to a load with an electrical resistance of 39 Ω, showed an output power of 1.13 nW at $\Delta T = 1.5$ °C after exposure to TDAE for 10 min [364]. Since PSS is hydrophilic and PEDOT is hydrophobic in nature, a hydrophilic solvent can selectively de-dope the PSS and can optimize the TE properties of PEDOT:PSS. Inspired by this, Kim et al. [365] de-doped the mixture of PEDOT:PSS and DMSO with ethylene glycol (EG) for 100 min, resulting in a ZT of 0.42 at 300 K due to a simultaneous increase of the Seebeck coefficient and the electrical conductivity, and a reduction of the thermal conductivity [365]. These enhancements originated from the de-doping and formation of highly ordered structures in PEDOT:PSS through the EG and DMSO treatments. The former effect raises the polaron or bipolaron concentration while the latter effect increases the mobility of charge carriers [394]. Likewise, PF of 7.26 μW $m^{-1}K^{-2}$ and 22.28 μW $m^{-1}K^{-2}$ were achieved in PEDOT:PSS treated by sorbitol and TDAE, respectively [395]. In the case of the TDAE treated PEDOT:PSS, a ZT of 0.026 at 300 K was obtained [395]. To avoid using common and toxic organic solvents for the de-doping process, new "green" solvents such as deep eutectic solvents (DES) have been used to treat PEDOT:PSS. For instance, a mixture of choline chloride and EG increased the PF of PEDOT:PSS to 24.08 μW $m^{-1}K^{-2}$ [396].

As stated above, the secondary doping process leads to improved electrical conductivity due to a morphological change in the PEDOT:PSS structure while the de-doping process significantly increases the Seebeck coefficient due to a change in the oxidation level of PEDOT (Fig. 15a, b). A sequential treatment that includes both secondary doping and de-doping processes has been suggested to increase the electrical conductivity and Seebeck coefficient simultaneously to obtain maximum PF. For instance, H_2SO_4 and NaOH were used to treat PEDOT:PSS films through the sequential treatment, which resulted in a Seebeck coefficient of 39.2 μV K^{-1}, an electrical conductivity of 2170 S cm^{-1}, and a PF of 334 μW $m^{-1}K^{-2}$ [367]. The significant improvements observed were due to a sequential treatment which contributed to an increase in charge carrier mobility through the conformational change of PEDOT:PSS and the alteration of carrier concentration by adjusting the oxidation level of PEDOT. Moreover, it has been recently reported that a combination of solution-shearing deposition and directionally applied solvent treatments can drastically improve the TE properties of PEDOT:PSS thin films to obtain a high power factor of 800 μW $m^{-1}K^{-2}$ [397]. This significant improvement resulted from the structural alignment of PEDOT chains and larger-sized domains. A schematic of the sheared deposition of PEDOT:PSS and a postdeposition sheared solvent treatment are illustrated in Fig. 15c, d.

Another strategy to enhance the TE properties of organic semiconductors is the fabrication of a hetero-structure of conducting polymer and other materials based on the concept of interfacial energy filtering. As an example, the hetero-structures of several ionic liquids (ILs) such as 1-ethyl-3-methylimidazolium tetrafluoroborate, 1-ethyl-3-methylimidazolium bis(trifluoromethylsulfonyl)imide and 1-ethyl-3-methylimidazolium dicyanamide) and PEDOT:PSS were fabricated that significantly enhanced their TE properties. A PF of 754 μW $m^{-1}K^{-2}$ and a ZT of 0.75 at 300 K were obtained for the 1-ethyl-3-methylimidazolium dicyanamide/PEDOT:PSS hetero-structure [368]. These results are comparable to the well-established TE properties of Bi_2Te_3 at RT. Moreover, the authors suggested that this significant enhancement originated from the surface energy filtering of low energy charge carriers through the accumulated ions of IL on top of the PEDOT:PSS layer (Fig. 15e). Characterization of the open circuit voltage (V_{OC}) vs. time, and electrical conductivity and Seebeck coefficient vs. relative humidity in IL/PEDOT:PSS hetero-structures revealed that the nature of conduction was purely electronic in these systems, with no evidence of ionic conduction.

The TE properties of PEDOT:PSS can also be improved through the fabrication of one-dimensional fibers for increasing the chain packing order and the proportions of quinoid PEDOT by the spatial confinement effect originating from the specific fiber configuration. As shown in Fig. 15f, PEDOT:PSS fibers were constructed through a continuous wet-spinning process followed by sulfuric acid treatment [398]. The optimized fibers resulted in an electrical conductivity of 4029.5 S cm^{-1}, a Seebeck coefficient of 19.2 μV K^{-1}, and a power factor of 147.8 μW $m^{-1}K^{-2}$. The obtained PF was 15 times higher than that of a PEDOT:PSS film fabricated at the same condition. These results were due to the high order of polymer chain conformations and chain stacking structures. Similarly, as illustrated in Fig. 15g, PEDOT:Nafion fibers were fabricated through melt extrusion followed by fiber spinning [399]. The fabricated melt-spun fibers showed high flexibility that kept their conductivity of about 3 S cm^{-1} upon stretching to 100% elongation.

Moreover, lightweight, elastic, and conformal TEGs are needed for wearable applications. Although PEDOT:PSS has shown promising TE

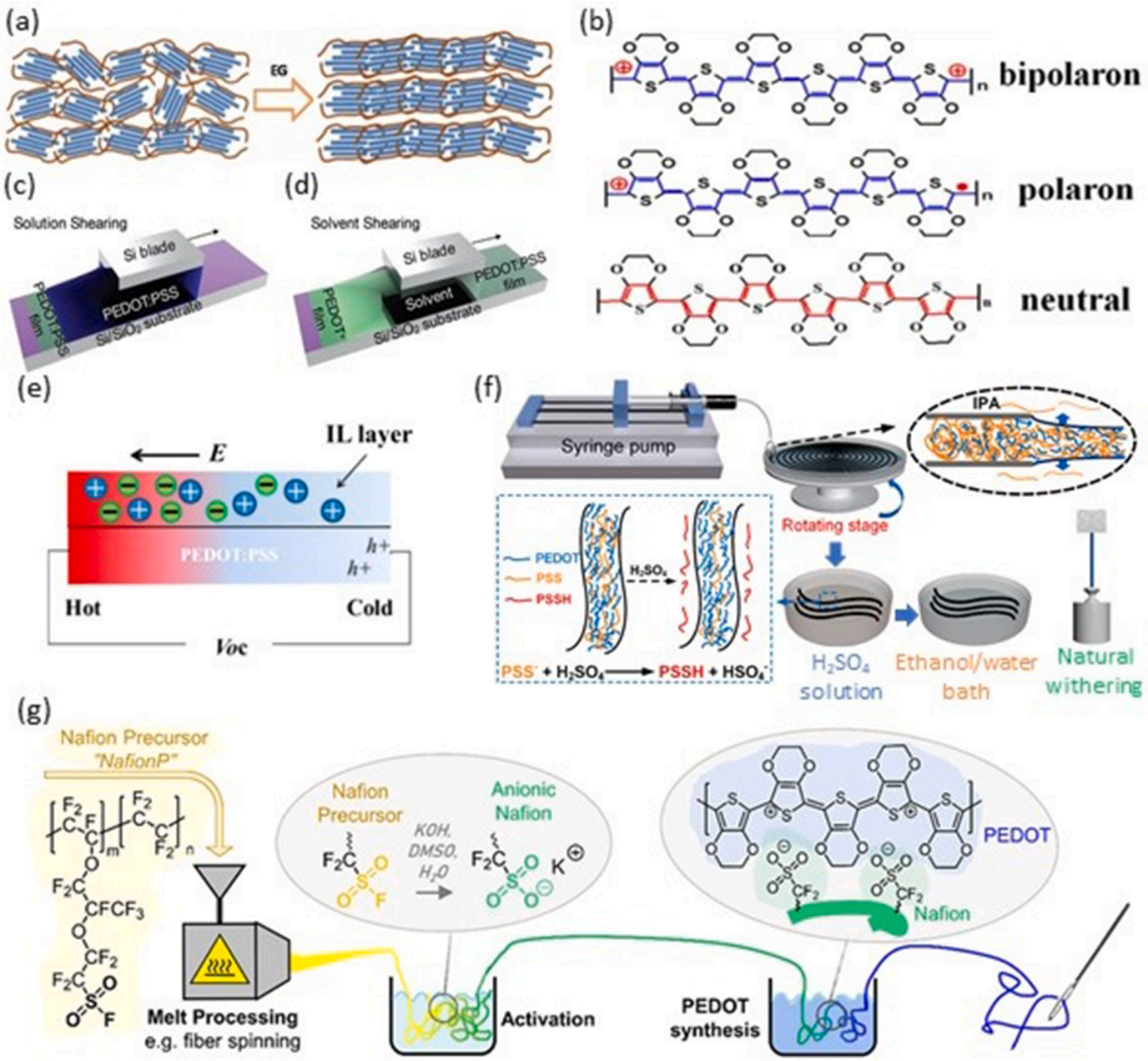

Fig. 15. (a) Morphological change in the PEDOT:PSS films caused by the addition of EG in the secondary doping process. (Reprint permission from Ref. [394]) (b) Schematic plot of transition of PEDOT chains from bipolaron to polaron and neutral state during the dedoping process (Reprint permission from Ref. [407]). (c) Schematic of sheared deposition of PEDOT:PSS. (d) Postdeposition sheared solvent treatment. (Reprint permission from Ref. [397]) (e) Surface energy filtering effect in IL/PEDOT:PSS hetero-structures under temperature gradient. (Reprint permission from Ref. [368]). (f) schematic illustration of the set-up for producing PEDOT:PSS fibers. (Reprint permission from Ref. [398]) (g) Chemical structures and the processing scheme for the Nafion precursor, activated Nafion, and PEDOT. (Reprint permission from Ref. [399]).

performance, its thick layers are hard and brittle, making it challenging to fabricate effective wearable TEGs from them. To address this issue, elastomer composites including PEDOT:PSS, polyurethane, and three types of ILs comprising a common 1-ethyl-3-methylimidazolium (EMIM) cation and various anions (ethyl sulfate (ES), tricyanomethanide (TCM), and tetracyanoborate (TCB)) were developed by aqueous processing [400]. These composites showed high conductivity (>140 S cm^{-1}), superior stretchability (>600%), and excellent elasticity. These outstanding results originated from favorable percolation networks on the nano- and microscale and the plasticizing effect of the IL.

Another well-established conducting polymer is poly(3-hexylthiophene) (P3HT) which possesses the advantages of good electrical conductivity, commercial availability, and ease of solution processability [401]. It has been reported that the doping of a P3HT film, fabricated by drop casting with 20–31% acetonitrile, significantly enhanced its PF up to 0.14 μW $m^{-1}K^{-2}$ which was three orders of magnitude higher than that of the bare sample [401]. Also, doping of a P3HT film with a ferric salt of triflimide ($TFSI^{-}$) anions resulted in a PF of 20 μW $m^{-1}K^{-2}$, and a ZT of 0.04 at 340 K [402]. This is one of the highest reported TE properties of P3HT.

Polyaniline (PANI) [403] is a conducting polymer with several promising features such as a tunable oxidation state, and a doping process that is compatible with base and acid. These characteristics enable precise control of the electrical conductivity and Seebeck

coefficient through altering dopant type, level of pH, and oxidation state. For instance, the doping of PANI with camphor sulphonic acid resulted in a Seebeck coefficient of 0.58 $V^{-1}K$, and a ZT of 2.14 at 17 K [404]. These results implied that PANI can be utilized for TE cooling devices, *e.g.*, Peltier coolers for low temperature applications.

Polypyrrole (PPy) is a conducting polymer that acts as a quasi 1D polymer and which possesses good mechanical flexibility for application in flexible TEGs [405]. Many attempts have been made to produce flexible PPy films [405,406]. However, several drawbacks such as poor adhesion to substrates and non-uniform thickness have been reported for the fabricated PPy films, which were circumvented to a certain degree by using free-standing films of PPy. PPy films fabricated by electro-polymerization methods demonstrated a PF of 3.9 $\mu W\ m^{-1}K^{-2}$ and a ZT of 6.8×10^{-3} [406], which is one of the highest values reported for PPy films.

Polycarbazole (PCz) is a conducting polymer with a well-ordered molecular structure. It has been utilized in optoelectronics, nanoelectronics, and sensory devices because of its good chemical, physical, and electrical properties, and its compatibility with different synthesis techniques [408]. The Seebeck coefficient of poly(2,7-carbazole) derivatives can be increased by localizing the charge carriers in their backbone chain, however the electrical conductivity reduces during this process [408]. Lévesque et al. [409] synthesized poly(2,7-carbazolylenevinylene) by substituting alkyl side chains to the 3,6 positions of the carbazole. They showed a maximum PF of 7.5×10^{-2} $\mu W\ m^{-1}K^{-2}$ through simultaneously keeping the Seebeck coefficient constant and increasing the electrical conductivity. Subsequently, different types of alkyl side chains have been added to the backbone of this polymer. The highest PF of $\sim 10^{-1}$ $\mu W\ m^{-1}K^{-2}$ was achieved in the derivatives with the substitution of indolocarbazole on thiophene units [410]. The best TE properties have been reported in one of the poly(2,7-carbazole) derivatives, poly[*N*-9′-heptadecanyl-2,7-carbazole-alt-5,5′-(4′,7′-di-2-thienyl-2′,1′,3′-benzothiadiazole], which was doped with $FeCl_3$ [411]. This copolymer resulted in electrical conductivity, Seebeck coefficient, and PF of 500 S cm^{-1}, 70 $\mu V\ K^{-1}$, and 19 $\mu W\ m^{-1}K^{-2}$, respectively [411].

The polymerization of acetylene results in a conducting polymer called polyacetylene (PA). This conducting polymer has been utilized in TE applications. It has been reported that the electrical conductivity of PA doped with chlorine, halogens, bromine, and iodine was increased by up to 11 orders of magnitude [412]. For instance, a free-standing PA film doped with iodine illustrated an electrical conductivity of 20,000 S cm^{-1} at RT [412]. It has been reported that the electrical conductivity of PA films doped with iodine can be significantly decreased by temperature and pressure [412] and increased by stretching [413]. Also, the electrical conductivity of PA increased up to 28,500 S cm^{-1} by doping with chlorine-based dopants [414]. The tunable electrical conductivity of PA leads to the optimization of its PF effectively. However, poor air stability and lack of solubility in different types of solvents have limited the use of PA for fabricating practical flexible TEGs [415]. Consequently, more research must be oriented to address these issues for PA as a high-performance flexible TE material.

The development of high-performance conducting polymer TE materials is strongly related to electrical doping. Although many efforts have been made in this area, an in-depth study on the efficiency of doping in highly doped conducting polymers is still missing. More recently, it has been reported that the distribution of dopant molecules in a specific position in highly doped conducting polymers strongly influences the Seebeck coefficient and the electrical conductivity [416]. Poly(2,5-bis(3-hexadecylthiophen-2-yl)thieno[3,2-b]thiophene) (PBTTT) films were highly doped with 2,3,5,6-tetrafluoro-7,7,8,8-tetracyanoquinodimethane (F4TCNQ) by solution-sequential (SSq) and vapor doping methods. As shown in Fig. 16a, the SSq doping procedure induced F4TCNQ in the amorphous domains of PBTTT films while the vapor method deposited the dopant in both the amorphous and crystalline domains. The results indicated that the F4TCNQ dopant in crystalline domains can significantly increase the PF. However, as shown in Fig. 16b, Brinkmann et al. reported that the highest TE performance was obtained in the preferential location of the dopant tris (4-bromophenyl)ammoniumyl hexachloroantimonate), magic blue, in the amorphous phase of P3HT [417]. This doping procedure kept the structure of P3HT nanocrystals almost unchanged and resulted in an electrical conductivity of 3000 S cm^{-1} and a PF of 170 ± 30 $\mu W\ m^{-1}K^{-2}$ due to significant improvement of charge carrier mobility. Interestingly, it has been reported that mobile electrons contribute substantially to charge carrier transport in highly *p*-type doped conducting polymers leading to Seebeck coefficient inversion [418]. Kemerink et al. experimental and theoretically revealed that this phenomenon was attributed to the density of states filling and opening of a hard Coulomb gap around the Fermi energy at high doping levels [419].

4.1.2. Small molecules

Small molecules are another category of organic TE materials that generally possess a Seebeck coefficient in the order of mV K^{-1} [420]. Some examples of small molecules are pentacene, polydopamine (PDA), C_{60}, dinaphtho[2,3-b:2′,3′-f] thieno[3,2-b]thiophene (DNTT), polydopamine (PDA), and 2,7-dioctyl[1]benzothieno[3,2-b][1]benzothiophene (C8BTBT) [421,422]. Their chemical structures are shown in Fig. 17. von Mühlenen et al. fabricated a field-effect transistor made of pentacene and carried out TE measurements [423]. They obtained a high Seebeck coefficient between 240 and 500 $\mu V\ K^{-1}$ which was due to the surface treatment of the field-effect transistor's dielectric layer on top of the channel. The Seebeck coefficient was independent of the channel thickness and applied gate voltage. The authors inferred the formation of polarons and the localization of charge carriers in the pentacene channel of the field effect transistor. These results showed that the transport mechanism in organic materials was influenced by electronic polarization phenomena.

4.1.3. Single molecules

Charge dynamics at the molecular level can be analyzed using single-molecule heterojunctions, by capturing a single molecule between metal electrodes. It is desired to develop a device that achieves a balance between the electrical conductivity and Seebeck coefficient. Experimental and theoretical research has shown that a system that possesses a discrete or even sharp electronic density of state could provide this compromise [424]. Single-molecule heterojunctions can meet this criterion, and their TE characterization can shed light on the transport mechanism at molecular levels and open a new direction in the field of thermoelectricity. For TE characterization in single molecules, one of the most appropriate techniques is the scanning tunneling microscope (STM). In this method, a single molecule is captured between a conducting tip and the substrate [424]. The measurement procedure of conductance and Seebeck voltage in a single molecule is depicted in Fig. 18. The conductance is calculated from the measured current passed through a single molecule by means of the STM tip. For Seebeck voltage measurement, firstly the formation of a junction between the single molecule and the tip is evaluated by applying a voltage bias and monitoring the corresponding current. After removing the applied voltage bias, the generated V_{OC} is the Seebeck voltage which corresponds to the applied temperature difference along the single molecule between the substrate and tip. A voltage amplifier is used for measuring the Seebeck voltage precisely [424].

The electrical conductance measurement of single molecules is an innovative approach for thermoelectric transport characterization of single molecules [425]. Generally, conductance measurement cannot give any information about the type of conduction in a single molecule, and the position of the Fermi level between the HOMO and the LUMO after forming the contact with metal tips. In this regard, the pioneering work on TE characterization of single molecules including both conductance and Seebeck coefficient measurements was performed on 1,4-benzenedithiol (BDT), 4,4′-dibenzenedithiol (DBDT), and 4,

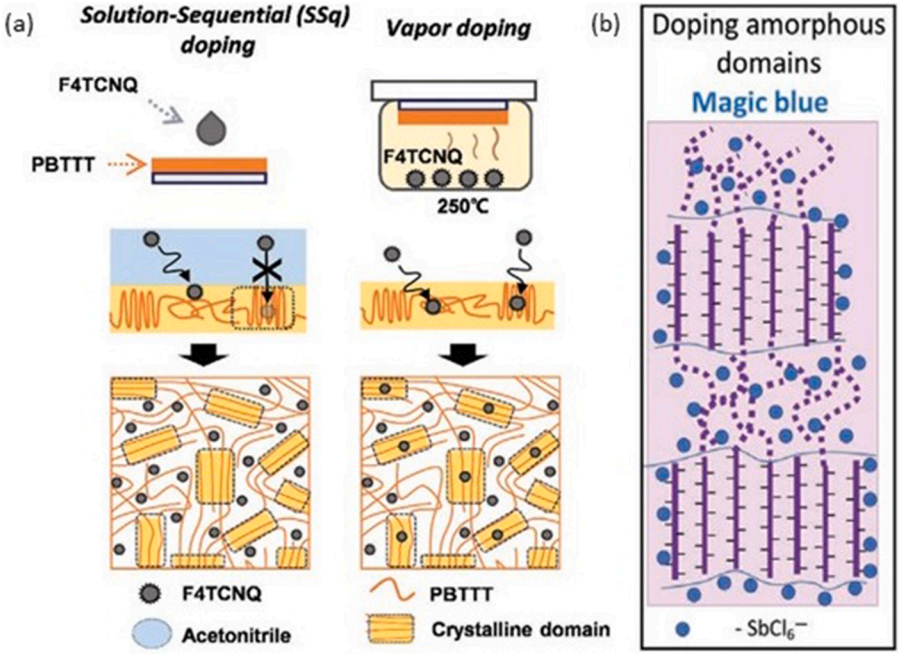

Fig. 16. (a) Schematic descriptions on the experimental process and the resulting dopant positions yielded by SSq doping and vapor doping. (Reprint permission from Ref. [416]) (b) Various doped P3HT microstructures: doping of the crystalline domains for F4TCNQ and F6TCNNQ; doping of both crystalline and amorphous zones for FeCl3 and Mo(tdf-COCF3)3 and doping of the amorphous zones of P3HT with magic blue. (Reprint permission from Ref. [417]) (For interpretation of the references to color in this figure legend, the reader is referred to the web version of this article.).

4″-tribenzenedithiol (TBDT) by the STM method with a gold tip. Seebeck coefficients of +14.2 ± 3.2 μV K^{-1}, +12.9 ± 2.2 μV K^{-1}, and +8.7 ± 2.1 μV K^{-1} were measured for TBDT, DBDT, and BDT, respectively. The obtained results revealed *p*-type conduction, 1.2 eV energy gap between the Fermi level and HOMO of BDT, and a positive linear relation between the Seebeck coefficient and the length of single molecules [426]. Recently, a combination of experimental and theoretical work revealed that the Seebeck coefficient and electrical conductance of single organic radical molecules can be simultaneously enhanced due to their intrinsic spin state [427]. 1,2,4-benzotriazin-4-yl (Blatter) radical molecules with pseudo-meta (meta) and pseudo-para (para) connections to two gold electrodes and the closed-shell (non-radical) quinazoline analogue have been designed to test this idea. A schematic presentation of a single-molecule junction formed by Blatter with para connections to two gold electrodes is illustrated in Fig. 18c. Also, the observed counterintuitive quantum interference (QI) effect in stable Blatter radical molecules with meta-connected radicals resulted in an enhancement of TE properties. As a consequence, the PF was improved by more than one order of magnitude in radicals compared to an analogous closed-shell molecule. These results opened a new research pathway for developing OTE materials working at RT.

4.2. *n*-type organic TE materials

4.2.1. Coordination polymers

A major class of *n*-type organic TE materials are coordination polymers [421]. These polymers are made of metal ions and ligands which act as connectors and linkers in their backbones, respectively [428]. Fundamentally, the entropy of electrons located in the d-orbitals of transition metals determines the Seebeck coefficient of coordination polymers. Historically, coordination polymers including 4,4'-dihydroxy-3,3'-diacetyl biphenyl bis-thiosemicarbazone (L-1) and 4, 4'-dihydroxy- 3,3'-dipropionyl biphenyl bis-thiosemicarbazone (L-2) were introduced as a pioneering group of organic TE materials. The synthesized Cu(II) chelate polymer of (L-1) and (L-2) showed an electrical conductivity of ~10^{-5} S cm^{-1}, and Seebeck coefficient of ~1.1–1.2 mV K^{-1} [429]. These findings illustrated a very low PF which was far from the practical performance. Much attention has been oriented toward the TE properties of coordination polymers since Zhu et al. introduced poly[A_x(M-ett)] (A = Na^+, K^+, Ni^{2+} and Cu^{2+} M= Ni and Cu and ett = 1,1,2,2-ethenetetrathiolate) as a high performance TE material [421,428] (Fig. 19a). Many efforts have been carried out to explore the synthesis method, structural, magnetic, and TE properties of poly[A_x(M-ett)] and their related derivatives [421]. The poly[Na_x(Ni-ett)] and poly[K_x(Ni-ett)] showed *n*-type electrical conductivity from 40 to 44 S cm^{-1} and negative Seebeck coefficient from -75 to -121 μV K^{-1} at RT. The poly[Na_x(Ni-ett)] and poly[K_x(Ni-ett)] resulted in the ZT of ~ 0.042, and ~ 0.1 at 300 K, respectively. On the other hand, poly[Cu_x(-Cu-ett)] showed a *p*-type conductivity, and a ZT value of ~ 0.005 at RT. Based on these results, the authors fabricated a TEG made of 35 legs of *n*-type poly[K_x(Ni-ett)] and *p*-type poly[Cu_x(Cu-ett)] which resulted in a maximum power of 750 μW with a load resistance of 33 Ω at $\Delta T = 82$ K (Fig. 19b and c) [430].

Coordination polymers suffer from poor solubility in common organic solvents. To address this problem, a large area of flexible poly (Ni-ett) was fabricated through the electrochemical deposition technique (Fig. 19d and e), resulting in the enhancement of solubility and TE properties [373]. A maximum PF of 453 μW $m^{-1}K^{-2}$ and a ZT of 0.21 at RT were obtained, owing to the polycrystalline microstructure of the produced films [373]. The insolubility of coordination polymers can be attenuated by hybridization with other polymers, then the composite polymer solution can be used for printing processes. For instance, a flexible TEG made from the composite of poly[A_x(M-ett)], PVDF, and DMSO was fabricated by ink-jet printing on a PET substrate [431]. Recently, a sol–gel technique with oxidation was used to improve the solubility issue of P(Na_x[Niett]) resulting in fabrication of smooth films [432], as illustrated in Fig. 19f. An electrical conductivity of 80.3 S cm^{-1}, a Seebeck coefficient of -35.4 μV K^{-1}, and a maximum power factor of 10.1 μW $m^{-1}K^{-2}$ were achieved at 100°C by controlling the annealing temperature.

Recently, low dimensional coordination polymers have attracted extensive attention in the field of thermoelectricity. For instance, *n*-type two dimensional Cu-BHT (BHT = benzenehexathiol) has been developed with a high value of electrical conductivity (1580 S cm^{-1}) at RT [433]. The measured Seebeck coefficient was in the range of - 4– - 10 μV K^{-1} [433]. This coordination polymer opens a new pathway for developing high performance flexible organic TE materials. Recently, metal-organic frameworks (MOFs) have been introduced as a new class of organic TE materials that possess two main features of microstructural verities, and tailor-ability. For example, *n*-type nanostructured Ni_3(2,3,6,7,10,

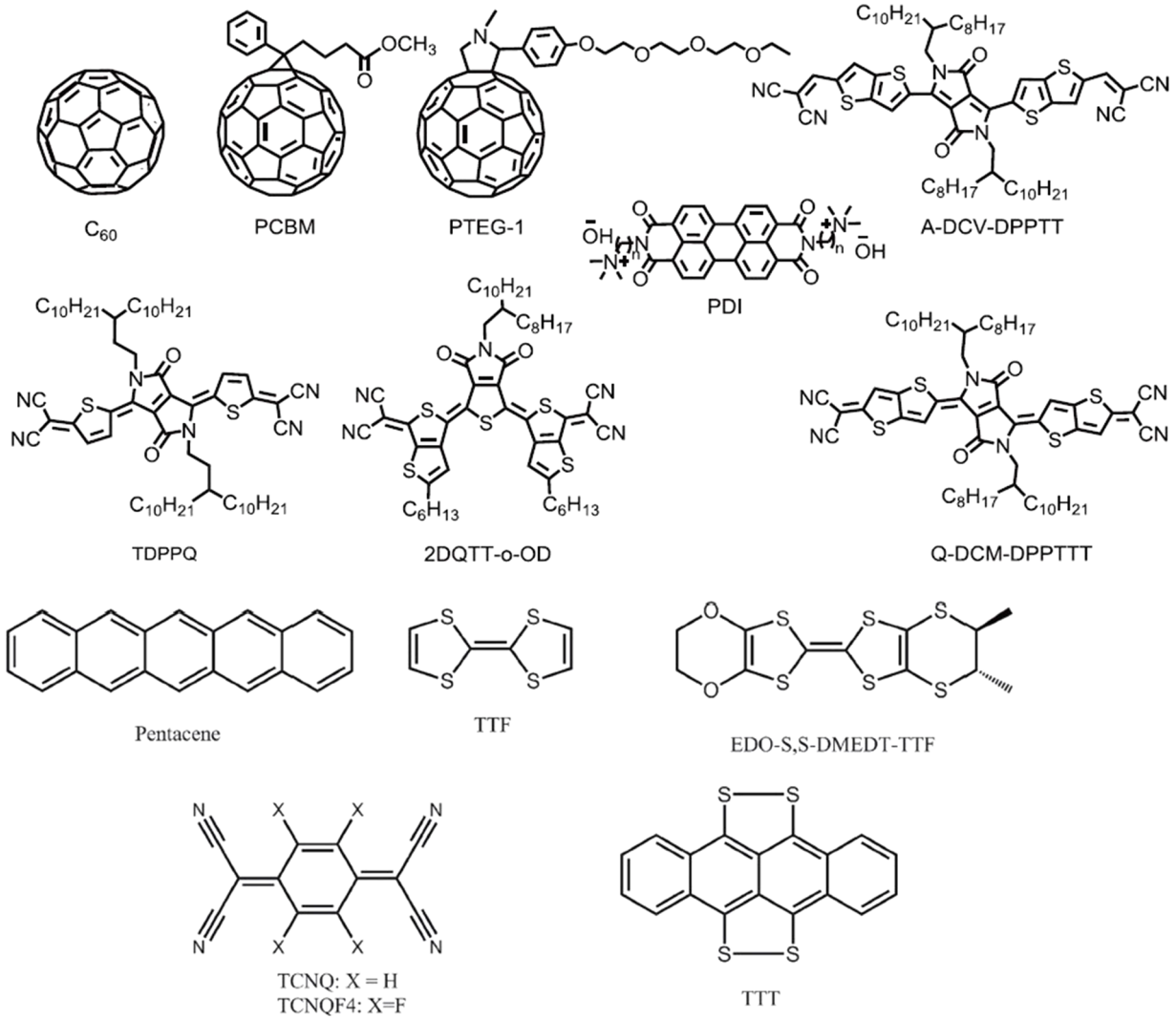

Fig. 17. Chemical structures of several small molecular organic semiconductors used as TE materials. (Reprint permission from Refs. [421,422]).

11-hexaiminotriphenylene)$_2$ pellets resulted in an electrical conductivity of 58.8 S cm^{-1}, a Seebeck coefficient of −11.9 μV K^{-1}, a low thermal conductivity of 0.2 W m^{-1}K^{-1}, and a ZT of ∼10^{-3} [434]. The solution process compatibility, high crystallinity, and tunable pore structure of MOFs show promise as organic TE materials for next generation flexible TEG.

4.2.2. *Conducting polymers*

Although various conducting polymers have been introduced as highly efficient *p*-type OTE materials, their *n*-type counterparts have not been developed due to the lack of good *n*-type conducting polymers and stable *n*-type dopants. However, recent advances have been made in this regard [435]. A major class of high-performance conducting polymers is donor-acceptor (D-A) type polymers comprising electron-donating (D) and electron-accepting (A) building blocks [436]. Among them, the family of the naphthalene diimide (NDI)-based copolymers has been investigated extensively and poly(N,N''-bis(2-octyl-dodecyl)-1,4,5,8-naphthalenedicarboximide-2,6-diyl]-alt-5,5'-(2,2'-bithiophene)), known as PNDI-T2, is the most well-known example of this family [436]. Recently, the PNDI-TVT copolymer was synthesized by substituting T2 with thienylenevinylene-thienylene (TVT), offering an appropriate backbone for enhancing TE properties upon doping [436]. PNDI-TVT doped with H-benzimidazoles resulted in a maximum in-plane electrical conductivity of 2.4 × 10^{-2} S cm^{-1} at RT, being almost four times larger with respect to both similar n-doped PNDI-T2 and to DMBI-doped PNDI-Tz2. Moreover, a complex of NDI with tetrabutylammonium fluoride (TBAF) has been used as a dopant for two new *n*-type conducting polymers including PNDIClTVT (synthesized based on a weak donor unit dichlorodithienylethene (ClTVT) by Stille coupling in ortho-dichlorobenzene (o-DCB)) and PBDOPVTT (synthesized by Stille coupling PNDIClTVT in chlorobenzene) [437]. The NDIClTVT doped with NDI-TBAF resulted in an electrical conductivity of 0.20 S cm^{-1}, a Seebeck coefficient of -1854 μV K^{-1}, and a power factor of 67 μW m^{-1}K^{-2}, which is the highest reported PF in solution-processed *n*-type conducting polymers.

Another effective strategy to develop *n*-type conducting polymers is acceptor–acceptor (A-A) copolymerization [438]. Recently, a distannylated monomer of strong electron-deficient double B←N bridged bipyridine (BNBP) unit has been synthesized as an A-A type conducting polymer through Stille polycondenzation [438]. The doped polymers with TDAE showed an electrical conductivity of 7.8 S cm^{-1} and a high power factor of 24.8 μW m^{-1}K^{-2}. More recently, McCulloch et al. developed three lactone-based rigid backbone conducting polymers with A-A properties by molecular engineering [439]. They experimentally and theoretically showed that the increase of lactone group density by raising the benzene content led to increasing the electron affinities, hence improving the *n*-type doping process by N-DMBI as the dopant. In their work, the electrical conductivity was improved by three orders of magnitude and reached 12 S cm^{-1}, resulting in a PF of 13.2 μW m^{-1}K^{-2}.

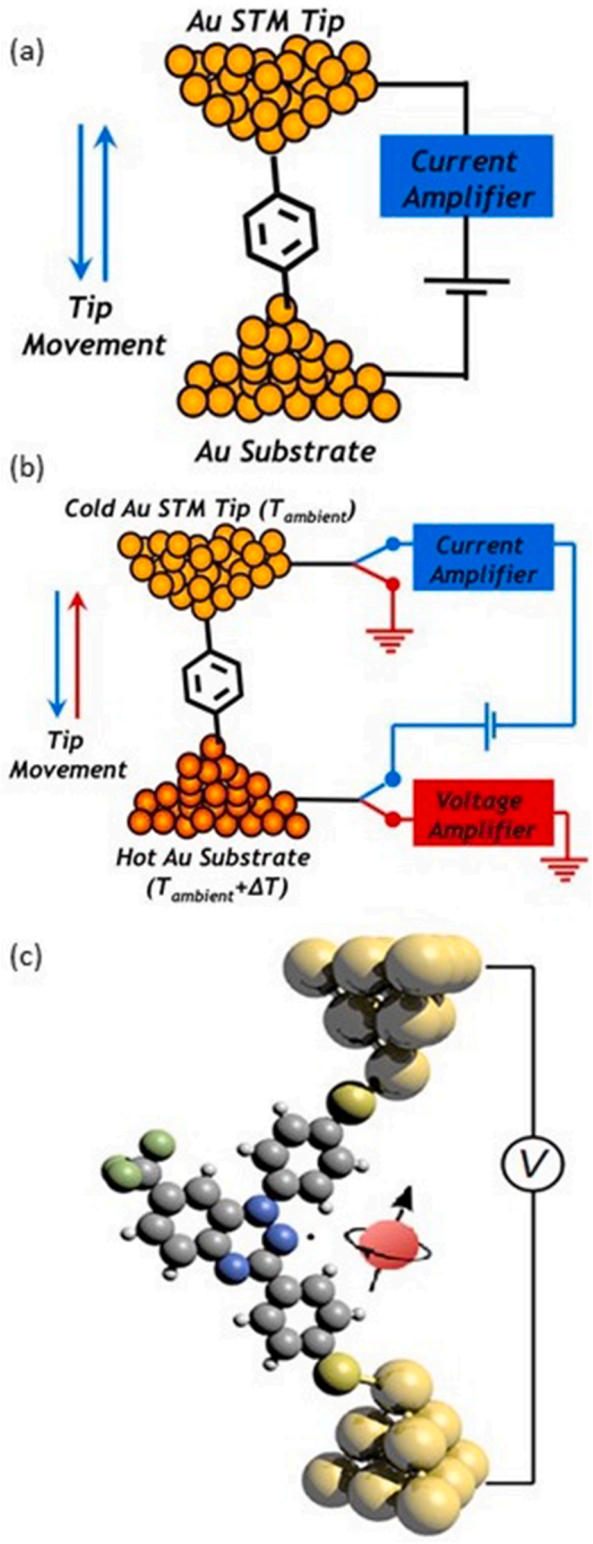

Fig. 18. STM-break junction technique for measurement of: (a) electronic conductance, and (b) Seebeck voltage. (Reprint permission from Ref. [424]) (c) Schematic diagram of a single-molecule junction formed by meta-connected Blatter radical between gold electrodes. (Reprint permission from Ref. [427]).

4.2.3. Small molecules

Small molecules have attracted extensive attention as TE materials due to their stable *n*-type conductivity and facile purification and crystallization processes [420]. C_{60} has been introduced as a candidate for *n*-type TE materials. It was doped with Cs_2CO_3, displaying a PF of 28.8 μW $m^{-1}K^{-2}$ [440]. Moreover, its derivative, [6,6]-phenyl-C_{61}-butyric acid methyl ester (PCBM), resulted in an *n*-type electrical conductivity of 10^{-8} S cm^{-1}, and extremely low thermal conductivity of 0.03 W $m^{-1}K^{-1}$ at RT [441]. C_{60} and its derivatives have been subjected to 3,6-Bis(dimethylamino)acridine (AOB) [442] and (4-(1,3-dimethyl-2,3-dihydro-1H-benzoimidazol-2-yl)phenyl) dimethylamine (N-DMBI) [443] as doping agents to increase the TE efficiency. As an example, an electrical conductivity, Seebeck coefficient, and PF of 2 S cm^{-1}, -500 μV K^{-1}, and 1 μW $m^{-1}K^{-2}$, respectively, were achieved in PCBM doped with N-DPBI and AOB [443]. In the case of another small molecule, 2DQTT-o-OD, doping with $(2\text{-Cyc-DMBI-Me})_2$ showed a PF of 33.3 μW $m^{-1}K^{-2}$ [444]. Recently, new *n*-type small molecule TE materials have been developed based on B←N-incorporated dibenzo-azaacenes 1,2-DBNA-2 and 1,2-DBNA-5 [445]. The low LUMO energy levels of 1,2-DBNA-2 and 1,2-DBNA-5 resulted in the efficient *n*-type doping. For instance, the doped 1,2-DBNA-5 with N-DMBI showed an electrical conductivity of 0.01 S cm^{-1}, a Seebeck coefficient of −244.4 μV K^{-1}, and a PF of 0.06 μW $m^{-1}K^{-2}$.

In the past two decades, the "phonon-glass electron-crystal (PGEC)" concept has been explored extensively in inorganic TE materials. In the case of OTE materials, they are mostly "phonon-glasses" but far from being "electron-crystal". Recently, a molecularly n-doped fullerene derivative with an accurate design of the side chain was reported as a PGEC OTE material [446]. It resulted in an excellent electrical conductivity of >10 S cm^{-1} and an ultralow thermal conductivity of <0.1 W$m^{-1}K^{-1}$, and a ZT = 0.34 at 120°C.

Other approaches to enhance the TE properties of *n*-type small molecules are self-doping and tailoring of the host and dopant miscibility. Though self-doping of perylene diimides (PDI) resulted in a very low PF of 1.4 μW $m^{-1}K^{-2}$, it triggered research interest in self-doped *n*-type small molecules [447], whereas a tailored fullerene derivative (a host) and N-DMBI (a dopant) resulted in electrical conductivity, Seebeck coefficient, and maximum PF of 2.05 S cm^{-1}, - 284 μV K^{-1}, and 16.7 μW $m^{-1}K^{-2}$, respectively, at dopant concentration of 40% [448].

Despite many efforts to improve their TE properties, the low electrical conductivity of *n*-type small molecules limits the PF. To address this issue, organic field-effect transistors with modulated gate voltage have been proposed to regulate the TE parameters [449]. The dropyrrolo [3,4-c]pyrrole-1,4-diylidenebis(thieno[3,2-b]thiophene) [374], NDI (2OD)(4t-BuPh)-DTYM2 [449], NDI3HU-DTYM2 [449], and TDPPQ [450] have been incorporated in this kind of organic field-effect transistor. The aromatic structure of the former small molecule's derivative doped with N-DMBI resulted in an electrical conductivity of 3 S cm^{-1}, a Seebeck coefficient of -580 μV K^{-1}, PF of 100 μW $m^{-1}K^{-2}$, and a ZT of 0.11 at RT [374]. This significant enhancement originated from tuning the electronic structure and mobility by modulating the conjugated backbone of organic semiconductors, hence improving the TE performance by adjusting the electrical conductivity and Seebeck coefficient.

Recently, both *n*- and *p*-type small molecule TE materials were constructed by low dimensional TTT_2I_3 (TTT = Tetrathiotetracene) and $(DMe\text{-}DCNQI)_2Cu$ (DMe-DCNQI = Dimethyl-Dicyanoquinonediimine) [451]. The *p*-type TTT_2I_3 showed an electrical conductivity of 3.3×10^3 S cm^{-1}, Seebeck coefficient of 40 μV K^{-1}, a PF of 300 μW $m^{-1}K^{-2}$, and ZT of 0.04 at RT. The *n*-type $(DMe\text{-}DCNQI)_2Cu$, based on the concept of phonon drag, demonstrated a relatively high ZT of ≥ 0.15 below 40 K. A TEG made of one leg of TTT_2I_3 (*p*-type) and a leg of $DCNQI_2Cu$ (*n*-type) resulted in output power of 125 nW at $\Delta T = 92$ K. This work opens a new research direction to develop organic TE materials based on crystalline low-dimensional molecular metals for low temperature TE applications.

4.2.4. Single molecule

Fullerenes and their derivative (C_{60}, PCBM, and C_{70}) were the first reported *n*-type single molecule TE materials reported by Segalman et al. [452]. The thermoelectric measurements were carried out using different electrodes including Pt, Au, and Ag. The results indicated that the variation of electrical conductivity with type of electrode was related

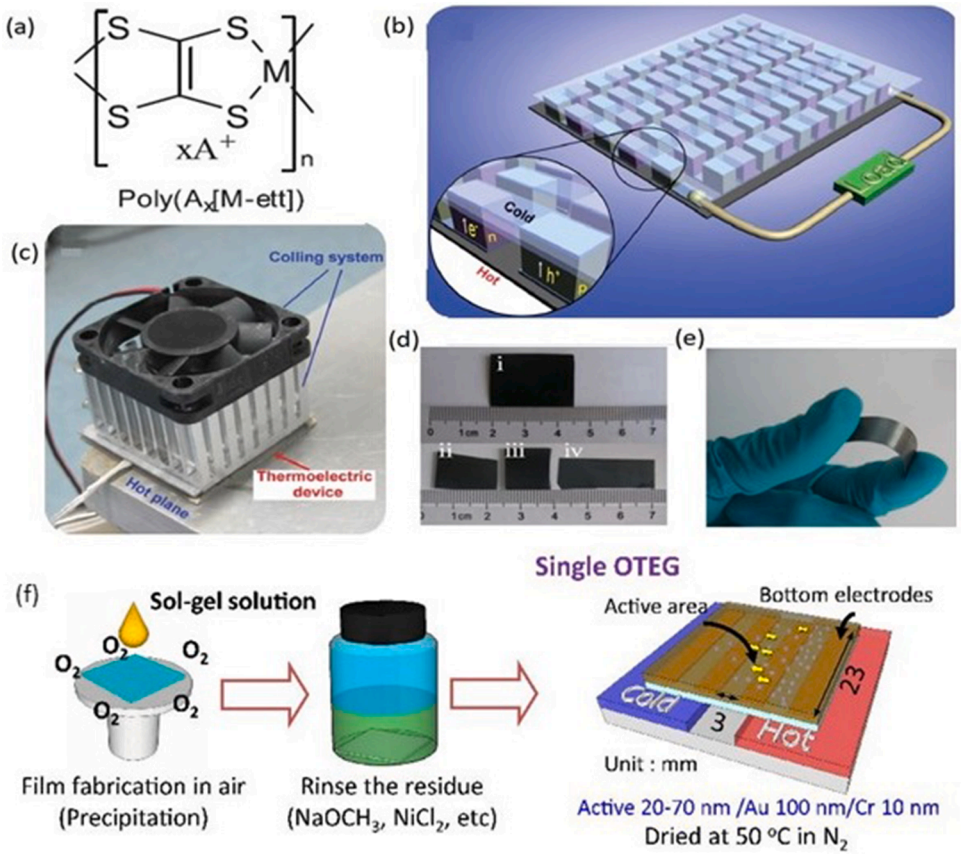

Fig. 19. (a) The molecular structure of poly [A_x(M-ett)]. (b) Schematic of the TE module consisting of 35 couples. (c) Photograph of the module and the measurement system with hot plane and cooling fan. (Reprint permission from Ref. [430]) (d) Images of poly(Ni-ett) films deposited on PI (i), Teflon (ii), quartz (iii), and PET (iv) substrates. (e) Flexibility of the thin film deposited on PET. (Reprint permission from Ref. [373]) (f) Fabrication process of P (Na_x[Niett]) thin films. (Reprint permission from Ref. [432]).

to the different binding properties of fullerene and electrodes. In the case of Seebeck coefficient, the variation was determined by the alignment of electrodes work functions and the energy level of LUMO. The most important contribution of this work was introducing a new class of *n*-type organic TE materials based on single molecules. Until then, magnetic single molecules including $[(Cp^{iPr5})Dy(Cp^*)]^+$ [453],$[Dy(O^tBu)_2(py)_5]^+$ [454], and the conjugated polymers, *e.g.*, EDOT-based molecules [455], were studied as single molecule TE materials. Furthermore, numerous techniques for controlling electron and phonon transport in molecular devices have recently been established, including size effect, chemical modulation, mechanical regulation, electrostatics gating, and quantum interference effect in single molecules [456]. For instance, constructive quantum interference (CQI) can be translated from single molecules to self-assembled monolayers (SAMs) and effectively boost both the electrical conductivity and the Seebeck coefficient [457]. Recently, multi-component thin films were assembled by using a bottom-up method. These films comprised a rigid, highly conductive 'sticky'-linker (formed from alkynyl-functionalised anthracenes) and a 'slippery'-linker (consisting of a functionalized metalloporphyrin) [457]. It has been shown that the addition of either a porphyrin layer or a graphene layer to an anthracene-based SAM raises the Seebeck coefficient, and the addition of both porphyrin and graphene boosts the Seebeck coefficient. These findings have opened a new avenue for designing thin film OTE materials using SAMs.

4.3. Carbon nano tubes (CNTs)

Low dimensional structures of carbon-based materials such as graphene, carbon nanotubes (CNTs), and fullerene, have been extensively studied as TE materials [458]. Particular attention has been paid to CNTs due to their remarkable electrical and mechanical properties suited for fabricating flexible, low cost, and lightweight TEGs [458]. Sumio Iijima synthesized the first CNT in 1991 [459]. Two years after that, Hicks and Dresselhaus reported ultra-high TE performance in nanostructure and low dimensional systems due to the quantum confinement of charge carriers [460]. These two prominent findings provided a fertile platform for TE materials to exploit the advantage of CNT for flexible TEGs. Although CNTs illustrated *p*-type conductivity due to oxygen doping in air [461], many investigations have been performed to obtain *p*-type and *n*-type conductions by means of different dopants [462]. In the case of *p*-type doping, oxidative dopants such as oxygen, acids, and organic molecules are often used for CNTs [458]. As an example, *p*-type CNTs were fabricated using three different dispersants such as chlorosulfonic acid (CSA), N-methyl-2-pyrrolidone (NMP), and deionized water with sodium dodecylbenzenesulfonate (SDBS) through three types of fabrication techniques including high-pressure carbon monoxide, chemical vapor deposition, and arc discharge [463]. The best PF of 550.8 μW $m^{-1}K^{-2}$ was achieved from an electrical conductivity of 1.7×10^4 S cm^{-1} and a Seebeck coefficient of 18 μV K^{-1} for double-wall CNTs fabricated by chemical vapor deposition utilizing CSA solvent [463].

In general, the presence of oxygen in air leads to a difficulty for producing *n*-type CNTs. Reduction agents such as $NaBH_4$ and hydrazine have been used to achieve *n*-type CNTs but the doped CNTs were unstable in air [464]. So far, several other *n*-type molecular dopants have been developed for obtaining *n*-type CNTs (Fig. 20a) [465]. Typically, poly(ethyleneimine) (PEI) [466], reduced viologen [467], prylene diimide [468], and their derivatives, are used as *n*-type dopant for CNTs. The doped single wall CNTs (SWCNTs) with perylene diimide (PDINE) or naphthalene diimide (NDINE) resulted in *n*-type stable SWCNTs with PFs of 112 μW $m^{-1}K^{-2}$ and 135 μW $m^{-1}K^{-2}$, respectively [468]. This stability originated from a strong $\pi-\pi$ interaction between dopant molecules and CNTs. An output power of 3.3 μW at $\Delta T = 50°C$ was obtained from a TEG made of five unicouples of SWCNTs doped with SDBS (*p*-type leg) and NDINE (*n*-type leg) [468]. Recently, Wang et al. utilized a solution-processable method to prepare doped SWCNTs with

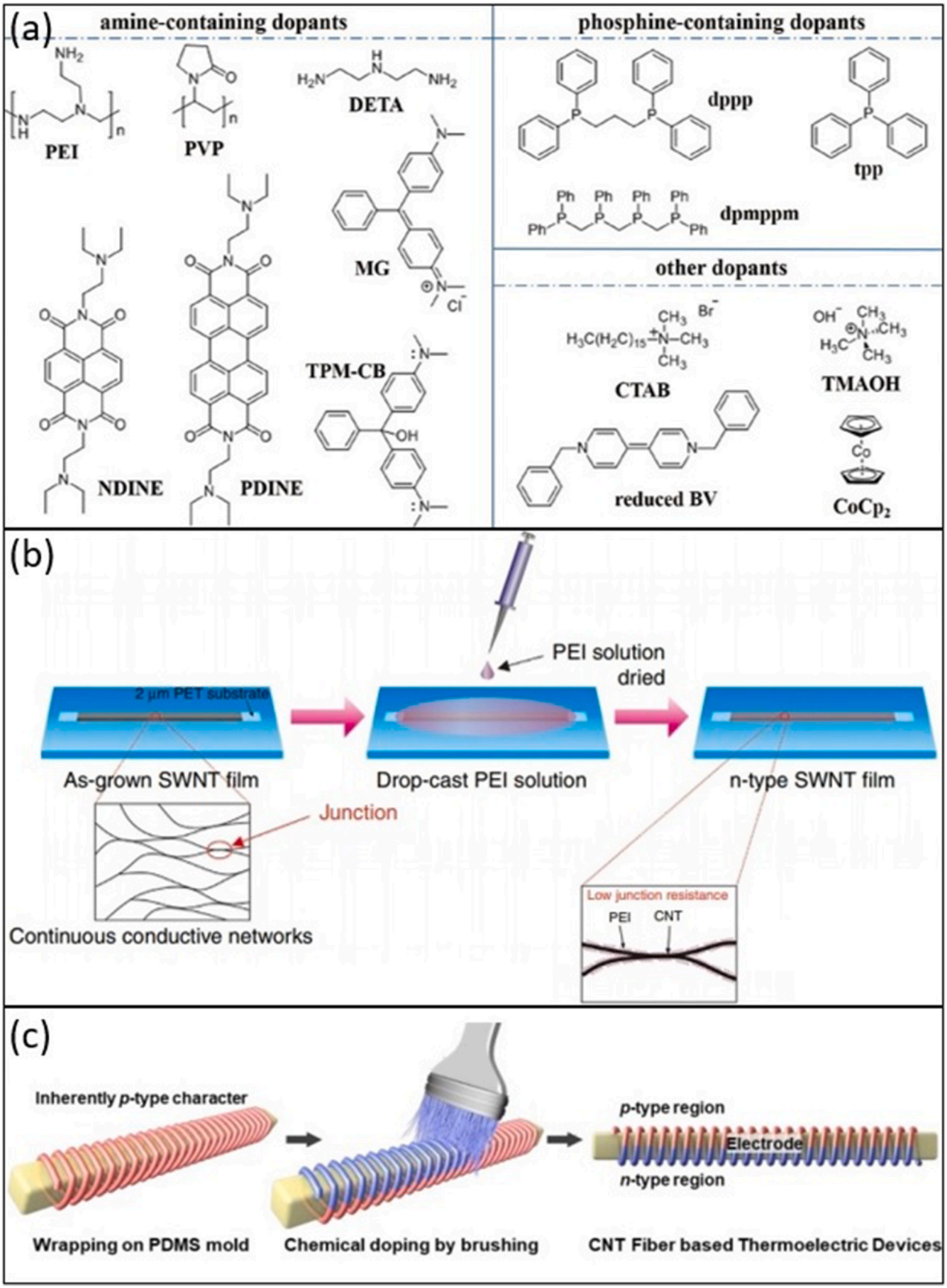

Fig. 20. (a) Chemical structures of molecular dopants used for the preparation of *n*-doped CNTs. (Reprint permission from Ref. [465]) (b) Schematic of the fabrication process for *n*-type SWCNT films based on as-grown SWCNT continuous networks. (Reprint permission from Ref. [470]). (c) Illustration showing the fabrication of CNT fiber based-TEGs (Reprint permission from Ref. [473]).

N-DMBI in a DMSO solution [469]. High electrical conductivity of 2298 S cm^{-1} was obtained at RT which was higher than other solution processed SWCNTs. At 373 K, the high electrical conductivity of 3490 S cm^{-1} resulted in a high n-type power factor of 195 μW $m^{-1}K^{-2}$. They concluded that the *n*-type electrical conductivity was affected by the wrapping morphology of the surfactant on SWCNTs.

Recently, as shown in Fig. 20b, the PEI solution was drop casted on SWCNT to produce a stable *n*-type conductivity [470]. A large PF of 1500 μW $m^{-1}K^{-2}$ was achieved in the film with PEI concentration of 1 wt.% due to low inter tube junction resistance and contact resistance. Over 180 days of testing, the electrical conductivity and Seebeck coefficient showed <5% variation away from their average value [470]. Typically, organic molecules containing phosphine or nitrogen are used for transferring electrons to CNTs as *n*-type dopants. Former dopant group examples are 1,3-bis(diphenylphosphino)propane (dppp), triphenylphosphine (tpp), and bis[(diphenylphosphinomethyl)phenylphosphino] methane (dpmppm). Moreover, common surfactants have been introduced as another type of effective *n*-type dopants for CNTs. Flexible *n*-type SWCNT films were prepared through alkylammonium cationic surfactant and resulted in a PF of 185.7 μW $m^{-1}K^{-2}$ at RT [471]. This improvement was obtained from the regulation of different parameters such as dispersion medium, the length of alkyl chain, cationic surfactant types, and type of dopants [471]. In summary, the adsorption of dopant molecules on the outer surfaces of CNTs is the basis of the doping mechanism. An alternative method for *n*-type doping of CNT for improving its TE properties is encapsulating the dopant molecules, *e.g.* $CoCp_2$, inside the nanotubes [472].

Recently, the well-aligned CNT fibers were fabricated by the wet-spinning method which enabled the regulation of the longitudinal charge carrier mobility [473]. The maximum PF of 432 μW $m^{-1}K^{-2}$ was achieved and is attributed to enhanced electrical conductivity due to improved charge carrier mobility, without significant alteration of the carrier concentration and Seebeck coefficient. The *p*-type and *n*-type CNTs were produced by doping with 4-hydroxycarbazole (H-carbazole) and 1,3-bis(diphenyl phosphino) propane (dppp), respectively (Fig. 20c). A flexible TEG constructed from 40 legs of *p*- and *n*-type CNT fibers resulted in an output power of 2 μW at $\Delta T = 20$ K.

4.4. Composites of organic TE materials

Although many efforts have been made to improve the TE properties of organic materials, they still suffer from relatively low electrical conductivity and Seebeck coefficient. To address this issue, one effective strategy is to fabricate organic semiconductor-based composites by incorporating either organic or inorganic fillers. The fabricated composites can improve the electrical conductivity and Seebeck coefficient, making them comparable to state-of-the-art inorganic TE materials. Owing to these capabilities, organic TE composites have been widely investigated over the years [387,421]. Two main class of materials have been introduced as fillers in these composites: (1) carbon-based materials such as CNTs and graphene, and (2) inorganic TE materials such as Bi_2Te_3, SnSe, Te, and PbTe related compounds and nanostructures [387, 421].

4.4.1. Carbon fillers

CNT and graphene are popular organic fillers due to their high electron mobility and electrical conductivity, flexibility, and large specific surface area providing low contact resistance between host and filler in the composites. These carbon fillers are mostly incorporated in PEDOT:PSS, P3HT, PPy, and PANI for fabricating high performance flexible organic TE composites.

The PANI/CNT composite is a promising TE material because PANI chains wrap around CNTs to create a hybrid structure and also the PANI chains get aligned parallel to the CNTs . As an example, the well-aligned nanofiber composite of PANI/CNT produced by combination of *in-situ* polymerization and electro-spinning is shown in Fig. 21a [474]. The ordered microstructure led to a decrease of defects in the backbone of PANI and electron localization, increasing the mobility of charge carrier in the composite. In this case, the fabricated sample resulted in a PF of 0.17 μW $m^{-1}K^{-2}$ [474]. Recently, a composite based on SWCNT and a copolymer poly(aniline-co-pyrrole) (PANIPy) resulted in a high PF of 70 μW $m^{-1}K^{-2}$ at RT [475].

So far, several strategies applied to PANI-based composites, such as cryogenic assisted grinding [476], *in-situ* polymerization [477], camphorsulfonic acid doping [478], and fabrication of complex oxide composites [479], have resulted in improved TE properties. For instance, the *in-situ* polymerization followed by solution processing was used for fabricating well-ordered SWCNTs/PANI composite films [480]. The produced devices showed a PF of 217 μW $m^{-1}K^{-2}$ at SWCNT content of 65% [480]. The reasonably good TE performance was attributed to high charge carrier mobility due to the combination of these two fabrication processes.

PEDOT:PSS/CNTs is another promising composite. Historically, PEDOT:PSS was used to enhance the binding of carbon materials to the host polymer. For example, doped PEDOT:PSS with DMSO has been used for the proper dispersion of CNT into a gum Arabic as a host which illustrated a PF of 25 μW $m^{-1}K^{-2}$ at 35 wt% of PEDOT:PSS and CNTs [481]. Grunlan et al. later [482] showed that by further increasing the content of SWCNTs to 60% and PEDOT:PSS to 30% in the composite, enhanced device parameters can be achieved with Seebeck coefficient of 41 μV K^{-1}, electrical conductivity of 950 S cm^{-1}, a PF of 160 μW $m^{-1}K^{-2}$, and a ZT of 0.12 - 0.24 at RT. Subsequently, synthesis of an organic composite made of MWCNTs, DWCNTs, and PEDOT:PSS and meso-tetra(4-carboxyphenyl) porphine (TCPP) as the stabilizer resulted in an electrical conductivity of 960 S cm^{-1}, a Seebeck coefficient of 70 μV K^{-1}, and a PF of 500 μW $m^{-1}K^{-2}$ at 40 wt% DWCNTs. As shown in Fig. 21b and c, the creation of a strong junction between the CNTs by PEDOT:PSS and TCPP results in the improvement of charge transport and consequently a significant enhancement of TE performance [483].

The treatment of PEDOT:PSS and CNTs composites with various types of dopants through secondary doping and de-doping processes can optimize the PF [484,485]. For instance, the PF of SWCNT/PEDOT:PSS composite reached 464 μW $m^{-1}K^{-2}$ at RT by treating the composite with DMSO [485]. Moreover, a nanocomposite of PEDOT:PSS and SWCNT treated with DMSO and NaOH resulted in a PF of 526 μW $m^{-1}K^{-2}$ calculated from an electrical conductivity of 1701 S cm^{-1}, and a Seebeck coefficient of 55.6 μV K^{-1}, and a ZT of 0.39 at RT [486].

Several fabrication methods such as layer-by-layer (LbL) assembly, template synthesis, melt intercalation, direct mixing, sol-gel process, solution processing, and *in-situ* polymerization have been developed to fabricate organic composites [487]. For instance, as shown in Fig. 21d, a composite comprising PANI, graphene, PEDOT:PSS, and DWCNT was constructed by the LbL deposition method in 20 and 80 cycles [488]. A composite consisting of 80 units of PANI/graphene-PEDOT:PSS/PANI/DWCNT-PEDOT:PSS layer showed a maximum PF of 2710 μW $m^{-1}K^{-2}$ which was attributed to enhanced charge carrier mobility as a result of a layered structure of composite and interconnected graphene sheets [488]. Many efforts have been put into preparing different composites of organic TE materials and graphene nanosheets, graphene nanoplatelets, and reduced graphene oxide (rGO) [489,490]. Among them, a composite of PEDOT:PSS and 3 wt% graphene nanosheets treated with hydrazine exhibited a PF of 53.3 μW $m^{-1}K^{-2}$ [489].

Another good candidate for preparing composite TE materials with CNTs is P3HT due to its good solubility in organic solvents and adjustable molecular structure [491]. The composites of P3HT with different weight percentages of MWCNT and SWCNT have been fabricated by the solution process method [491]. Doping of composites with $FeCl_3$ has exhibited high electrical conductivity and PF. The doped P3HT/SWCNT composite resulted in an electrical conductivity of 1000 S cm^{-1}, a Seebeck coefficient of 29 μV K^{-1}, and a PF of 95 μW $m^{-1}K^{-2}$. The improvement of TE properties was attributed to the crystallization of P3HT on the surface of CNTs by means of a strong interaction between

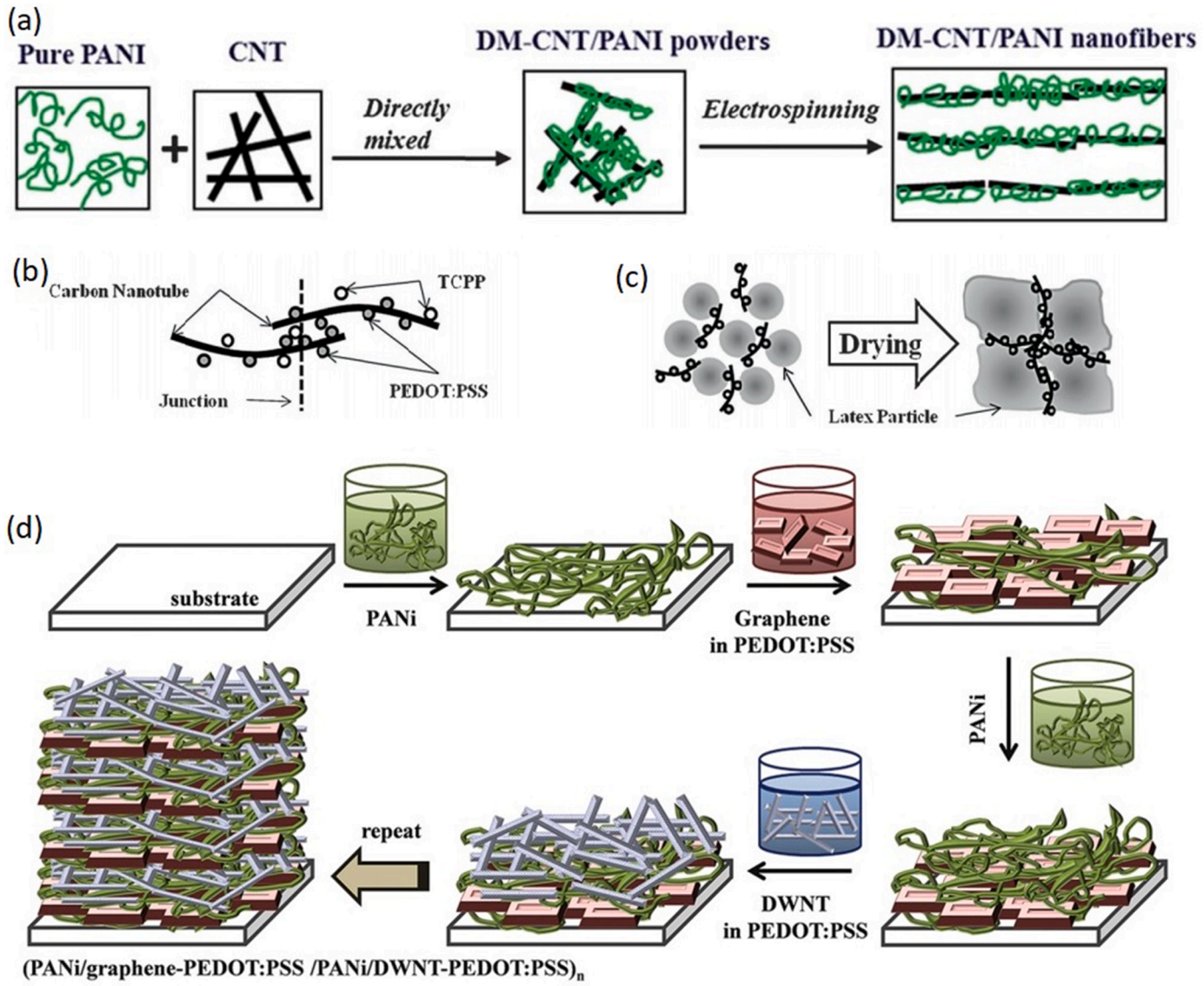

Fig. 21. (a) Schematic representations of the formation mechanism of DM-CNT/PANI nanofibers. (Reprint permission from Ref. [474]) (b) Schematic of carbon nanotubes decorated by PEDOT:PSS and TCPP molecules and the junction formed between them. (c) Schematic depicting the formation of a segregated network composite during polymer coalescence as it dries. (Reprint permission from Ref. [483]) (d) Schematic of the LbL deposition process. (Reprint permission from Ref. [488]).

them. In the composites comprising CNT fillers, the good connection of CNT networks results in a significant enhancement of the electrical conductivity. However, a comprehensive applied model is needed to describe the underlying mechanisms of these enhancements in the composites of organic TE materials and CNTs. On the other hand, the use of graphene as a filler in polymer matrices improves electrical conductivity by providing additional electron transport channels and thereby enhanced carrier mobility. However, owing to the high thermal conductivity of graphene, further efforts are required to achieve high TE properties by compromising the electrical and thermal conductivities.

Recently, CNT has been incorporated in other OTE materials including GO, MOFs, and small molecules to enhance their TE properties. Recently, mass-produced MWCNT/GO hybrids doped with an *n*-type dopant of NDMBI resulted in a maximum PF of 195 μW $m^{-1}K^{-2}$ at 373 K [492]. This outstanding result originated from the high n-type Seebeck coefficient of metallic MWCNTs and created a connection between GO and MWCNTs electrically by using dopants containing amine groups. Although MOFs have high Seebeck coefficient and low thermal conductivity, the TE performance is reduced due to their low electrical conductivity. In this case, both p- and *n*-type composites of $Ni_3(HITP)_2$ were synthesized by introducing *p*-type pristine CNTs and *n*-type PEI-doped CNTs, respectively [493]. It has been concluded that CNTs played a dominant role in the determination of charge carrier types. By selective tuning of TE properties, not only the maximum ZT value was increased up to 270 times compared with the ZT of a pristine MOF, but also it is seven times higher than the reported ZT for MOFs. Moreover, the composites of different types of novel butterfly-shaped small molecules with SWCNTs have been synthesized as high-performance *p*-type OTE materials [494]. The results indicated that butterfly-shaped small molecules significantly enhanced the TE properties in comparison with that of the composite based on the analogous planar small molecules. The developed composite with SWCNTs resulted in a high PF of 312 μW $m^{-1}K^{-2}$. This significant result was attributed to the higher activation energy, improved doping level, and charge transport process between the small molecules and SWCNTs.

The performance of *n*-type organic TE composites is usually lower than their *p*-type counterparts due to the instability of *n*-type conductivity in air, and inhomogeneous microstructure. To attenuate these

issues, a composite of DWCNT and graphene stabilized by polyethyleneimine (PEI) and polyvinylpyrrolidone (PVP), respectively, was fabricated by the LbL deposition technique which resulted in an electrical conductivity of 300 S cm^{-1}, a Seebeck coefficient of -80 μV K^{-1}, and a PF of 190 μW $m^{-1}K^{-2}$ at RT [464]. Creating the bridge between graphene sheets by DWCNTs increases the electron mobility, electrical conductivity and Seebeck coefficient. The achieved results were stable for a period greater than two months in ambient air atmosphere because the graphene sheets protected the films from oxygen [464]. Recently, it has been reported that composite films comprising P(NDI2OD-T2) copolymer and SWCNTs doped with 10 wt% N-DMBI resulted in *n*-type TE performance with the highest PF of 18.1 μW $m^{-1}K^{-2}$ for the 45.5 wt% SWCNT. Also, the negative Seebeck coefficient of the *n*-type film was stable in air for 8 months [495].

4.4.2. Inorganic TE material fillers

Significant attempts have been made to enhance the TE properties of organic TE materials and their composites with inorganic compounds. However, their efficiency is still behind conventional inorganic TE materials due to their low electrical conductivity and Seebeck coefficient. One strategy to meet this issue is the fabrication of the composites comprising high ZT organic and inorganic TE materials to simultaneously benefit from their respective advantages.

Inorganic TE materials such as Te, Bi_2Te_3, and SnSe have successfully been incorporated in organic TE materials such as PEDOT:PSS to prepare organic/inorganic composites. For instance, a Te/PEDOT:PSS composite at 10% of PEDOT:PSS concentration was fabricated through drop-casting of PEDOT:PSS and Te NWs solution followed by sonicating [496]. This composite resulted in a maximum PF of 25 μW $m^{-1}K^{-2}$ at RT [496]. Since the secondary doping of PEDOT:PSS with H_2SO_4, H_3PO_4, and DMSO can remarkably enhance the TE properties, a PEDOT:PSS coated Te (PC-Te) nanorod/PEDOT:PSS composite produced by drop-casting was treated with H_2SO_4 [497]. In this case, a composite made of 90 wt% PC-Te nanorods, treated with 12 M H_2SO_4, demonstrated a maximum PF of 141.9 μW $m^{-1}K^{-2}$, corresponding to an electrical conductivity of 204.6 S cm^{-1} and a Seebeck coefficient of 83.27 μV K^{-1} at RT [497]. Recently, the effect of length, diameter, and aspect ratio of a Te/PEDOT:PSS nanowire composite on TE properties was investigated by changing the experimental parameter of ligand molecular weight during the synthesis process [498]. Increasing the ligand molecular weight led to a larger nanowire aspect ratio that resulted in an optimal power factor of ~130 μW $m^{-1}K^{-2}$ at RT for a modest aspect ratio of 73. Numerous studies have been carried out to improve the TE efficiency of Te/PEDOT:PSS composites [499,500]. However, commercialization of these composites is difficult due to the scarcity and high cost of Te. To address this issue, the amount of Te inclusion can be decreased by incorporating CNT and BiTe-based materials into PANI and PEDOT:PSS composites without deteriorating their TE properties [501]. Compositionally graded Bi_2Te_3 nanoparticles or Sb_2Te_3 nanoflakes/PEDOT:PSS nanocomposites have been introduced to optimize the PF along the applied temperature gradient by systematically tuning the composition of nanocomposites along the length of the TEG [502]. This method improved the capability of organic/inorganic composite-based TEGs.

SnSe is another well-established inorganic TE material with a high Seebeck coefficient and relatively low thermal conductivity which can be employed to fabricate organic/inorganic composites [503]. SnSe nanosheets/PEDOT:PSS composites fabricated by drop-casting resulted in a PF of 390 μW $m^{-1}K^{-2}$ and a ZT of 0.32 at RT at 20 wt% of SnSe nanosheets [366]. The formation of potential barriers in the composite at the interface of SnSe and PEDOT:PSS led to a significant increase in the Seebeck coefficient by filtering low energy charge carriers, and a slight decrease in the electrical conductivity, hence the improvement in PF.

In another approach, a composite of chemically exfoliated MoS_2 nanosheets (ce-MoS_2) and PEDOT:PSS was prepared by the LbL deposition method to increase the Seebeck coefficient and electrical conductivity simultaneously [504]. The fabricated composite illustrated an electrical conductivity of 867 S cm^{-1}, a Seebeck coefficient of 21.9 μV K^{-1}, and a PF of 41.6 μW $m^{-1}K^{-2}$. The improvement of electrical conductivity was attributed to the microstructural change and the removal of PSS through the secondary doping process. The energy filtering effect through the formed potential barrier in the composite and the alteration of oxidation level through de-doping with negative charged ce-MoS_2 led to an increase in Seebeck coefficient.

Moreover, several inorganic TE materials such as CuI, SnO_x, and SiO_2 have been added to OTE materials for developing high performance OTE composites. In this case, composites of PEDOT:PSS and SnO_x nanoparticles were fabricated without any ligand termination inside PEDOT:PSS thin films [505]. SnO_x nanoparticles generated by spark discharge were homogeneously deposited on PEDOT:PSS thin film via a low-energy diffusion mode. Strong interactions between the SnO_x nanoparticles and PSS chains at the top layer resulted in PEDOT chains crystalline packing at the bottom layers that effectively enhanced the electrical conductivity. Also, the SnO_x nanoparticles introduced de-doping and energy filtering effects and intensively increased the Seebeck coefficient. Ultimately, a power factor of 116 μW $m^{-1}K^{-2}$ was achieved that is six times higher than that of the film without SnO_x nanoparticles. Also, the developed three-dimensional paper PEDOT:tosylate/CuI composites resulted in a power density of 4.8 nW cm^{-2} at $\Delta T = 6$ K. This value was 10 times higher than that of the pristine paper PEDOT:Tos composites [506]. This significant improvement was attributed to the addition of the CuI nanocrystals that increase the Seebeck coefficient from 65 μV K^{-1} to 225 μV K^{-1}. Recently, self-healable and stretchable ionic TE composites have been developed by integrating SiO_2 nanoparticles in a PANI: poly (2-acrylamido-2-methyl-1-propanesulfonic acid): phytic acid (PANI:PAAMPSA:PA) ternary polymer [507]. The molecular interaction among PANI, PAAMPSA, PA, and SiO_2 are illustrated in Fig. 22a. A high ionic ZT of 3.74 was obtained in this composite at 80% relative humidity. The incorporation of SiO_2 nanoparticles effectively led to autonomous self-healability and stretchability, and the increase of the mobile proton concentration in the composites.

Decreasing the contact resistance at the interface between the organic and inorganic component in the composite is desirable to improve both electrical conductivity and Seebeck coefficient at the same time. Recently, Nan et al. investigated the mechanisms of multiple interfaces on thermal and electrical transport properties in CNTs-Te-PEDOT:PSS composite by spatially resolved current and thermal measurements [508]. The results indicated that interfacial interactions and interface density played critical roles in determining the carrier and phonon transport in organic/inorganic composites. Particularly, the formation of the highly conductive layers at the interfaces of Te-PEDOT:PSS and CNTs-PEDOT:PSS can improve the electrical conductivity and Seebeck coefficient simultaneously. Finally, a high power factor of 224 μW $m^{-1}K^{-2}$ and a ZT of 0.24 at 410 K were achieved by tuning carrier mobility and phonon scattering at the multiple interfaces in this composite. Moreover, the TE properties of PEDOT:PSS/Bi_2Te_3 composite were improved by creating defects in the crystal structure of Bi_2Te_3 through proton irradiation which resulted in a PF of 432 μW $m^{-1}K^{-2}$ and ZT of 0.18 at RT [509]. The exceptional PF of 4600 μW $m^{-1}K^{-2}$ and ZT of 1.29 at RT was achieved in a composite of $(Bi_2Te_3)_{0.2}(Sb_2Te_3)_{0.8}$ and graphene nanosheets [510]. Here, increasing the carrier concentration and mobility led to an enhancement of electrical conductivity, whereas incorporation of graphene nanosheets into the BiSbTe alloy enhanced the phonon scattering by decreasing the lattice thermal conductivity [510]. However, the aggregation of nano phases in the composite has hindered the wide use of organic/inorganic composites. To address this problem, Wang et al. [511] fabricated a flexible PEDOT/Bi_2Te_3 composite with monodispersed and periodically spaced Bi_2Te_3 particles into the PEDOT medium. The size and distance of Bi_2Te_3 particles were precisely tuned from tens to hundreds of nanometers. Also, the samples

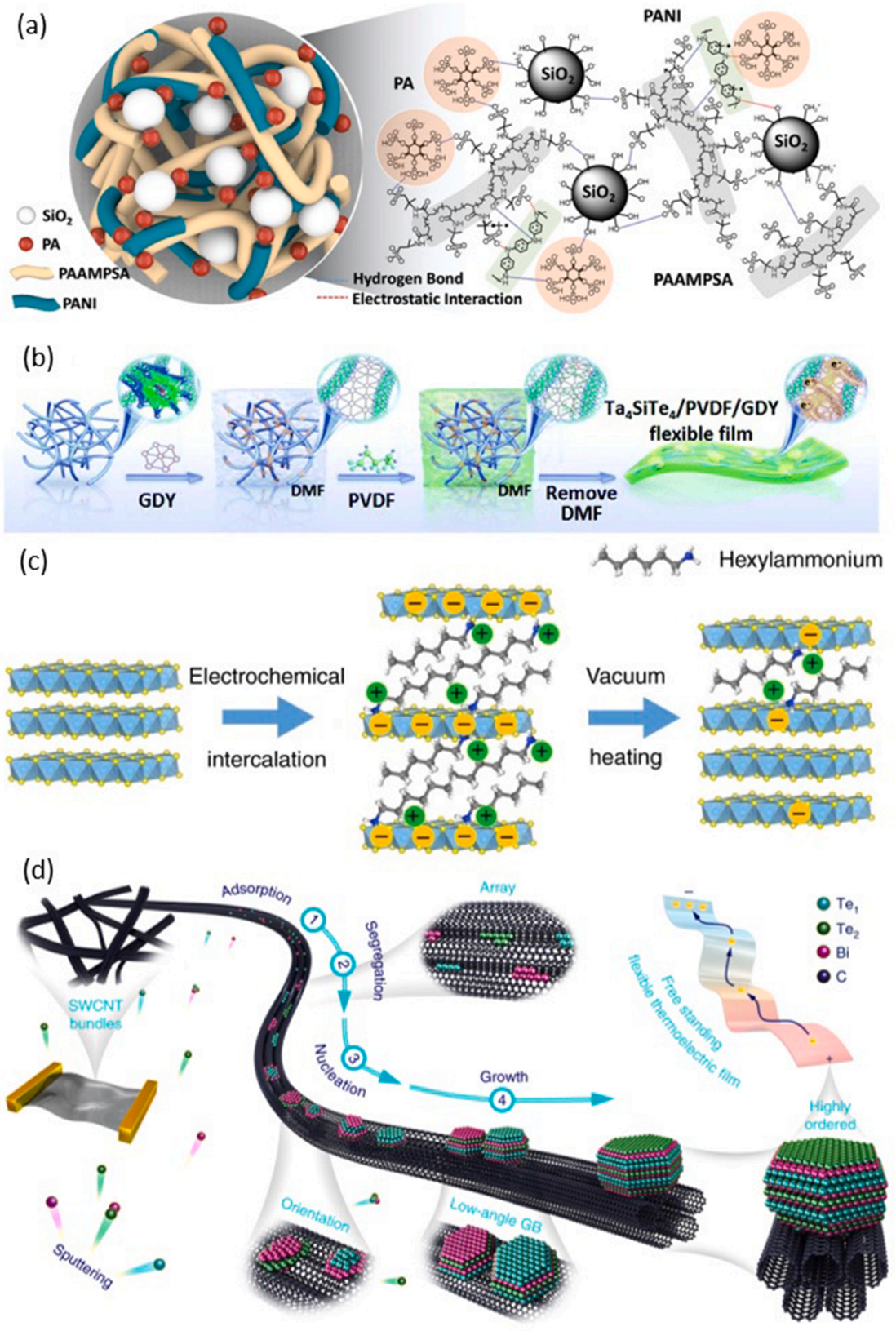

Fig. 22. (a) Schematic illustration and molecular interaction among PANI, PAAMPSA, PA, and SiO_2 in the structure of the organic/inorganic ionic TE composites. (Reprint permission from Ref. [507]) (b) Fabrication process of the Ta_4SiTe_4/GDY/PVDF composite films. (Reprint permission from Ref. [378]) (c) Evolution of structure and carrier concentration of TiS_2 single crystal with the electrochemical intercalation of HA/TBA molecules and vacuum heating. (Reprint permission from Ref. [516]) (d) Illustration of the fabrication and structure of a free-standing highly ordered Bi_2Te_3/SWCNT hybrid TE material. (Reprint permission from Ref. [376]).

were doped by tosylate. This composite showed a PF of ~1350 μW $m^{-1}K^{-2}$, and ZT of 0.58 at RT. These promising values originated from the high electrical conductivity of tosylate doped PEDOT, the high Seebeck coefficient of Bi_2Te_3 fillers, the filtering of low energy carriers at the interface of PEDOT and Bi_2Te_3 phases, and the reduction of thermal conductivity by phonon scattering at the established interfaces [511].

Although *p*-type organic/inorganic TE composites have been developed successfully, the fabrication of flexible TEGs remains challenging due to the instability of *n*-type organic/inorganic composites in the air. In this regard, many attempts have been carried out to improve the stability of organic/inorganic composites. As an example, a composite of Perylene diimide (PDI)/Te nanowires (NWs) showed good air stability and a PF of 17.6 μW $m^{-1}K^{-2}$ at 80 vol% PDI concentration [512]. The findings showed that ligand templating on inorganic nanostructures was essential for electrical and thermal transport in organic/inorganic composites. In another work, Bi_2Te_3 nanosheets were *in situ* grown on SWCNTs aided by PVP [513]. Various flexible Bi_2Te_3 nanosheets/SWCNTs composites were fabricated on PVDF membranes by vacuum-assisted filtration. Electrical conductivity of 253.9 S cm^{-1} and a power factor of 57.8 μW m^{-1} K^{-2} were achieved at 386 K. The fabricated composite kept its TE and mechanical performances for 9 months in an Ar atmosphere. Furthermore, the flexible composite of Ni NWs/PVDF illustrated stable *n*-type conductivity in air [514]. The fabricated composite containing 80 wt% of Ni NWs resulted in an electrical conductivity of 4701 S cm^{-1}, a Seebeck coefficient of - 20.6 μV K^{-1}, a PF of 200 μW $m^{-1}K^{-2}$, and a ZT of 0.1 at RT. The improved device parameters were primarily attributed to the formation of electron transport pathway through the Ni NWs networks in the host polymer [514]. Also, Liang et al. developed N2200/Co NWs/SWCNTs to fabricate a high-performance *n*-type organic/inorganic composite [515]. The presence of N2200 and SWCNTs improved the Seebeck coefficient and electrical conductivity of the composite, respectively. The optimized composite showed an electrical conductivity of 1860 S cm^{-1}, a Seebeck coefficient of -45 μV K^{-1}, a power factor of 483 μW m^{-1} K^{-2}, and a ZT of 0.18 at 380 K. Recently, semiconducting graphdiyne (GDY) has been used for developing high-performance *n*-type organic/inorganic flexible TE composites. In this case, as shown in Fig. 22b, Chen et al. developed *n*-type Ta_4SiTe_4/PVDF/GDY composite films where the homogenous distributed GDY inside the composites led to enhancement of electrical conductivity by bridging between the Ta_4SiTe_4 whiskers [378]. The optimized composite film had a maximum ZT value of 0.2 at 300 K.

The formation of layered structures and superlattices is another strategy for improving the TE efficiency of *n*-type organic/inorganic composites. These complex structures provide a platform that provides ease of transport for charge carriers as well as efficient blocking of phonons. For instance, the TiS_2[tetrabutylammonium]$_x$[hexylammonium]$_y$ layered structure comprising a random mixture of tetrabutylammonium (TBA) and hexylammonium (HA) molecules illustrated a PF of 904 μW $m^{-1}K^{-2}$ and a ZT of 0.23 at 300 K [516] (Fig. 22c).

Another strategy to attain high performance *n*-type flexible TE composites is decorating conventional inorganic TE materials with nanostructures on top of organic TE materials, which formed the highly ordered organic/inorganic TE composites. For instance, a flexible, high-performance and stable organic/inorganic composite was fabricated through scaffolding the nanocrystal of Bi_2Te_3 on top of the SWCNT belts (Fig. 22d) [376]. The fabricated composite exhibited a PF of ~1600 μW $m^{-1}K^{-2}$ and ZT of 0.89 at RT which was attributed to filtering of low-energy carriers and phonon scattering.

4.5. Summary of approaches for improving organic-based TE materials

Organic TE materials possess intrinsic low thermal conductivity but improving the electrical conductivity and Seebeck coefficient is vital for improving the TE efficiency. So far, several approaches have been introduced to enhance the TE properties of organic TE materials [384]. These strategies are briefly summarized below:

(a) The TE properties of organic materials strongly relate to their physical and chemical properties. Particularly, a polymer with a highly ordered microstructure leads to high carrier mobility and high TE performance. For example, in the case of PEDOT films doped with p-toluenesulfonate molecules, improving the charge carrier mobility due to well-oriented PEDOT chains along the substrate resulted in a three-fold increase in the electrical conductivity. While the Seebeck coefficient remained constant, the PF significantly increased from 25 to 78.5 μW $m^{-1}K^{-2}$ [517]. Furthermore, the polymer molecular weight, chemical structure and thin-film microstructure can influence the electronic and thermal charge transport mechanisms [518]. As an example, in the case of poly(3-alkylthiophene)s, the shorter alkyl side chains resulted in longer nanofibres and also higher electrical conductivity while the Seebeck coefficient was independent of the length of alkyl side chains [519].

(b) The doping process is one of the main methods to regulate the TE properties of organic materials. Since an optimal charge carrier concentration in TE materials leads to the maximum PF, molecular doping of organic materials can effectively optimize the concentration of charge carriers in the backbone of polymer, e.g., polaron and bipolaron through chemical oxidation or reduction process [520]. For instance, the electrical conductivity of the polar polythiophene derivative (p($g_4$2T-T)) was increased by four orders of magnitude by molecular doping with 2,3,5,6-tetrafluoro-7,7,8,8-tetracyanoquinodimethane (F4TCNQ) through the co-processing method [521].

(c) The fabrication of organic composites with low dimensional carbon-based materials such as CNT, graphene, and C_{60} can significantly enhance their TE properties due to promising chemical, physical, thermal, and electrical properties of carbon-based materials [33]. One of the main reasons for this improvement is the formation of well-aligned polymer chains, which results in an enhanced charge carrier mobility. For example, applying the CNTs to PANI resulted in the alignment of PANI chains, reduction of π-π conjugated defects, and the charge carriers' localization which resulted in higher charge carrier mobility and enhanced TE properties [474].

(d) Another promising approach to enhance the TE properties of organic materials is fabricating organic/inorganic composites [370]. These types of materials have been introduced as the new class of flexible TE materials, which have the advantages of both organic and inorganic TE materials. These composites contain two main contributions: (1) enhancing the Seebeck coefficient by filtering the charge carriers with lower energy at the energy barrier formed at the interface of organic and inorganic parts, (2) reducing the thermal conductivity by phonon scattering at the formed interface [522,523]. The weight of these two contributions depends on the type of organic and inorganic materials, and the features of established energy barriers. The rational design of interfaces between inorganic and organic materials in a composite and understanding the underlying mechanism of formed interfaces are the effective methods for obtaining an efficient organic/inorganic TE composite. For instance, the PF of P3HT/Bi_2Te_3 composite was improved from 3.9 μW $m^{-1}K^{-2}$ for P3HT to 13.6 μW $m^{-1}K^{-2}$ for the composite, as a result of enhanced Seebeck coefficient due to the filtering of lower energy charge carriers [524].

4.6. Fabrication of organic TE devices

4.6.1. Drop casting

Drop casting is a simple method for the fabrication of thin films based on solutions made of nanoparticles, nanocomposites, and general

organic and inorganic compounds [525]. In this method, as shown in Fig. 23a, firstly a predetermined amount of solution is dropped onto a substrate followed by evaporation at ambient conditions or by heating the substrate. The substrate material can be organic or inorganic, in flexible or rigid forms. Generally, in this method, a ring pattern named the coffee ring effect is produced in the thin film due to the liquid-solid surface tension between the edge of the droplet and substrate [525]. So far, different approaches, e.g., using anisotropic particles [526], have been utilized to suppress the coffee ring effect. Several organic and inorganic TE materials and their composites such as P3HT/CNT [480], CNT/poly(vinylidene fluoride) (PVDF) [527], SWCNT/PEI [470], PEDOT:PSS/Bi_2Te_3 nanosheet [528] and Bi_2Te_3 nanoplate [529] have been fabricated by this method.

4.6.2. Spin coating

Spin coating is a simple solution-based method for the fabrication of thin films with thickness in the range of nm to μm. Spin coating can be applied to a wide range of organic and inorganic materials and their composite materials [530]. In this process, as shown in Fig. 23b, firstly the solution is cast on top of a planar substrate which can be spun either before or after drop casting. After that, the substrate is spun at a predetermined speed followed by the evaporation of the solvent. Finally, a thin film is fabricated. The solution viscosity, the solution and substrate surface energies, spinning speed, and spinning duration, are the four key parameters of the spin coating process which determine the thin film physical, electrical, and thermal properties [530]. One of the most prominent applications of this method is coating the resist layer in the photolithography process used in fabrication technology, e.g., for the fabrication of TEGs. Several organic TE materials such as PEDOT:PSS [365], PEDOT/Si composite [531], and SWCNT/P3HT composite [532] have been fabricated through the spin coating process.

4.6.3. Electrospinning

Nanofibers can be produced from polymer solutions or melts using the electrospinning method, under a high electrical voltage [533]. So far, several organic TE materials such as carbon nanofibers (CNFs) [534], CNT/PANI composite [474] and PANI/(polystyrene and polyethylene oxide) blends [535] have been developed by this method. The required high voltage for starting the spinning process is applied to the solution. This voltage is connected between a needle of a syringe and collectors, then the material is deposited on the collector (Fig. 23c). The formation of nanofibers begins when the applied electrical voltage prevails over the solution's surface tension. The chemical and physical properties of the produced fibers depend on the solution parameters, the process factors, and the ambient conditions during the electrospinning process [533].

4.6.4. Printing technology

Printing is a fabrication technique for creating complicated geometry in comparison with the subtractive fabrication method. Printing technology creates a new research pathway to thermoelectricity through the easy fabrication of TE devices with complex geometry and higher conversion performance [383,536]. The printing processes that use ink for the fabrication of TE devices are mainly classified into inkjet, dispenser, and screen-printing methods. The physiochemical parameters of inks such as dispersibility, concentration, and rheological properties play a key role in obtaining high quality products with the desired chemical, physical, thermal, magnetic, and electrical properties [537]. In this regard, understanding these factors is crucial for the printing process of TE materials. One of the significant properties of organic TE materials is their good compatibility with the ink printing process. Fig. 23d schematically shows the inkjet printing technique which consists of continuous and drop-on-demand (DOD) methods [538]. Fig. 23e, f illustrates the working principle of screen printing and dispenser printing techniques [539,540]. As a recent example, the ink of hybrid Te NWs and PEDOT:PSS was formulated followed by the fabrication of high performance and flexible TEGs by the dispensing printing method [541]. The fabricated composites and flexible TEGs illustrated a maximum power factor of 102.42 μW m^{-1} K^{-2} and a power output of ~ 4.5 μW at $\Delta T = 100$ K, respectively. Moreover, a monolithic micro-OTEG was fabricated on a plastic substrate by a combination of direct lasering and inkjet printing methods [542]. The p- and *n*-type legs of the micro-OTEG comprised PEDOT:PSS and a doped fullerene derivative. The fabricated micro-OTEG demonstrated a power density of 30.5 nW cm^{-2} under a temperature gradient of 25 K around RT. Also, as shown in Fig. 23g, h, an OTEG consisting of 100 leg pairs of *p*-type PEDOT:Nafion composite was fabricated using melt extrusion followed by fused filament 3D printing [399]. The TE legs were connected by an ABS/Carbon black blend. The fabricated OTEGs resulted in a maximum output power of ~0.7 nW at $\Delta T = 53$ K.

5. Hybrid PV-TEG systems

The sun is undeniably one of the key renewable energy sources [546]. PV panels directly convert radiation energy to electricity and TEGs directly convert the heat of infrared energy to electricity. Therefore, the combination of PV and TE could be utilized for producing more electrical energy than the electricity produced by a single PV or TE system. The two most common technologies for fabricating hybrid PV-TEG systems to utilize the full solar spectrum are spectrum splitting PV-TEG systems and integrated PV-TEG systems. The advantages of hybrid PV-TEG systems over single PV and TEG systems are the reduced heat dissipation of PV by incorporation of TEGs and using a wide range of the solar radiation spectrum from infrared to ultraviolet. A summary of different PV-TEG hybrid systems developed so far are discussed in the following sections.

5.1. Spectrum splitting PV-TEG system

PV devices usually operate optimally when the photon energy is close to the band gap energy. However, photons with energy smaller or larger than the PV band gap energy can only be used partly. In the spectrum splitting PV-TEG system, the solar spectrum is divided into two parts: the suitable wavelength for PV in the range of 200 nm to 800 nm, and remaining wavelengths in the range of 800 nm to 3000 nm for the TEG. In general, spectrum splitting PV-TEG systems consist of a solar concentrator, the spectrum splitting device, PV devices, TEGs, and cooling systems (Fig. 24a). For the spectrum splitting PV-TEG system, several studies have been carried out to investigate their performance and practical application [547], including optimization of the cut-off wavelength and the power fractions of each segment [548], thermal management [549], and the influence of concentration ratio and cooling condition [550].

5.2. Integrated PV-TEG system

In integrated PV-TEG systems, the TEG is attached to the back of PV modules for thermal energy harvesting (Fig. 24b). Many experimental and theoretical works have been performed to study different aspects of the integrated PV-TEG system such as optimization of the absorbing layer, conducting layer, and insulating layer between the PV and the TEG for heat collection [551], providing a sun tracking system [552], optimization of the hybrid system structure [553], and the impact of high ZT value on total efficiency [554].

5.3. Optimization and development of hybrid PV-TEG system

The hybrid PV-TEG system is a complex system which involves additional energy transfer and conversion processes. In general, the use of high ZT materials for TEGs, the use of highly efficient PV cells and optimizing thermal management of the hybrid system are introduced to improve the performance of a hybrid PV-TEG system. Moreover, more

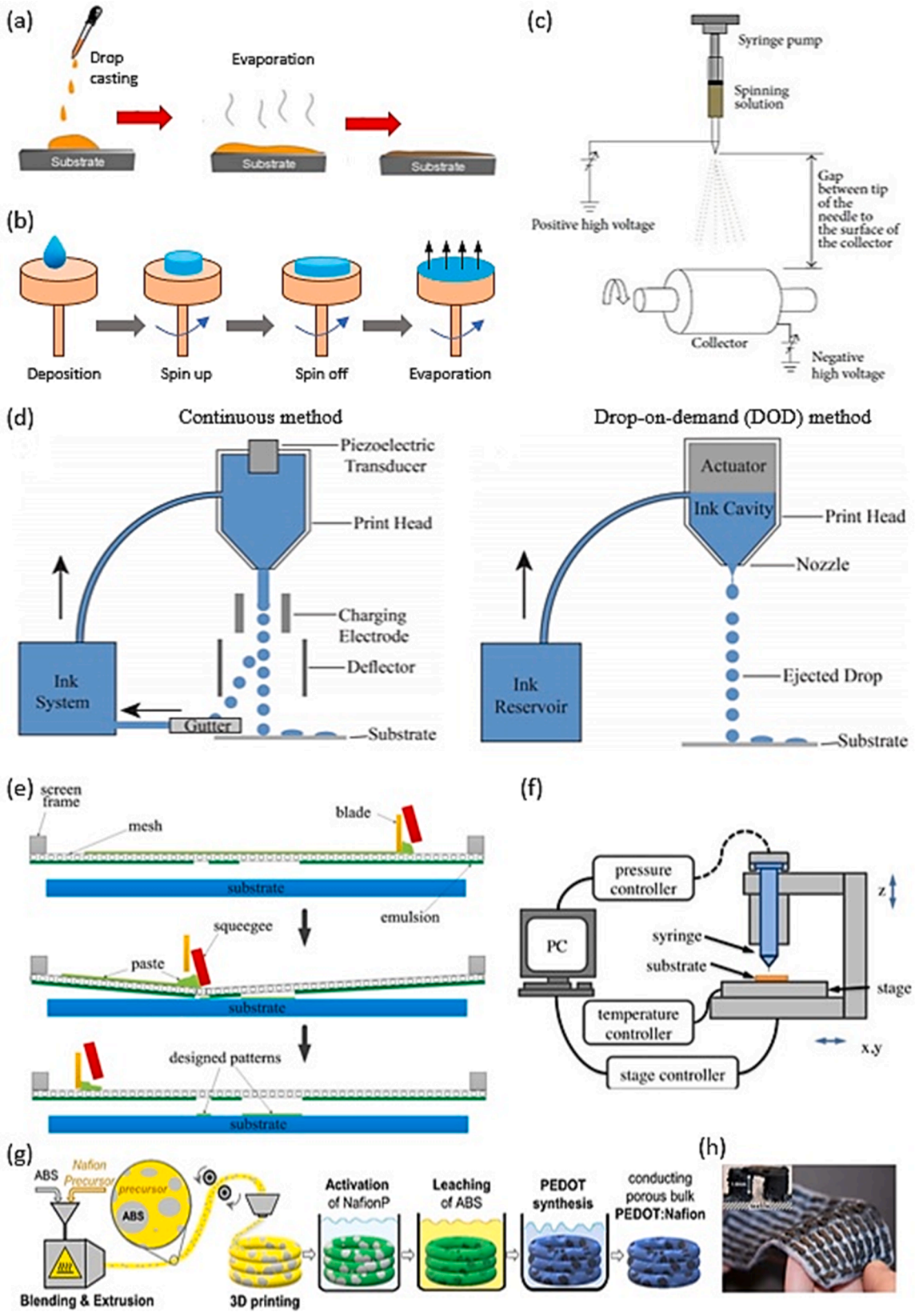

Fig. 23. The schematic diagram of: (a) a drop casting method (Reprint permission from Ref. [543]), (b) a spin coating method, (c) a basic electrospinning setup (Reprint permission from Ref. [544]), (d) continuous inkjet printing and drop-on-demand inkjet printing (Reprint permission from Ref. [545]), (e) screen printing process (Reprint permission from Ref. [540]), and (f) dispenser printing process (Reprint permission from Ref. [539]). (g) Processing schematic for the fused filament fabrication 3D printing of the precursor/ABS blend to obtain PEDOT:Nafion bulk structures. (h) Photograph of 100-leg OTEG and the inset shows a single leg pair. (Reprint permission from Ref. [399]).

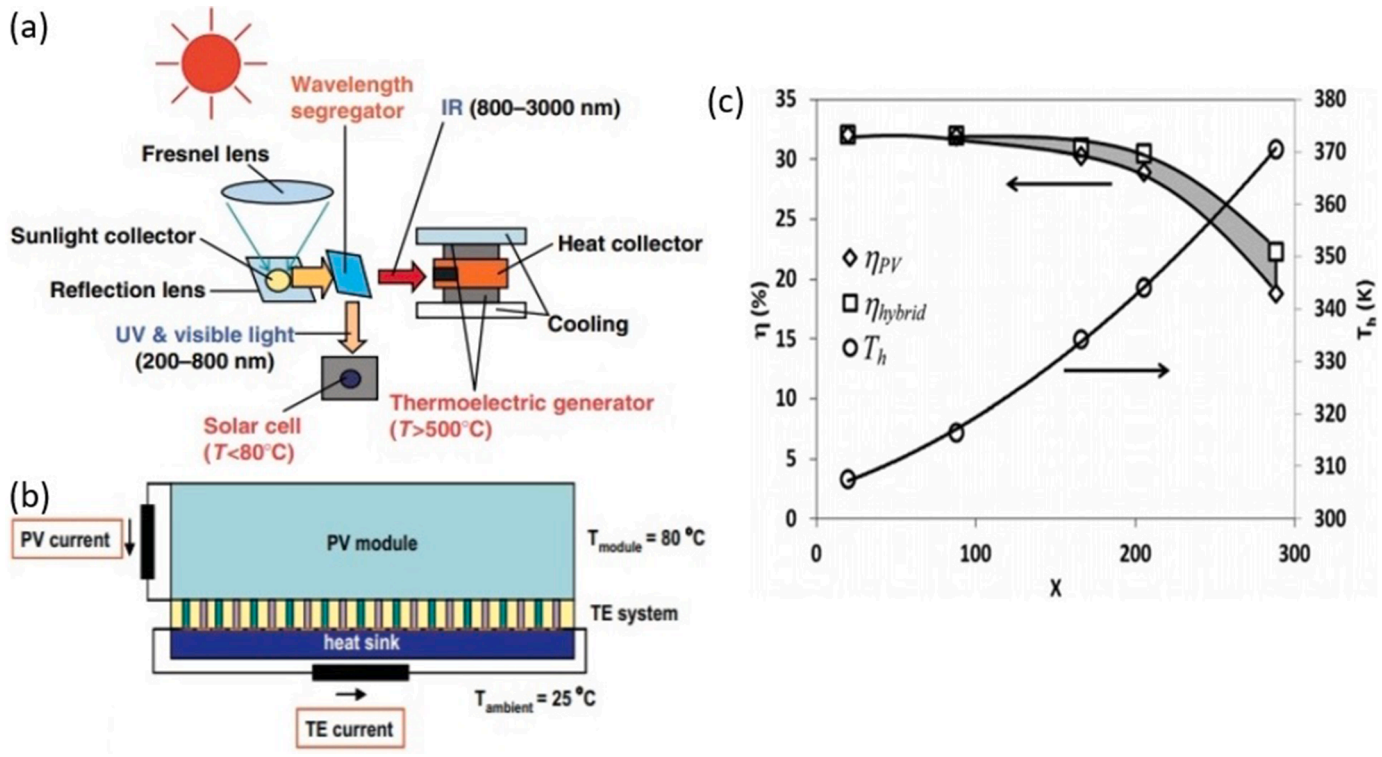

Fig. 24. (a) Spectrum splitting in a hybrid PV-TEG system (Reprint permission from Ref. [571]). (b) Schematic of an integrated PV-TEG system. (Reprint permission from Ref. [554]) (c) Variation of electrical efficiency of a PV, efficiency of a hybrid PV-TEG, and hot side temperature (T_h) of a TEG with concentration factor (X). (Reprint permission from Ref. [569]).

components such as cooling medium, concentrator, the geometrical parameters of individual PV and TEGs and their hybrid system can be optimized to improve the overall efficiency. Additionally, TEG and PV cell modules have different behavior with temperature; the former's efficiency improves with higher temperature gradient while the latter's efficiency declines with temperature. This discrepancy makes the optimization of hybrid PV-TEG system parameters challenging. Hybrid PV-TE performance optimization can be classified into the following sections.

5.3.1. *Efficiency temperature coefficient of the PV cell*

The temperature coefficient defines the sensitivity of PV cells to temperature rise which is a key factor for designing hybrid PV-TEG systems. In this system, for providing temperature differences for TEG operation, the intensity of the incident solar radiation on the PV cell is increased by a concentrator which leads to an increase PV cell temperature. This increasing temperature impacts the electron–hole recombination and consequently decreases the performance of the PV cells. Consequently, this temperature regulation is important in the design of hybrid PV-TEG systems. It has been reported that the reduction of efficiency in hybrid systems can be compensated by the energy generated from the TEG when the hybrid system uses PV cells which are not sensitive to the temperature rise [555].

5.3.2. *Material optimization*

The ZT of TE materials is a key parameter of the performance of the TEG which strongly affects the total performance of the hybrid PV-TEG systems. Therefore, selecting a material with high ZT for a TEG depends on the operating temperature of PV-TEG systems. Bi_2Te_3, PbTe, and SiGe were mostly used for operating PV-TEG systems below 500 K, 500 K to 900 K, and above 900K, respectively. The efficiency of PV-TEG hybrid systems can be enhanced using higher ZT materials. However, high thermal loss in the TEG causes poor efficiency even when using high ZT materials. Furthermore, it has been shown that both organic and inorganic materials used in PV play a key role in the development of hybrid PV-TEG systems. Both organic and inorganic PV based on dye-sensitized [556], polymer [557], Perovskite [558], GaAs [559], and silicon-based [554] materials were utilized for the fabrication of PV-TEG hybrid systems.

5.3.3. *Structural optimization*

Structural optimization of TEGs implies the determination of the number of thermoelements [560], the area ratio of the hot and cold junctions [561], the thermoelement area ratio [562], and the geometry of TE legs [563] that will result in maximum electrical power. It has been reported that the optimal design for a TEG-only system might not be the same as that for a hybrid PV-TEG system. For instance, maximum output power of a hybrid PV-TEG system has been achieved with symmetric thermoelements area while this does not happen in TEGs [564]. In the case of PV cells, the use of nanostructured surfaces in the PV cells enhanced the solar energy conversion efficiency due to more irradiance absorption. Zhou et al. illustrated in two different works that the nanostructured surface of the PV cell improved the overall conversion efficiency of the PV-TEG system [565,566].

5.3.4. *Concentration ratio*

Solar concentration affects the performance, and the cost of hybrid PV-TEG systems which depend on the type of solar cells employed and subsequently on the temperature coefficient [567]. Higher concentration ratios provide greater contribution of the TEG in terms of power generation, but there is a trade-off between efficiency contribution of the TEG and the PV cell [568]. Beeri et al. [569] experimentally and numerically calculated that maximum efficiency of 32% could be reached with a concentrated factor (the ratio of the radiant power density at the collector to the radiant power density of the sun light without any concentration) below 200 in hybrid PV-TEG systems, while the TEG efficiency contribution reached 40% at a concentrated factor of 200 (Fig. 24c).

5.3.5. Convective heat transfer coefficient of the cooling system

The heat transfer coefficient strongly influences the performance of PV-TEG systems due to the dependency of the temperature distribution through the layers of the coupled PV-TEG to the level of cooling, especially at higher concentration ratios. Low heat transfer coefficients lead to increased cell temperatures and a low temperature difference across the TEG, subsequently resulting in lower efficiency of the PV cell and low output power generated by the TEG. Conversely, high heat transfer coefficient for PV-TEG systems leads to enhancement of the temperature distribution across the PV system and a higher temperature difference between the junctions of the TEG. Falah et al. [570] developed a 3D model of PV-TEG system and showed that the contribution of the TEG to the overall performance of the hybrid system increased marginally at a convective coefficient of $h = 35\ W\ m^{-2}K^{-1}$, and subsequently decreased at higher convective coefficients due to the additional thermal resistance produced by attaching TEG to the PV module. Moreover, they reported that using an efficient cooling system can improve the total hybrid system output at the same operating condition.

5.4. Inorganic PV-inorganic TEG hybrids

Many experimental and theoretical studies have been performed to design, fabricate, and characterize PV devices. According to these investigations, PV devices can be categorized into the following groups: PV devices based on (1) single crystal and polycrystalline silicon which are commercialized, (2) thin film amorphous silicon, and CdTe, and (3) organic materials and III-V compounds [572,573]. On the other hand, TE devices based on inorganic materials such as Bi_2Te_3 and its related compounds are commercially available [574]. Consequently, the hybrid PV-TE devices not only can improve the solar conversion efficiency of PV, but also may enhance the overall energy conversion efficiency. The hybridization of inorganic PV and TE devices has attracted attention due to their commercial availability and high energy conversion efficiency. In these hybrid systems, the PV part was mostly made of polycrystalline and crystalline silicon, multi junctional structure, perovskites, and GaAs [574] and the TE part was typically constructed from Bi_2Te_3 [574]. Most of the reported theoretical and experimental investigations have been oriented towards thermal management strategies [575], design and evaluation of systems with optical concentration tools [576], increasing the material efficiency [577], and TE and PV structural optimizations [578]. These works have revealed that the hybrid inorganic PV-TE system is unable to improve the overall efficiency and can only compensate for the decrease of PV efficiency due to rising the temperature.

5.5. Organic PV-inorganic TEG hybrids

Organic PV devices have been employed in hybrid PV-TE systems due to their low-cost fabrication and compatibility with mass production process like roll-to-roll printing techniques [574,579,580]. Moreover, since organic PV devices are typically semi-transparent in comparison with their inorganic counterpart in the range of the visible spectrum, the TE parts can effectively utilize this range of light through the adsorption layer for converting the thermal energy to electricity [581,582]. Owing to relatively low thermal stability of organic materials, the operating temperature of these hybrid systems is restricted to below 400 K [583]. The inorganic TE module made of Bi_2Te_3 compounds is used in these PV-TEG hybrid devices [556]. In the case of organic PV devices, the polymer [584,585], and dye-sensitized [556,586] PV devices have been used in these hybrid systems. For instance, a hybrid PV-TE device was fabricated in which the PV part was made of P3HT/indene-C_{60} and PEDOT:PSS layers, and the TE part was the commercial TGP-715 chip [585]. While a temperature difference along the TE parts was introduced through the wasted solar radiation in the form of thermal energy, the output power of the hybrid system improved compared with that of the PV device alone. At a temperature difference of 9.5 K, the hybrid system increased the maximum output power from 6.02 mW cm^{-2} to 11.29 mW cm^{-2}, and the *Voc* from 0.87 V to 1.72 V [585].

5.6. Organic PV-organic TEG hybrids

Many inorganic PV devices have been utilized for the fabrication of hybrid PV-TEG systems while fewer investigations have been performed on organic PV-based hybrid systems. Surprisingly, almost all the research used commercial TEGs or inorganic based TEGs to integrate with PV cells. All organic PV-TEG systems can have the advantages of being cost-effective, light-weight, flexible, and scalable via solution processing. In this regard, for the first time, Suzuki et al. [584] fabricated an all organic hybrid PV-TEG system which operated selectively in PV or TEG mode using P3HT and $PC_{61}BM$. However, the efficiency of the fabricated device was low, and it could not work in both PV and TEG modes at the same time. Subsequently, Lee et al. [557] fabricated non-flexible an all organic-based PV-TEG using PEDOT:PSS (Fig. 25). More recently, Campoy-Quiles et al. [382] investigated the effect of geometry on energy conversion efficiency in all organic PV-TE device. They considered reflection, non-contact, and contact transmissions geometries in their work. They concluded that the contact transmission geometry resulted in a high energy conversion efficiency due to the production of high temperature differences for the TEG. It is worth mentioning that apart from the aforementioned reports, work on all organic flexible PV-TEG hybrid device systems is yet to be reported. Consequently, increased research focus is needed for the development of all organic PV-TEG systems, and the realization of wearable and flexible energy devices based on this technology.

6. Summary and outlook

There has been remarkable progress in the development of organic solar cells (OSC) in the last few years, particularly with the emergence of NFA materials. Continuing efforts on the design and development of novel high-performing materials and devices would be greatly benefited by further understanding the direct correlation between the resultant material energetics in BHJ blends, to the resultant morphology, voltage losses and stability of respective devices. Further research efforts in developing water/alcohol processable and sustainable solvent alternatives for active layers and compatible HTL materials are likely to accelerate the transition of OSC technology from the laboratory scale to real-world low-cost technologies with a high power-to-weight ratio for future electricity generation.

Based on recent progress made in the field of organic photovoltaics (OPV) at large, it is reasonable to believe that in the next decades, photovoltaic technology would be one of the most accessible and predominantly used methods of generating energy. OPV technology is expected to complement rather than entirely replace the silicon-based first-generation solar cells, as the advent of low-cost, semitransparent, and flexible OSCs in the consumer market will open enormous opportunities for novel applications such as building-integrated photovoltaics, green house installations, powering smart wearables and portable electronics, and harvesting indoor-lighting for IoT. Unlike electricity, which is generated and distributed over long distances, large scale use of OPV technology would result in a scenario where clean and portable renewable energy would be in ample supply and harvested local to the source of consumption. Therefore, future works should focus on methods to enhance and consistently evaluate the outdoor reliability of OSCs. Further research efforts should also be made to develop low-cost, sustainable, and environmentally benign energy storage solutions as well as energy-efficient recycling of organic electronic devices.

The use of flexible organic TEGs to harvest energy from the human body to provide a power source for portable and wearable electronic devices has sparked much scientific interest. Despite significant improvements in *p*-type organic TE materials and a confirmed RT dimensionless figure of merit (ZT) of 0.42 in PEDOT:PSS, *p*-type organic TE

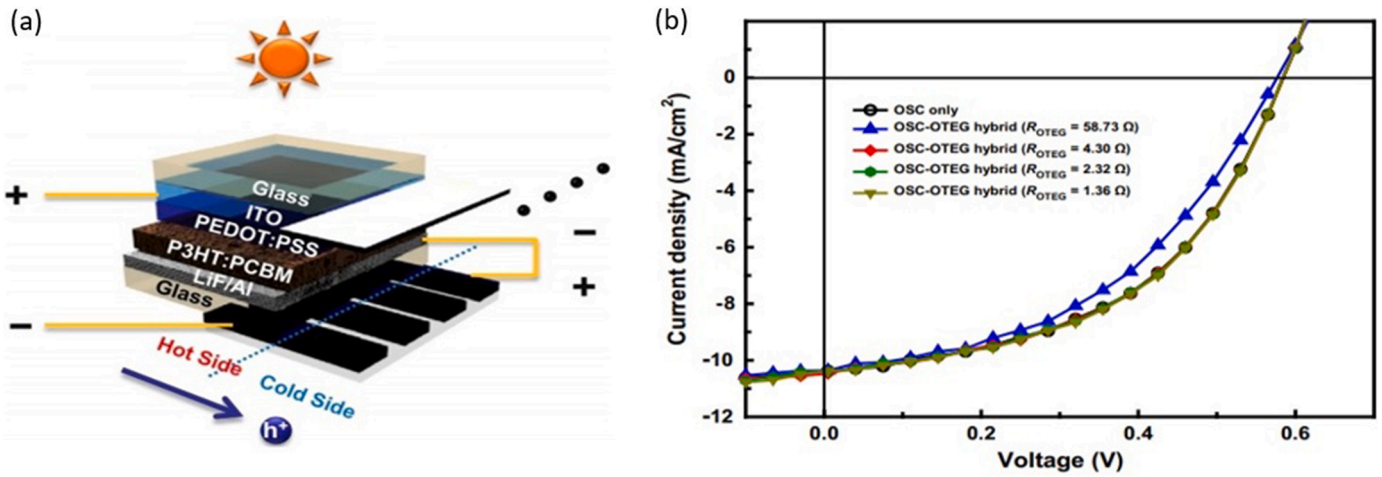

Fig. 25. (a) Schematic illustration of a PV-organic TEG hybrid device using a highly conductive PEDOT:PSS film, and (b) Photocurrent density - voltage curves of the PV-TEG hybrid device for various PEDOT:PSS films as the TEG. (Reprint permission from Ref. [557]).

materials' performance remains poor as compared to their inorganic counterparts. The preparation of organic/inorganic composites for achieving high ZT organic based TE materials has recently been introduced as a promising research approach. In this area, interfacial engineering and the underlying mechanisms for electronic/thermal transport from the viewpoint of analytical and numerical models should be well studied. In addition to theoretical studies, further experimental work is required to analyze the design of interfacial phases towards lowering the electrical resistance and enhancing thermal resistance in order to improve the TE efficiency. In contrast to *p*-type organic TE materials, *n*-type counterparts with comparable flexibility, stability, and ZT values are yet to be developed. In this case, small molecules and MOFs are good candidates for future research. For instance, butterfly-shaped small molecule/SWCNT composites open a new pathway for developing a new class of OTE materials.

In comparison to traditional fabrication methods, printing technologies, which cover a wide range of materials from organics to inorganics and allow for the manufacturing of complex structures with tailored geometry and functionality, have sparked a new wave of interest in next-generation modular organic TE products. However, it should be mentioned that printing-based manufacturing of flexible organic TEGs is still in its infancy. Nevertheless, these technologies not only illustrate a great potential for fabricating highly efficient TEGs for niche energy harvesting applications, but also provide the ability to fabricate high ZT flexible organic TE materials. For instance, much research should be oriented toward improving the durability and enhancing the TE properties of ink-processed and printed TE materials. Future works should focus on comprehensive understanding of host-dopant interactions and dopant stability in TE inks, for future development of flexible organic TEGs. Electrode materials, bonding methods, and metallization of materials in printing technology should be further developed to fabricate high-performance flexible organic TEGs.

Furthermore, the concept of hybrid PV-TEG systems to co-power generate from light and heat has attracted extensive attention recently. However, there are a limited number of reports in the literature for flexible PV-TEG hybrid systems. Consequently, extensive research is needed to expound flexible PV-TEG hybrid devices based on organic materials for wearables applications. In this context, future directions should be oriented towards; (i) novel device-level designs of flexible PV-TEG hybrid systems using current state-of-the-art organic semiconductors, (ii) reduction of the thermal resistance between the PV and the TEG, (iii) investigation on the effect of outdoor ambient air atmosphere during a full year on the total efficiency of PV-TEG devices, and (iv) optimization of PV-TEG hybrid systems towards mass production and cost-effectiveness.

Declaration of Competing Interest

The authors affirm that there are no conflicts of interest to declare.

Data Availability

No data was used for the research described in the article.

Acknowledgment

AP is thankful for the financial support of Science Foundation Ireland (SFI) under Grant No. 18/SIRG/5621. AS and DB acknowledge the support of KAUST Office of Sponsored Research (OSR) under award number OSR-2019-CARF/CCF-3079.

References

[1] A.E. Becquerel, Recherches sur les effets de la radiation chimique de la lumiere solaire au moyen des courants electriques, Comptes Rendus de L'Acad. Sci. 9 (1839) 145–149.
[2] C.E. Fritts, On a new form of selenium cell, and some electrical discoveries made by its use, Am. J. Sci. s3-26 (1883) 465–472, https://doi.org/10.2475/ajs.s3-26.156.465.
[3] D.M. Chapin, C.S. Fuller, G.L. Pearson, A new silicon *p-n* junction photocell for converting solar radiation into electrical power, J. Appl. Phys. 25 (1954) 676–677, https://doi.org/10.1063/1.1721711.
[4] M.A. Green, Silicon photovoltaic modules: a brief history of the first 50 years, Prog. Photovolt. 13 (2005) 447–455, https://doi.org/10.1002/pip.612.
[5] S.S. Sun, N.S. Sariciftci, Organic Photovoltaics: Mechanisms, Materials and Devices, Taylor & Francis, Boca Raton, FL, 2005.
[6] Photovoltaic report, Fraunhofer Institute for Solar Energy Systems, 2019.
[7] R.G. Kepler, Charge carrier production and mobility in anthracene crystals, Phys. Rev. 119 (1960) 1226–1229, https://doi.org/10.1103/PhysRev.119.1226.
[8] H. Shirakawa, E.J. Louis, A.G. MacDiarmid, C.K. Chiang, A.J. Heeger, Synthesis of electrically conducting organic polymers: halogen derivatives of polyacetylene, (ch), J. Chem. Soc. Chem. Commun. (1977) 578–580, https://doi.org/10.1039/C39770000578.
[9] D.M. Ivory, G.G. Miller, J.M. Sowa, L.W. Shacklette, R.R. Chance, R. H. Baughman, Highly conducting charge-transfer complexes of poly(p-phenylene), J. Chem. Phys. 71 (1979) 1506–1507, https://doi.org/10.1063/1.438420.
[10] M. Brie, R. Turcu, C. Neamtu, S. Pruneanu, The effect of initial conductivity and doping anions on gas sensitivity of conducting polypyrrole films to nh3, Sens. Actuators B Chem. 37 (1996) 119–122, https://doi.org/10.1016/S0925-4005(97)80125-6.
[11] G.E. Wnek, J.C.W. Chien, F.E. Karasz, C.P. Lillya, Electrically conducting derivative of poly(p-phenylene vinylene), Polymer 20 (1979) 1441–1443, https://doi.org/10.1016/0032-3861(79)90002-8.
[12] P.N. Bartlett, S.K. Ling-Chung, Conducting polymer gas sensors part iii: results for four different polymers and five different vapours, Sens. Actuators 20 (1989) 287–292, https://doi.org/10.1016/0250-6874(89)80127-1.

[13] J.J. Langer, Conformations of aniline black (polyaniline) molecules, Synth. Met. 20 (1987) 35–41, https://doi.org/10.1016/0379-6779(87)90542-X.

[14] M.R. Andersson, M. Berggren, O. Inganaes, G. Gustafsson, J.C. Gustafsson-Carlberg, D. Selse, T. Hjertberg, O. Wennerstroem, Electroluminescence from substituted poly(thiophenes): from blue to near-infrared, Macromolecules 28 (1995) 7525–7529, https://doi.org/10.1021/ma00126a033.

[15] X. Pan, A. Sharma, R. Kroon, D. Gedefaw, S. Elmas, Y.T. Yin, G.G. Andersson, D. A. Lewis, M.R. Andersson, Water/ethanol soluble *p*-type conjugated polymers for the use in organic photovoltaics, Front. Mater. 7 (2020) 1–13, https://doi.org/10.3389/fmats.2020.00281.

[16] M. Seri, M. Bolognesi, Z. Chen, S. Lu, W. Koopman, A. Facchetti, M. Muccini, Fine structural tuning of cyanated dithieno[3,2-b:2′,3′-d]silole–oligothiophene copolymers: Synthesis, characterization, and photovoltaic response, Macromolecules 46 (2013) 6419–6430, https://doi.org/10.1021/ma4011186.

[17] L. Valentini, D. Bagnis, A. Marrocchi, M. Seri, A. Taticchi, J.M. Kenny, Novel anthracene-core molecule for the development of efficient PCBM-based solar cells, Chem. Mater. 20 (2008) 32–34, https://doi.org/10.1021/cm703011k.

[18] A. Abbotto, M. Seri, M.S. Dangate, F. De Angelis, N. Manfredi, E. Mosconi, M. Bolognesi, R. Ruffo, M.M. Salamone, M. Muccini, A vinylene-linked benzo[1,2-b:4,5-b′]dithiophene-2,1,3-benzothiadiazole low-bandgap polymer, J. Polym. Sci. Part A Polym. Chem. 50 (2012) 2829–2840, https://doi.org/10.1002/pola.26046.

[19] A.J. Heeger, Semiconducting polymers: the third generation, Chem. Soc. Rev. 39 (2010) 2354–2371, https://doi.org/10.1039/B914956M.

[20] A.C. Arias, J.D. MacKenzie, I. McCulloch, J. Rivnay, A. Salleo, Materials and applications for large area electronics: solution-based approaches, Chem. Rev. 110 (2010) 3–24, https://doi.org/10.1021/cr900150b.

[21] J.H. Burroughes, D.D.C. Bradley, A.R. Brown, R.N. Marks, K. Mackay, R. H. Friend, P.L. Burns, A.B. Holmes, Light-emitting diodes based on conjugated polymers, Nature 347 (1990) 539–541, https://doi.org/10.1038/347539a0.

[22] V. Ahmad, A. Shukla, J. Sobus, A. Sharma, D. Gedefaw, G.G. Andersson, M. R. Andersson, S.C. Lo, E.B. Namdas, High-speed oleds and area-emitting light-emitting transistors from a tetracyclic lactim semiconducting polymer, Adv. Opt. Mater. 6 (2018), 1800768, https://doi.org/10.1002/adom.201800768.

[23] A. Sharma, S. Singh, X. Song, D. Rosas Villalva, J. Troughton, D. Corzo, L. Toppare, G. Gunbas, B.C. Schroeder, D. Baran, A nonionic alcohol soluble polymer cathode interlayer enables efficient organic and perovskite solar cells, Chem. Mater. 33 (2021) 8602–8611, https://doi.org/10.1021/acs.chemmater.1c01430.

[24] C.M. Benavides, P. Murto, C.L. Chochos, V.G. Gregoriou, A. Avgeropoulos, X. Xu, K. Bini, A. Sharma, M.R. Andersson, O. Schmidt, C.J. Brabec, E. Wang, S.F. Tedde, High-performance organic photodetectors from a high-bandgap indacenodithiophene-based π-conjugated donor–acceptor polymer, ACS Appl. Mater. Interfaces 10 (2018) 12937–12946, https://doi.org/10.1021/acsami.8b03824.

[25] D. Rosas Villalva, S. Singh, L.A. Galuska, A. Sharma, J. Han, J. Liu, M.A. Haque, S. Jang, A.H. Emwas, L.J.A. Koster, X. Gu, B.C. Schroeder, D. Baran, Backbone-driven host–dopant miscibility modulates molecular doping in ndi conjugated polymers, Mater. Horiz. 9 (2022) 500–508, https://doi.org/10.1039/D1MH01357B.

[26] T. Cao, X.L. Shi, J. Zou, Z.G. Chen, Advances in conducting polymer-based thermoelectric materials and devices, Microstructures 1 (2021) 1–33, https://doi.org/10.20517/microstructures.2021.06.

[27] S. Xu, X.L. Shi, M. Dargusch, C. Di, J. Zou, Z.G. Chen, Conducting polymer-based flexible thermoelectric materials and devices: from mechanisms to applications, Prog. Mater. Sci. (2021), 100840, https://doi.org/10.1016/j.pmatsci.2021.100840.

[28] L. Zhang, X.L. Shi, Y.L. Yang, Z.G. Chen, Flexible thermoelectric materials and devices: from materials to applications, Mater. Today (2021), https://doi.org/10.1016/j.mattod.2021.02.016.

[29] Z. Fan, Y. Zhang, L. Pan, J. Ouyang, Q. Zhang, Recent developments in flexible thermoelectrics: from materials to devices, Renew. Sustain. Energy Rev. (2020), 110448, https://doi.org/10.1016/j.rser.2020.110448.

[30] W.Y. Chen, X.L. Shi, J. Zou, Z.G. Chen, Wearable fiber-based thermoelectrics from materials to applications, Nano Energy 81 (2021), 105684, https://doi.org/10.1016/j.nanoen.2020.105684.

[31] J. Wei, L. Yang, Z. Ma, P. Song, M. Zhang, J. Ma, F. Yang, X. Wang, Review of current high-zt thermoelectric materials, J. Mater. Sci. 55 (2020) 1–63, https://doi.org/10.1007/s10853-020-04949-0.

[32] F. Hossein-Babaei, M. Akbari-Saatlu, Growth of ZnO nanorods on the surface and edges of a multilayer graphene sheet, Scr. Mater. 139 (2017) 77–82, https://doi.org/10.1016/j.scriptamat.2017.06.025.

[33] S. Masoumi, S. O'Shaughnessy, A. Pakdel, Organic-based flexible thermoelectric generators: from materials to devices, Nano Energy 92 (2022), 106774, https://doi.org/10.1016/j.nanoen.2021.106774.

[34] S. Masoumi, A. Noori, M. Shokrani, F. Hossein-Babaei, Apparatus for seebeck coefficient measurements on high-resistance bulk and thin-film samples, IEEE Trans. Instrum. Meas. 69 (2019) 3070–3077, https://doi.org/10.1109/TIM.2019.2931066.

[35] M.N. Hasan, H. Wahid, N. Nayan, M.S. Mohamed Ali, Inorganic thermoelectric materials: a review, Int. J. Energy Res. 44 (2020) 6170–6222, https://doi.org/10.1002/er.5313.

[36] B. Poudel, Q. Hao, Y. Ma, Y. Lan, A. Minnich, B. Yu, X. Yan, D. Wang, A. Muto, D. Vashaee, High-thermoelectric performance of nanostructured bismuth antimony telluride bulk alloys, Science 320 (2008) 634–638, https://doi.org/10.1126/science.1156446.

[37] Y. Zhang, W. Wang, F. Zhang, K. Dai, C. Li, Y. Fan, G. Chen, Q. Zheng, Soft organic thermoelectric materials: principles, current state of the art and applications, Small 18 (2022), 2104922, https://doi.org/10.1002/smll.202104922.

[38] J. Wang, L. Liu, F. Wu, Z. Liu, Z. Fan, L. Chen, Y. Chen, Recent developments of *n*-type organic thermoelectric materials: influence of structure modification on molecule arrangement and solution processing, ChemSusChem 15 (2022), e202102420, https://doi.org/10.1002/cssc.202102420.

[39] M. Vafaei, A. Amini, A. Siadatan, Breakthrough in co 2 measurement with a chamberless ndir optical gas sensor, IEEE Trans. Instrum. Meas. 69 (2019) 2258–2268, https://doi.org/10.1109/TIM.2019.2920702.

[40] M. Vafaei, A. Amini, Chamberless ndir co2 sensor robust against environmental fluctuations, ACS Sens. 6 (2021) 1536–1542, https://doi.org/10.1021/acssensors.0c01863.

[41] F. Hossein-Babaei, S. Masoumi, S. Aghili, M. Shokrani, Atmospheric dependence of thermoelectric generation in sno2 thin films with different intergranular potential barriers utilized for self-powered H_2S sensor fabrication, ACS Appl. Electron. Mater. 3 (2021) 353–361, https://doi.org/10.1021/acsaelm.0c00893.

[42] T. Kim, Y. Ko, Y. Lee, C. Cha, N. Kim, Experimental analysis of flexible thermoelectric generators used for self-powered devices, Energy (2020), 117544, https://doi.org/10.1016/j.energy.2020.117544.

[43] M. Akbari-Saatlu, M. Procek, C. Mattsson, G.r. Thungström, T. Törndahl, B. Li, J. Su, W. Xiong, H.H. Radamson, Nanometer-thick ZnO/SnO_2 heterostructures grown on alumina for H_2S sensing, ACS Appl. Nano Mater. (2022), https://doi.org/10.1021/acsanm.2c00940.

[44] R. Liu, Z.L. Wang, K. Fukuda, T. Someya, Flexible self-charging power sources, Nat. Rev. Mater. (2022) 1–17, https://doi.org/10.1038/s41578-022-00441-0.

[45] M. Akbari-Saatlu, M. Procek, C. Mattsson, G. Thungström, H.-E. Nilsson, W. Xiong, B. Xu, Y. Li, H.H. Radamson, Silicon nanowires for gas sensing: a review, Nanomaterials 10 (2020) 2215, https://doi.org/10.3390/nano10112215.

[46] R. Feng, F. Tang, N. Zhang, X. Wang, Flexible, high-power density, wearable thermoelectric nanogenerator and self-powered temperature sensor, ACS Appl. Mater. Interfaces 11 (2019) 38616–38624, https://doi.org/10.1021/acsami.9b11435.

[47] M. Zeng, D. Zavanelli, J. Chen, M. Saeidi-Javash, Y. Du, S. LeBlanc, G.J. Snyder, Y. Zhang, Printing thermoelectric inks toward next-generation energy and thermal devices, Chem. Soc. Rev. (2021), https://doi.org/10.1039/D1CS00490E.

[48] Y.S. Jung, D.H. Jeong, S.B. Kang, F. Kim, M.H. Jeong, K.S. Lee, J.S. Son, J.M. Baik, J.S. Kim, K.J. Choi, Wearable solar thermoelectric generator driven by unprecedentedly high temperature difference, Nano Energy 40 (2017) 663–672, https://doi.org/10.1016/j.nanoen.2017.08.061.

[49] L. Zhang, B. Xia, X.L. Shi, W.D. Liu, Y. Yang, X. Hou, X. Ye, G. Suo, Z.G. Chen, Achieving high thermoelectric properties in pedot: PSS/SWCNTs composite films by a combination of dimethyl sulfoxide doping and nabh4 dedoping, Carbon (2022), https://doi.org/10.1016/j.carbon.2022.05.043.

[50] S. Xu, M. Hong, X. Shi, M. Li, Q. Sun, Q. Chen, M. Dargusch, J. Zou, Z.G. Chen, Computation-guided design of high-performance flexible thermoelectric modules for sunlight-to-electricity conversion, Energy Environ. Sci. 13 (2020) 3480–3488, https://doi.org/10.1039/D0EE01895C.

[51] H. Ishii, K. Sugiyama, E. Ito, K. Seki, Energy level alignment and interfacial electronic structures at organic/metal and organic/organic interfaces, Adv. Mater. 11 (1999) 605–625, https://doi.org/10.1002/(SICI)1521-4095(199906)11:8<605::AID-ADMA605>3.0.CO;2-Q.

[52] H. Bronstein, C.B. Nielsen, B.C. Schroeder, I. McCulloch, The role of chemical design in the performance of organic semiconductors, Nat. Rev. Chem. 4 (2020) 66–77, https://doi.org/10.1038/s41570-019-0152-9.

[53] M.S. Vezie, S. Few, I. Meager, G. Pieridou, B. Dörling, R.S. Ashraf, A.R. Goñi, H. Bronstein, I. McCulloch, S.C. Hayes, M. Campoy-Quiles, J. Nelson, Exploring the origin of high optical absorption in conjugated polymers, Nat. Mater. 15 (2016) 746–753, https://doi.org/10.1038/nmat4645.

[54] S. Günes, H. Neugebauer, N.S. Sariciftci, Conjugated polymer-based organic solar cells, Chem. Rev. 107 (2007) 1324–1338, https://doi.org/10.1021/cr050149z.

[55] B.A. Gregg, M.C. Hanna, Comparing organic to inorganic photovoltaic cells: theory, experiment, and simulation, J. Appl. Phys. 93 (2003) 3605–3614, https://doi.org/10.1063/1.1544413.

[56] I. Olle, Organic photovoltaics over three decades, Adv. Mater. (2018), 1800388, https://doi.org/10.1002/adma.201800388.

[57] G.A. Chamberlain, Organic solar cells: a review, Solar Cells 8 (1983) 47–83, https://doi.org/10.1016/0379-6787(83)90039-X.

[58] Paul.M. Blom, V.D. Mihailetchi, L.J.A. Koster, D.E. Markov, Device physics of polymer:fullerene bulk hetrojuction solar cells, Adv. Mater. 19 (2007) 1551–1566.

[59] M. Knupfer, Exciton binding energies in organic semiconductors, Appl. Phys. A 77 (2003) 623–626, https://doi.org/10.1007/s00339-003-2182-9.

[60] C.W. Tang, Two-layer organic photovoltaic cell, Appl. Phys. Lett. 48 (1986) 183–185, https://doi.org/10.1063/1.96937.

[61] M. Theander, A. Yartsev, D. Zigmantas, V. Sundstrom, W. Mammo, M. R. Andersson, O. Inganas, Photoluminescence quenching at a polythiophene C_{60} heterojunction, Phys. Rev. B 61 (2000) 12957–12963, https://doi.org/10.1103/PhysRevB.61.12957.

[62] G. Yu, J. Gao, J.C. Hummelen, F. Wudl, A.J. Heeger, Polymer photovoltaic cells: enhanced efficiencies via a network of internal donor-acceptor heterojunctions, Science 270 (1995) 1789–1791, https://doi.org/10.1126/science.270.5243.1789.

[63] J.J.M. Halls, C.A. Walsh, N.C. Greenham, E.A. Marseglia, R.H. Friend, S. C. Moratti, A.B. Holmes, Efficient photodiodes from interpenetrating polymer networks, Nature 376 (1995) 498–500, https://doi.org/10.1038/376498a0.

[64] C. McDowell, M. Abdelsamie, M.F. Toney, G.C. Bazan, Solvent additives: key morphology-directing agents for solution-processed organic solar cells, Adv. Mater. 30 (2018), 1707114, https://doi.org/10.1002/adma.201707114.

[65] S. Bi, X. Leng, Y. Li, Z. Zheng, X. Zhang, Y. Zhang, H. Zhou, Interfacial modification in organic and perovskite solar cells, Adv. Mater. 31 (2019), 1805708, https://doi.org/10.1002/adma.201805708.

[66] Y. Cui, Y. Xu, H. Yao, P. Bi, L. Hong, J. Zhang, Y. Zu, T. Zhang, J. Qin, J. Ren, Z. Chen, C. He, X. Hao, Z. Wei, J. Hou, Single-junction organic photovoltaic cell with 19% efficiency, Adv. Mater. 33 (2021), 2102420, https://doi.org/10.1002/adma.202102420.

[67] L. Meng, Y. Zhang, X. Wan, C. Li, X. Zhang, Y. Wang, X. Ke, Z. Xiao, L. Ding, R. Xia, H.L. Yip, Y. Cao, Y. Chen, Organic and solution-processed tandem solar cells with 17.3% efficiency, Science 361 (2018) 1094–1098, https://doi.org/10.1126/science.aat2612.

[68] N. Gasparini, A. Salleo, I. McCulloch, D. Baran, The role of the third component in ternary organic solar cells, Nat. Rev. Mater. 4 (2019) 229–242, https://doi.org/10.1038/s41578-019-0093-4.

[69] S. Langner, F. Häse, J.D. Perea, T. Stubhan, J. Hauch, L.M. Roch, T. Heumueller, A. Aspuru-Guzik, C.J. Brabec, Beyond ternary OPV: high-throughput experimentation and self-driving laboratories optimize multicomponent systems, Adv. Mater. (2020), 1907801, https://doi.org/10.1002/adma.201907801.

[70] G. Horowitz, Organic semiconductors for new electronic devices, Adv. Mater. 2 (1990) 287–292, https://doi.org/10.1002/adma.19900020604.

[71] T. Kietzke, H.H. Hörhold, D. Neher, Efficient polymer solar cells based on M3EH−PPV, Chem. Mater. 17 (2005) 6532–6537, https://doi.org/10.1021/cm050148n.

[72] T. Yamamoto, K. Sanechika, A. Yamamoto, Preparation of thermostable and electric-conducting poly(2,5-thienylene), J. Polym. Sci. Polym. Lett. Ed. 18 (1980) 9–12, https://doi.org/10.1002/pol.1980.130180103.

[73] M. Granström, K. Petritsch, A.C. Arias, A. Lux, M.R. Andersson, R.H. Friend, Laminated fabrication of polymeric photovoltaic diodes, Nature 395 (1998) 257–260, https://doi.org/10.1038/26183.

[74] R.D. McCullough, R.D. Lowe, Enhanced electrical conductivity in regioselectively synthesized poly(3-alkylthiophenes), J. Chem. Soc. Chem. Commun. (1992) 70–72, https://doi.org/10.1039/C39920000070.

[75] R.D. McCullough, R.D. Lowe, M. Jayaraman, D.L. Anderson, Design, synthesis, and control of conducting polymer architectures: structurally homogeneous poly (3-alkylthiophenes), J. Org. Chem. 58 (1993) 904–912, https://doi.org/10.1021/jo00056a024.

[76] M.T. Dang, L. Hirsch, G. Wantz, P3HT:PCBM, best seller in polymer photovoltaic research, Adv. Mater. 23 (2011) 3597–3602, https://doi.org/10.1002/adma.201100792.

[77] L.S. Roman, M.R. Andersson, T. Yohannes, O. Inganás, Photodiode performance and nanostructure of polythiophene/C_{60} blends, Adv. Mater. 9 (1997) 1164–1168, https://doi.org/10.1002/adma.19970091508.

[78] X. Guo, C. Cui, M. Zhang, L. Huo, Y. Huang, J. Hou, Y. Li, High efficiency polymer solar cells based on poly(3-hexylthiophene)/indene-C_{70} bisadduct with solvent additive, Energy Environ. Sci. 5 (2012) 7943–7949, https://doi.org/10.1039/C2EE21481D.

[79] F.C. Krebs, Low band gap polymer materials for organic solar cells, Solar Energy Mater. Solar Cells 91 (2007) 953, https://doi.org/10.1016/j.solmat.2007.02.019.

[80] M.A. Ansari, S. Mohiuddin, F. Kandemirli, M.I. Malik, Synthesis and characterization of poly(3-hexylthiophene): improvement of regioregularity and energy band gap, RSC Adv. 8 (2018) 8319–8328, https://doi.org/10.1039/C8RA00555A.

[81] E.E. Havinga, W. ten Hoeve, H. Wynberg, A new class of small band gap organic polymer conductors, Polym. Bull. 29 (1992) 119–126, https://doi.org/10.1007/BF00558045.

[82] Y.J. Cheng, S.H. Yang, C.S. Hsu, Synthesis of conjugated polymers for organic solar cell applications, Chem. Rev. 109 (2009) 5868–5923, https://doi.org/10.1021/cr900182s.

[83] G. Brocks, A. Tol, Small band gap semiconducting polymers made from dye molecules: Polysquaraines, J. Phys. Chem. 100 (1996) 1838–1846, https://doi.org/10.1021/jp952276c.

[84] A. Gadisa, W. Mammo, L.M. Andersson, S. Admassie, F. Zhang, M.R. Andersson, O. Inganäs, A new donor–acceptor–donor polyfluorene copolymer with balanced electron and hole mobility, Adv. Funct. Mater. 17 (2007) 3836–3842, https://doi.org/10.1002/adfm.200700441.

[85] Y. Zhou, D.A. Gedefaw, S. Hellström, I. Krätschmer, F. Zhang, W. Mammo, O. Inganäs, M.R. Andersson, Black polymers in bulk-heterojunction solar cells, IEEE J. Sel. Top. Quantum Electron. 16 (2010) 1565–1572, https://doi.org/10.1109/JSTQE.2010.2049002.

[86] D. Gedefaw, Y. Zhou, S. Hellström, L. Lindgren, L.M. Andersson, F. Zhang, W. Mammo, O. Inganäs, M.R. Andersson, Alternating copolymers of fluorene and donor–acceptor–donor segments designed for miscibility in bulk heterojunction photovoltaics, J. Mater. Chem. 19 (2009) 5359–5363, https://doi.org/10.1039/B823137K.

[87] F. Zhang, J. Bijleveld, E. Perzon, K. Tvingstedt, S. Barrau, O. Inganäs, M. R. Andersson, High photovoltage achieved in low band gap polymer solar cells by adjusting energy levels of a polymer with the lumos of fullerene derivatives, J. Mater. Chem. 18 (2008) 5468–5474, https://doi.org/10.1039/B811957K.

[88] T. Yohannes, F. Zhang, M. Svensson, J.C. Hummelen, M.R. Andersson, O. Inganäs, Polyfluorene copolymer based bulk heterojunction solar cells, Thin. Solid. Films 449 (2004) 152–157, https://doi.org/10.1016/S0040-6090(03)01348-8.

[89] J.F. Morin, M. Leclerc, D. Adès, A. Siove, Polycarbazoles: 25 years of progress, Macromol. Rapid Commun. 26 (2005) 761–778, https://doi.org/10.1002/marc.200500096.

[90] J.F. Morin, M. Leclerc, Syntheses of conjugated polymers derived from N-Alkyl-2,7-carbazoles, Macromolecules 34 (2001) 4680–4682, https://doi.org/10.1021/ma010152u.

[91] N. Blouin, A. Michaud, M. Leclerc, A low-bandgap poly(2,7-carbazole) derivative for use in high-performance solar cells, Adv. Mater. 19 (2007) 2295–2300, https://doi.org/10.1002/adma.200602496.

[92] S. Beaupré, M. Leclerc, PCDTBT: en route for low cost plastic solar cells, J. Mater. Chem. A 1 (2013) 11097–11105, https://doi.org/10.1039/C3TA12420G.

[93] M.C. Scharber, M. Koppe, J. Gao, F. Cordella, M.A. Loi, P. Denk, M. Morana, H. J. Egelhaaf, K. Forberich, G. Dennler, R. Gaudiana, D. Waller, Z. Zhu, X. Shi, C. J. Brabec, Influence of the bridging atom on the performance of a low-bandgap bulk heterojunction solar cell, Adv. Mater. 22 (2010) 367–370, https://doi.org/10.1002/adma.200900529.

[94] H.Y. Chen, J. Hou, A.E. Hayden, H. Yang, K.N. Houk, Y. Yang, Silicon atom substitution enhances interchain packing in a thiophene-based polymer system, Adv. Mater. 22 (2010) 371–375, https://doi.org/10.1002/adma.200902469.

[95] E. Wang, L. Hou, Z. Wang, S. Hellström, F. Zhang, O. Inganäs, M.R. Andersson, An easily synthesized blue polymer for high-performance polymer solar cells, Adv. Mater. 22 (2010) 5240–5244, https://doi.org/10.1002/adma.201002225.

[96] Y. Kim, H.R. Yeom, J.Y. Kim, C. Yang, High-efficiency polymer solar cells with a cost-effective quinoxaline polymer through nanoscale morphology control induced by practical processing additives, Energy Environ. Sci. 6 (2013) 1909–1916, https://doi.org/10.1039/C3EE00110E.

[97] Y. Lu, Z. Xiao, Y. Yuan, H. Wu, Z. An, Y. Hou, C. Gao, J. Huang, Fluorine substituted thiophene–quinoxaline copolymer to reduce the homo level and increase the dielectric constant for high open-circuit voltage organic solar cells, J. Mater. Chem. C 1 (2013) 630–637, https://doi.org/10.1039/C2TC00327A.

[98] W. Zhuang, H. Zhen, R. Kroon, Z. Tang, S. Hellström, L. Hou, E. Wang, D. Gedefaw, O. Inganäs, F. Zhang, M.R. Andersson, Molecular orbital energy level modulation through incorporation of selenium and fluorine into conjugated polymers for organic photovoltaic cells, J. Mater. Chem. A 1 (2013) 13422–13425, https://doi.org/10.1039/C3TA13040A.

[99] Y. Liu, J. Zhao, Z. Li, C. Mu, W. Ma, H. Hu, K. Jiang, H. Lin, H. Ade, H. Yan, Aggregation and morphology control enables multiple cases of high-efficiency polymer solar cells, Nat. Commun. 5 (2014) 5293, https://doi.org/10.1038/ncomms6293.

[100] D. Gedefaw, M. Tessarolo, W. Zhuang, R. Kroon, E. Wang, M. Bolognesi, M. Seri, M. Muccini, M.R. Andersson, Conjugated polymers based on benzodithiophene and fluorinated quinoxaline for bulk heterojunction solar cells: thiophene versus thieno[3,2-b]thiophene as π-conjugated spacers, Polym. Chem. 5 (2014) 2083–2093, https://doi.org/10.1039/C3PY01519J.

[101] M. Bolognesi, D. Gedefaw, D. Dang, P. Henriksson, W. Zhuang, M. Tessarolo, E. Wang, M. Muccini, M. Seri, M.R. Andersson, 2d π-conjugated benzo[1,2-b:4,5-b′]dithiophene- and quinoxaline-based copolymers for photovoltaic applications, RSC Adv. 3 (2013) 24543–24552, https://doi.org/10.1039/C3RA44238A.

[102] M. Tessarolo, D. Gedefaw, M. Bolognesi, F. Liscio, P. Henriksson, W. Zhuang, S. Milita, M. Muccini, E. Wang, M. Seri, M.R. Andersson, Structural tuning of quinoxaline-benzodithiophene copolymers via alkyl side chain manipulation: synthesis, characterization and photovoltaic properties, J. Mater. Chem. A 2 (2014) 11162–11170, https://doi.org/10.1039/C4TA01479K.

[103] Z. He, C. Zhong, S. Su, M. Xu, H. Wu, Y. Cao, Enhanced power-conversion efficiency in polymer solar cells using an inverted device structure, Nat. Photonics 6 (2012) 591–595, https://doi.org/10.1038/nphoton.2012.190.

[104] Q. Wan, X. Guo, Z. Wang, W. Li, B. Guo, W. Ma, M. Zhang, Y. Li, 10.8% efficiency polymer solar cells based on PTB7-Th and $PC_{71}BM$ via binary solvent additives treatment, Adv. Funct. Mater. 26 (2016) 6635–6640, https://doi.org/10.1002/adfm.201602181.

[105] C. Piliego, T.W. Holcombe, J.D. Douglas, C.H. Woo, P.M. Beaujuge, J.M. J. Fréchet, Synthetic control of structural order in N-Alkylthieno[3,4-c]pyrrole-4,6-dione-based polymers for efficient solar cells, J. Am. Chem. Soc. 132 (2010) 7595–7597, https://doi.org/10.1021/ja103275u.

[106] Y. Ie, J. Huang, Y. Uetani, M. Karakawa, Y. Aso, Synthesis, properties, and photovoltaic performances of donor–acceptor copolymers having dioxocycloalkene-annelated thiophenes as acceptor monomer units, Macromolecules 45 (2012) 4564–4571, https://doi.org/10.1021/ma300742r.

[107] D. Qian, L. Ye, M. Zhang, Y. Liang, L. Li, Y. Huang, X. Guo, S. Zhang, Z.a. Tan, J. Hou, Design, application, and morphology study of a new photovoltaic polymer with strong aggregation in solution state, Macromolecules 45 (2012) 9611–9617, https://doi.org/10.1021/ma301900h.

[108] W. Zhao, D. Qian, S. Zhang, S. Li, O. Inganäs, F. Gao, J. Hou, Fullerene-free polymer solar cells with over 11% efficiency and excellent thermal stability, Adv. Mater. 28 (2016) 4734–4739, https://doi.org/10.1002/adma.201600281.

[109] M. Zhang, X. Guo, W. Ma, H. Ade, J. Hou, A large-bandgap conjugated polymer for versatile photovoltaic applications with high performance, Adv. Mater. 27 (2015) 4655–4660, https://doi.org/10.1002/adma.201502110.

[110] Q. Fan, Y. Wang, M. Zhang, B. Wu, X. Guo, Y. Jiang, W. Li, B. Guo, C. Ye, W. Su, J. Fang, X. Ou, F. Liu, Z. Wei, T.C. Sum, T.P. Russell, Y. Li, High-performance as-cast nonfullerene polymer solar cells with thicker active layer and large area exceeding 11% power conversion efficiency, Adv. Mater. 30 (2018), 1704546, https://doi.org/10.1002/adma.201704546.

[111] J. Yuan, Y. Zhang, L. Zhou, G. Zhang, H.L. Yip, T.K. Lau, X. Lu, C. Zhu, H. Peng, P. A. Johnson, M. Leclerc, Y. Cao, J. Ulanski, Y. Li, Y. Zou, Single-junction organic solar cell with over 15% efficiency using fused-ring acceptor with electron-deficient core, Joule 3 (2019) 1140–1151, https://doi.org/10.1016/j.joule.2019.01.004.
[112] W. Zhao, S. Li, H. Yao, S. Zhang, Y. Zhang, B. Yang, J. Hou, Molecular optimization enables over 13% efficiency in organic solar cells, J. Am. Chem. Soc. 139 (2017) 7148–7151, https://doi.org/10.1021/jacs.7b02677.
[113] J. Xiong, K. Jin, Y. Jiang, J. Qin, T. Wang, J. Liu, Q. Liu, H. Peng, X. Li, A. Sun, X. Meng, L. Zhang, L. Liu, W. Li, Z. Fang, X. Jia, Z. Xiao, Y. Feng, X. Zhang, K. Sun, S. Yang, S. Shi, L. Ding, Thiolactone copolymer donor gifts organic solar cells a 16.72% efficiency, Sci. Bull. 64 (2019) 1573–1576, https://doi.org/10.1016/j.scib.2019.10.002.
[114] Q. Liu, Y. Jiang, K. Jin, J. Qin, J. Xu, W. Li, J. Xiong, J. Liu, Z. Xiao, K. Sun, S. Yang, X. Zhang, L. Ding, 18% efficiency organic solar cells, Sci. Bull. 65 (2020) 272–275, https://doi.org/10.1016/j.scib.2020.01.001.
[115] A. Mishra, P. Bäuerle, Small molecule organic semiconductors on the move: promises for future solar energy technology, Angew. Chem. Int. Ed. 51 (2012) 2020–2067, https://doi.org/10.1002/anie.201102326.
[116] Y. Sun, G.C. Welch, W.L. Leong, C.J. Takacs, G.C. Bazan, A.J. Heeger, Solution-processed small-molecule solar cells with 6.7% efficiency, Nat. Mater. 11 (2012) 44–48, https://doi.org/10.1038/nmat3160.
[117] K. Sun, Z. Xiao, S. Lu, W. Zajaczkowski, W. Pisula, E. Hanssen, J.M. White, R. M. Williamson, J. Subbiah, J. Ouyang, A.B. Holmes, W.W.H. Wong, D.J. Jones, A molecular nematic liquid crystalline material for high-performance organic photovoltaics, Nat. Commun. 6 (2015) 6013, https://doi.org/10.1038/ncomms7013.
[118] D. Deng, Y. Zhang, J. Zhang, Z. Wang, L. Zhu, J. Fang, B. Xia, Z. Wang, K. Lu, W. Ma, Z. Wei, Fluorination-enabled optimal morphology leads to over 11% efficiency for inverted small-molecule organic solar cells, Nat. Commun. 7 (2016) 13740, https://doi.org/10.1038/ncomms13740.
[119] L. Yang, S. Zhang, C. He, J. Zhang, Y. Yang, J. Zhu, Y. Cui, W. Zhao, H. Zhang, Y. Zhang, Z. Wei, J. Hou, Modulating molecular orientation enables efficient nonfullerene small-molecule organic solar cells, Chem. Mater. 30 (2018) 2129–2134, https://doi.org/10.1021/acs.chemmater.8b00287.
[120] Q. Yue, H. Wu, Z. Zhou, M. Zhang, F. Liu, X. Zhu, 13.7% efficiency small-molecule solar cells enabled by a combination of material and morphology optimization, Adv. Mater. 31 (2019), 1904283, https://doi.org/10.1002/adma.201904283.
[121] N.S. Sariciftci, L. Smilowitz, A.J. Heeger, F. Wudl, Photoinduced electron transfer from a conducting polymer to buckminsterfullerene, Science 258 (1992) 1474–1476, https://doi.org/10.1126/science.258.5087.1474. %J.
[122] S. Morita, S. Kiyomatsu, X.H. Yin, A.A. Zakhidov, T. Noguchi, T. Ohnishi, K. Yoshino, Doping effect of buckminsterfullerene in poly(2,5-dialkoxy-p-phenylene vinylene), J. Appl. Phys. 74 (1993) 2860–2865, https://doi.org/10.1063/1.354639.
[123] N.S. Sariciftci, D. Braun, C. Zhang, V.I. Srdanov, A.J. Heeger, G. Stucky, F. Wudl, Semiconducting polymer-buckminsterfullerene heterojunctions: diodes, photodiodes, and photovoltaic cells, Appl. Phys. Lett. 62 (1993) 585–587, https://doi.org/10.1063/1.108863.
[124] G. Yu, J. Gao, J.C. Hummelen, F. Wudl, A.J. Heeger, Polymer photovoltaic cells - enhanced efficiencies via a network of internal donor-acceptor heterojunctions, Science 270 (1995) 1789–1791, https://doi.org/10.1126/science.270.5243.1789.
[125] N.S. Sariciftci, L. Smilowitz, A.J. Heeger, F. Wudl, Semiconducting polymers (as donors) and buckminsterfullerene (as acceptor): photoinduced electron transfer and heterojunction devices, Synth. Met. 59 (1993) 333–352, https://doi.org/10.1016/0379-6779(93)91166-Y.
[126] Y. He, Y. Li, Fullerene derivative acceptors for high performance polymer solar cells, Phys. Chem. Chem. Phys. 13 (2011) 1970–1983, https://doi.org/10.1039/C0CP01178A.
[127] D.F. Kronholm, J.C. Hummelen, Organic photovoltaics, eds., Wiley-VCH Verlag GmbH & Co. KGaA, 2009, pp. 153–178.
[128] J.L. Delgado, N. Martín, P. de la Cruz, F. Langa, Pyrazolinofullerenes: a less known type of highly versatile fullerene derivatives, Chem. Soc. Rev. 40 (2011) 5232–5241, https://doi.org/10.1039/C1CS15105C.
[129] M. Drees, H. Hoppe, C. Winder, H. Neugebauer, N.S. Sariciftci, W. Schwinger, F. Schäffler, C. Topf, M.C. Scharber, Z. Zhu, R. Gaudiana, Stabilization of the nanomorphology of polymer–fullerene "bulk heterojunction" blends using a novel polymerizable fullerene derivative, J. Mater. Chem. 15 (2005) 5158–5163, https://doi.org/10.1039/B505361G.
[130] B.C. Thompson, J.M.J. Fréchet, Polymer–fullerene composite solar cells, Angew. Chem. Int. Ed. 47 (2008) 58–77, https://doi.org/10.1002/anie.200702506.
[131] Y.Y. Lai, Y.J. Cheng, C.S. Hsu, Applications of functional fullerene materials in polymer solar cells, Energy Environ. Sci. 7 (2014) 1866–1883, https://doi.org/10.1039/C3EE43080D.
[132] M. Jørgensen, K. Norrman, S.A. Gevorgyan, T. Tromholt, B. Andreasen, F. C. Krebs, Stability of polymer solar cells, Adv. Mater. 24 (2012) 580–612, https://doi.org/10.1002/adma.201104187.
[133] P. Cheng, G. Li, X. Zhan, Y. Yang, Next-generation organic photovoltaics based on non-fullerene acceptors, Nat. Photonics 12 (2018) 131–142, https://doi.org/10.1038/s41566-018-0104-9.
[134] T. Earmme, Y.J. Hwang, N.M. Murari, S. Subramaniyan, S.A. Jenekhe, All-polymer solar cells with 3.3% efficiency based on naphthalene diimide-selenophene copolymer acceptor, J. Am. Chem. Soc. 135 (2013) 14960–14963, https://doi.org/10.1021/ja4085429.
[135] K. Nakano, M. Nakano, B. Xiao, E. Zhou, K. Suzuki, I. Osaka, K. Takimiya, K. Tajima, Naphthodithiophene diimide-based copolymers: ambipolar semiconductors in field-effect transistors and electron acceptors with near-infrared response in polymer blend solar cells, Macromolecules 49 (2016) 1752–1760, https://doi.org/10.1021/acs.macromol.5b02658.
[136] X. Zhan, Z.A. Tan, B. Domercq, Z. An, X. Zhang, S. Barlow, Y. Li, D. Zhu, B. Kippelen, S.R. Marder, A high-mobility electron-transport polymer with broad absorption and its use in field-effect transistors and all-polymer solar cells, J. Am. Chem. Soc. 129 (2007) 7246–7247, https://doi.org/10.1021/ja071760d.
[137] X. Long, Z. Ding, C. Dou, J. Zhang, J. Liu, L. Wang, Polymer acceptor based on double B←N bridged bipyridine (BNBP) unit for high-efficiency all-polymer solar cells, Adv. Mater. 28 (2016) 6504–6508, https://doi.org/10.1002/adma.201601205.
[138] Y. Wang, Z. Yan, H. Guo, M.A. Uddin, S. Ling, X. Zhou, H. Su, J. Dai, H.Y. Woo, X. Guo, Effects of bithiophene imide fusion on the device performance of organic thin-film transistors and all-polymer solar cells, Angew. Chem. Int. Ed. 56 (2017) 15304–15308, https://doi.org/10.1002/anie.201708421.
[139] C. Mu, P. Liu, W. Ma, K. Jiang, J. Zhao, K. Zhang, Z. Chen, Z. Wei, Y. Yi, J. Wang, S. Yang, F. Huang, A. Facchetti, H. Ade, H. Yan, High-efficiency all-polymer solar cells based on a pair of crystalline low-bandgap polymers, Adv. Mater. 26 (2014) 7224–7230, https://doi.org/10.1002/adma.201402473.
[140] J. Liu, S. Chen, D. Qian, B. Gautam, G. Yang, J. Zhao, J. Bergqvist, F. Zhang, W. Ma, H. Ade, O. Inganäs, K. Gundogdu, F. Gao, H. Yan, Fast charge separation in a non-fullerene organic solar cell with a small driving force, Nat. Energy 1 (2016) 16089, https://doi.org/10.1038/nenergy.2016.89.
[141] H. Yan, Z. Chen, Y. Zheng, C. Newman, J.R. Quinn, F. Dötz, M. Kastler, A. Facchetti, A high-mobility electron-transporting polymer for printed transistors, Nature 457 (2009) 679–686, https://doi.org/10.1038/nature07727.
[142] Y. An, J. Oh, S. Chen, B. Lee, S.M. Lee, D. Han, C. Yang, Effects of incorporating different chalcogenophene comonomers into random acceptor terpolymers on the morphology and performance of all-polymer solar cells, Polym. Chem. 9 (2018) 593–602, https://doi.org/10.1039/C7PY01907F.
[143] Z. Genene, W. Mammo, E. Wang, M.R. Andersson, Recent advances in *n*-type polymers for all-polymer solar cells, Adv. Mater. 31 (2019), 1807275, https://doi.org/10.1002/adma.201807275.
[144] X. Xu, K. Feng, Z. Bi, W. Ma, G. Zhang, Q. Peng, Single-junction polymer solar cells with 16.35% efficiency enabled by a platinum(ii) complexation strategy, Adv. Mater. 31 (2019), 1901872, https://doi.org/10.1002/adma.201901872.
[145] H. Tan, X. Zheng, J. Zhu, J. Yu, W. Zhu, An A–D–D–A-type non-fullerene small-molecule acceptor with strong near-infrared absorption for high performance polymer solar cells, J. Mater. Chem. C 7 (2019) 13301–13306, https://doi.org/10.1039/C9TC04898G.
[146] A. Wadsworth, M. Moser, A. Marks, M.S. Little, N. Gasparini, C.J. Brabec, D. Baran, I. McCulloch, Critical review of the molecular design progress in non-fullerene electron acceptors towards commercially viable organic solar cells, Chem. Soc. Rev. 48 (2019) 1596–1625, https://doi.org/10.1039/C7CS00892A.
[147] J. Hou, O. Inganäs, R.H. Friend, F. Gao, Organic solar cells based on non-fullerene acceptors, Nat. Mater. 17 (2018) 119–128, https://doi.org/10.1038/nmat5063.
[148] Y. Cui, H. Yao, J. Zhang, T. Zhang, Y. Wang, L. Hong, K. Xian, B. Xu, S. Zhang, J. Peng, Z. Wei, F. Gao, J. Hou, Over 16% efficiency organic photovoltaic cells enabled by a chlorinated acceptor with increased open-circuit voltages, Nat. Commun. 10 (2019) 2515, https://doi.org/10.1038/s41467-019-10351-5.
[149] Y. Firdaus, V.M. Le Corre, J.I. Khan, Z. Kan, F. Laquai, P.M. Beaujuge, T. D. Anthopoulos, Key parameters requirements for non-fullerene-based organic solar cells with power conversion efficiency >20%, Adv. Sci. 6 (2019), 1802028 https://doi.org/10.1002/advs.201802028.
[150] Y. Lin, J. Wang, Z.G. Zhang, H. Bai, Y. Li, D. Zhu, X. Zhan, An electron acceptor challenging fullerenes for efficient polymer solar cells, Adv. Mater. 27 (2015) 1170–1174, https://doi.org/10.1002/adma.201404317.
[151] M.H. Hoang, G.E. Park, S. Choi, C.G. Park, S.H. Park, T.V. Nguyen, S. Kim, K. Kwak, M.J. Cho, D.H. Choi, High-efficiency non-fullerene polymer solar cell fabricated by a simple process using new conjugated terpolymers, J. Mater. Chem. C 7 (2019) 111–118, https://doi.org/10.1039/C8TC05035J.
[152] H. Yao, Y. Cui, R. Yu, B. Gao, H. Zhang, J. Hou, Design, synthesis, and photovoltaic characterization of a small molecular acceptor with an ultra-narrow band gap, Angew. Chem. Int. Ed. 56 (2017) 3045–3049, https://doi.org/10.1002/anie.201610944.
[153] S. Holliday, R.S. Ashraf, A. Wadsworth, D. Baran, S.A. Yousaf, C.B. Nielsen, C. H. Tan, S.D. Dimitrov, Z. Shang, N. Gasparini, M. Alamoudi, F. Laquai, C. J. Brabec, A. Salleo, J.R. Durrant, I. McCulloch, High-efficiency and air-stable P3HT-based polymer solar cells with a new non-fullerene acceptor, Nat. Commun. 7 (2016) 11585, https://doi.org/10.1038/ncomms11585.
[154] S. Choi, H. Lee, R. Ghaffari, T. Hyeon, D.H. Kim, Recent advances in flexible and stretchable bio-electronic devices integrated with nanomaterials, Adv. Mater. 28 (2016) 4203–4218, https://doi.org/10.1002/adma.201504150.
[155] Y. Zhang, S.W. Ng, X. Lu, Z. Zheng, Solution-processed transparent electrodes for emerging thin-film solar cells, Chem. Rev. 120 (2020) 2049–2122, https://doi.org/10.1021/acs.chemrev.9b00483.
[156] J. Ben-David, A.J. Stapleton, C.T. Gibson, A. Sharma, A.R. Gentle, D.A. Lewis, A. V. Ellis, Poly(3,4-ethylenedioxythiophene):Polystyrene sulfonate-free silver nanowire/single walled carbon nanotube transparent electrodes using graphene oxide, Thin Solid Films 616 (2016) 515–520, https://doi.org/10.1016/j.tsf.2016.09.014.
[157] X. Chen, G. Xu, G. Zeng, H. Gu, H. Chen, H. Xu, H. Yao, Y. Li, J. Hou, Y. Li, Realizing ultrahigh mechanical flexibility and >15% efficiency of flexible organic

solar cells via a "welding" flexible transparent electrode, Adv. Mater. 32 (2020), 1908478, https://doi.org/10.1002/adma.201908478.
[158] L. Lucera, F. Machui, P. Kubis, H.D. Schmidt, J. Adams, S. Strohm, T. Ahmad, K. Forberich, H.J. Egelhaaf, C.J. Brabec, Highly efficient, large area, roll coated flexible and rigid OPV modules with geometric fill factors up to 98.5% processed with commercially available materials, Energy Environ. Sci. 9 (2016) 89–94, https://doi.org/10.1039/C5EE03315B.
[159] E. Bihar, D. Corzo, T.C. Hidalgo, D. Rosas-Villalva, K.N. Salama, S. Inal, D. Baran, Fully inkjet-printed, ultrathin and conformable organic photovoltaics as power source based on cross-linked PEDOT:PSS electrodes, Adv. Mater. Technol. 5 (2020), 2000226, https://doi.org/10.1002/admt.202000226.
[160] J. Bergqvist, T. Österberg, A. Melianas, L. Ever Aguirre, Z. Tang, W. Cai, Z. Ma, M. Kemerink, D. Gedefaw, M.R. Andersson, O. Inganäs, Asymmetric photocurrent extraction in semitransparent laminated flexible organic solar cells, npj Flex. Electron. 2 (2018) 4, https://doi.org/10.1038/s41528-017-0017-6.
[161] J. Kim, W.J. da Silva, A.R. bin Mohd Yusoff, J. Jang, Organic devices based on nickel nanowires transparent electrode, Sci. Rep. 6 (2016) 19813, https://doi.org/10.1038/srep19813.
[162] Y. Xiong, R.E. Booth, T. Kim, L. Ye, Y. Liu, Q. Dong, M. Zhang, F. So, Y. Zhu, A. Amassian, B.T. O'Connor, H. Ade, Novel bimodal silver nanowire network as top electrodes for reproducible and high-efficiency semitransparent organic photovoltaics, Solar RRL (2020), 2000328, https://doi.org/10.1002/solr.202000328 n/a.
[163] K. Vandewal, S. Albrecht, E.T. Hoke, K.R. Graham, J. Widmer, J.D. Douglas, M. Schubert, W.R. Mateker, J.T. Bloking, G.F. Burkhard, A. Sellinger, J.M. J. Fréchet, A. Amassian, M.K. Riede, M.D. McGehee, D. Neher, A. Salleo, Efficient charge generation by relaxed charge-transfer states at organic interfaces, Nat. Mater. 13 (2014) 63–68, https://doi.org/10.1038/nmat3807.
[164] S. Gélinas, A. Rao, A. Kumar, S.L. Smith, A.W. Chin, J. Clark, T.S. van der Poll, G. C. Bazan, R.H. Friend, Ultrafast long-range charge separation in organic semiconductor photovoltaic diodes, Science 343 (2014) 512–516, https://doi.org/10.1126/science.1246249.
[165] Y. Fang, A.K. Pandey, A.M. Nardes, N. Kopidakis, P.L. Burn, P. Meredith, A narrow optical gap small molecule acceptor for organic solar cells, Adv. Energy Mater. 3 (2013) 54–59, https://doi.org/10.1002/aenm.201200372.
[166] T.M. Clarke, J.R. Durrant, Charge photogeneration in organic solar cells, Chem. Rev. 110 (2010) 6736–6767, https://doi.org/10.1021/cr900271s.
[167] C. Göhler, A. Wagenpfahl, C. Deibel, Nongeminate recombination in organic solar cells, Adv. Electron. Mater. 4 (2018), 1700505, https://doi.org/10.1002/aelm.201700505.
[168] J.J. Benson-Smith, L. Goris, K. Vandewal, K. Haenen, J.V. Manca, D. Vanderzande, D.D.C. Bradley, J. Nelson, Formation of a ground-state charge-transfer complex in polyfluorene//[6,6]-phenyl-c61 butyric acid methyl ester (PCBM) blend films and its role in the function of polymer/PCBM solar cells, Adv. Funct. Mater. 17 (2007) 451–457, https://doi.org/10.1002/adfm.200600484.
[169] M.A. Loi, S. Toffanin, M. Muccini, M. Forster, U. Scherf, M. Scharber, Charge transfer excitons in bulk heterojunctions of a polyfluorene copolymer and a fullerene derivative, Adv. Funct. Mater. 17 (2007) 2111–2116, https://doi.org/10.1002/adfm.200601098.
[170] C. Kästner, K. Vandewal, D.A.M. Egbe, H. Hoppe, Revelation of interfacial energetics in organic multiheterojunctions, Adv. Sci. 4 (2017), 1600331, https://doi.org/10.1002/advs.201600331.
[171] T.A. Dela Peña, J.I. Khan, N. Chaturvedi, R. Ma, Z. Xing, J. Gorenflot, A. Sharma, F.L. Ng, D. Baran, H. Yan, F. Laquai, K.S. Wong, Understanding the charge transfer state and energy loss trade-offs in non-fullerene-based organic solar cells, ACS Energy Lett. (2021) 3408–3416, https://doi.org/10.1021/acsenergylett.1c01574.
[172] V. Coropceanu, X.K. Chen, T. Wang, Z. Zheng, J.L. Brédas, Charge-transfer electronic states in organic solar cells, Nat. Rev. Mater. 4 (2019) 689–707, https://doi.org/10.1038/s41578-019-0137-9.
[173] X.K. Chen, D.P. Qian, Y.M. Wang, T. Kirchartz, W. Tress, H.F. Yao, J. Yuan, M. Hulsbeck, M.J. Zhang, Y.P. Zou, Y.M. Sun, Y.F. Li, J.H. Hou, O. Inganas, V. Coropceanu, J.L. Bredas, F. Gao, A unified description of non-radiative voltage losses in organic solar cells, Nat. Energy 6 (2021) 799–806, https://doi.org/10.1038/s41560-021-00843-4.
[174] H. Cha, G. Fish, J. Luke, A. Alraddadi, H.H. Lee, W. Zhang, Y. Dong, S. Limbu, A. Wadsworth, I.P. Maria, L. Francàs, H.L. Sou, T. Du, J.S. Kim, M.A. McLachlan, I. McCulloch, J.R. Durrant, Suppression of recombination losses in polymer: nonfullerene acceptor organic solar cells due to aggregation dependence of acceptor electron affinity, Adv. Energy Mater. 9 (2019), 1901254, https://doi.org/10.1002/aenm.201901254.
[175] S. Karuthedath, J. Gorenflot, Y. Firdaus, N. Chaturvedi, C.S.P. De Castro, G. T. Harrison, J.I. Khan, A. Markina, A.H. Balawi, T.A.D. Peña, W. Liu, R.Z. Liang, A. Sharma, S.H.K. Paleti, W. Zhang, Y. Lin, E. Alarousu, D.H. Anjum, P. M. Beaujuge, S. De Wolf, I. McCulloch, T.D. Anthopoulos, D. Baran, D. Andrienko, F. Laquai, Intrinsic efficiency limits in low-bandgap non-fullerene acceptor organic solar cells, Nat. Mater. 20 (2021) 378–384, https://doi.org/10.1038/s41563-020-00835-x.
[176] L. Dou, J. You, Z. Hong, Z. Xu, G. Li, R.A. Street, Y. Yang, 25th anniversary article: a decade of organic/polymeric photovoltaic research, Adv. Mater. 25 (2013) 6642–6671, https://doi.org/10.1002/adma.201302563.
[177] T. Unger, S. Wedler, F.J. Kahle, U. Scherf, H. Bässler, A. Köhler, The impact of driving force and temperature on the electron transfer in donor–acceptor blend systems, J. Phys. Chem. C 121 (2017) 22739–22752, https://doi.org/10.1021/acs.jpcc.7b09213.
[178] K. Kawashima, Y. Tamai, H. Ohkita, I. Osaka, K. Takimiya, High-efficiency polymer solar cells with small photon energy loss, Nat. Commun. 6 (2015) 10085, https://doi.org/10.1038/ncomms10085.
[179] C. Yang, J. Zhang, N. Liang, H. Yao, Z. Wei, C. He, X. Yuan, J. Hou, Effects of energy-level offset between a donor and acceptor on the photovoltaic performance of non-fullerene organic solar cells, J. Mater. Chem. A 7 (2019) 18889–18897, https://doi.org/10.1039/C9TA04789A.
[180] A.J. Ward, A. Ruseckas, M.M. Kareem, B. Ebenhoch, L.A. Serrano, M. Al-Eid, B. Fitzpatrick, V.M. Rotello, G. Cooke, I.D.W. Samuel, The impact of driving force on electron transfer rates in photovoltaic donor–acceptor blends, Adv. Mater. 27 (2015) 2496–2500, https://doi.org/10.1002/adma.201405623.
[181] K. Nakano, Y. Chen, B. Xiao, W. Han, J. Huang, H. Yoshida, E. Zhou, K. Tajima, Anatomy of the energetic driving force for charge generation in organic solar cells, Nat. Commun. 10 (2019) 2520, https://doi.org/10.1038/s41467-019-10434-3.
[182] H. Cha, S. Wheeler, S. Holliday, S.D. Dimitrov, A. Wadsworth, H.H. Lee, D. Baran, I. McCulloch, J.R. Durrant, Influence of blend morphology and energetics on charge separation and recombination dynamics in organic solar cells incorporating a nonfullerene acceptor, Adv. Funct. Mater. 28 (2018), 1704389, https://doi.org/10.1002/adfm.201704389.
[183] S.M. Menke, N.A. Ran, G.C. Bazan, R.H. Friend, Understanding energy loss in organic solar cells: toward a new efficiency regime, Joule 2 (2018) 25–35, https://doi.org/10.1016/j.joule.2017.09.020.
[184] J. Zhang, W. Liu, G. Zhou, Y. Yi, S. Xu, F. Liu, H. Zhu, X. Zhu, Accurate determination of the minimum homo offset for efficient charge generation using organic semiconducting alloys, Adv. Energy Mater. 10 (2020), 1903298, https://doi.org/10.1002/aenm.201903298.
[185] Y. Li, D. Qian, L. Zhong, J.D. Lin, Z.Q. Jiang, Z.G. Zhang, Z. Zhang, Y. Li, L.S. Liao, F. Zhang, A fused-ring based electron acceptor for efficient non-fullerene polymer solar cells with small homo offset, Nano Energy 27 (2016) 430–438, https://doi.org/10.1016/j.nanoen.2016.07.019.
[186] S. Chen, Y. Liu, L. Zhang, P.C.Y. Chow, Z. Wang, G. Zhang, W. Ma, H. Yan, A wide-bandgap donor polymer for highly efficient non-fullerene organic solar cells with a small voltage loss, J. Am. Chem. Soc. 139 (2017) 6298–6301, https://doi.org/10.1021/jacs.7b01606.
[187] S. Li, L. Zhan, C. Sun, H. Zhu, G. Zhou, W. Yang, M. Shi, C.Z. Li, J. Hou, Y. Li, H. Chen, Highly efficient fullerene-free organic solar cells operate at near zero highest occupied molecular orbital offsets, J. Am. Chem. Soc. 141 (2019) 3073–3082, https://doi.org/10.1021/jacs.8b12126.
[188] Z. Zhou, W. Liu, G. Zhou, M. Zhang, D. Qian, J. Zhang, S. Chen, S. Xu, C. Yang, F. Gao, H. Zhu, F. Liu, X. Zhu, Subtle molecular tailoring induces significant morphology optimization enabling over 16% efficiency organic solar cells with efficient charge generation, Adv. Mater. 32 (2020), 1906324, https://doi.org/10.1002/adma.201906324.
[189] Y. Zhong, M. Causa', G.J. Moore, P. Krauspe, B. Xiao, F. Günther, J. Kublitski, R. Shivhare, J. Benduhn, E. BarOr, S. Mukherjee, K.M. Yallum, J. Réhault, S.C. B. Mannsfeld, D. Neher, L.J. Richter, D.M. DeLongchamp, F. Ortmann, K. Vandewal, E. Zhou, N. Banerji, Sub-picosecond charge-transfer at near-zero driving force in polymer:non-fullerene acceptor blends and bilayers, Nat. Commun. 11 (2020) 833, https://doi.org/10.1038/s41467-020-14549-w.
[190] C. Yan, S. Barlow, Z. Wang, H. Yan, A.K.Y. Jen, S.R. Marder, X. Zhan, Non-fullerene acceptors for organic solar cells, Nat. Rev. Mater. 3 (2018) 18003, https://doi.org/10.1038/natrevmats.2018.3.
[191] D. Baran, T. Kirchartz, S. Wheeler, S. Dimitrov, M. Abdelsamie, J. Gorman, R. S. Ashraf, S. Holliday, A. Wadsworth, N. Gasparini, P. Kaienburg, H. Yan, A. Amassian, C.J. Brabec, J.R. Durrant, I. McCulloch, Reduced voltage losses yield 10% efficient fullerene free organic solar cells with >1 V open circuit voltages, Energy Environ. Sci. 9 (2016) 3783–3793, https://doi.org/10.1039/C6EE02598F.
[192] S. Chen, Y. Wang, L. Zhang, J. Zhao, Y. Chen, D. Zhu, H. Yao, G. Zhang, W. Ma, R. H. Friend, P.C.Y. Chow, F. Gao, H. Yan, Efficient nonfullerene organic solar cells with small driving forces for both hole and electron transfer, Adv. Mater. 30 (2018), 1804215, https://doi.org/10.1002/adma.201804215.
[193] M.P. Aplan, J.M. Munro, Y. Lee, A.N. Brigeman, C. Grieco, Q. Wang, N.C. Giebink, I. Dabo, J.B. Asbury, E.D. Gomez, Revealing the importance of energetic and entropic contributions to the driving force for charge photogeneration, ACS Appl. Mater. Interfaces 10 (2018) 39933–39941, https://doi.org/10.1021/acsami.8b12077.
[194] X. Wan, C. Li, M. Zhang, Y. Chen, Acceptor–donor–acceptor type molecules for high performance organic photovoltaics – chemistry and mechanism, Chem. Soc. Rev. 49 (2020) 2828–2842, https://doi.org/10.1039/D0CS00084A.
[195] L. Perdigón-Toro, H. Zhang, A. Markina, J. Yuan, S.M. Hosseini, C.M. Wolff, G. Zuo, M. Stolterfoht, Y. Zou, F. Gao, D. Andrienko, S. Shoaee, D. Neher, Barrierless free charge generation in the high-performance pm6:Y6 bulk heterojunction non-fullerene solar cell, Adv. Mater. 32 (2020), 1906763, https://doi.org/10.1002/adma.201906763.
[196] R. Wang, C. Zhang, Q. Li, Z. Zhang, X. Wang, M. Xiao, Charge separation from an intra-moiety intermediate state in the high-performance pm6:Y6 organic photovoltaic blend, J. Am. Chem. Soc. 142 (2020) 12751–12759, https://doi.org/10.1021/jacs.0c04890.
[197] J.Y. Wu, J. Lee, Y.C. Chin, H.F. Yao, H. Cha, J. Luke, J.H. Hou, J.S. Kim, J. R. Durrant, Exceptionally low charge trapping enables highly efficient organic bulk heterojunction solar cells, Energy Environ. Sci. 13 (2020) 2422–2430, https://doi.org/10.1039/d0ee01338b.

[198] R.A.J. Janssen, J. Nelson, Factors limiting device efficiency in organic photovoltaics, Adv. Mater. 25 (2013) 1847–1858, https://doi.org/10.1002/adma.201202873.
[199] H. Yao, Y. Cui, D. Qian, C.S. Ponseca, A. Honarfar, Y. Xu, J. Xin, Z. Chen, L. Hong, B. Gao, R. Yu, Y. Zu, W. Ma, P. Chabera, T. Pullerits, A. Yartsev, F. Gao, J. Hou, 14.7% efficiency organic photovoltaic cells enabled by active materials with a large electrostatic potential difference, J. Am. Chem. Soc. 141 (2019) 7743–7750, https://doi.org/10.1021/jacs.8b12937.
[200] M. Wang, Y.Z. Li, H.C. Chen, C.W. Liu, Y.S. Chen, Y.C. Lo, C.S. Tsao, Y.C. Huang, S.W. Liu, K.T. Wong, B. Hu, Unveiling the underlying mechanism of record-high efficiency organic near-infrared photodetector harnessing a single-component photoactive layer, Mater. Horiz. 7 (2020) 1171–1179, https://doi.org/10.1039/C9MH01524H.
[201] M. Schwarze, K.S. Schellhammer, K. Ortstein, J. Benduhn, C. Gaul, A. Hinderhofer, L. Perdigón Toro, R. Scholz, J. Kublitski, S. Roland, M. Lau, C. Poelking, D. Andrienko, G. Cuniberti, F. Schreiber, D. Neher, K. Vandewal, F. Ortmann, K. Leo, Impact of molecular quadrupole moments on the energy levels at organic heterojunctions, Nat. Commun. 10 (2019) 2466, https://doi.org/10.1038/s41467-019-10435-2.
[202] C. Poelking, D. Andrienko, Long-range embedding of molecular ions and excitations in a polarizable molecular environment, J. Chem. Theory Comput. 12 (2016) 4516–4523, https://doi.org/10.1021/acs.jctc.6b00599.
[203] C. Poelking, M. Tietze, C. Elschner, S. Olthof, D. Hertel, B. Baumeier, F. Würthner, K. Meerholz, K. Leo, D. Andrienko, Impact of mesoscale order on open-circuit voltage in organic solar cells, Nat. Mater. 14 (2015) 434–439, https://doi.org/10.1038/nmat4167.
[204] Y. Dong, V.C. Nikolis, F. Talnack, Y.C. Chin, J. Benduhn, G. Londi, J. Kublitski, X. Zheng, S.C.B. Mannsfeld, D. Spoltore, L. Muccioli, J. Li, X. Blase, D. Beljonne, J. S. Kim, A.A. Bakulin, G. D'Avino, J.R. Durrant, K. Vandewal, Orientation dependent molecular electrostatics drives efficient charge generation in homojunction organic solar cells, Nat. Commun. 11 (2020) 4617, https://doi.org/10.1038/s41467-020-18439-z.
[205] Y. Wu, J. Guo, W. Wang, Z. Chen, Z. Chen, R. Sun, Q. Wu, T. Wang, X. Hao, H. Zhu, J. Min, A conjugated donor-acceptor block copolymer enables over 11% efficiency for single-component polymer solar cells, Joule 5 (2021) 1800–1815, https://doi.org/10.1016/j.joule.2021.05.002.
[206] Y. Gao, Surface analytical studies of interfaces in organic semiconductor devices, Mater. Sci. Eng. R 68 (2010) 39–87, https://doi.org/10.1016/j.mser.2010.01.001.
[207] S.H. Choi, S.M. Jeong, W.H. Koo, S.J. Jo, H.K. Baik, S.J. Lee, K.M. Song, D. W. Han, Diamond-like carbon as a buffer layer in polymeric electroluminescent device, Thin Solid Films 483 (2005) 351–357, https://doi.org/10.1016/j.tsf.2004.12.040.
[208] S. Braun, W.R. Salaneck, M. Fahlman, Energy-level alignment at organic/metal and organic/organic interfaces, Adv. Mater. 21 (2009) 1450–1472, https://doi.org/10.1002/adma.200802893.
[209] A. Sharma, R. Berger, D.A. Lewis, G.G. Andersson, Invisible high workfunction materials on heterogeneous surfaces, Appl. Surf. Sci. 327 (2015) 22–26, https://doi.org/10.1016/j.apsusc.2014.11.089.
[210] J. Bertrandie, J. Han, C.S.P. De Castro, E. Yengel, J. Gorenflot, T. Anthopoulos, F. Laquai, A. Sharma, D. Baran, The energy level conundrum of organic semiconductors in solar cells, Adv. Mater. (2022), 2202575, https://doi.org/10.1002/adma.202202575 n/a.
[211] X.E. Li, Q. Zhang, J. Yu, Y. Xu, R. Zhang, C. Wang, H. Zhang, S. Fabiano, X. Liu, J. Hou, F. Gao, M. Fahlman, Mapping the energy level alignment at donor/acceptor interfaces in non-fullerene organic solar cells, Nat. Commun. 13 (2022) 2046, https://doi.org/10.1038/s41467-022-29702-w.
[212] R.E.M. Willems, C.H.L. Weijtens, X. de Vries, R. Coehoorn, R.A.J. Janssen, Relating frontier orbital energies from voltammetry and photoelectron spectroscopy to the open-circuit voltage of organic solar cells, Adv. Energy Mater. 9 (2019), 1803677, https://doi.org/10.1002/aenm.201803677.
[213] L. Jong-Hoon, J.S. Yi, K. Geunjin, P. Byoungwook, K. Junghwan, K. Seyoung, K. Bongseong, L. Kwanghee, Reinforcing the built-in field for efficient charge collection in polymer solar cells, Adv. Funct. Mater. 28 (2018), 1705079, https://doi.org/10.1002/adfm.201705079.
[214] W. Tress, K. Leo, M. Riede, Influence of hole-transport layers and donor materials on open-circuit voltage and shape of I–V curves of organic solar cells, Adv. Funct. Mater. 21 (2011) 2140–2149, https://doi.org/10.1002/adfm.201002669.
[215] C.J. Brabec, S.E. Shaheen, C. Winder, N.S. Sariciftci, P. Denk, Effect of lif/metal electrodes on the performance of plastic solar cells, Appl. Phys. Lett. 80 (2002) 1288–1290, https://doi.org/10.1063/1.1446988.
[216] D. Gupta, M. Bag, K.S. Narayan, Correlating reduced fill factor in polymer solar cells to contact effects, Appl. Phys. Lett. 92 (2008) 093301–093303, https://doi.org/10.1063/1.2841062.
[217] J. Hwang, A. Wan, A. Kahn, Energetics of metal–organic interfaces: new experiments and assessment of the field, Mater. Sci. Eng. R. Rep. 64 (2009) 1–31, https://doi.org/10.1016/j.mser.2008.12.001.
[218] L.M. Chen, Z. Xu, Z. Hong, Y. Yang, Interface investigation and engineering - achieving high performance polymer photovoltaic devices, J. Mater. Chem. 20 (2010) 2575–2598, https://doi.org/10.1039/B925382C.
[219] A. Sharma, G. Andersson, D.A. Lewis, Role of humidity on indium and tin migration in organic photovoltaic devices, Phys. Chem. Chem. Phys. 13 (2011) 4381–4387, https://doi.org/10.1039/c0cp02203a.
[220] A. Sharma, S.E. Watkins, D.A. Lewis, G. Andersson, Effect of indium and tin contamination on the efficiency and electronic properties of organic bulk heterojunction solar cells, Sol. Energy Mater. Sol. Cells 95 (2011) 3251–3255, https://doi.org/10.1016/j.solmat.2011.07.012.
[221] M. Jørgensen, K. Norrman, F.C. Krebs, Stability/degradation of polymer solar cells, Sol. Energy Mater. Sol. Cells 92 (2008) 686–714, https://doi.org/10.1016/j.solmat.2008.01.005.
[222] F.C. Krebs, Air stable polymer photovoltaics based on a process free from vacuum steps and fullerenes, Sol. Energy Mater. Sol. Cells 92 (2008) 715–726, https://doi.org/10.1016/j.solmat.2008.01.013.
[223] W.H. Baek, I. Seo, T.S. Yoon, H.H. Lee, C.M. Yun, Y.S. Kim, Hybrid inverted bulk heterojunction solar cells with nanoimprinted tio2 nanopores, Sol. Energy Mater. Sol. Cells 93 (2009) 1587–1591, https://doi.org/10.1016/j.solmat.2009.04.014.
[224] Z. Liang, Q. Zhang, O. Wiranwetchayan, J. Xi, Z. Yang, K. Park, C. Li, G. Cao, Effects of the morphology of a ZnO buffer layer on the photovoltaic performance of inverted polymer solar cells, Adv. Funct. Mater. 22 (2012) 2194–2201, https://doi.org/10.1002/adfm.201101915.
[225] Y. Sun, J.H. Seo, C.J. Takacs, J. Seifter, A.J. Heeger, Inverted polymer solar cells integrated with a low-temperature-annealed sol-gel-derived ZnO film as an electron transport layer, Adv. Mater. 23 (2011) 1679–1683, https://doi.org/10.1002/adma.201004301.
[226] A. Sharma, M. Ionescu, G.G. Andersson, D.A. Lewis, Role of zinc oxide thickness on the photovoltaic performance of laminated organic bulk-heterojunction solar cells, Sol. Energy Mater. Sol. Cells 115 (2013) 64–70, https://doi.org/10.1016/j.solmat.2013.03.012.
[227] A. Sharma, S.E. Watkins, G. Andersson, D.A. Lewis, Effect of annealing temperature of ZnO on the energy level alignment in inverted organic photovoltaics (OPVs), Energy Tech. 2 (2014) 462–468, https://doi.org/10.1002/ente.201300186.
[228] Z. George, Y. Xia, A. Sharma, C. Lindqvist, G. Andersson, O. Inganas, E. Moons, C. Muller, M.R. Andersson, Two-in-one: cathode modification and improved solar cell blend stability through addition of modified fullerenes, J. Mater. Chem. A 4 (2016) 2663–2669, https://doi.org/10.1039/C5TA06420A.
[229] C.V. Hoven, A. Garcia, G.C. Bazan, T.Q. Nguyen, Recent applications of conjugated polyelectrolytes in optoelectronic devices, Adv. Mater. 20 (2008) 3793–3810, https://doi.org/10.1002/adma.200800533.
[230] C. Duan, K. Zhang, C. Zhong, F. Huang, Y. Cao, Recent advances in water/alcohol-soluble [small pi]-conjugated materials: new materials and growing applications in solar cells, Chem. Soc. Rev. 42 (2013) 9071–9104, https://doi.org/10.1039/C3CS60200A.
[231] J.M. Bjuggren, A. Sharma, D. Gedefaw, S. Elmas, C. Pan, B. Kirk, X. Zhao, G. Andersson, M.R. Andersson, Facile synthesis of an efficient and robust cathode interface material for polymer solar cells, ACS Appl. Energy Mater. 1 (2018) 7130–7139, https://doi.org/10.1021/acsaem.8b01554.
[232] A. Sharma, R. Kroon, D.A. Lewis, G.G. Andersson, M.R. Andersson, Poly(4-vinylpyridine): a new interface layer for organic solar cells, ACS Appl. Mater. Interfaces (2017) 10929–10936, https://doi.org/10.1021/acsami.6b12687.
[233] A. Sharma, Z. George, T. Bennett, D.A. Lewis, G.F. Metha, G.G. Andersson, M. R. Andersson, Stability of polymer interlayer modified ito electrodes for organic solar cells, Aust. J. Chem. 69 (2016) 735–740, https://doi.org/10.1071/CH15806.
[234] D. Ma, M. Lv, M. Lei, J. Zhu, H. Wang, X. Chen, Self-organization of amine-based cathode interfacial materials in inverted polymer solar cells, ACS Nano 8 (2014) 1601–1608, https://doi.org/10.1021/nn4059067.
[235] W.Y. Tan, R. Wang, M. Li, G. Liu, P. Chen, X.C. Li, S.M. Lu, H.L. Zhu, Q.M. Peng, X.H. Zhu, W. Chen, W.C.H. Choy, F. Li, J. Peng, Y. Cao, Lending triarylphosphine oxide to phenanthroline: a facile approach to high-performance organic small-molecule cathode interfacial material for organic photovoltaics utilizing air-stable cathodes, Adv. Funct. Mater. 24 (2014) 6540–6547, https://doi.org/10.1002/adfm.201401685.
[236] Y. Zhou, C. Fuentes-Hernandez, J. Shim, J. Meyer, A.J. Giordano, H. Li, P. Winget, T. Papadopoulos, H. Cheun, J. Kim, M. Fenoll, A. Dindar, W. Haske, E. Najafabadi, T.M. Khan, H. Sojoudi, S. Barlow, S. Graham, J.L. Brédas, S.R. Marder, A. Kahn, B. Kippelen, A universal method to produce low–work function electrodes for organic electronics, Science 336 (2012) 327–332, https://doi.org/10.1126/science.1218829.
[237] S. Venkatesan, E. Ngo, D. Khatiwada, C. Zhang, Q. Qiao, Enhanced lifetime of polymer solar cells by surface passivation of metal oxide buffer layers, ACS Appl. Mater. Interfaces 7 (2015) 16093–16100, https://doi.org/10.1021/acsami.5b04687.
[238] Z. Tang, W. Tress, Q. Bao, M.J. Jafari, J. Bergqvist, T. Ederth, M.R. Andersson, O. Inganäs, Improving cathodes with a polymer interlayer in reversed organic solar cells, Adv. Energy Mater. 4 (2014), 1400643, https://doi.org/10.1002/aenm.201400643.
[239] Z. He, H. Wu, Y. Cao, Recent advances in polymer solar cells: realization of high device performance by incorporating water/alcohol-soluble conjugated polymers as electrode buffer layer, Adv. Mater. 26 (2014) 1006–1024, https://doi.org/10.1002/adma.201303391.
[240] P. Xiang, H. Lin, Q. Fei, Z. Yinhua, C.P. K, Low work function surface modifiers for solution-processed electronics: a review, Adv. Mater. Interfaces 5 (2018), 1701404, https://doi.org/10.1002/admi.201701404.
[241] Z. Yin, J. Wei, Q. Zheng, Interfacial materials for organic solar cells: recent advances and perspectives, Adv. Sci. 3 (2016), 1500362, https://doi.org/10.1002/advs.201500362.
[242] K. Zhang, C. Zhong, S. Liu, C. Mu, Z. Li, H. Yan, F. Huang, Y. Cao, Highly efficient inverted polymer solar cells based on a cross-linkable water-/alcohol-soluble conjugated polymer interlayer, ACS Appl. Mater. Interfaces 6 (2014) 10429–10435, https://doi.org/10.1021/am501920z.

[243] Z.G. Zhang, B. Qi, Z. Jin, D. Chi, Z. Qi, Y. Li, J. Wang, Perylene diimides: a thickness-insensitive cathode interlayer for high performance polymer solar cells, Energy Environ. Sci. 7 (2014) 1966–1973, https://doi.org/10.1039/C4EE00022F.
[244] L. Hu, Y. Liu, L. Mao, S. Xiong, L. Sun, N. Zhao, F. Qin, Y. Jiang, Y. Zhou, Chemical reaction between an itic electron acceptor and an amine-containing interfacial layer in non-fullerene solar cells, J. Mater. Chem. A 6 (2018) 2273–2278, https://doi.org/10.1039/C7TA10306A.
[245] S. Xiong, L. Hu, L. Hu, L. Sun, F. Qin, X. Liu, M. Fahlman, Y. Zhou, 12.5% flexible nonfullerene solar cells by passivating the chemical interaction between the active layer and polymer interfacial layer, Adv. Mater. 31 (2019), 1806616, https://doi.org/10.1002/adma.201806616.
[246] J. Yao, B. Qiu, Z.G. Zhang, L. Xue, R. Wang, C. Zhang, S. Chen, Q. Zhou, C. Sun, C. Yang, M. Xiao, L. Meng, Y. Li, Cathode engineering with perylene-diimide interlayer enabling over 17% efficiency single-junction organic solar cells, Nat. Commun. 11 (2020) 2726, https://doi.org/10.1038/s41467-020-16509-w.
[247] F.J. Lim, K. Ananthanarayanan, J. Luther, G.W. Ho, Influence of a novel fluorosurfactant modified PEDOT:PSS hole transport layer on the performance of inverted organic solar cells, J. Mater. Chem. 22 (2012) 25057–25064, https://doi.org/10.1039/C2JM35646E.
[248] J. Bertrandie, A. Sharma, N. Gasparini, D.R. Villalva, S.H.K. Paleti, N. Wehbe, J. Troughton, D. Baran, Air-processable and thermally stable hole transport layer for non-fullerene organic solar cells, ACS Appl. Energy Mater. 5 (2022) 1023–1030, https://doi.org/10.1021/acsaem.1c03378.
[249] Z. Zheng, Q. Hu, S. Zhang, D. Zhang, J. Wang, S. Xie, R. Wang, Y. Qin, W. Li, L. Hong, N. Liang, F. Liu, Y. Zhang, Z. Wei, Z. Tang, T.P. Russell, J. Hou, H. Zhou, A highly efficient non-fullerene organic solar cell with a fill factor over 0.80 enabled by a fine-tuned hole-transporting layer, Adv. Mater. 30 (2018), 1801801, https://doi.org/10.1002/adma.201801801.
[250] H. Zhou, Y. Zhang, C.K. Mai, J. Seifter, T.Q. Nguyen, G.C. Bazan, A.J. Heeger, Solution-processed ph-neutral conjugated polyelectrolyte improves interfacial contact in organic solar cells, ACS Nano 9 (2015) 371–377, https://doi.org/10.1021/nn505378m.
[251] Y. Cui, B. Xu, B. Yang, H. Yao, S. Li, J. Hou, A novel ph neutral self-doped polymer for anode interfacial layer in efficient polymer solar cells, Macromolecules 49 (2016) 8126–8133, https://doi.org/10.1021/acs.macromol.6b01595.
[252] Y. Cui, G. Jia, J. Zhu, Q. Kang, H. Yao, L. Lu, B. Xu, J. Hou, The critical role of anode work function in non-fullerene organic solar cells unveiled by counterion-size-controlled self-doping conjugated polymers, Chem. Mater. 30 (2018) 1078–1084, https://doi.org/10.1021/acs.chemmater.7b04982.
[253] K.C. Kwon, C. Kim, Q.V. Le, S. Gim, J.M. Jeon, J.Y. Ham, J.L. Lee, H.W. Jang, S. Y. Kim, Synthesis of atomically thin transition metal disulfides for charge transport layers in optoelectronic devices, ACS Nano 9 (2015) 4146–4155, https://doi.org/10.1021/acsnano.5b01504.
[254] Y. Lin, B. Adilbekova, Y. Firdaus, E. Yengel, H. Faber, M. Sajjad, X. Zheng, E. Yarali, A. Seitkhan, O.M. Bakr, A. El-Labban, U. Schwingenschlögl, V. Tung, I. McCulloch, F. Laquai, T.D. Anthopoulos, 17% efficient organic solar cells based on liquid exfoliated WS_2 as a replacement for PEDOT:PSS, Adv. Mater. (2019), 1902965, https://doi.org/10.1002/adma.201902965.
[255] M. Timpel, H. Li, M.V. Nardi, B. Wegner, J. Frisch, P.J. Hotchkiss, S.R. Marder, S. Barlow, J.L. Brédas, N. Koch, Electrode work function engineering with phosphonic acid monolayers and molecular acceptors: charge redistribution mechanisms, Adv. Funct. Mater. 28 (2018), 1704438, https://doi.org/10.1002/adfm.201704438.
[256] y. lin, Y. Firdaus, F.H. Isikgor, M.I. Nugraha, E. Yengel, G.T. Harrison, R. Hallani, A. El Labban, H. Faber, C. Ma, X. Zheng, A.S. Subbiah, C.T. Howells, O.M. Bakr, I. McCulloch, S. De Wolf, L. Tsetseris, T.D. Anthopoulos, Self-assembled monolayer enables htl-free organic solar cells with 18% efficiency and improved operational stability, ACS Energy Lett. (2020), https://doi.org/10.1021/acsenergylett.0c01421.
[257] C. Lindqvist, J. Bergqvist, C.C. Feng, S. Gustafsson, O. Bäcke, N.D. Treat, C. Bounioux, P. Henriksson, R. Kroon, E. Wang, A. Sanz-Velasco, P.M. Kristiansen, N. Stingelin, E. Olsson, O. Inganäs, M.R. Andersson, C. Müller, Fullerene nucleating agents: a route towards thermally stable photovoltaic blends, Adv. Energy Mater. 4 (2014), 1301437, https://doi.org/10.1002/aenm.201301437.
[258] C. Zhong, J.A. Bartelt, M.D. McGehee, D. Cao, F. Huang, Y. Cao, A.J. Heeger, Influence of intermixed donor and acceptor domains on the ultrafast charge generation in bulk heterojunction materials, J. Phys. Chem. C 119 (2015) 26889–26894, https://doi.org/10.1021/acs.jpcc.5b09572.
[259] X. Song, N. Gasparini, L. Ye, H. Yao, J. Hou, H. Ade, D. Baran, Controlling blend morphology for ultrahigh current density in nonfullerene acceptor-based organic solar cells, ACS Energy Lett. 3 (2018) 669–676, https://doi.org/10.1021/acsenergylett.7b01266.
[260] G. Li, V. Shrotriya, J. Huang, Y. Yao, T. Moriarty, K. Emery, Y. Yang, High-efficiency solution processable polymer photovoltaic cells by self-organization of polymer blends, Nat. Mater. 4 (2005) 864–868, https://doi.org/10.1038/nmat1500.
[261] W. Cai, C. Zhong, C. Duan, Z. Hu, S. Dong, D. Cao, M. Lei, F. Huang, Y. Cao, The influence of amino group on PCDTBT-based and P3HT-based polymer solar cells: hole trapping processes, Appl. Phys. Lett. 106 (2015), 233302, https://doi.org/10.1063/1.4922467.
[262] W. Li, K.H. Hendriks, A. Furlan, W.S.C. Roelofs, S.C.J. Meskers, M.M. Wienk, R.A. J. Janssen, Effect of the fibrillar microstructure on the efficiency of high molecular weight diketopyrrolopyrrole-based polymer solar cells, Adv. Mater. 26 (2014) 1565–1570, https://doi.org/10.1002/adma.201304360.
[263] Z. Li, X. Xu, W. Zhang, X. Meng, W. Ma, A. Yartsev, O. Inganäs, M.R. Andersson, R.A.J. Janssen, E. Wang, High performance all-polymer solar cells by synergistic effects of fine-tuned crystallinity and solvent annealing, J. Am. Chem. Soc. 138 (2016) 10935–10944, https://doi.org/10.1021/jacs.6b04822.
[264] C. Lindqvist, J. Bergqvist, O. Bäcke, S. Gustafsson, E. Wang, E. Olsson, O. Inganäs, M.R. Andersson, C. Müller, Fullerene mixtures enhance the thermal stability of a non-crystalline polymer solar cell blend, Appl. Phys. Lett. 104 (2014), 153301, https://doi.org/10.1063/1.4870997.
[265] M. Campoy-Quiles, T. Ferenczi, T. Agostinelli, P.G. Etchegoin, Y. Kim, T. D. Anthopoulos, P.N. Stavrinou, D.D.C. Bradley, J. Nelson, Morphology evolution via self-organization and lateral and vertical diffusion in polymer:Fullerene solar cell blends, Nat. Mater. 7 (2008) 158–164, https://doi.org/10.1038/nmat2102.
[266] W. Ma, C. Yang, X. Gong, K. Lee, A.J. Heeger, Thermally stable, efficient polymer solar cells with nanoscale control of the interpenetrating network morphology, Adv. Funct. Mater. 15 (2005) 1617–1622, https://doi.org/10.1002/adfm.200500211.
[267] J. Bergqvist, C. Lindqvist, O. Backe, Z. Ma, Z. Tang, W. Tress, S. Gustafsson, E. Wang, E. Olsson, M.R. Andersson, O. Inganas, C. Muller, Sub-glass transition annealing enhances polymer solar cell performance, J. Mater. Chem. A 2 (2014) 6146–6152, https://doi.org/10.1039/C3TA14165A.
[268] A.D. de Zerio, C. Müller, Glass forming acceptor alloys for highly efficient and thermally stable ternary organic solar cells, Adv. Energy Mater. 8 (2018), 1702741, https://doi.org/10.1002/aenm.201702741.
[269] L. Yu, D. Qian, S. Marina, F.A.A. Nugroho, A. Sharma, S. Hultmark, A.I. Hofmann, R. Kroon, J. Benduhn, D.M. Smilgies, K. Vandewal, M.R. Andersson, C. Langhammer, J. Martín, F. Gao, C. Müller, Diffusion-limited crystallization: a rationale for the thermal stability of non-fullerene solar cells, ACS Appl. Mater. Interfaces 11 (2019) 21766–21774, https://doi.org/10.1021/acsami.9b04554.
[270] C. Müller, On the glass transition of polymer semiconductors and its impact on polymer solar cell stability, Chem. Mater. 27 (2015) 2740–2754, https://doi.org/10.1021/acs.chemmater.5b00024.
[271] D.S. Kaplan, Structure–property relationships in copolymers to composites: molecular interpretation of the glass transition phenomenon, J. Appl. Polym. Sci. 20 (1976) 2615–2629, https://doi.org/10.1002/app.1976.070201001.
[272] D.J. Lipomi, Stretchable figures of merit in deformable electronics, Adv. Mater. 28 (2016) 4180–4183, https://doi.org/10.1002/adma.201504196.
[273] J. Zhao, A. Swinnen, G. Van Assche, J. Manca, D. Vanderzande, B.V. Mele, Phase diagram of P3HT/PCBM blends and its implication for the stability of morphology, J. Phys. Chem. B 113 (2009) 1587–1591, https://doi.org/10.1021/jp804151a.
[274] R. Noriega, J. Rivnay, K. Vandewal, F.P.V. Koch, N. Stingelin, P. Smith, M. F. Toney, A. Salleo, A general relationship between disorder, aggregation and charge transport in conjugated polymers, Nat. Mater. 12 (2013) 1038, https://doi.org/10.1038/nmat3722.
[275] A. Sharma, X. Pan, J.M. Bjuggren, D. Gedefaw, X. Xu, R. Kroon, E. Wang, J. A. Campbell, D.A. Lewis, M.R. Andersson, Probing the relationship between molecular structures, thermal transitions, and morphology in polymer semiconductors using a woven glass-mesh-based dmta technique, Chem. Mater. 31 (2019) 6740–6749, https://doi.org/10.1021/acs.chemmater.9b01213.
[276] C. Lindqvist, A. Sanz-Velasco, E. Wang, O. Backe, S. Gustafsson, E. Olsson, M. R. Andersson, C. Muller, Nucleation-limited fullerene crystallisation in a polymer-fullerene bulk-heterojunction blend, J. Mater. Chem. A 1 (2013) 7174–7180, https://doi.org/10.1039/C3TA11018D.
[277] C. Muller, J. Bergqvist, K. Vandewal, K. Tvingstedt, A.S. Anselmo, R. Magnusson, M.I. Alonso, E. Moons, H. Arwin, M. Campoy-Quiles, O. Inganas, Phase behaviour of liquid-crystalline polymer/fullerene organic photovoltaic blends: thermal stability and miscibility, J. Mater. Chem. 21 (2011) 10676–10684.
[278] S.E. Root, M.A. Alkhadra, D. Rodriquez, A.D. Printz, D.J. Lipomi, Measuring the glass transition temperature of conjugated polymer films with ultraviolet–visible spectroscopy, Chem. Mater. 29 (2017) 2646–2654, https://doi.org/10.1021/acs.chemmater.7b00242.
[279] F.A.A. Nugroho, A. Diaz de Zerio Mendaza, C. Lindqvist, T.J. Antosiewicz, C. Müller, C. Langhammer, Plasmonic nanospectroscopy for thermal analysis of organic semiconductor thin films, Anal. Chem. 89 (2017) 2575–2582, https://doi.org/10.1021/acs.analchem.6b04807.
[280] R. Xie, Y. Lee, M.P. Aplan, N.J. Caggiano, C. Müller, R.H. Colby, E.D. Gomez, Glass transition temperature of conjugated polymers by oscillatory shear rheometry, Macromolecules 50 (2017) 5146–5154, https://doi.org/10.1021/acs.macromol.7b00712.
[281] J. Martín, N. Stingelin, D. Cangialosi, Direct calorimetric observation of the rigid amorphous fraction in a semiconducting polymer, J. Phys. Chem. Lett. 9 (2018) 990–995, https://doi.org/10.1021/acs.jpclett.7b03110.
[282] P.E. Hopkinson, P.A. Staniec, A.J. Pearson, A.D.F. Dunbar, T. Wang, A.J. Ryan, R. A.L. Jones, D.G. Lidzey, A.M. Donald, A phase diagram of the P3HT:PCBM organic photovoltaic system: implications for device processing and performance, Macromolecules 44 (2011) 2908–2917, https://doi.org/10.1021/ma102524a.
[283] B.C. Schroeder, Y.C. Chiu, X. Gu, Y. Zhou, J. Xu, J. Lopez, C. Lu, M.F. Toney, Z. Bao, Non-conjugated flexible linkers in semiconducting polymers: a pathway to improved processability without compromising device performance, Adv. Electron. Mater. 2 (2016), 1600104, https://doi.org/10.1002/aelm.201600104.
[284] A. Sharma, X. Pan, J.A. Campbell, M.R. Andersson, D.A. Lewis, Unravelling the thermomechanical properties of bulk heterojunction blends in polymer solar cells, Macromolecules 50 (2017) 3347–3354, https://doi.org/10.1021/acs.macromol.7b00430.
[285] N.P. Holmes, M. Marks, J.M. Cave, K. Feron, M.G. Barr, A. Fahy, A. Sharma, X. Pan, D.A.L. Kilcoyne, X. Zhou, D.A. Lewis, M.R. Andersson, J. van Stam, A.

B. Walker, E. Moons, W.J. Belcher, P.C. Dastoor, Engineering two-phase and three-phase microstructures from water-based dispersions of nanoparticles for eco-friendly polymer solar cell applications, Chem. Mater. 30 (2018) 6521–6531, https://doi.org/10.1021/acs.chemmater.8b03222.
[286] X. Pan, A. Sharma, D. Gedefaw, R. Kroon, A. Diaz de Zerio, N.P. Holmes, A.L. D. Kilcoyne, M.G. Barr, A. Fahy, M. Marks, X. Zhou, W. Belcher, P.C. Dastoor, M. R. Andersson, Environmentally friendly preparation of nanoparticles for organic photovoltaics, Org. Electron. 59 (2018) 432–440, https://doi.org/10.1016/j.orgel.2018.05.040.
[287] M. Marks, N.P. Holmes, A. Sharma, X. Pan, R. Chowdhury, M.G. Barr, C. Fenn, M. J. Griffith, K. Feron, A.L.D. Kilcoyne, D.A. Lewis, M.R. Andersson, W.J. Belcher, P. C. Dastoor, Building intermixed donor–acceptor architectures for water-processable organic photovoltaics, Phys. Chem. Chem. Phys. 21 (2019) 5705–5715, https://doi.org/10.1039/C8CP07137C.
[288] L. Yu, E. Davidson, A. Sharma, M.R. Andersson, R. Segalman, C. Müller, Isothermal crystallization kinetics and time–temperature–transformation of the conjugated polymer: poly(3-(2′-ethyl)hexylthiophene), Chem. Mater. 29 (2017) 5654–5662, https://doi.org/10.1021/acs.chemmater.7b01393.
[289] P. Murto, Z. Genene, C.M. Benavides, X. Xu, A. Sharma, X. Pan, O. Schmidt, C. J. Brabec, M.R. Andersson, S.F. Tedde, W. Mammo, E. Wang, High performance all-polymer photodetector comprising a donor–acceptor–acceptor structured indacenodithiophene–bithieno[3,4-c]pyrroletetrone copolymer, ACS Macro Lett. 7 (2018) 395–400, https://doi.org/10.1021/acsmacrolett.8b00009.
[290] F. Machui, M. Hösel, N. Li, G.D. Spyropoulos, T. Ameri, R.R. Søndergaard, M. Jørgensen, A. Scheel, D. Gaiser, K. Kreul, D. Lenssen, M. Legros, N. Lemaitre, M. Vilkman, M. Välimäki, S. Nordman, C.J. Brabec, F.C. Krebs, Cost analysis of roll-to-roll fabricated ito free single and tandem organic solar modules based on data from manufacture, Energy Environ. Sci. 7 (2014) 2792–2802, https://doi.org/10.1039/C4EE01222D.
[291] A. Teichler, J. Perelaer, U.S. Schubert, Inkjet printing of organic electronics – comparison of deposition techniques and state-of-the-art developments, J. Mater. Chem. C 1 (2013) 1910–1925, https://doi.org/10.1039/C2TC00255H.
[292] Z.B. Henson, P. Zalar, X. Chen, G.C. Welch, T.Q. Nguyen, G.C. Bazan, Towards environmentally friendly processing of molecular semiconductors, J. Mater. Chem. A 1 (2013) 11117–11120, https://doi.org/10.1039/C3TA12690K.
[293] F.C. Krebs, Fabrication and processing of polymer solar cells: a review of printing and coating techniques, Sol. Energy Mater. Sol. Cells 93 (2009) 394–412, https://doi.org/10.1016/j.solmat.2008.10.004.
[294] L.M. Andersson, Fully slot–die-coated all-organic solar cells, Energy Tech. 3 (2015) 437–442, https://doi.org/10.1002/ente.201402153.
[295] F.C. Krebs, M. Jørgensen, K. Norrman, O. Hagemann, J. Alstrup, T.D. Nielsen, J. Fyenbo, K. Larsen, J. Kristensen, A complete process for production of flexible large area polymer solar cells entirely using screen printing–first public demonstration, Sol. Energy Mater. Sol. Cells 93 (2009) 422–441, https://doi.org/10.1016/j.solmat.2008.12.001.
[296] F.C. Krebs, Polymer solar cell modules prepared using roll-to-roll methods: knife-over-edge coating, slot-die coating and screen printing, Sol. Energy Mater. Sol. Cells 93 (2009) 465–475, https://doi.org/10.1016/j.solmat.2008.12.012.
[297] C. Yang, E. Zhou, S. Miyanishi, K. Hashimoto, K. Tajima, Preparation of active layers in polymer solar cells by aerosol jet printing, ACS Appl. Mater. Interfaces 3 (2011) 4053–4058, https://doi.org/10.1021/am200907k.
[298] S.W. Heo, J.Y. Lee, H.J. Song, J.R. Ku, D.K. Moon, Patternable brush painting process for fabrication of flexible polymer solar cells, Sol. Energy Mater. Sol. Cells 95 (2011) 3041–3046, https://doi.org/10.1016/j.solmat.2011.06.029.
[299] K.H. Yim, Z. Zheng, Z. Liang, R.H. Friend, W.T.S. Huck, J.S. Kim, Efficient conjugated-polymer optoelectronic devices fabricated by thin-film transfer-printing technique, Adv. Funct. Mater. 18 (2008) 1012–1019, https://doi.org/10.1002/adfm.200701321.
[300] Y. Kim, G. Kim, J. Lee, K. Lee, Morphology controlled bulk-heterojunction layers of fully electro-spray coated organic solar cells, Sol. Energy Mater. Sol. Cells 105 (2012) 272–279, https://doi.org/10.1016/j.solmat.2012.06.027.
[301] J.H. Chang, Y.H. Chen, H.W. Lin, Y.T. Lin, H.F. Meng, E.C. Chen, Highly efficient inverted rapid-drying blade-coated organic solar cells, Org. Electron. 13 (2012) 705–709, https://doi.org/10.1016/j.orgel.2011.12.025.
[302] B.A. Bailey, M.O. Reese, D.C. Olson, S.E. Shaheen, N. Kopidakis, Air-processed organic photovoltaic devices fabricated with hot press lamination, Org. Electron. 12 (2011) 108–112, https://doi.org/10.1016/j.orgel.2010.10.008.
[303] S.Y. Park, Y.J. Kang, S. Lee, D.G. Kim, J.K. Kim, J.H. Kim, J.W. Kang, Spray-coated organic solar cells with large-area of 12.25 cm^2, Sol. Energy Mater. Sol. Cells 95 (2011) 852–855, https://doi.org/10.1016/j.solmat.2010.10.033.
[304] X. Meng, L. Zhang, Y. Xie, X. Hu, Z. Xing, Z. Huang, C. Liu, L. Tan, W. Zhou, Y. Sun, W. Ma, Y. Chen, A general approach for lab-to-manufacturing translation on flexible organic solar cells, Adv. Mater. 31 (2019), 1903649, https://doi.org/10.1002/adma.201903649.
[305] H.W. Ro, J.M. Downing, S. Engmann, A.A. Herzing, D.M. DeLongchamp, L. J. Richter, S. Mukherjee, H. Ade, M. Abdelsamie, L.K. Jagadamma, A. Amassian, Y. Liu, H. Yan, Morphology changes upon scaling a high-efficiency, solution-processed solar cell, Energy Environ. Sci. 9 (2016) 2835–2846, https://doi.org/10.1039/C6EE01623E.
[306] S. Cros, R. de Bettignies, S. Berson, S. Bailly, P. Maisse, N. Lemaitre, S. Guillerez, Definition of encapsulation barrier requirements: a method applied to organic solar cells, Sol. Energy Mater. Sol. Cells 95 (2011) S65–S69, https://doi.org/10.1016/j.solmat.2011.01.035.
[307] M. Granstrom, K. Petritsch, A.C. Arias, A. Lux, M.R. Andersson, R.H. Friend, Laminated fabrication of polymeric photovoltaic diodes, Nature 395 (1998) 257–260, https://doi.org/10.1038/26183.
[308] J. Huang, G. Li, Y. Yang, A semi-transparent plastic solar cell fabricated by a lamination process, Adv. Mater. 20 (2008) 415–419, https://doi.org/10.1002/adma.200701101.
[309] R. Søndergaard, M. Hösel, D. Angmo, T.T. Larsen-Olsen, F.C. Krebs, Roll-to-roll fabrication of polymer solar cells, Mater. Today 15 (2012) 36–49, https://doi.org/10.1016/S1369-7021(12)70019-6.
[310] M.J. Moran, J.S. Zogorski, P.J. Squillace, Chlorinated solvents in groundwater of the united states, Environ. Sci. Technol. 41 (2007) 74–81, https://doi.org/10.1021/es061553y.
[311] N. Brautbar, J. Williams, Industrial solvents and liver toxicity: risk assessment, risk factors and mechanisms, Int. J. Hyg. Environ. Health 205 (2002) 479–491, https://doi.org/10.1078/1438-4639-00175.
[312] C. McDowell, G.C. Bazan, Organic solar cells processed from green solvents, Curr. Opin. Green Sustain. Chem. 5 (2017) 49–54, https://doi.org/10.1016/j.cogsc.2017.03.007.
[313] G. Kocak, D. Gedefaw, M.R. Andersson, Optimizing polymer solar cells using non-halogenated solvent blends, Polymers 11 (2019) 544, https://doi.org/10.3390/polym11030544.
[314] M. Lv, M. Lei, J. Zhu, T. Hirai, X. Chen, [6,6]-phenyl-C_{61}-butyric acid 2-((2-(dimethylamino)ethyl)(methyl)amino)-ethyl ester as an acceptor and cathode interfacial material in polymer solar cells, ACS Appl. Mater. Interfaces 6 (2014) 5844–5851, https://doi.org/10.1021/am5007047.
[315] J. Yang, A. Garcia, T.Q. Nguyen, Organic solar cells from water-soluble poly (thiophene)/fullerene heterojunction, Appl. Phys. Lett. 90 (2007), 103514, https://doi.org/10.1063/1.2711707.
[316] T.L. Nguyen, C. Lee, H. Kim, Y. Kim, W. Lee, J.H. Oh, B.J. Kim, H.Y. Woo, Ethanol-processable, highly crystalline conjugated polymers for eco-friendly fabrication of organic transistors and solar cells, Macromolecules 50 (2017) 4415–4424, https://doi.org/10.1021/acs.macromol.7b00452.
[317] C. Duan, W. Cai, B.B.Y. Hsu, C. Zhong, K. Zhang, C. Liu, Z. Hu, F. Huang, G. C. Bazan, A.J. Heeger, Y. Cao, Toward green solvent processable photovoltaic materials for polymer solar cells: the role of highly polar pendant groups in charge carrier transport and photovoltaic behavior, Energy Environ. Sci. 6 (2013) 3022–3034, https://doi.org/10.1039/C3EE41838C.
[318] W. Zhao, S. Zhang, Y. Zhang, S. Li, X. Liu, C. He, Z. Zheng, J. Hou, Environmentally friendly solvent-processed organic solar cells that are highly efficient and adaptable for the blade-coating method, Adv. Mater. 30 (2018), 1704837, https://doi.org/10.1002/adma.201704837.
[319] S. Venkatesan, Q. Chen, E.C. Ngo, N. Adhikari, K. Nelson, A. Dubey, J. Sun, V. Bommisetty, C. Zhang, D. Galipeau, Q. Qiao, Polymer solar cells processed using anisole as a relatively nontoxic solvent, Energy Tech. 2 (2014) 269–274, https://doi.org/10.1002/ente.201300174.
[320] B. Fan, L. Ying, Z. Wang, B. He, X.F. Jiang, F. Huang, Y. Cao, Optimisation of processing solvent and molecular weight for the production of green-solvent-processed all-polymer solar cells with a power conversion efficiency over 9%, Energy Environ. Sci. 10 (2017) 1243–1251, https://doi.org/10.1039/C7EE00619E.
[321] S. Dong, K. Zhang, B. Xie, J. Xiao, H.-L. Yip, H. Yan, F. Huang, Y. Cao, High-performance large-area organic solar cells enabled by sequential bilayer processing via nonhalogenated solvents, Adv. Energy Mater. 9 (2019), 1802832, https://doi.org/10.1002/aenm.201802832.
[322] L. Ye, Y. Xiong, H. Yao, A. Gadisa, H. Zhang, S. Li, M. Ghasemi, N. Balar, A. Hunt, B.T. O'Connor, J. Hou, H. Ade, High performance organic solar cells processed by blade coating in air from a benign food additive solution, Chem. Mater. 28 (2016) 7451–7458, https://doi.org/10.1021/acs.chemmater.6b03083.
[323] J. Zhao, Y. Li, G. Yang, K. Jiang, H. Lin, H. Ade, W. Ma, H. Yan, Efficient organic solar cells processed from hydrocarbon solvents, Nat. Energy 1 (2016) 15027, https://doi.org/10.1038/nenergy.2015.27.
[324] A. Wadsworth, R.S. Ashraf, M. Abdelsamie, S. Pont, M. Little, M. Moser, Z. Hamid, M. Neophytou, W. Zhang, A. Amassian, J.R. Durrant, D. Baran, I. McCulloch, Highly efficient and reproducible nonfullerene solar cells from hydrocarbon solvents, ACS Energy Lett. 2 (2017) 1494–1500, https://doi.org/10.1021/acsenergylett.7b00390.
[325] A.S. Gertsen, M.F. Castro, R.R. Søndergaard, J.W. Andreasen, Scalable fabrication of organic solar cells based on non-fullerene acceptors, Flex. Print. Electron. 5 (2020), 014004, https://doi.org/10.1088/2058-8585/ab5f57.
[326] S. Zhang, L. Ye, H. Zhang, J. Hou, Green-solvent-processable organic solar cells, Mater. Today 19 (2016) 533–543, https://doi.org/10.1016/j.mattod.2016.02.019.
[327] S. Gärtner, M. Christmann, S. Sankaran, H. Röhm, E.-M. Prinz, F. Penth, A. Pütz, A.E. Türeli, B. Penth, B. Baumstümmler, A. Colsmann, Eco-friendly fabrication of 4% efficient organic solar cells from surfactant-free P3HT:Icba nanoparticle dispersions, Adv. Mater. 26 (2014) 6653–6657, https://doi.org/10.1002/adma.201402360.
[328] K. Landfester, R. Montenegro, U. Scherf, R. Güntner, U. Asawapirom, S. Patil, D. Neher, T. Kietzke, Semiconducting polymer nanospheres in aqueous dispersion prepared by a miniemulsion process, Adv. Mater. 14 (2002) 651–655, https://doi.org/10.1002/1521-4095(20020503)14:9<651::Aid-adma651>3.0.Co;2-v.
[329] J. Cho, S. Yoon, K. Min Sim, Y. Jin Jeong, C. Eon Park, S.K. Kwon, Y.H. Kim, D. S. Chung, Universal selection rule for surfactants used in miniemulsion processes for eco-friendly and high performance polymer semiconductors, Energy Environ. Sci. 10 (2017) 2324–2333, https://doi.org/10.1039/C7EE01943B.
[330] F.J.M. Colberts, M.M. Wienk, R.A.J. Janssen, Aqueous nanoparticle polymer solar cells: effects of surfactant concentration and processing on device performance, ACS Appl. Mater. Interfaces 9 (2017) 13380–13389, https://doi.org/10.1021/acsami.7b00557.

[331] D. Darwis, N. Holmes, D. Elkington, A.L. David Kilcoyne, G. Bryant, X. Zhou, P. Dastoor, W. Belcher, Surfactant-free nanoparticulate organic photovoltaics, Sol. Energy Mater. Sol. Cells 121 (2014) 99–107, https://doi.org/10.1016/j.solmat.2013.10.010.

[332] C. Xie, X. Tang, M. Berlinghof, S. Langner, S. Chen, A. Späth, N. Li, R.H. Fink, T. Unruh, C.J. Brabec, Robot-based high-throughput engineering of alcoholic polymer: fullerene nanoparticle inks for an eco-friendly processing of organic solar cells, ACS Appl. Mater. Interfaces 10 (2018) 23225–23234, https://doi.org/10.1021/acsami.8b03621.

[333] L. D'Olieslaeger, G. Pirotte, I. Cardinaletti, J. D'Haen, J. Manca, D. Vanderzande, W. Maes, A. Ethirajan, Eco-friendly fabrication of PBDTTPD:$PC_{71}BM$ solar cells reaching a pce of 3.8% using water-based nanoparticle dispersions, Org. Electron. 42 (2017) 42–46, https://doi.org/10.1016/j.orgel.2016.12.018.

[334] N.P. Holmes, M. Marks, P. Kumar, R. Kroon, M.G. Barr, N. Nicolaidis, K. Feron, A. Pivrikas, A. Fahy, A.D.d.Z. Mendaza, A.L.D. Kilcoyne, C. Müller, X. Zhou, M. R. Andersson, P.C. Dastoor, W.J. Belcher, Nano-pathways: bridging the divide between water-processable nanoparticulate and bulk heterojunction organic photovoltaics, Nano Energy 19 (2016) 495–510, https://doi.org/10.1016/j.nanoen.2015.11.021.

[335] S. Ulum, N. Holmes, M. Barr, A.L.D. Kilcoyne, B.B. Gong, X. Zhou, W. Belcher, P. Dastoor, The role of miscibility in polymer:Fullerene nanoparticulate organic photovoltaic devices, Nano Energy 2 (2013) 897–905, https://doi.org/10.1016/j.nanoen.2013.03.009.

[336] K.N. Schwarz, S.B. Farley, T.A. Smith, K.P. Ghiggino, Charge generation and morphology in P3HT : PCBM nanoparticles prepared by mini-emulsion and reprecipitation methods, Nanoscale 7 (2015) 19899–19904, https://doi.org/10.1039/C5NR06244F.

[337] L. D'Olieslaeger, M. Pfannmöller, E. Fron, I. Cardinaletti, M. Van Der Auweraer, G. Van Tendeloo, S. Bals, W. Maes, D. Vanderzande, J. Manca, A. Ethirajan, Tuning of PCDTBT:$PC_{71}BM$ blend nanoparticles for eco-friendly processing of polymer solar cells, Sol. Energy Mater. Sol. Cells 159 (2017) 179–188, https://doi.org/10.1016/j.solmat.2016.09.008.

[338] J. Kosco, M. Bidwell, H. Cha, T. Martin, C.T. Howells, M. Sachs, D.H. Anjum, S. Gonzalez Lopez, L. Zou, A. Wadsworth, W. Zhang, L. Zhang, J. Tellam, R. Sougrat, F. Laquai, D.M. DeLongchamp, J.R. Durrant, I. McCulloch, Enhanced photocatalytic hydrogen evolution from organic semiconductor heterojunction nanoparticles, Nat. Mater. (2020), https://doi.org/10.1038/s41563-019-0591-1.

[339] C. Xie, T. Heumüller, W. Gruber, X. Tang, A. Classen, I. Schuldes, M. Bidwell, A. Späth, R.H. Fink, T. Unruh, I. McCulloch, N. Li, C.J. Brabec, Overcoming efficiency and stability limits in water-processing nanoparticular organic photovoltaics by minimizing microstructure defects, Nat. Commun. 9 (2018) 5335, https://doi.org/10.1038/s41467-018-07807-5.

[340] M. Bag, T.S. Gehan, L.A. Renna, D.D. Algaier, P.M. Lahti, D. Venkataraman, Fabrication conditions for efficient organic photovoltaic cells from aqueous dispersions of nanoparticles, RSC Adv. 4 (2014) 45325–45331, https://doi.org/10.1039/C4RA07463G.

[341] N.P. Holmes, S. Ulum, P. Sista, K.B. Burke, M.G. Wilson, M.C. Stefan, X. Zhou, P. C. Dastoor, W.J. Belcher, The effect of polymer molecular weight on P3HT:PCBM nanoparticulate organic photovoltaic device performance, Sol. Energy Mater. Sol. Cells 128 (2014) 369–377, https://doi.org/10.1016/j.solmat.2014.05.046.

[342] S.A. Hashemi, S. Ramakrishna, A.G. Aberle, Recent progress in flexible–wearable solar cells for self-powered electronic devices, Energy Environ. Sci. 13 (2020) 685–743, https://doi.org/10.1039/c9ee03046h.

[343] Y. Liu, M. Pharr, G.A. Salvatore, Lab-on-skin: a review of flexible and stretchable electronics for wearable health monitoring, ACS Nano 11 (2017) 9614–9635, https://doi.org/10.1021/acsnano.7b04898.

[344] Y. Li, G. Xu, C. Cui, Y. Li, Flexible and semitransparent organic solar cells, Adv. Energy Mater. 8 (2018), 1701791, https://doi.org/10.1002/aenm.201701791.

[345] M. Manceau, D. Angmo, M. Jørgensen, F.C. Krebs, Ito-free flexible polymer solar cells: from small model devices to roll-to-roll processed large modules, Org. Electron. 12 (2011) 566–574, https://doi.org/10.1016/j.orgel.2011.01.009.

[346] K. Yu, S. Rich, S. Lee, K. Fukuda, T. Yokota, T. Someya, Organic photovoltaics: toward self-powered wearable electronics, Proc. IEEE 107 (2019) 2137–2154, https://doi.org/10.1109/JPROC.2019.2929797.

[347] D. Koo, S. Jung, J. Seo, G. Jeong, Y. Choi, J. Lee, S.M. Lee, Y. Cho, M. Jeong, J. Lee, J. Oh, C. Yang, H. Park, Flexible organic solar cells over 15% efficiency with polyimide-integrated graphene electrodes, Joule 4 (2020) 1021–1034, https://doi.org/10.1016/j.joule.2020.02.012Get.

[348] A. Hübler, B. Trnovec, T. Zillger, M. Ali, N. Wetzold, M. Mingebach, A. Wagenpfahl, C. Deibel, V. Dyakonov, Printed paper photovoltaic cells, Adv. Energy Mater. 1 (2011) 1018–1022, https://doi.org/10.1002/aenm.201100394.

[349] Y. Liu, N. Qi, T. Song, M. Jia, Z. Xia, Z. Yuan, W. Yuan, K.Q. Zhang, B. Sun, Highly flexible and lightweight organic solar cells on biocompatible silk fibroin, ACS Appl. Mater. Interfaces 6 (2014) 20670–20675, https://doi.org/10.1021/am504163r.

[350] S. Lee, Y. Lee, J. Park, D. Choi, Stitchable organic photovoltaic cells with textile electrodes, Nano Energy 9 (2014) 88–93, https://doi.org/10.1016/j.nanoen.2014.06.017.

[351] X. Wang, H. Jin, R.C.R. Nagiri, B.Z.L. Poliquit, J. Subbiah, D.J. Jones, N. Kopidakis, P.L. Burn, J. Yu, Flexible ito-free organic photovoltaics on ultra-thin flexible glass substrates with high efficiency and improved stability, Solar RRL 3 (2019), 1800286, https://doi.org/10.1002/solr.201800286.

[352] T. Yan, W. Song, J. Huang, R. Peng, L. Huang, Z. Ge, 16.67% rigid and 14.06% flexible organic solar cells enabled by ternary heterojunction strategy, Adv. Mater. 31 (2019), 1902210, https://doi.org/10.1002/adma.201902210.

[353] H. Zhen, K. Li, C. Chen, Y. Yu, Z. Zheng, Q. Ling, Water-borne foldable polymer solar cells: one-step transferring free-standing polymer films onto woven fabric electrodes, J. Mater. Chem. A 5 (2017) 782–788, https://doi.org/10.1039/C6TA08309A.

[354] X. Xu, X. Zhou, K. Zhou, Y. Xia, W. Ma, O. Inganäs, Large-area, semitransparent, and flexible all-polymer photodetectors, Adv. Funct. Mater. 28 (2018), 1805570, https://doi.org/10.1002/adfm.201805570.

[355] T. Lei, M. Guan, J. Liu, H.C. Lin, R. Pfattner, L. Shaw, A.F. McGuire, T.C. Huang, L. Shao, K.T. Cheng, J.B.H. Tok, Z. Bao, Biocompatible and totally disintegrable semiconducting polymer for ultrathin and ultralightweight transient electronics, Proc. Natl. Acad. Sci. 114 (2017) 5107–5112, https://doi.org/10.1073/pnas.1701478114.

[356] M. Kaltenbrunner, M.S. White, E.D. Głowacki, T. Sekitani, T. Someya, N. S. Sariciftci, S. Bauer, Ultrathin and lightweight organic solar cells with high flexibility, Nat. Commun. 3 (2012) 770, https://doi.org/10.1038/ncomms1772.

[357] H. Jinno, K. Fukuda, X. Xu, S. Park, Y. Suzuki, M. Koizumi, T. Yokota, I. Osaka, K. Takimiya, T. Someya, Stretchable and waterproof elastomer-coated organic photovoltaics for washable electronic textile applications, Nat. Energy 2 (2017) 780–785, https://doi.org/10.1038/s41560-017-0001-3.

[358] S. Park, S.W. Heo, W. Lee, D. Inoue, Z. Jiang, K. Yu, H. Jinno, D. Hashizume, M. Sekino, T. Yokota, K. Fukuda, K. Tajima, T. Someya, Self-powered ultra-flexible electronics via nano-grating-patterned organic photovoltaics, Nature 561 (2018) 516–521, https://doi.org/10.1038/s41586-018-0536-x.

[359] J. Jean, A. Wang, V. Bulović, *In situ* vapor-deposited parylene substrates for ultra-thin, lightweight organic solar cells, Org. Electron. 31 (2016) 120–126, https://doi.org/10.1016/j.orgel.2016.01.022.

[360] M. Jakešová, T.A. Sjöström, V. Đerek, D. Poxson, M. Berggren, E.D. Głowacki, D. T. Simon, Wireless organic electronic ion pumps driven by photovoltaics, npj Flex. Electron. 3 (2019) 14, https://doi.org/10.1038/s41528-019-0060-6.

[361] X. Xu, K. Fukuda, A. Karki, S. Park, H. Kimura, H. Jinno, N. Watanabe, S. Yamamoto, S. Shimomura, D. Kitazawa, T. Yokota, S. Umezu, T.Q. Nguyen, T. Someya, Thermally stable, highly efficient, ultraflexible organic photovoltaics, Proc. Natl. Acad. Sci. 115 (2018) 4589–4594, https://doi.org/10.1073/pnas.1801187115.

[362] T.Y. Qu, L.J. Zuo, J.D. Chen, X. Shi, T. Zhang, L. Li, K.C. Shen, H. Ren, S. Wang, F. M. Xie, Y.Q. Li, A.K.Y. Jen, J.X. Tang, Biomimetic electrodes for flexible organic solar cells with efficiencies over 16%, Adv. Opt. Mater. (2020), 2000669 https://doi.org/10.1002/adom.202000669 n/a.

[363] K.C. See, J.P. Feser, C.E. Chen, A. Majumdar, J.J. Urban, R.A. Segalman, Water-processable polymer– nanocrystal hybrids for thermoelectrics, Nano Lett. 10 (2010) 4664–4667, https://doi.org/10.1021/nl102880k.

[364] O. Bubnova, Z.U. Khan, A. Malti, S. Braun, M. Fahlman, M. Berggren, X. Crispin, Optimization of the thermoelectric figure of merit in the conducting polymer poly (3, 4-ethylenedioxythiophene), Nat. Mater. 10 (2011) 429–433, https://doi.org/10.1038/nmat3012.

[365] G.H. Kim, L. Shao, K. Zhang, K.P. Pipe, Engineered doping of organic semiconductors for enhanced thermoelectric efficiency, Nat. Mater. 12 (2013) 719–723, https://doi.org/10.1038/nmat3635.

[366] H. Ju, J. Kim, Chemically exfoliated snse nanosheets and their snse/poly (3, 4-ethylenedioxythiophene): poly (styrenesulfonate) composite films for polymer based thermoelectric applications, ACS Nano 10 (2016) 5730–5739, https://doi.org/10.1021/acsnano.5b07355.

[367] Z. Fan, P. Li, D. Du, J. Ouyang, Significantly enhanced thermoelectric properties of PEDOT: PSS films through sequential post-treatments with common acids and bases, Adv. Energy Mater. 7 (2017), 1602116, https://doi.org/10.1002/aenm.201602116.

[368] Z. Fan, D. Du, X. Guan, J. Ouyang, Polymer films with ultrahigh thermoelectric properties arising from significant seebeck coefficient enhancement by ion accumulation on surface, Nano Energy 51 (2018) 481–488, https://doi.org/10.1016/j.nanoen.2018.07.002.

[369] X. Wang, J. Cheng, L. Yin, Z. Zhang, X. Wang, J. Sui, X. Liu, J. Mao, F. Cao, Q. Zhang, Organic/inorganic hybrid design as a route for promoting the $Bi_{0.5}Sb_{1.5}Te_3$ for high-performance thermoelectric power generation, Adv. Funct. Mater. (2022), 2200307, https://doi.org/10.1002/adfm.202200307.

[370] B. Zhang, J. Sun, H. Katz, F. Fang, R. Opila, Promising thermoelectric properties of commercial PEDOT: PSS materials and their Bi_2Te_3 powder composites, ACS Appl. Mater. Interfaces 2 (2010) 3170–3178, https://doi.org/10.1021/am100654p.

[371] M. Sumino, K. Harada, M. Ikeda, S. Tanaka, K. Miyazaki, C. Adachi, Thermoelectric properties of *n*-type C_{60} thin films and their application in organic thermovoltaic devices, Appl. Phys. Lett. 99 (2011) 188, https://doi.org/10.1063/1.3631633.

[372] J.H. We, S.J. Kim, B.J. Cho, Hybrid composite of screen-printed inorganic thermoelectric film and organic conducting polymer for flexible thermoelectric power generator, Energy 73 (2014) 506–512, https://doi.org/10.1016/j.energy.2014.06.047.

[373] Y. Sun, L. Qiu, L. Tang, H. Geng, H. Wang, F. Zhang, D. Huang, W. Xu, P. Yue, Y. S. Guan, Flexible *n*-type high-performance thermoelectric thin films of poly (nickel-ethylenetetrathiolate) prepared by an electrochemical method, Adv. Mater. 28 (2016) 3351–3358, https://doi.org/10.1002/adma.201505922.

[374] D. Huang, H. Yao, Y. Cui, Y. Zou, F. Zhang, C. Wang, H. Shen, W. Jin, J. Zhu, Y. Diao, Conjugated-backbone effect of organic small molecules for *n*-type thermoelectric materials with ZT over 0.2, JACS 139 (2017) 13013–13023, https://doi.org/10.1021/jacs.7b05344.

[375] L. Wang, Z. Zhang, L. Geng, T. Yuan, Y. Liu, J. Guo, L. Fang, J. Qiu, S. Wang, Solution-printable fullerene/TiS_2 organic/inorganic hybrids for high-performance

flexible *n*-type thermoelectrics, Energy Environ. Sci. 11 (2018) 1307–1317, https://doi.org/10.1039/C7EE03617E.
[376] Q. Jin, S. Jiang, Y. Zhao, D. Wang, J. Qiu, D.M. Tang, J. Tan, D.M. Sun, P.X. Hou, X.Q. Chen, Flexible layer-structured Bi_2Te_3 thermoelectric on a carbon nanotube scaffold, Nat. Mater. 18 (2019) 62–68, https://doi.org/10.1038/s41563-018-0217-z.
[377] Y. Lu, Y. Qiu, K. Cai, X. Li, M. Gao, J. He, Ultrahigh performance PEDOT/Ag_2Se/CuAgSe composite film for wearable thermoelectric power generators, Mater. Today Phys. 14 (2020), 100223, https://doi.org/10.1016/j.mtphys.2020.100223.
[378] S. Qu, C. Ming, P. Qiu, K. Xu, Q. Xu, Q. Yao, P. Lu, H. Zeng, X. Shi, L. Chen, High-performance *n*-type Ta_4SiTe_4/polyvinylidene fluoride (PVDF)/graphdiyne organic–inorganic flexible thermoelectric composites, Energy Environ. Sci. 14 (2021) 6586–6594, https://doi.org/10.1039/D1EE02552J.
[379] F. Zhang, Y. Zang, D. Huang, C.A. Di, D. Zhu, Flexible and self-powered temperature–pressure dual-parameter sensors using microstructure-frame-supported organic thermoelectric materials, Nat. Commun. 6 (2015) 1–10, https://doi.org/10.1038/ncomms9356.
[380] D. Zhao, H. Wang, Z.U. Khan, J. Chen, R. Gabrielsson, M.P. Jonsson, M. Berggren, X. Crispin, Ionic thermoelectric supercapacitors, Energy Environ. Sci. 9 (2016) 1450–1457, https://doi.org/10.1039/C6EE00121A.
[381] K. Liu, T. Ding, J. Li, Q. Chen, G. Xue, P. Yang, M. Xu, Z.L. Wang, J. Zhou, Thermal–electric nanogenerator based on the electrokinetic effect in porous carbon film, Adv. Energy Mater. 8 (2018), 1702481, https://doi.org/10.1002/aenm.201702481.
[382] J.P. Jurado, B. Dörling, O. Zapata-Arteaga, A.R. Goñi, M. Campoy-Quiles, Comparing different geometries for photovoltaic-thermoelectric hybrid devices based on organics, J. Mater. Chem. C 9 (2021) 2123–2132, https://doi.org/10.1039/D0TC05067A.
[383] C.Y. Yang, M.A. Stoeckel, T.P. Ruoko, H.Y. Wu, X. Liu, N.B. Kolhe, Z. Wu, Y. Puttisong, C. Musumeci, M. Massetti, A high-conductivity *n*-type polymeric ink for printed electronics, Nat. Commun. 12 (2021) 1–8, https://doi.org/10.1038/s41467-021-22528-y.
[384] S. Peng, D. Wang, J. Lu, M. He, C. Xu, Y. Li, S. Zhu, A review on organic polymer-based thermoelectric materials, J. Polym. Environ. 25 (2017) 1208–1218, https://doi.org/10.1007/s10924-016-0895-z.
[385] D.R. Villalva, S. Singh, L.A. Galuska, A. Sharma, J. Han, J. Liu, M.A. Haque, S. Jang, A.H. Emwas, L.J.A. Koster, Backbone-driven host–dopant miscibility modulates molecular doping in ndi conjugated polymers, Mater. Horiz. (2022), https://doi.org/10.1039/D1MH01357B.
[386] L. Beverina, G. Pagani, M. Sassi, Multichromophoric electrochromic polymers: colour tuning of conjugated polymers through the side chain functionalization approach, Chem. Commun. 50 (2014) 5413–5430, https://doi.org/10.1039/C4CC00163J.
[387] C.J. Yao, H.L. Zhang, Q. Zhang, Recent progress in thermoelectric materials based on conjugated polymers, Polym 11 (2019) 107, https://doi.org/10.3390/polym11010107.
[388] Z. Rahimzadeh, S.M. Naghib, Y. Zare, K.Y. Rhee, An overview on the synthesis and recent applications of conducting poly (3, 4-ethylenedioxythiophene)(pedot) in industry and biomedicine, J. Mater. Sci. 55 (2020) 7575–7611, https://doi.org/10.1007/s10853-020-04561-2.
[389] F. Hossein-Babaei, T. Akbari, B. Harkinezhad, Dopant passivation by adsorbed water monomers causes high humidity sensitivity in PEDOT: PSS thin films at ppm-level humidity, Sens. Actuators B 293 (2019) 329–335, https://doi.org/10.1016/j.snb.2019.05.018.
[390] N. Kim, S. Kee, S.H. Lee, B.H. Lee, Y.H. Kahng, Y.R. Jo, B.J. Kim, K. Lee, Highly conductive PEDOT: PSS nanofibrils induced by solution-processed crystallization, Adv. Mater. 26 (2014) 2268–2272, https://doi.org/10.1002/adma.201304611.
[391] M. Culebras, C. Gómez, A. Cantarero, Enhanced thermoelectric performance of pedot with different counter-ions optimized by chemical reduction, J. Mater. Chem. A 2 (2014) 10109–10115, https://doi.org/10.1039/c4ta01012d.
[392] M. Scholdt, H. Do, J. Lang, A. Gall, A. Colsmann, U. Lemmer, J.D. Koenig, M. Winkler, H. Boettner, Organic semiconductors for thermoelectric applications, J. Electron. Mater. 39 (2010) 1589–1592, https://doi.org/10.1007/s11664-010-1271-8.
[393] D.A. Mengistie, C.H. Chen, K.M. Boopathi, F.W. Pranoto, L.J. Li, C.W. Chu, Enhanced thermoelectric performance of PEDOT: PSS flexible bulky papers by treatment with secondary dopants, ACS Appl. Mater. Interfaces 7 (2015) 94–100, https://doi.org/10.1021/am507032e.
[394] Q. Wei, M. Mukaida, Y. Naitoh, T. Ishida, Morphological change and mobility enhancement in PEDOT: PSS by adding co-solvents, Adv. Mater. 25 (2013) 2831–2836, https://doi.org/10.1002/adma.201205158.
[395] E. Yang, J. Kim, B.J. Jung, J. Kwak, Enhanced thermoelectric properties of sorbitol-mixed PEDOT: PSS thin films by chemical reduction, J. Mater. Sci. Mater. Electron. 26 (2015) 2838–2843, https://doi.org/10.1007/s10854-015-2766-0.
[396] Z. Zhu, C. Liu, H. Shi, Q. Jiang, J. Xu, F. Jiang, J. Xiong, E. Liu, An effective approach to enhanced thermoelectric properties of PEDOT: PSS films by a des post-treatment, J. Polym. Sci. Part B Polym. Phys. 53 (2015) 885–892, https://doi.org/10.1002/polb.23718.
[397] A.C. Hinckley, S.C. Andrews, M.T. Dunham, A. Sood, M.T. Barako, S. Schneider, M.F. Toney, K.E. Goodson, Z. Bao, Achieving high thermoelectric performance and metallic transport in solvent-sheared PEDOT: PSS, Adv. Electron. Mater. 7 (2021), 2001190, https://doi.org/10.1002/aelm.202001190.
[398] N. Wen, Z. Fan, S. Yang, Y. Zhao, T. Cong, S. Xu, H. Zhang, J. Wang, H. Huang, C. Li, Highly conductive, ultra-flexible and continuously processable PEDOT: PSS fibers with high thermoelectric properties for wearable energy harvesting, Nano Energy 78 (2020), 105361, https://doi.org/10.1016/j.nanoen.2020.105361.
[399] A.I. Hofmann, I. Östergren, Y. Kim, S. Fauth, M. Craighero, M.-H. Yoon, A. Lund, C. Müller, All-polymer conducting fibers and 3d prints via melt processing and templated polymerization, ACS Appl. Mater. Interfaces 12 (2020) 8713–8721, https://doi.org/10.1021/acsami.9b20615.
[400] N. Kim, S. Lienemann, I. Petsagkourakis, D.A. Mengistie, S. Kee, T. Ederth, V. Gueskine, P. Leclère, R. Lazzaroni, X. Crispin, Elastic conducting polymer composites in thermoelectric modules, Nat. Commun. 11 (2020) 1–10, https://doi.org/10.1038/s41467-020-15135-w.
[401] Y. Xuan, X. Liu, S. Desbief, P. Leclère, M. Fahlman, R. Lazzaroni, M. Berggren, J. Cornil, D. Emin, X. Crispin, Thermoelectric properties of conducting polymers: the case of poly(3-hexylthiophene), Phys. Rev. B Condens. Matter 82 (2010), 115454, https://doi.org/10.1103/PhysRevB.82.115454.
[402] Q. Zhang, Y. Sun, W. Xu, D. Zhu, Thermoelectric energy from flexible P3HT films doped with a ferric salt of triflimide anions, Energy Environ. Sci. 5 (2012) 9639–9644, https://doi.org/10.1039/c2ee23006b.
[403] N.K. Jangid, S. Jadoun, N. Kaur, A review on high-throughput synthesis, deposition of thin films and properties of polyaniline, Eur. Polym. J. 125 (2020), 109485, https://doi.org/10.1016/j.eurpolymj.2020.109485.
[404] C. Nath, A. Kumar, Y.K. Kuo, G.S. Okram, High thermoelectric figure of merit in nanocrystalline polyaniline at low temperatures, Appl. Phys. Lett. 105 (2014), 133108, https://doi.org/10.1063/1.4897146.
[405] J. Stejskal, M. Trchová, Conducting polypyrrole nanotubes: a review, Chem. Pap. 72 (2018) 1563–1595, https://doi.org/10.1007/s11696-018-0394-x.
[406] M. Culebras, B. Uriol, C.M. Gómez, A. Cantarero, Controlling the thermoelectric properties of polymers: application to PEDOT and polypyrrole, Phys. Chem. Chem. Phys. 17 (2015) 15140–15145, https://doi.org/10.1039/C5CP01940K.
[407] J. Wang, K. Cai, S. Shen, A facile chemical reduction approach for effectively tuning thermoelectric properties of PEDOT films, Org. Electron. 17 (2015) 151–158, https://doi.org/10.1016/j.orgel.2014.12.007.
[408] S. Wakim, B.R. Aïch, Y. Tao, M. Leclerc, Charge transport, photovoltaic, and thermoelectric properties of poly (2, 7-carbazole) and poly (indolo [3, 2-b] carbazole) derivatives, Polym. Rev. 48 (2008) 432–462, https://doi.org/10.1080/15583720802231726.
[409] I. Lévesque, X. Gao, D.D. Klug, S.T. John, C.I. Ratcliffe, M. Leclerc, Highly soluble poly (2, 7-carbazolenevinylene) for thermoelectrical applications: from theory to experiment, React. Funct. Polym. 65 (2005) 23–36, https://doi.org/10.1016/j.reactfunctpolym.2004.11.008.
[410] I. Lévesque, P.O. Bertrand, N. Blouin, M. Leclerc, S. Zecchin, G. Zotti, C. I. Ratcliffe, D.D. Klug, X. Gao, F. Gao, Synthesis and thermoelectric properties of polycarbazole, polyindolocarbazole, and polydiindolocarbazole derivatives, Chem. Mater. 19 (2007) 2128–2138, https://doi.org/10.1021/cm070063h.
[411] R.B. Aïch, N. Blouin, A. Bouchard, M. Leclerc, Electrical and thermoelectric properties of poly (2, 7-carbazole) derivatives, Chem. Mater. 21 (2009) 751–757, https://doi.org/10.1021/cm8031175.
[412] N. Basescu, Z.X. Liu, D. Moses, A.J. Heeger, H. Naarmann, N. Theophilou, High electrical conductivity in doped polyacetylene, Nature 327 (1987) 403–405, https://doi.org/10.1038/327403a0.
[413] R. Zuzok, A. Kaiser, W. Pukacki, S. Roth, Thermoelectric power and conductivity of iodine-doped "new''polyacetylene, J. Chem. Phys. 95 (1991) 1270–1275, https://doi.org/10.1063/1.461107.
[414] Y. Park, C. Yoon, B. Na, H. Shirakawa, K. Akagi, Metallic properties of transition metal halides doped polyacetylene: the soliton liquid state, Synth. Met. 41 (1991) 27–32, https://doi.org/10.1016/0379-6779(91)90989-I.
[415] H. Kaneko, T. Ishiguro, A. Takahashi, J. Tsukamoto, Magnetoresistance and thermoelectric power studies of metal-nonmetal transition in iodine-doped polyacetylene, Synth. Met. 57 (1993) 4900–4905, https://doi.org/10.1016/0379-6779(93)90836-l.
[416] J. Min, D. Kim, S.G. Han, C. Park, H. Lim, W. Sung, K. Cho, Position-induced efficient doping for highly doped organic thermoelectric materials, Adv. Electron. Mater. 8 (2022), 2101142, https://doi.org/10.1002/aelm.202101142.
[417] Y. Zhong, V. Untilova, D. Muller, S. Guchait, C. Kiefer, L. Herrmann, N. Zimmermann, M. Brosset, T. Heiser, M. Brinkmann, Preferential location of dopants in the amorphous phase of oriented regioregular poly (3-hexylthiophene-2, 5-diyl) films helps reach charge conductivities of 3000 S cm^{-1}, Adv. Funct. Mater. (2022), 2202075, https://doi.org/10.1002/adfm.202202075.
[418] Z. Liang, H.H. Choi, X. Luo, T. Liu, A. Abtahi, U.S. Ramasamy, J.A. Hitron, K. N. Baustert, J.L. Hempel, A.M. Boehm, *n*-type charge transport in heavily *p*-doped polymers, Nat. Mater. 20 (2021) 518–524, https://doi.org/10.1038/s41563-020-00859-3.
[419] K. Xu, T.P. Ruoko, M. Shokrani, D. Scheunemann, H. Abdalla, H. Sun, C.Y. Yang, Y. Puttisong, N.B. Kolhe, J.S.M. Figueroa, On the origin of seebeck coefficient inversion in highly doped conducting polymers, Adv. Funct. Mater. (2022), 2112276, https://doi.org/10.1002/adfm.202112276.
[420] A. Tripathi, Y. Lee, S. Lee, H.Y. Woo, Recent advances in *n*-type organic thermoelectric materials, dopants, and doping strategies, J. Mater. Chem. C (2022), https://doi.org/10.1039/D1TC06175E.
[421] Y. Sun, C.A. Di, W. Xu, D. Zhu, Advances in *n*-type organic thermoelectric materials and devices, Adv. Electron. Mater. 5 (2019), 1800825, https://doi.org/10.1002/aelm.201800825.
[422] Q. Zhang, Y. Sun, W. Xu, D. Zhu, Organic thermoelectric materials: emerging green energy materials converting heat to electricity directly and efficiently, Adv. Mater. 26 (2014) 6829–6851, https://doi.org/10.1002/adma.201305371.
[423] A. von Mühlenen, N. Errien, M. Schaer, M.N. Bussac, L. Zuppiroli, Thermopower measurements on pentacene transistors, Phys. Rev. B Condens. Matter 75 (2007), 115338, https://doi.org/10.1103/PhysRevB.75.115338.

[424] J.A. Malen, S.K. Yee, A. Majumdar, R.A. Segalman, Fundamentals of energy transport, energy conversion, and thermal properties in organic–inorganic heterojunctions, Chem. Phys. Lett. 491 (2010) 109–122, https://doi.org/10.1016/j.cplett.2010.03.028.
[425] M.A. Reed, C. Zhou, C. Muller, T. Burgin, J. Tour, Conductance of a molecular junction, Science 278 (1997) 252–254, https://doi.org/10.1126/science.278.5336.252.
[426] P. Reddy, S.Y. Jang, R.A. Segalman, A. Majumdar, Thermoelectricity in molecular junctions, Science 315 (2007) 1568–1571, https://doi.org/10.1126/science.1137149.
[427] J. Hurtado-Gallego, S. Sangtarash, R. Davidson, L. Rincón-García, A. Daaoub, G. Rubio-Bollinger, C.J. Lambert, V.S. Oganesyan, M.R. Bryce, N. Agraït, Thermoelectric enhancement in single organic radical molecules, Nano Lett. 22 (2022) 948–953, https://doi.org/10.1021/acs.nanolett.1c03698.
[428] Y. Sun, P. Sheng, C. Di, F. Jiao, W. Xu, D. Qiu, D. Zhu, Organic thermoelectric materials and devices based on *p*- and *n*-type poly(metal 1,1,2,2-ethenetetrathiolate)s, Adv. Mater. 24 (2012) 932–937, https://doi.org/10.1002/adma.201104305.
[429] J. D'sa, V. Rao, K. Patel, R. Patel, A study on the synthesis and electrical properties of chelate polymers, Appl. Macromol. Chem. Phys. 79 (1979) 133–145, https://doi.org/10.1002/apmc.1979.050790111.
[430] Y. Sun, P. Sheng, C. Di, F. Jiao, W. Xu, D. Qiu, D. Zhu, Organic thermoelectric materials and devices based on *p*-and *n*-type poly (metal 1, 1, 2, 2-ethenetetrathiolate) s, Adv. Mater. 24 (2012) 932–937, https://doi.org/10.1002/adma.201104305.
[431] F. Jiao, C.A. Di, Y. Sun, P. Sheng, W. Xu, D. Zhu, Inkjet-printed flexible organic thin-film thermoelectric devices based on *p*-and *n*-type poly (metal 1, 1, 2, 2-ethenetetrathiolate) s/polymer composites through ball-milling, Philos. Trans. R. Soc. A 372 (2014), 20130008, https://doi.org/10.1098/rsta.2013.0008.
[432] S. Hwang, W.J. Potscavage Jr, T.W. Kim, C. Adachi, Interplay among thermoelectric properties, atmospheric stability, and electronic structures in solution-deposited thin films of *p* (nax [niett]), Adv. Electron. Mater. 6 (2020), 1901172, https://doi.org/10.1002/aelm.201901172.
[433] X. Huang, P. Sheng, Z. Tu, F. Zhang, J. Wang, H. Geng, Y. Zou, C.A. Di, Y. Yi, Y. Sun, A two-dimensional π–d conjugated coordination polymer with extremely high electrical conductivity and ambipolar transport behaviour, Nat. Commun. 6 (2015) 1–8, https://doi.org/10.1038/ncomms8408.
[434] L. Sun, B. Liao, D. Sheberla, D. Kraemer, J. Zhou, E.A. Stach, D. Zakharov, V. Stavila, A.A. Talin, Y. Ge, A microporous and naturally nanostructured thermoelectric metal-organic framework with ultralow thermal conductivity, Joule 1 (2017) 168–177, https://doi.org/10.1016/j.joule.2017.07.018.
[435] T.L.D. Tam, M. Lin, A.D. Handoko, T.T. Lin, J. Xu, High-performance & thermally stable *n*-type polymer thermoelectrics based on a benzyl viologen radical cation-doped ladder-type conjugated polymer, J. Mater. Chem. A 9 (2021) 11787–11793, https://doi.org/10.1039/D1TA01645H.
[436] M. Cassinelli, S. Cimò, T. Biskup, X. Jiao, A. Luzio, C.R. McNeill, Y.Y. Noh, Y. H. Kim, C. Bertarelli, M. Caironi, Enhanced *n*-type doping of a naphthalene diimide based copolymer by modification of the donor unit, Adv. Electron. Mater. 7 (2021), 2100407, https://doi.org/10.1002/aelm.202100407.
[437] J. Han, C. Ganley, Q. Hu, X. Zhao, P. Clancy, T.P. Russell, H.E. Katz, Using preformed meisenheimer complexes as dopants for *n*-type organic thermoelectrics with high seebeck coefficients and power factors, Adv. Funct. Mater. 31 (2021), 2010567, https://doi.org/10.1002/adfm.202010567.
[438] C. Dong, S. Deng, B. Meng, J. Liu, L. Wang, A distannylated monomer of a strong electron-accepting organoboron building block: enabling acceptor–acceptor-type conjugated polymers for *n*-type thermoelectric applications, Angew. Chem. 133 (2021) 16320–16326, https://doi.org/10.1002/ange.202105127.
[439] M. Alsufyani, M.A. Stoeckel, X. Chen, K. Thorley, R.K. Hallani, Y. Puttisong, X. Ji, D. Meli, B.D. Paulsen, J. Strzalka, Lactone backbone density in rigid electron-deficient semiconducting polymers enabling high *n*-type organic thermoelectric performance, Angew. Chem. 134 (2022), e202113078, https://doi.org/10.1002/ange.202113078.
[440] A. Barbot, C. Di Bin, B. Lucas, B. Ratier, M. Aldissi, *n*-type doping and thermoelectric properties of co-sublimed cesium-carbonate-doped fullerene, J. Mater. Sci. 48 (2013) 2785–2789, https://doi.org/10.1007/s10853-012-6824-1.
[441] J.C. Duda, P.E. Hopkins, Y. Shen, M.C. Gupta, Exceptionally low thermal conductivities of films of the fullerene derivative PCBM, Phys. Rev. Lett. 110 (2013), 015902, https://doi.org/10.1103/PhysRevLett.110.015902.
[442] C. Waldauf, P. Schilinsky, M. Perisutti, J. Hauch, C.J. Brabec, Solution-processed organic *n*-type thin-film transistors, Adv. Mater. 15 (2003) 2084–2088, https://doi.org/10.1002/adma.200305623.
[443] F. Gao, Y. Liu, Y. Xiong, P. Wu, B. Hu, L. Xu, Fabricate organic thermoelectric modules use modified PCBM and PEDOT: PSS materials, Front. Optoelectron. 10 (2017) 117–123, https://doi.org/10.1007/s12200-017-0712-x.
[444] D. Yuan, D. Huang, C. Zhang, Y. Zou, C.A. Di, X. Zhu, D. Zhu, Efficient solution-processed *n*-type small-molecule thermoelectric materials achieved by precisely regulating energy level of organic dopants, ACS Appl. Mater. Interfaces 9 (2017) 28795–28801, https://doi.org/10.1021/acsami.7b07282.
[445] Y. Min, C. Dong, H. Tian, J. Liu, L. Wang, B←N-incorporated dibenzo-azaacenes as *n*-type thermoelectric materials, ACS Appl. Mater. Interfaces 13 (2021) 33321–33327, https://doi.org/10.1021/acsami.1c08514.
[446] J. Liu, B. van der Zee, R. Alessandri, S. Sami, J. Dong, M.I. Nugraha, A.J. Barker, S. Rousseva, L. Qiu, X. Qiu, *n*-type organic thermoelectrics: demonstration of ZT>0.3, Nat. Commun. 11 (2020) 1–9, https://doi.org/10.1038/s41467-020-19537-8.
[447] B. Russ, M.J. Robb, F.G. Brunetti, P.L. Miller, E.E. Perry, S.N. Patel, V. Ho, W. B. Chang, J.J. Urban, M.L. Chabinyc, Power factor enhancement in solution-processed organic *n*-type thermoelectrics through molecular design, Adv. Mater. 26 (2014) 3473–3477, https://doi.org/10.1002/adma.201306116.
[448] J. Liu, L. Qiu, G. Portale, M. Koopmans, G. Ten Brink, J.C. Hummelen, L.J. A. Koster, *n*-type organic thermoelectrics: improved power factor by tailoring host–dopant miscibility, Adv. Mater. 29 (2017), 1701641, https://doi.org/10.1002/adma.201701641.
[449] F. Zhang, Y. Zang, D. Huang, C.A. Di, X. Gao, H. Sirringhaus, D. Zhu, Modulated thermoelectric properties of organic semiconductors using field-effect transistors, Adv. Funct. Mater. 25 (2015) 3004–3012, https://doi.org/10.1002/adfm.201404397.
[450] D. Huang, C. Wang, Y. Zou, X. Shen, Y. Zang, H. Shen, X. Gao, Y. Yi, W. Xu, C. A. Di, Bismuth interfacial doping of organic small molecules for high performance *n*-type thermoelectric materials, Angew. Chem. Int. Ed. 55 (2016) 10672–10675, https://doi.org/10.1002/anie.201604478.
[451] F. Huewe, A. Steeger, K. Kostova, L. Burroughs, I. Bauer, P. Strohriegl, V. Dimitrov, S. Woodward, J. Pflaum, Low-cost and sustainable organic thermoelectrics based on low-dimensional molecular metals, Adv. Mater. 29 (2017), 1605682, https://doi.org/10.1002/adma.201605682.
[452] S.K. Yee, J.A. Malen, A. Majumdar, R.A. Segalman, Thermoelectricity in fullerene–metal heterojunctions, Nano Lett. 11 (2011) 4089–4094, https://doi.org/10.1021/nl2014839.
[453] Y.S. Ding, N.F. Chilton, R.E. Winpenny, Y.Z. Zheng, On approaching the limit of molecular magnetic anisotropy: a near-perfect pentagonal bipyramidal dysprosium (iii) single-molecule magnet, Angew. Chem. Int. Ed. 55 (2016) 16071–16074, https://doi.org/10.1002/anie.201609685.
[454] F.S. Guo, B.M. Day, Y.C. Chen, M.L. Tong, A. Mansikkamäki, R.A. Layfield, Magnetic hysteresis up to 80 kelvin in a dysprosium metallocene single-molecule magnet, Science 362 (2018) 1400–1403, https://doi.org/10.1126/science.aav0652.
[455] M. Famili, I.M. Grace, Q. Al-Galiby, H. Sadeghi, C.J. Lambert, Toward high thermoelectric performance of thiophene and ethylenedioxythiophene (EDOT) molecular wires, Adv. Funct. Mater. 28 (2018), 1703135, https://doi.org/10.1002/adfm.201703135.
[456] Y.J. Zeng, D. Wu, X.H. Cao, W.X. Zhou, L.M. Tang, K.Q. Chen, Nanoscale organic thermoelectric materials: measurement, theoretical models, and optimization strategies, Adv. Funct. Mater. 30 (2020), 1903873, https://doi.org/10.1002/adfm.201903873.
[457] T.L. Bennett, M. Alshammari, S. Au-Yong, A. Almutlg, X. Wang, L.A. Wilkinson, T. Albrecht, S.P. Jarvis, L.F. Cohen, A. Ismael, Multi-component self-assembled molecular-electronic films: towards new high-performance thermoelectric systems, Chem. Sci. 13 (2022) 5176–5185, https://doi.org/10.1039/D2SC00078D.
[458] X. Wang, H. Wang, B. Liu, Carbon nanotube-based organic thermoelectric materials for energy harvesting, Polymers 10 (2018) 1196, https://doi.org/10.3390/polym10111196.
[459] S. Iijima, Helical microtubules of graphitic carbon, Nature 354 (1991) 56–58, https://doi.org/10.1038/354056a0.
[460] L. Hicks, M.S. Dresselhaus, Thermoelectric figure of merit of a one-dimensional conductor, Phys. Rev. B Condens. Matter 47 (1993) 16631, https://doi.org/10.1103/physrevb.47.16631.
[461] P.G. Collins, K. Bradley, M. Ishigami, D.A. Zettl, Extreme oxygen sensitivity of electronic properties of carbon nanotubes, Science 287 (2000) 1801–1804, https://doi.org/10.1126/science.287.5459.1801.
[462] J.S. Yun, S. Choi, S.H. Im, Advances in carbon-based thermoelectric materials for high-performance, flexible thermoelectric devices, Carbon Energy 3 (2021) 667–708, https://doi.org/10.1002/cey2.121.
[463] Y. Ryu, L. Yin, C. Yu, Dramatic electrical conductivity improvement of carbon nanotube networks by simultaneous de-bundling and hole-doping with chlorosulfonic acid, J. Mater. Chem. 22 (2012) 6959–6964, https://doi.org/10.1039/c2jm16000e.
[464] C. Cho, M. Culebras, K.L. Wallace, Y. Song, K. Holder, J.-H. Hsu, C. Yu, J. C. Grunlan, Stable *n*-type thermoelectric multilayer thin films with high power factor from carbonaceous nanofillers, Nano Energy 28 (2016) 426–432, https://doi.org/10.1016/j.nanoen.2016.08.063.
[465] J. Tang, Y. Chen, S.R. McCuskey, L. Chen, G.C. Bazan, Z. Liang, Recent advances in *n*-type thermoelectric nanocomposites, Adv. Electron. Mater. 5 (2019), 1800943, https://doi.org/10.1002/aelm.201800943.
[466] M. Shim, A. Javey, N.W. Shi Kam, H. Dai, Polymer functionalization for air-stable *n*-type carbon nanotube field-effect transistors, JACS 123 (2001) 11512–11513, https://doi.org/10.1021/ja0169670.
[467] S.M. Kim, J.H. Jang, K.K. Kim, H.K. Park, J.J. Bae, W.J. Yu, I.H. Lee, G. Kim, D. D. Loc, U.J. Kim, Reduction-controlled viologen in bisolvent as an environmentally stable *n*-type dopant for carbon nanotubes, JACS 131 (2009) 327–331, https://doi.org/10.1021/ja807480g.
[468] G. Wu, Z.G. Zhang, Y. Li, C. Gao, X. Wang, G. Chen, Exploring high-performance *n*-type thermoelectric composites using amino-substituted rylene dimides and carbon nanotubes, ACS Nano 11 (2017) 5746–5752, https://doi.org/10.1021/acsnano.7b01279.
[469] Y. Wang, Q. Li, J. Wang, Z. Li, K. Li, X. Dai, J. Pan, H. Wang, Understanding the solvent effects on polarity switching and thermoelectric properties changing of solution-processable *n*-type single-walled carbon nanotube films, Nano Energy 93 (2022), 106804, https://doi.org/10.1016/j.nanoen.2021.106804.
[470] W. Zhou, Q. Fan, Q. Zhang, L. Cai, K. Li, X. Gu, F. Yang, N. Zhang, Y. Wang, H. Liu, High-performance and compact-designed flexible thermoelectric modules

enabled by a reticulate carbon nanotube architecture, Nat. Commun. 8 (2017) 1–9, https://doi.org/10.1038/ncomms14886.
[471] X. Cheng, X. Wang, G. Chen, A convenient and highly tunable way to *n*-type carbon nanotube thermoelectric composite film using common alkylammonium cationic surfactant, J. Mater. Chem. A 6 (2018) 19030–19037, https://doi.org/10.1039/c8ta07746k.
[472] L.J. Li, A. Khlobystov, J. Wiltshire, G. Briggs, R. Nicholas, Diameter-selective encapsulation of metallocenes in single-walled carbon nanotubes, Nat. Mater. 4 (2005) 481–485, https://doi.org/10.1038/nmat1396.
[473] T. Lee, K.T. Park, B.C. Ku, H. Kim, Carbon nanotube fibers with enhanced longitudinal carrier mobility for high-performance all-carbon thermoelectric generators, Nanoscale 11 (2019) 16919–16927, https://doi.org/10.1039/c9nr05757a.
[474] Q. Wang, Q. Yao, J. Chang, L. Chen, Enhanced thermoelectric properties of CNT/PANI composite nanofibers by highly orienting the arrangement of polymer chains, J. Mater. Chem. 22 (2012) 17612–17618, https://doi.org/10.1039/c2jm32750c.
[475] S. Wang, F. Liu, C. Gao, T. Wan, L. Wang, L. Wang, L. Wang, Enhancement of the thermoelectric property of nanostructured polyaniline/carbon nanotube composites by introducing pyrrole unit onto polyaniline backbone via a sustainable method, Chem. Eng. J. 370 (2019) 322–329, https://doi.org/10.1016/j.cej.2019.03.155.
[476] Q. Zhang, W. Wang, J. Li, J. Zhu, L. Wang, M. Zhu, W. Jiang, Preparation and thermoelectric properties of multi-walled carbon nanotube/polyaniline hybrid nanocomposites, J. Mater. Chem. A 1 (2013) 12109–12114, https://doi.org/10.1039/c3ta12353g.
[477] K. Zhang, M. Davis, J. Qiu, L. Hope-Weeks, S. Wang, Thermoelectric properties of porous multi-walled carbon nanotube/polyaniline core/shell nanocomposites, Nanotechnol 23 (2012), 385701, https://doi.org/10.1088/0957-4484/23/38/385701.
[478] H. Wang, S.I. Yi, X. Pu, C. Yu, Simultaneously improving electrical conductivity and thermopower of polyaniline composites by utilizing carbon nanotubes as high mobility conduits, ACS Appl. Mater. Interfaces 7 (2015) 9589–9597, https://doi.org/10.1021/acsami.5b01149.
[479] Y. Wang, J. Yang, L. Wang, K. Du, Q. Yin, Q. Yin, Polypyrrole/graphene/polyaniline ternary nanocomposite with high thermoelectric power factor, ACS Appl. Mater. Interfaces 9 (2017) 20124–20131, https://doi.org/10.1021/acsami.7b05357.
[480] L. Wang, Q. Yao, J. Xiao, K. Zeng, S. Qu, W. Shi, Q. Wang, L. Chen, Engineered molecular chain ordering in single-walled carbon nanotubes/polyaniline composite films for high-performance organic thermoelectric materials, Chem. Asian J. 11 (2016) 1804–1810, https://doi.org/10.1002/asia.201600212.
[481] D. Kim, Y. Kim, K. Choi, J.C. Grunlan, C. Yu, Improved thermoelectric behavior of nanotube-filled polymer composites with poly (3, 4-ethylenedioxythiophene) poly (styrenesulfonate), ACS Nano 4 (2010) 513–523, https://doi.org/10.1021/nn9013577.
[482] C. Yu, K. Choi, L. Yin, J.C. Grunlan, Light-weight flexible carbon nanotube based organic composites with large thermoelectric power factors, ACS Nano 5 (2011) 7885–7892, https://doi.org/10.1021/nn202868a.
[483] G.P. Moriarty, K. Briggs, B. Stevens, C. Yu, J.C. Grunlan, Fully organic nanocomposites with high thermoelectric power factors by using a dual-stabilizer preparation, Energy Technol. 1 (2013) 265–272, https://doi.org/10.1002/ente.201300018.
[484] W. Lee, Y.H. Kang, J.Y. Lee, K.S. Jang, S.Y. Cho, Improving the thermoelectric power factor of cnt/PEDOT: PSS nanocomposite films by ethylene glycol treatment, RSC Adv. 6 (2016) 53339–53344, https://doi.org/10.1039/c6ra08599g.
[485] J.H. Hsu, W. Choi, G. Yang, C. Yu, Origin of unusual thermoelectric transport behaviors in carbon nanotube filled polymer composites after solvent/acid treatments, Org. Electron. 45 (2017) 182–189, https://doi.org/10.1016/j.orgel.2017.03.007.
[486] S. Liu, H. Li, C. He, Simultaneous enhancement of electrical conductivity and seebeck coefficient in organic thermoelectric swnt/PEDOT: PSS nanocomposites, Carbon 149 (2019) 25–32, https://doi.org/10.1016/j.carbon.2019.04.007.
[487] Z. Soleimani, S. Zoras, B. Ceranic, S. Shahzad, Y. Cui, A review on recent developments of thermoelectric materials for room-temperature applications, Sustain. Energy Tech. 37 (2020), 100604, https://doi.org/10.1016/j.seta.2019.100604.
[488] C. Cho, K.L. Wallace, P. Tzeng, J.H. Hsu, C. Yu, J.C. Grunlan, Outstanding low temperature thermoelectric power factor from completely organic thin films enabled by multidimensional conjugated nanomaterials, Adv. Energy Mater. 6 (2016), 1502168, https://doi.org/10.1002/aenm.201502168.
[489] J. Xiong, F. Jiang, H. Shi, J. Xu, C. Liu, W. Zhou, Q. Jiang, Z. Zhu, Y. Hu, Liquid exfoliated graphene as dopant for improving the thermoelectric power factor of conductive PEDOT: PSS nanofilm with hydrazine treatment, ACS Appl. Mater. Interfaces 7 (2015) 14917–14925, https://doi.org/10.1021/acsami.5b03692.
[490] P.A. Zong, J. Liang, P. Zhang, C. Wan, Y. Wang, K. Koumoto, Graphene-based thermoelectrics, ACS Appl. Energy Mater. 3 (2020) 2224–2239, https://doi.org/10.1021/acsaem.9b02187.
[491] C. Bounioux, P. Díaz-Chao, M. Campoy-Quiles, M.S. Martín-González, A.R. Goni, R. Yerushalmi-Rozen, C. Müller, Thermoelectric composites of poly (3-hexylthiophene) and carbon nanotubes with a large power factor, Energy Environ. Sci. 6 (2013) 918–925, https://doi.org/10.1039/c2ee23406h.
[492] Y. Wang, Z. Lu, Q. Hu, X. Qi, Q. Li, Z. Wu, H.L. Zhang, C. Yu, H. Wang, Mass-produced metallic multiwalled carbon nanotube hybrids exhibiting high *n*-type thermoelectric performances, J. Mater. Chem. A 9 (2021) 3341–3352, https://doi.org/10.1039/D0TA10113C.
[493] X. Qi, Y. Wang, K. Li, J. Wang, H.L. Zhang, C. Yu, H. Wang, Enhanced electrical properties and restrained thermal transport in p-and *n*-type thermoelectric metal–organic framework hybrids, J. Mater. Chem. A 9 (2021) 310–319, https://doi.org/10.1039/D0TA10051J.
[494] L. Wei, H. Huang, C. Gao, D. Liu, L. Wang, Novel butterfly-shaped organic semiconductor and single-walled carbon nanotube composites for high performance thermoelectric generators, Mater. Horiz. 8 (2021) 1207–1215, https://doi.org/10.1039/D0MH01679A.
[495] Y. Liu, D.R. Villalva, A. Sharma, M.A. Haque, D. Baran, Molecular doping of a naphthalene diimide–bithiophene copolymer and swcnts for *n*-type thermoelectric composites, ACS Appl. Mater. Interfaces 13 (2020) 411–418, https://doi.org/10.1021/acsami.0c16740.
[496] C. Li, F. Jiang, C. Liu, W. Wang, X. Li, T. Wang, J. Xu, A simple thermoelectric device based on inorganic/organic composite thin film for energy harvesting, Chem. Eng. J. 320 (2017) 201–210, https://doi.org/10.1016/j.cej.2017.03.023.
[497] Q. Meng, Q. Jiang, K. Cai, L. Chen, Preparation and thermoelectric properties of PEDOT: PSS coated te nanorod/PEDOT: PSS composite films, Org. Electron. 64 (2019) 79–85, https://doi.org/10.1016/j.orgel.2018.10.010.
[498] M.P. Gordon, K. Haas, E. Zaia, A.K. Menon, L. Yang, A. Bruefach, M.D. Galluzzo, M.C. Scott, R.S. Prasher, A. Sahu, Understanding diameter and length effects in a solution-processable tellurium-poly (3, 4-ethylenedioxythiophene) polystyrene sulfonate hybrid thermoelectric nanowire mesh, Adv. Electron. Mater. 7 (2021), 2000904, https://doi.org/10.1002/aelm.202000904.
[499] Q. Meng, K. Cai, Y. Du, L. Chen, Preparation and thermoelectric properties of SWCNT/PEDOT: PSS coated tellurium nanorod composite films, J. Alloys Compd. 778 (2019) 163–169, https://doi.org/10.1016/j.jallcom.2018.10.381.
[500] X. Hu, K. Zhang, J. Zhang, S. Wang, Y. Qiu, Thermoelectric properties of conducting polymer nanowire–tellurium nanowire composites, ACS Appl. Energy Mater. 1 (2018) 4883–4890, https://doi.org/10.1021/acsaem.8b00909.
[501] Y. Wang, C. Yu, M. Sheng, S. Song, Y. Deng, Individual adjustment of electrical conductivity and thermopower enabled by multiple interfaces in polyaniline-based ternary hybrid nanomaterials for high thermoelectric performances, Adv. Mater. Interfaces 5 (2018), 1701168, https://doi.org/10.1002/admi.201701168.
[502] C. Ou, L. Zhang, Q. Jing, V. Narayan, S. Kar-Narayan, Compositionally graded organic–inorganic nanocomposites for enhanced thermoelectric performance, Adv. Electron. Mater. 6 (2020), 1900720, https://doi.org/10.1002/aelm.201900720.
[503] Z.G. Chen, X. Shi, L.D. Zhao, J. Zou, High-performance snse thermoelectric materials: progress and future challenge, Prog. Mater. Sci. 97 (2018) 283–346, https://doi.org/10.1016/j.pmatsci.2018.04.005.
[504] X. Wang, F. Meng, Q. Jiang, W. Zhou, F. Jiang, T. Wang, X. Li, S. Li, Y. Lin, J. Xu, Simple layer-by-layer assembly method for simultaneously enhanced electrical conductivity and thermopower of PEDOT: PSS/*ce*-MoS_2 heterostructure films, ACS Appl. Energy Mater. 1 (2018) 3123–3133, https://doi.org/10.1021/acsaem.8b00315.
[505] J. Dong, D. Gerlach, P. Koutsogiannis, P. Rudolf, G. Portale, Boosting the thermoelectric properties of PEDOT: PSS via low-impact deposition of tin oxide nanoparticles, Adv. Electron. Mater. 7 (2021), 2001284, https://doi.org/10.1002/aelm.202001284.
[506] T. Maji, A.M. Rousti, A.P. Kazi, C. Drew, J. Kumar, D.C. Christodouleas, Wearable thermoelectric devices based on three-dimensional PEDOT: tosylate/cui paper composites, ACS Appl. Mater. Interfaces 13 (2021) 46919–46926, https://doi.org/10.1021/acsami.1c12237.
[507] Y.T. Malik, Z.A. Akbar, J.Y. Seo, S. Cho, S.Y. Jang, J.W. Jeon, Self-healable organic–inorganic hybrid thermoelectric materials with excellent ionic thermoelectric properties, Adv. Energy Mater. 12 (2022), 2103070, https://doi.org/10.1002/aenm.202103070.
[508] C. Liu, D.L. Shan, Z.H. Shen, G.K. Ren, Z.F. Zhou, J.Y. Li, D. Yi, J.L. Lan, L. Q. Chen, G.J. Snyder, Role of interfaces in organic–inorganic flexible thermoelectrics, Nano Energy 89 (2021), 106380, https://doi.org/10.1016/j.nanoen.2021.106380.
[509] G. Goo, G. Anoop, S. Unithrattil, W.S. Kim, H.J. Lee, H.B. Kim, M.H. Jung, J. Park, H.C. Ko, J.Y. Jo, Proton-irradiation effects on the thermoelectric properties of flexible Bi_2Te_3/PEDOT: PSS composite films, Adv. Electron. Mater. 5 (2019), 1800786, https://doi.org/10.1002/aelm.201800786.
[510] C. Li, X. Qin, Y. Li, D. Li, J. Zhang, H. Guo, H. Xin, C. Song, Simultaneous increase in conductivity and phonon scattering in a graphene nanosheets/$(Bi_2Te_3)_{0.2}(Sb_2Te_3)_{0.8}$ thermoelectric nanocomposite, J. Alloys Compd. 661 (2016) 389–395, https://doi.org/10.1016/j.jallcom.2015.11.217.
[511] L. Wang, Z. Zhang, Y. Liu, B. Wang, L. Fang, J. Qiu, K. Zhang, S. Wang, Exceptional thermoelectric properties of flexible organic− inorganic hybrids with monodispersed and periodic nanophase, Nat. Commun. 9 (2018) 1–8, https://doi.org/10.1038/s41467-018-06251-9.
[512] E.W. Zaia, M.P. Gordon, V. Niemann, J. Choi, R. Chatterjee, C.H. Hsu, J. Yano, B. Russ, A. Sahu, J.J. Urban, Molecular level insight into enhanced *n*-type transport in solution-printed hybrid thermoelectrics, Adv. Energy Mater. 9 (2019), 1803469, https://doi.org/10.1002/aenm.201803469.
[513] X. Chen, L. Feng, P. Yu, C. Liu, J. Lan, Y.H. Lin, X. Yang, Flexible thermoelectric films based on Bi_2Te_3 nanosheets and carbon nanotube network with high *n*-type performance, ACS Appl. Mater. Interfaces 13 (2021) 5451–5459, https://doi.org/10.1021/acsami.0c21396.
[514] Y. Chen, M. He, B. Liu, G.C. Bazan, J. Zhou, Z. Liang, Bendable *n*-type metallic nanocomposites with large thermoelectric power factor, Adv. Mater. 29 (2017), 1604752, https://doi.org/10.1002/adma.201604752.

[515] J. Tang, R. Chen, L. Chen, G.C. Bazan, Z. Liang, Semiconducting polymer contributes favorably to the seebeck coefficient in multi-component, high-performance *n*-type thermoelectric nanocomposites, J. Mater. Chem. A 8 (2020) 9797–9805, https://doi.org/10.1039/d0ta02388d.
[516] C. Wan, R. Tian, M. Kondou, R. Yang, P. Zong, K. Koumoto, Ultrahigh thermoelectric power factor in flexible hybrid inorganic-organic superlattice, Nat. Commun. 8 (2017) 1–9, https://doi.org/10.1038/s41467-017-01149-4.
[517] I. Petsagkourakis, E. Pavlopoulou, G. Portale, B.A. Kuropatwa, S. Dilhaire, G. Fleury, G. Hadziioannou, Structurally-driven enhancement of thermoelectric properties within poly (3, 4-ethylenedioxythiophene) thin films, Sci. Rep. 6 (2016) 30501, https://doi.org/10.1038/srep30501.
[518] D.X. Crispin, Retracted article: towards polymer-based organic thermoelectric generators, Energy Environ. Sci. (2012), https://doi.org/10.1039/C2EE23401G.
[519] B.Z. Endrődi, J.N. Mellár, Z.N. Gingl, C. Visy, C. Janáky, Molecular and supramolecular parameters dictating the thermoelectric performance of conducting polymers: a case study using poly (3-alkylthiophene) s, J. Phys. Chem. C 119 (2015) 8472–8479, https://doi.org/10.1021/acs.jpcc.5b00135.
[520] S.E. Yoon, Y. Kang, S.Y. Noh, J. Park, S.Y. Lee, J. Park, D.W. Lee, D.R. Whang, T. Kim, G.H. Kim, High efficiency doping of conjugated polymer for investigation of intercorrelation of thermoelectric effects with electrical and morphological properties, ACS Appl. Mater. Interfaces 12 (2019) 1151–1158, https://doi.org/10.1021/acsami.9b17825.
[521] R. Kroon, D. Kiefer, D. Stegerer, L. Yu, M. Sommer, C. Müller, Polar side chains enhance processability, electrical conductivity, and thermal stability of a molecularly p-doped polythiophene, Adv. Mater. 29 (2017), 1700930, https://doi.org/10.1002/adma.201700930.
[522] F. Hossein-Babaei, S. Masoumi, A. Noori, Linking thermoelectric generation in polycrystalline semiconductors to grain boundary effects sets a platform for novel seebeck effect-based sensors, J. Mater. Chem. A 6 (2018) 10370–10378, https://doi.org/10.1039/c8ta02732c.
[523] A. Pakdel, Q. Guo, V. Nicolosi, T. Mori, Enhanced thermoelectric performance of Bi–Sb–Te/Sb_2O_3 nanocomposites by energy filtering effect, J. Mater. Chem. A 6 (2018) 21341–21349, https://doi.org/10.1039/C8TA08238C.
[524] M. He, J. Ge, Z. Lin, X. Feng, X. Wang, H. Lu, Y. Yang, F. Qiu, Thermopower enhancement in conducting polymer nanocomposites via carrier energy scattering at the organic–inorganic semiconductor interface, Energy Environ. Sci. 5 (2012) 8351–8358, https://doi.org/10.1039/c2ee21803h.
[525] A.K.S. Kumar, Y. Zhang, D. Li, R.G. Compton, A mini-review: how reliable is the drop casting technique? Electrochem. Commun. (2020), 106867 https://doi.org/10.1016/j.elecom.2020.106867.
[526] P.J. Yunker, T. Still, M.A. Lohr, A. Yodh, Suppression of the coffee-ring effect by shape-dependent capillary interactions, Nature 476 (2011) 308–311, https://doi.org/10.1038/nature10344.
[527] D.S. Montgomery, C.A. Hewitt, R. Barbalace, T. Jones, D.L. Carroll, Spray doping method to create a low-profile high-density carbon nanotube thermoelectric generator, Carbon 96 (2016) 778–781, https://doi.org/10.1016/j.carbon.2015.09.029.
[528] Y. Du, K. Cai, S. Chen, P. Cizek, T. Lin, Facile preparation and thermoelectric properties of Bi_2Te_3 based alloy nanosheet/PEDOT: PSS composite films, ACS Appl. Mater. Interfaces 6 (2014) 5735–5743, https://doi.org/10.1021/am5002772.
[529] Y. Hosokawa, K. Wada, M. Tanaka, K. Tomita, M. Takashiri, Thermal annealing effect on structural and thermoelectric properties of hexagonal Bi_2Te_3 nanoplate thin films by drop-casting technique, Jpn. J. Appl. Phys. 57 (2017) 02CC02, https://doi.org/10.7567/JJAP.57.02CC02.
[530] N. Sahu, B. Parija, S. Panigrahi, Fundamental understanding and modeling of spin coating process: a review, Indian J. Phys. 83 (2009) 493–502, https://doi.org/10.1007/s12648-009-0009-z.
[531] D. Lee, S.Y. Sayed, S. Lee, C.A. Kuryak, J. Zhou, G. Chen, Y. Shao-Horn, Quantitative analyses of enhanced thermoelectric properties of modulation-doped PEDOT: PSS/undoped si (001) nanoscale heterostructures, Nanoscale 8 (2016) 19754–19760, https://doi.org/10.1039/c6nr06950a.
[532] C.T. Hong, W. Lee, Y.H. Kang, Y. Yoo, J. Ryu, S.Y. Cho, K.-S. Jang, Effective doping by spin-coating and enhanced thermoelectric power factors in SWCNT/P3HT hybrid films, J. Mater. Chem. A 3 (2015) 12314–12319, https://doi.org/10.1039/c5ta02443a.
[533] N. Bhardwaj, S.C. Kundu, Electrospinning: a fascinating fiber fabrication technique, Biotechnol. Adv. 28 (2010) 325–347, https://doi.org/10.1016/j.biotechadv.2010.01.004.
[534] N. Dalton, R.P. Lynch, M.N. Collins, M. Culebras, Thermoelectric properties of electrospun carbon nanofibres derived from lignin, Int. J. Biol. Macromol. 121 (2019) 472–479, https://doi.org/10.1016/j.ijbiomac.2018.10.051.
[535] P.K. Kahol, N. Pinto, An epr investigation of electrospun polyaniline-polyethylene oxide blends, Synth. Met. 140 (2004) 269–272, https://doi.org/10.1016/S0379-6779(03)00370-9.
[536] S. Jo, S. Choo, F. Kim, S.H. Heo, J.S. Son, Ink processing for thermoelectric materials and power-generating devices, Adv. Mater. 31 (2019), 1804930, https://doi.org/10.1002/adma.201804930.
[537] M. Orrill, S. LeBlanc, Printed thermoelectric materials and devices: fabrication techniques, advantages, and challenges, J. Appl. Polym. Sci. 134 (2017), https://doi.org/10.1002/App.44256.
[538] L. Lan, J. Zou, C. Jiang, B. Liu, L. Wang, J. Peng, Inkjet printing for electroluminescent devices: emissive materials, film formation, and display prototypes, Front. Optoelectron. 10 (2017) 329–352, https://doi.org/10.1007/s12200-017-0765-x.
[539] A. Chen, D. Madan, P. Wright, J. Evans, Dispenser-printed planar thick-film thermoelectric energy generators, J. Micromech. Microeng. 21 (2011), 104006, https://doi.org/10.1088/0960-1317/21/10/104006.
[540] Z. Cao, E. Koukharenko, M. Tudor, R. Torah, S. Beeby, Flexible screen printed thermoelectric generator with enhanced processes and materials, Sens. Actuators A 238 (2016) 196–206, https://doi.org/10.1016/j.sna.2015.12.016.
[541] G. Karalis, L. Tzounis, C.K. Mytafides, K. Tsirka, P. Formanek, M. Stylianakis, E. Kymakis, A.S. Paipetis, A high performance flexible and robust printed thermoelectric generator based on hybridized te nanowires with PEDOT: PSS, Appl. Energy 294 (2021), 117004, https://doi.org/10.1016/j.apenergy.2021.117004.
[542] M. Massetti, S. Bonfadini, D. Nava, M. Butti, L. Criante, G. Lanzani, L. Qiu, J. Hummelen, J. Liu, L. Koster, Fully direct written organic micro-thermoelectric generators embedded in a plastic foil, Nano Energy 75 (2020), 104983, https://doi.org/10.1016/j.nanoen.2020.104983.
[543] P. Kajal, K. Ghosh, S. Powar, Applications of Solar Energy, eds., Springer, 2018, pp. 341–364.
[544] S. Dhakate, B. Singla, M. Uppal, R. Mathur, Effect of processing parameters on morphology and thermal properties of electrospun polycarbonate nanofibers, Adv. Mater. Lett. 1 (2010) 200–204, https://doi.org/10.5185/amlett.2010.8148.
[545] H. Zhang, S.K. Moon, T.H. Ngo, 3d printed electronics of non-contact ink writing techniques: status and promise, Int. J. Precis. Eng. Manuf. Green Technol. 7 (2020) 511–524, https://doi.org/10.1007/s40684-019-00139-9.
[546] M. Thirugnanasambandam, S. Iniyan, R. Goic, A review of solar thermal technologies, Renew. Sustain. Energy Rev. 14 (2010) 312–322, https://doi.org/10.1016/j.rser.2009.07.014.
[547] Y. Vorobiev, J. González-Hernández, P. Vorobiev, L. Bulat, Thermal-photovoltaic solar hybrid system for efficient solar energy conversion, Sol. Energy 80 (2006) 170–176, https://doi.org/10.1016/j.solener.2005.04.022.
[548] D. Kraemer, L. Hu, A. Muto, X. Chen, G. Chen, M. Chiesa, Photovoltaic-thermoelectric hybrid systems: a general optimization methodology, Appl. Phys. Lett. 92 (2008), 243503, https://doi.org/10.1063/1.2947591.
[549] J.P. Fleurial, Thermoelectric power generation materials: technology and application opportunities, J. Miner. Met. Mater. Soc. 61 (2009) 79–85, https://doi.org/10.1007/s11837-009-0057-z. TMS.
[550] X. Ju, Z. Wang, G. Flamant, P. Li, W. Zhao, Numerical analysis and optimization of a spectrum splitting concentration photovoltaic–thermoelectric hybrid system, Sol. Energy 86 (2012) 1941–1954, https://doi.org/10.1016/j.solener.2012.02.024.
[551] T. Liao, B. Lin, Z. Yang, Performance characteristics of a low concentrated photovoltaic–thermoelectric hybrid power generation device, Int. J. Therm. Sci. 77 (2014) 158–164, https://doi.org/10.1016/j.ijthermalsci.2013.10.013.
[552] M. Mohsenzadeh, M.B. Shafii, A novel concentrating photovoltaic/thermal solar system combined with thermoelectric module in an integrated design, Renew. Energy 113 (2017) 822–834, https://doi.org/10.1016/j.renene.2017.06.047.
[553] S. Soltani, A. Kasaeian, T. Sokhansefat, M.B. Shafii, Performance investigation of a hybrid photovoltaic/thermoelectric system integrated with parabolic trough collector, Energy Convers. Manag. 159 (2018) 371–380, https://doi.org/10.1016/j.enconman.2017.12.091.
[554] W. Van Sark, Feasibility of photovoltaic–thermoelectric hybrid modules, Appl. Energy 88 (2011) 2785–2790, https://doi.org/10.1016/j.apenergy.2011.02.008.
[555] W. Gu, T. Ma, A. Song, M. Li, L. Shen, Mathematical modelling and performance evaluation of a hybrid photovoltaic-thermoelectric system, Energy Convers. Manag. 198 (2019), 111800, https://doi.org/10.1016/j.enconman.2019.111800.
[556] N. Wang, L. Han, H. He, N.H. Park, K. Koumoto, A novel high-performance photovoltaic–thermoelectric hybrid device, Energy Environ. Sci. 4 (2011) 3676–3679, https://doi.org/10.1039/c1ee01646f.
[557] J.J. Lee, D. Yoo, C. Park, H.H. Choi, J.H. Kim, All organic-based solar cell and thermoelectric generator hybrid device system using highly conductive PEDOT: PSS film as organic thermoelectric generator, Sol. Energy 134 (2016) 479–483, https://doi.org/10.1016/j.solener.2016.05.006.
[558] J. Zhang, Y. Xuan, L. Yang, A novel choice for the photovoltaic–thermoelectric hybrid system: the perovskite solar cell, Int. J. Energy Res. 40 (2016) 1400–1409, https://doi.org/10.1002/er.3532.
[559] Y. Da, Y. Xuan, Q. Li, From light trapping to solar energy utilization: a novel photovoltaic–thermoelectric hybrid system to fully utilize solar spectrum, Energy 95 (2016) 200–210, https://doi.org/10.1016/j.energy.2015.12.024.
[560] M. Hodes, Optimal pellet geometries for thermoelectric power generation, IEEE Trans Compon. Packag. Technol. 33 (2010) 307–318, https://doi.org/10.1109/Tcapt.2009.2039934.
[561] S. Shittu, G. Li, X. Zhao, X. Ma, Series of detail comparison and optimization of thermoelectric element geometry considering the PV effect, Renew. Energy 130 (2019) 930–942, https://doi.org/10.1016/j.renene.2018.07.002.
[562] G. Li, X. Chen, Y. Jin, Analysis of the primary constraint conditions of an efficient photovoltaic-thermoelectric hybrid system, Energies 10 (2017) 20, https://doi.org/10.3390/en10010020.
[563] A. Fabián-Mijangos, G. Min, J. Alvarez-Quintana, Enhanced performance thermoelectric module having asymmetrical legs, Energy Convers. Manag. 148 (2017) 1372–1381, https://doi.org/10.1016/j.enconman.2017.06.087.
[564] G. Li, X. Chen, Y. Jin, J. Ji, Optimizing on thermoelectric elements footprint of the photovoltaic-thermoelectric for maximum power generation, Enrgy Procedia 142 (2017) 730–735, https://doi.org/10.1016/j.egypro.2017.12.119.
[565] Y.P. Zhou, M.J. Li, W.W. Yang, Y.L. He, The effect of the full-spectrum characteristics of nanostructure on the PV-TE hybrid system performances within multi-physics coupling process, Appl. Energy 213 (2018) 169–178, https://doi.org/10.1016/j.apenergy.2018.01.027.

[566] Y.P. Zhou, Y.L. He, Y. Qiu, Q. Ren, T. Xie, Multi-scale investigation on the absorbed irradiance distribution of the nanostructured front surface of the concentrated PV-TE device by a MC-FDTD coupled method, Appl. Energy 207 (2017) 18–26, https://doi.org/10.1016/j.apenergy.2017.05.115.
[567] J. Zhang, Y. Xuan, L. Yang, Performance estimation of photovoltaic–thermoelectric hybrid systems, Energy 78 (2014) 895–903, https://doi.org/10.1016/j.energy.2014.10.087.
[568] R. Lamba, S. Kaushik, Solar driven concentrated photovoltaic-thermoelectric hybrid system: numerical analysis and optimization, Energy Convers. Manag. 170 (2018) 34–49, https://doi.org/10.1016/j.enconman.2018.05.048.
[569] O. Beeri, O. Rotem, E. Hazan, E.A. Katz, A. Braun, Y. Gelbstein, Hybrid photovoltaic-thermoelectric system for concentrated solar energy conversion: experimental realization and modeling, J. Appl. Phys. 118 (2015), 115104, https://doi.org/10.1063/1.4931428.
[570] H.F. Kohan, F. Lotfipour, M. Eslami, Numerical simulation of a photovoltaic thermoelectric hybrid power generation system, Sol. Energy 174 (2018) 537–548, https://doi.org/10.1016/j.solener.2018.09.046.
[571] U.A. Saleh, M.A. Johar, S.A.B. Jumaat, M.N. Rejab, W.A.W. Jamaludin, Evaluation of a PV-TEG hybrid system configuration for an improved energy output: a review, Int. J. Renew. Energy Dev. 10 (2020) 385–400, https://doi.org/10.14710/ijred.2021.33917.
[572] P.G.V. Sampaio, M.O.A. González, R.M. de Vasconcelos, M.A.T. dos Santos, J. C. de Toledo, J.P.P. Pereira, Photovoltaic technologies: mapping from patent analysis, Renew. Sustain. Energy Rev. 93 (2018) 215–224, https://doi.org/10.1016/j.rser.2018.05.033.
[573] S. Shittu, G. Li, Y.G. Akhlaghi, X. Ma, X. Zhao, E. Ayodele, Advancements in thermoelectric generators for enhanced hybrid photovoltaic system performance, Renew. Sustain. Energy Rev. 109 (2019) 24–54, https://doi.org/10.1016/j.rser.2019.04.023.
[574] D. Narducci, P. Bermel, B. Lorenzi, N. Wang, K. Yazawa, Hybrid and Fully Thermoelectric Solar Harvesting, eds., Springer, 2018, pp. 103–116.
[575] W. Zhu, Y. Deng, Y. Wang, S. Shen, R. Gulfam, High-performance photovoltaic-thermoelectric hybrid power generation system with optimized thermal management, Energy 100 (2016) 91–101, https://doi.org/10.1016/j.energy.2016.01.055.
[576] R. Lamba, S. Kaushik, Modeling and performance analysis of a concentrated photovoltaic–thermoelectric hybrid power generation system, Energy Convers. Manag. 115 (2016) 288–298, https://doi.org/10.1016/j.enconman.2016.02.061.
[577] Y. Deng, W. Zhu, Y. Wang, Y. Shi, Enhanced performance of solar-driven photovoltaic–thermoelectric hybrid system in an integrated design, Sol. Energy 88 (2013) 182–191, https://doi.org/10.1016/j.solener.2012.12.002.
[578] D. Kossyvakis, G. Voutsinas, E. Hristoforou, Experimental analysis and performance evaluation of a tandem photovoltaic–thermoelectric hybrid system, Energy Convers. Manag. 117 (2016) 490–500, https://doi.org/10.1016/j.enconman.2016.03.023.
[579] F.C. Krebs, N. Espinosa, M. Hösel, R.R. Søndergaard, M. Jørgensen, 25th anniversary article: rise to power–OPV-based solar parks, Adv. Mater. 26 (2014) 29–39, https://doi.org/10.1002/adma.201302031.
[580] F.C. Krebs, J. Fyenbo, D.M. Tanenbaum, S.A. Gevorgyan, R. Andriessen, B. van Remoortere, Y. Galagan, M. Jørgensen, The OE-A OPV demonstrator anno domini 2011, Energy Environ. Sci. 4 (2011) 4116–4123, https://doi.org/10.1039/c1ee01891d.
[581] A. Hagfeldt, G. Boschloo, L. Sun, L. Kloo, H. Pettersson, Dye-sensitized solar cells, Chem. Rev. 110 (2010) 6595–6663, https://doi.org/10.1021/cr900356p.
[582] S. Oh, P. Rai, M. Ramasamy, V.K. Varadan, Fishnet metastructure for ir band trapping for enhancement of photovoltaic–thermoelectric hybrid systems, Microelectron. Eng. 148 (2015) 117–121, https://doi.org/10.1016/j.mee.2015.10.016.
[583] K. Tvingstedt, C. Deibel, Temperature dependence of ideality factors in organic solar cells and the relation to radiative efficiency, Adv. Energy Mater. 6 (2016), 1502230, https://doi.org/10.1002/aenm.201502230.
[584] T. Suzuki, K. Yoshikawa, S. Momose, Integration of organic photovoltaic and thermoelectric hybrid module for energy harvesting applications, in: Proceedings of the International Electron Devices Meeting, 2010, https://doi.org/10.1109/IEDM.2010.5703460. IEEE.
[585] Y. Zhang, J. Fang, C. He, H. Yan, Z. Wei, Y. Li, Integrated energy-harvesting system by combining the advantages of polymer solar cells and thermoelectric devices, J. Phys. Chem. C 117 (2013) 24685–24691, https://doi.org/10.1021/jp4044573.
[586] H. Chang, M.J. Kao, K.C. Cho, S.L. Chen, K.H. Chu, C.C. Chen, Integration of cuo thin films and dye-sensitized solar cells for thermoelectric generators, Curr. Appl. Phys. 11 (2011) S19–S22, https://doi.org/10.1016/j.cap.2010.12.039.